

**University of Alberta**

Electron Transfer and Quinone Chemistry in *Escherichia coli*  
Dimethyl Sulfoxide Reductase and Succinate Dehydrogenase

by

Victor Wing Tai Cheng



A thesis submitted to the Faculty of Graduate Studies and Research  
in partial fulfillment of the requirements for the degree of

Doctor of Philosophy

Department of Biochemistry

Edmonton, Alberta

Fall, 2008



Library and  
Archives Canada

Published Heritage  
Branch

395 Wellington Street  
Ottawa ON K1A 0N4  
Canada

Bibliothèque et  
Archives Canada

Direction du  
Patrimoine de l'édition

395, rue Wellington  
Ottawa ON K1A 0N4  
Canada

*Your file    Votre référence*  
*ISBN: 978-0-494-46296-6*  
*Our file    Notre référence*  
*ISBN: 978-0-494-46296-6*

**NOTICE:**

The author has granted a non-exclusive license allowing Library and Archives Canada to reproduce, publish, archive, preserve, conserve, communicate to the public by telecommunication or on the Internet, loan, distribute and sell theses worldwide, for commercial or non-commercial purposes, in microform, paper, electronic and/or any other formats.

The author retains copyright ownership and moral rights in this thesis. Neither the thesis nor substantial extracts from it may be printed or otherwise reproduced without the author's permission.

**AVIS:**

L'auteur a accordé une licence non exclusive permettant à la Bibliothèque et Archives Canada de reproduire, publier, archiver, sauvegarder, conserver, transmettre au public par télécommunication ou par l'Internet, prêter, distribuer et vendre des thèses partout dans le monde, à des fins commerciales ou autres, sur support microforme, papier, électronique et/ou autres formats.

L'auteur conserve la propriété du droit d'auteur et des droits moraux qui protègent cette thèse. Ni la thèse ni des extraits substantiels de celle-ci ne doivent être imprimés ou autrement reproduits sans son autorisation.

---

In compliance with the Canadian Privacy Act some supporting forms may have been removed from this thesis.

Conformément à la loi canadienne sur la protection de la vie privée, quelques formulaires secondaires ont été enlevés de cette thèse.

While these forms may be included in the document page count, their removal does not represent any loss of content from the thesis.

Bien que ces formulaires aient inclus dans la pagination, il n'y aura aucun contenu manquant.

  
**Canada**

*for my wife, Helen*

## ABSTRACT

In living organisms, the majority of energy needed to maintain life is derived from the respiratory chain. In humans, respiration is strictly aerobic and is catalyzed by four enzyme complexes located at the inner mitochondrial membrane. In simpler prokaryotes, these complexes are either absent or substituted by other respiratory enzymes to allow them to thrive aerobically or anaerobically in diverse environments. The different respiratory chain enzymes contain a number of different prosthetic groups that form an electron transfer relay and are connected by the membrane-soluble quinone species. Using the *Escherichia coli* dimethyl sulfoxide reductase and succinate dehydrogenase enzymes as model systems, we set out to examine some underlying structure-function relationships that are common to respiratory chain enzymes in general. In this thesis, some questions regarding redox enzymes which we wanted to address include the elements that govern the biophysical properties of redox cofactors, the rate of electron transfer, and the mechanisms of proton transfer and quinone/quinol reduction/oxidation. This was accomplished by constructing site-directed mutants in the electron transfer subunits of dimethyl sulfoxide reductase and succinate dehydrogenase, followed by evaluations of enzyme function using *in vivo* complementation and *in vitro* biochemical, enzymology and spectroscopic techniques.

## **Acknowledgements**

First and foremost, I must thank my supervisor, Dr. Joel H. Weiner. He provided me with unwavering support through two summer studentships, an undergraduate biochemistry honors project, and of course through my Ph.D studies. His inclination to give me freedom to pursue questions which interested me, and his ability to steer me back on track when I started to go astray, are what every graduate student would desire in a supervisor. His wisdom, patience and support were greatly appreciated.

A big gratitude must be given to Gillian McCuaig, who taught me countless laboratory techniques, kept the lab running in tip-top form, and turned a blind eye (most of the time) when my bench was an unrecognizable mess during busy times. To Richard Rothery, the EPR guru, I also give many thanks for teaching me how to operate a machine that a handful of people in the world know how to use. His provisions of useful information during the last six years were certainly welcoming to me.

I want to thank Quang Tran, my Sdh partner-in-crime. He traveled with me to conferences and work projects, and was always a joyful companion during those times. His discussions, insights and knowledge on Sdh (as well as hockey, video games and poker) made him an extremely valuable colleague and a great friend. I would also like to thank Greg Workun, Nasim Boroumand, Huipo Tang, Glen Zhang, Zhongwei Zhao, Kamila Moquin, and Francois Chartier for helping me out on numerous occasions and making my time in the lab extremely enjoyable and memorable. I would also like to thank my two summer students,

Elysia Ma and Antonia Johnson, who helped me jump-start a couple of different projects and had the patience to learn from a graduate student. Much deserved gratitude also goes out to Dr. Simon de Vries and Marc Strampraad at the Delft University of Technology, Dr. Gary Cecchini at the U.C.S.F., as well as Dr. Les Dutton, Dr. Chris Moser, and Sarah Chobot from the University of Pennsylvania.

I am very grateful to have Drs. Bernard Lemire, Howard Young and Moira Glerum as my supervisory committee. They were very patient in listening to and understanding my research, and were very thoughtful and forthright with their guidance and suggestions. I would also like to thank Dr. Frank Nargang, who acted as an internal-external examiner, and Dr. Barry Rosen, who traveled from Detroit, Michigan to act as the external examiner.

Last but not least, I would like to thank those who are closest to me. These last few years would not have been possible without the support and love of my wife, who understood, somehow, that bacterial cultures may need to be harvested on the weekend or that the occasional all-nighter is needed to prepare a presentation. My Mom, Dad and my brother have also supported me throughout my graduate studies on many, many levels. Finally, a big thank you to all my fellow graduate students and friends for all those fun and unforgettable memories.

I am also extremely grateful for the financial support provided by Alberta Heritage Foundation for Medical Research and the Canadian Institutes for Health Research, which made these last few years possible.

## Table of Contents

### Chapter 1 – General Introduction.....1

- 1.1 Introduction
- 1.2 Respiration
- 1.3 Aerobic Respiration in Mitochondria
  - 1.3.1 NADH:ubiquinone oxidoreductase (complex I)
  - 1.3.2 Ubiquinol:cytochrome *c* oxidoreductase (*bc*<sub>1</sub> complex or complex III)
  - 1.3.3 Cytochrome *c* oxidase (complex IV)
  - 1.3.4 ATP Synthase (complex V)
- 1.4 Respiration in *Escherichia coli*
- 1.5 Common Prosthetic Groups of Respiratory Enzymes
- 1.6 Assembly and Targeting of Respiratory Enzymes

### Chapter 2 – *S*- and *N*-oxide Reductases.....23

- 2.1 Organization of the DMSO and TMAO respiratory chains
- 2.2 Dimethyl sulfoxide reductase
  - 2.2.1 Overview
  - 2.2.2 The *dms* Operon
  - 2.2.3 DmsA – The Catalytic Subunit
  - 2.2.4 DmsB – The Electron Transfer Subunit
  - 2.2.5 DmsC – The Membrane Anchor Subunit
  - 2.2.6 Membrane Targeting and Translocation of DMSO Reductase
  - 2.2.7 Topology of DmsABC
  - 2.2.8 YnfEFGH/DmsD – A Dms Paralogue
  - 2.2.9 DmsD – A DMSO Reductase Specific Chaperone
- 2.3 Trimethylamine *N*-oxide Reductase
  - 2.3.1 TMAO in the Natural Environment
  - 2.3.2 The *tor* Locus
  - 2.3.3 Tor Regulation
  - 2.3.4 TorA – The Catalytic Subunit
  - 2.3.5 TorC – The Pentaheme Cytochrome
  - 2.3.6 TorD – The Chaperone Protein
  - 2.3.7 The *torYZ* operon
- 2.4 Summary

### Chapter 3 – Investigation of the Environment Surrounding Iron-Cluster 4 of *Escherichia coli* Dimethyl Sulfoxide Reductase.....72

- 3.1 Introduction
- 3.2 Experimental Procedures
- 3.3 Results
- 3.4 Discussion

<b>Chapter 4 – Succinate:ubiquinone Oxidoreductase.....</b>	<b>101</b>
4.1 Overview	
4.2 The <i>sdh</i> operon	
4.3 Sdh and Disease Phenotypes in Humans	
4.4 X-ray Crystallographic Structures	
4.5 SdhA – The Catalytic Subunit	
4.6 SdhB – The Electron Transfer Subunit	
4.7 SdhCD – The Membrane Anchor Domain	
<b>Chapter 5 – Alternative Sites for Proton Entry from the Cytoplasm to the Quinone Binding Site in <i>Escherichia coli</i> Succinate Dehydrogenase.....</b>	<b>121</b>
5.1 Introduction	
5.2 Experimental Procedures	
5.3 Results	
5.4 Discussion	
<b>Chapter 6 – The Iron-Sulfur Clusters in <i>Escherichia coli</i> Succinate Dehydrogenase Direct Electron Flow.....</b>	<b>150</b>
6.1 Introduction	
6.2 Experimental Procedures	
6.3 Results	
6.4 Discussion	
<b>Chapter 7 – Calculation and Observation of Electron Transfer in <i>Escherichia coli</i> Succinate Dehydrogenase.....</b>	<b>171</b>
7.1 Introduction	
7.2 Experimental Procedures	
7.3 Results	
7.4 Discussion	
<b>Chapter 8 – Conclusions, Summary, and Future Directions.....</b>	<b>187</b>
8.1 DMSO Reductase	
8.2 Succinate Dehydrogenase	
8.3 Future Studies	
<b>References.....</b>	<b>199</b>



## List of Tables

<b>Table 2.1</b>	Summary of attributes for the four enzymes discussed in this review	<b>61</b>
<b>Table 3.1</b>	The growth rates of the DmsB mutants in glycerol-DMSO minimal media, and the BV <sup>+</sup> - and LPCH <sub>2</sub> -dependent reduction of TMAO	<b>92</b>
<b>Table 3.2</b>	HOQNO FQ titrations of DmsB mutants expressed in HB101 cells	<b>93</b>
<b>Table 3.3</b>	Mutations made in DmsB and the resultant $E_m$ values of the [3Fe-4S] cluster	<b>94</b>
<b>Table 5.1</b>	A list of residues studied by site-directed mutagenesis	<b>137</b>
<b>Table 5.2</b>	Succinate dependent reduction of PMS/MTT by mutant enzymes at pH 7, pH 8 and pD 7.4	<b>137</b>
<b>Table 5.3</b>	Succinate-dependent reduction of Q <sub>0</sub> by mutant enzymes	<b>138</b>
<b>Table 5.4</b>	Fumarate dependent oxidation of reduced plumbagin by mutant enzymes	<b>138</b>
<b>Table 5.5</b>	Kinetic isotope effect on enzyme activities	<b>139</b>
<b>Table 5.6</b>	Midpoint potentials of the [3Fe-4S] cluster and heme <i>b</i>	<b>140</b>
<b>Table 6.1</b>	Quantitation of cofactors and midpoint potentials (mV) of [Fe-S] clusters in Sdh	<b>164</b>
<b>Table 7.1</b>	Parameters to fit first-order rate equations to observed FS1 and FS3 reduction	<b>183</b>
<b>Table 7.2</b>	Midpoint potentials of the Fe-S clusters in WT and mutant Sdh	<b>183</b>

## List of Figures

<b>Figure 1.1</b>	Overview of the canonical aerobic respiratory chain	<b>20</b>
<b>Figure 1.2</b>	Variation in the <i>E. coli</i> respiratory chain	<b>21</b>
<b>Figure 1.3</b>	Stereo view of common prosthetic group in respiratory chain enzymes	<b>22</b>
<b>Figure 2.1</b>	A schematic representation of the TMAO and DMSO reductases	<b>62</b>
<b>Figure 2.2</b>	The reaction catalyzed by DMSO reductase	<b>62</b>
<b>Figure 2.3</b>	Organization of the chromosomal regions encoding <i>dmsABC</i> , <i>ynfEFGHdmsD</i> , <i>torCAD</i> , <i>torRTS</i> and <i>torYZ</i> operons	<b>63</b>
<b>Figure 2.4</b>	Organization of the upstream region preceding <i>dmsA</i>	<b>63</b>
<b>Figure 2.5</b>	Opposite views of the Mo-bisMGD cofactor	<b>64</b>
<b>Figure 2.6</b>	Space filling structures of DMSO reductase from <i>Rhodobacter capsulatus</i>	<b>64</b>
<b>Figure 2.7</b>	The active site funnel in <i>Rhodobacter capsulatus</i> DMSO reductase	<b>65</b>
<b>Figure 2.8</b>	Coordination of the molybdenum atom	<b>66</b>
<b>Figure 2.9</b>	Suggested catalytic mechanism for the catalytic cycle of <i>Rhodobacter</i> DMSO reductase	<b>67</b>
<b>Figure 2.10</b>	Cysteine coordination of the four [4Fe-4S] clusters in DmsB by four cysteine groups	<b>68</b>
<b>Figure 2.11</b>	A topology model based on <i>phoA</i> and <i>bla</i> fusions of DmsC	<b>68</b>
<b>Figure 2.12</b>	Ribbon model for the structure of <i>Salmonella typhimurium</i> DmsD	<b>69</b>
<b>Figure 2.13</b>	The reaction catalyzed by TMAO reductase	<b>70</b>
<b>Figure 2.14</b>	Organization of the divergently expressed intragenic region between <i>torC</i> and <i>torR</i>	<b>70</b>
<b>Figure 2.15</b>	The structure of TorA from <i>Shewanella massilia</i>	<b>71</b>
<b>Figure 3.1</b>	Electron transfer through DmsB and NarH	<b>95</b>
<b>Figure 3.2</b>	Local alignment of the amino acids around FS4 of DmsB with that of FdnH	<b>96</b>
<b>Figure 3.3</b>	Crystal Structure of FdnGHI, magnified and centered on FS4	<b>97</b>
<b>Figure 3.4</b>	A three-dimensional alignment of the backbones of the DmsB model and the structure of FdnH	<b>98</b>
<b>Figure 3.5</b>	Oxidized EPR spectra of the engineered [3Fe-4S] cluster in DmsB in the absence and presence of HOQNO	<b>99</b>
<b>Figure 3.6</b>	Redox titrations of FS4 from the DmsB <sup>C102S</sup> single mutant and the DmsB <sup>C102S/Y104D</sup> double mutant	<b>100</b>
<b>Figure 4.1</b>	Overview of <i>Escherichia coli</i> succinate dehydrogenase and fumarate reductase	<b>117</b>
<b>Figure 4.2</b>	Competitive inhibitors which have been co-crystallized with Sdh	<b>118</b>
<b>Figure 4.3</b>	The reactions catalyzed by SdhA and FrdA	<b>118</b>
<b>Figure 4.4</b>	The succinate binding site in <i>Escherichia coli</i> succinate dehydrogenase	<b>119</b>

<b>Figure 4.5</b>	The ubiquinone binding pocket in <i>Escherichia coli</i> Sdh	<b>120</b>
<b>Figure 5.1</b>	Two views of the putative water channel in <i>E. coli</i> Sdh leading from the cytoplasm to the Q-site	<b>141</b>
<b>Figure 5.2</b>	Assembly of mutant Sdh enzymes	<b>142</b>
<b>Figure 5.3</b>	Growth of <i>E. coli</i> DW35 with and without expression of wild-type and mutant Sdh enzymes	<b>143</b>
<b>Figure 5.4</b>	Relative enzyme activities in deuterium oxide	<b>144</b>
<b>Figure 5.5</b>	EPR spectra of the oxidized [3Fe-4S] cluster	<b>145</b>
<b>Figure 5.6</b>	EPR spectra of the oxidized heme <i>b</i>	<b>146</b>
<b>Figure 5.7</b>	The observed water molecules in porcine Sdh	<b>147</b>
<b>Figure 5.8</b>	The observed water molecules in chicken Sdh	<b>148</b>
<b>Figure 5.9</b>	An alternative proton entry point in <i>E. coli</i> Sdh	<b>149</b>
<b>Figure 6.1</b>	Iron-sulfur clusters in SdhB	<b>165</b>
<b>Figure 6.2</b>	SDS-PAGE gel stained by Coomassie blue	<b>166</b>
<b>Figure 6.3</b>	Aerobic growth with succinate as electron donor and anaerobic growth with fumarate as electron acceptor	<b>167</b>
<b>Figure 6.4</b>	Physiological and non-physiological enzyme activities of SdhB mutants	<b>168</b>
<b>Figure 6.5</b>	Stopped-flow traces of heme reduction by succinate in SdhB mutants	<b>169</b>
<b>Figure 6.6</b>	Production of reactive oxygen species by SdhB mutants during enzyme turnover	<b>170</b>
<b>Figure 7.1</b>	Pre-steady state heme reduction	<b>184</b>
<b>Figure 7.2</b>	Electron transfer in SdhCDAB	<b>185</b>
<b>Figure 7.3</b>	Electron transfer in SdhCDAB <sup>1150H</sup>	<b>186</b>

## List of Abbreviations

ADP	adenosine diphosphate
ALA	5-aminolevulinic acid
Arc	anoxic redox control
ATP	adenosine triphosphate
BV <sup>+</sup>	reduced benzyl viologen
complex I	NADH:ubiquinone oxidoreductase
complex II	succinate:ubiquinone oxidoreductase
complex III	ubiquinol:cytochrome <i>c</i> oxidoreductase
complex IV	cytochrome <i>c</i> oxidase
complex V	ATP synthase
DMQ	demethylmenaquinone
DMS	dimethyl sulfide
DMSO	dimethyl sulfoxide
DmsABC	DMSO reductase
EcDms	<i>Escherichia coli</i> DMSO reductase
EcFrd	<i>Escherichia coli</i> fumarate reductase
EcSdh	<i>Escherichia coli</i> succinate dehydrogenase
$E_m$	midpoint potential
EPR	electron paramagnetic resonance
ET	electron transfer
EXAFS	extended X-ray absorption fine structure
FAD	flavin adenine dinucleotide
FCP	four cluster protein
FdnGHI	formate dehydrogenase- <i>N</i>
[Fe-S]	iron-sulfur
FMN	flavin mononucleotide
FNR	fumarate and nitrate reduction
FQ	fluorescence quench
FrdABCD	fumarate reductase
G-F	glycerol-fumarate
H-bond	hydrogen bond
HIF	hypoxia-inducible factor
HOQNO	2- <i>n</i> -heptyl-4-hydroxyquinoline- <i>N</i> -oxide
Isc	iron sulfur cluster
KIE	kinetic isotope effect
LPCH <sub>2</sub>	reduced lapachol
MQ/MQH <sub>2</sub>	menaquinone/menaquinol
Mo-bisMGD	molybdo-bis(molybdopterin guanine dinucleotide)
MTT	2-(4,5-dimethyl-2-thiazolyl)-3,5-diphenyl-2 <i>H</i> -tetrazolium bromide
NAD <sup>+</sup>	nicotinamide adenine dinucleotide, oxidized form
NADH	nicotinamide adenine dinucleotide, reduced form
NarGHI	nitrate reductase
Nif	nitrogen fixation

NMR	nuclear magnetic resonance
OAA	oxaloacetate
P <sub>i</sub>	inorganic phosphate
pmf	proton motive force
PMS	phenazine methosulfate
Q <sub>0</sub>	ubiquinone analogue
Q-pool	quinone pool
Q-site	quinone binding site
Q <sub>i</sub> -site	quinone binding site, towards the “inside” of the membrane
Q <sub>o</sub> -site	quinone binding site, towards the “outside” of the membrane
Q <sub>D</sub> -site	quinone binding site distal to the soluble domain
Q <sub>P</sub> -site	quinone binding site proximal to the soluble domain
RhDms	<i>Rhodobacter</i> DMSO reductase
rmsd	root mean square deviation
ROS	reactive oxygen species
ScSdh	<i>Saccharomyces cerevisiae</i> succinate dehydrogenase
Sdh	succinate dehydrogenase
SdhCDAB	succinate dehydrogenase
SDS-PAGE	sodium dodecyl sulfate polyacrylamide gel electrophoresis
Suf	sulfur formation
Tat	twin arginine translocation
TCA	tricarboxylic acid
TMA/TMAO	trimethylamine/trimethylamine <i>N</i> -oxide
TorCA	TMAO reductase
TTFA	2-thenoyltrifluoroacetone
UQ/UQH <sub>2</sub>	ubiquinone/ubiquinol
WT	wild-type
Δ <i>p</i>	proton motive force

# **Chapter 1**

## **General Introduction**

## 1.1 Introduction

Eat. Play. Work. Reproduce. Finish writing this thesis. Admittedly, these are things which I like to do, but more importantly, they share a common denominator in that energy must be consumed if any of these are to be accomplished. In mammals, mitochondria are the power houses which churn out adenosine 5'-triphosphate (ATP) molecules, the energy currency of life on the cellular and molecular levels. This is accomplished by four multisubunit complexes (complexes I-IV) located at the inner mitochondrial membrane which, in transferring reducing equivalents to molecular oxygen, produce a proton motive force (pmf or  $\Delta p$ ) that is in turn used by ATP synthase (complex V) to generate ATP. Bacteria, such as the facultative anaerobe *Escherichia coli*, can harness energy from a wide diversity of substrates by utilizing an array of oxidoreductases. One such enzyme that is absent in the mitochondrion is dimethyl sulfoxide reductase (DmsABC) and will comprise a portion of this thesis. The remainder of the thesis will focus on succinate dehydrogenase (SdhCDAB), a complex II homologue that is highly conserved with the mammalian enzyme. During the course of the last 10 years, a wealth of structural information on membrane-bound oxidoreductases has become available. The aims of the studies presented herein are to identify structure-function relationships in DmsABC and SdhCDAB in regard to their abilities to transfer electrons and catalyze quinone oxidation/reduction.

## 1.2 Respiration

The 1978 Nobel Prize in Chemistry was awarded to Peter Mitchell for his discovery of the chemiosmotic mechanism of ATP synthesis. Mitchell hypothesized that

electron transfer is coupled to proton translocation across an energy conserving membrane and the resulting transmembrane electrochemical gradient or pmf is used to generate ATP (1). As the term electrochemical gradient implies, the pmf is comprised of two components: a proton concentration gradient ( $\Delta\text{pH}$ ) and a charge separation ( $\Delta\psi_m$ ). Mathematically, the three variables are related by the equation  $\Delta p = (-2.303RT\Delta\text{pH})/nF + \Delta\psi_m$  where  $R = 8.315 \text{ J K}^{-1} \text{ mol}^{-1}$ ,  $T =$  the temperature in Kelvin,  $n =$  moles of protons, and  $F = 96\,494 \text{ J V}^{-1} \text{ mol}^{-1}$ . Generation of  $\Delta p$  is accomplished by passing electrons from high energy reductants (e.g. NADH and succinate) to oxidants with a relatively low free energy (e.g.  $\text{O}_2$ ). In addition to ATP synthesis, the pmf can also be used to power flagellar rotation in bacteria (2,3), transport ions and metabolites (4), as well as translocate peptides across membranes (5,6).

### 1.3 Aerobic Respiration in Mitochondria

Mitochondrial respiration is carried out by five distinct multisubunit enzymes located at the inner membrane and oriented towards the matrix (Figure 1.1). NADH:ubiquinone oxidoreductase (complex I), succinate:ubiquinone oxidoreductase (succinate dehydrogenase or complex II), ubiquinol-cytochrome *c* oxidoreductase (*bc*<sub>1</sub> complex or complex III) and cytochrome *c* oxidase (complex IV) are responsible for extracting electrons from high energy substrates and passing them to molecular oxygen. Complexes I, III and IV are able to couple electron transfer to proton movement across the inner membrane, whereas complex II is an electroneutral enzyme and its turnover does not contribute to the pmf. Protons are transported from the matrix to the intermembrane space via two mechanisms: i) the scalar mechanism where oxidation and



reduction of substrates release and consume protons on opposite sides on the membrane and ii) the vectorial mechanism where protons are pumped directly across the membrane. The  $F_0F_1$ -ATPase (complex V) then utilizes the transmembrane electrochemical gradient to generate ATP.

### **1.3.1 NADH:ubiquinone oxidoreductase (complex I)**

The complex I enzyme serves as one of two major entry points for electrons to enter the electron transfer (ET) chain. At its active site, a noncovalent flavin mononucleotide (FMN) cofactor accepts two electrons from nicotinamide adenine dinucleotide (reduced form: NADH, oxidized form:  $NAD^+$ ), which are then shuttled through iron-sulfur ([Fe-S]) clusters and are ultimately used to reduce ubiquinone (UQ) to ubiquinol ( $UQH_2$ ) in the membrane-soluble domain. Complex I is an electrogenic enzyme and therefore plays a pivotal role in energy transduction. During NADH oxidation and UQ reduction, four protons are pumped across the energy conserving membrane (7,8).

Being the largest of all the mitochondrial respiratory complexes, complex I remains the only enzyme without a complete X-ray crystal structure. In fact, the number and assignment of cofactors in this enzyme remain ambiguous although it is known that it contains a noncovalent FMN molecule and a number of iron-sulfur clusters (7,9). The overall architecture of complex I, as determined by electron microscopy, is shaped like an “L” where one arm lies in the inner mitochondrial membrane and the other protrudes into the matrix (10-13). A similar electron microscopic structure was observed for the *E. coli* NADH:quinone oxidoreductase (14), which only contains the 14 core subunits of the

mitochondrial counterpart (15,16). Although structural data of the holoenzyme is absent, the peripheral hydrophilic domain of complex I from *Thermus thermophilus* has been determined by X-ray crystallography to a maximal resolution of 3.3Å by Hinchliffe and Sazanov (17). From the structure, one [2Fe-2S] and six [4Fe-4S] clusters were seen to comprise an electron transfer pathway that spans 84Å. An additional [2Fe-2S] (N1a) cluster and a [4Fe-4S] (N7) cluster were also observed in the protein but not on this pathway. It was proposed that the N1a cluster acts to distribute electrons away from the FMN molecule to minimize reactive oxygen species (ROS) generation (18). The distance between the N7 cluster and any other prosthetic group in the protein was observed to be much greater than the 14Å limit proposed for rapid electron transfer (19). As a result, it was suggested that the role of N7 is to aid protein folding, specifically that of the Nqo3 subunit (18).

Although the X-ray crystal structure of the soluble domain of complex I recently became available, structural information on the hydrophobic domain of the protein is still lacking. As such, the mechanism of proton translocation through the hydrophobic subunits remains unclear. Two hypotheses currently stand out. First, Dutton *et al.* have proposed that complex I works essentially in reverse compared to complex III (20) (see section 1.3.2) via a Q-cycle mechanism. The major drawback of this hypothesis is that such a mechanism would only allow 2 protons to be pumped across the membrane for every 2 electrons transferred between NADH and UQ, where experimental evidence clearly indicates a  $H^+/e^-$  ratio of 2 (7,8). The second hypothesis is that in complex I, electron transfer and proton pumping are directly coupled as is the case for cytochrome *c*

oxidase. Since no structural data are available for the complex I holoenzyme, the latter mechanism is difficult to support or discount.

### 1.3.2 Ubiquinol:cytochrome *c* oxidoreductase (*bc*<sub>1</sub> complex or complex III)

Of the mitochondrial respiratory chain enzymes, the *bc*<sub>1</sub> complex is the best understood. Crystal structures are available from a number of eukaryotes and prokaryotes (21-25), and these are often supplemented by a wealth of biochemical and biophysical data. In its simplest form, the *bc*<sub>1</sub> family of enzymes can be represented as a trimer comprised of a cytochrome *b* subunit (containing a heme *b*<sub>L</sub> and a heme *b*<sub>H</sub>), a cytochrome *c* subunit (containing a heme *c*<sub>1</sub>) and a Rieske iron-sulfur protein subunit (containing a [2Fe-2S] cluster). Complex III plays a fundamental role in energy transduction by transferring electrons from the reduced UQH<sub>2</sub> pool to the soluble cytochrome *c* protein and using the free energy from this reaction to translocate protons across the membrane at a H<sup>+</sup>/e<sup>-</sup> ratio of 1. The “Q-cycle” mechanism of UQ oxidation/reduction and proton translocation was first proposed by Mitchell over 30 years ago in the absence of any structural data and remains the working enzymatic model today (26-29).

The cytochrome *b* subunit contains two quinone binding sites; a Q<sub>o</sub>-site and a Q<sub>i</sub>-site representing the “outside” and “inside” of the membrane respectively. The initial step in catalysis is binding and oxidation of a UQH<sub>2</sub> molecule at the Q<sub>o</sub>-site; the two protons are released to the “outside” or positive side (*P*-side) of the membrane and the two electrons are bifurcated to the heme *b*<sub>L</sub> and the Rieske centre. Upon reduction of the [2Fe-2S] cluster, the iron sulfur protein subunit undergoes a conformational change that

moves the binuclear centre ( $\sim 25\text{\AA}$ ) closer to heme  $c_1$  to allow passage of an electron from the former to the latter (30,31). Reduced heme  $c_1$  subsequently passes the electron to the cytochrome  $c$  protein, which serves as a soluble electron carrier from complex III to complex IV. Meanwhile, heme  $b_L$  passes one electron to heme  $b_H$ , which in turn reduces a UQ molecule at the  $Q_i$ -site to form a stable semiquinone intermediate. A second molecule of UQH<sub>2</sub> then binds to and gets oxidized at the  $Q_o$ -site, and once again two protons are released to the “outside” and the two electrons are bifurcated. The Rieske pathway allows a second cytochrome  $c$  protein to get reduced. The heme  $b_H$  pathway donates a second electron to the  $Q_i$ -site, forming a UQH<sub>2</sub> molecule after taking up 2 protons from the “inside” or negative side of the membrane ( $N$ -side). Thus net consumption during enzyme turnover is 1 molecule of UQ which results in 2 protons released to the “outside”.

### 1.3.3 Cytochrome $c$ oxidase (complex IV)

Cytochrome  $c$  oxidase is the terminal oxidase in the respiratory chains of aerobic organisms. It catalyzes conversion of O<sub>2</sub> to 2 H<sub>2</sub>O and conserves the free energy by contributing to the pmf (32-35). X-ray crystal structures for cytochrome oxidase are available from several organisms (36-39). In essence, four redox centers are assembled in complex IV to carry out enzyme function: the binuclear Cu<sub>A</sub> center, Cu<sub>B</sub>, and two heme moieties (heme  $a$  and heme  $a_3$ ).

Electrons donated by the diffusible cytochromes  $c$  from the intermembrane space enter complex IV at the Cu<sub>A</sub> atom, transiently reduce heme  $a$ , and finally reach the Cu<sub>B</sub>/heme  $a_3$  catalytic reaction centre where molecular oxygen is consumed. During each

catalytic cycle, four  $H^+$  ions are consumed from the matrix to reduce oxygen and an additional four  $H^+$  ions are pumped across the energy conserving membrane. Thus, there is a charge separation and a proton gradient generated. Electron transfer from heme *a* to the  $Cu_B$ /heme *a*<sub>3</sub> center is generally thought to be coupled to proton transfer (34,35,40). A thorough understanding of  $H^+$  translocation by cytochrome *c* oxidase is complicated by the fact that three possible proton channels exist. The D-, K- and H- pathways are named according to conserved residues and contain ordered water molecules and polar amino acid sidechains that can facilitate proton transfer. The D-pathway begins at the intermembrane space side at a highly conserved Asp residue and leads to a conserved Glu residue ~24Å away that may serve as a branching point for protons (41-43). In fact, mutation of the conserved Glu residue in *E. coli* cytochrome oxidase cannot pump protons despite retaining significant oxidase activity (42). The K-pathway involves a conserved Lys residue, a Thr residue and the heme *a*<sub>3</sub> hydroxyl group (44,45). However, the K-pathway does not appear completely linked by hydrogen bonds and the Lys sidechain has been proposed to connect different parts of this pathway (46,47). The H-pathway partially overlaps with the D-pathway but does not lead to the conserved Glu residue or the catalytic site. This third pathway was suggested based on mutagenesis experiments in the mitochondrial cytochrome *c* oxidase and does not appear to be functionally important in the prokaryotic homologues (34,36,38,48,49).

#### **1.3.4 ATP Synthase (complex V)**

The  $F_0F_1$  ATP synthase is a highly conserved enzyme that is responsible for the majority of ATP synthesis in most organisms. The simplest ATP synthase is from *E. coli*

and it contains 8 subunits with a stoichiometry of  $\alpha_3\beta_3\gamma\delta\epsilon ab_2c_{10-14}$  and is ~530kDa in size (50,51). The  $F_0$  ( $ab_2c_{10-14}$ ) and  $F_1$  ( $\alpha_3\beta_3\gamma\delta\epsilon$ ) domains are rotary motors; the former is membrane bound and responds to the pmf while the latter is involved in ATP synthesis/hydrolysis (51-55). In the holoenzyme, the two domains are coupled so that pmf-driven rotation of the  $F_0$  domain drives rotation of the  $F_1$  domain and ATP synthesis.

X-ray crystal and NMR solution structures of portions of ATP synthase from a number of different organisms have been determined (56-65) but structure of the holoenzyme is limited to low resolution images from electron cryomicroscopy (66). A hexamer of alternating  $\alpha$  and  $\beta$  subunits comprise the catalytic domain where ATP synthesis/hydrolysis occurs at three distinct sites (67). Proton translocation down the electrochemical gradient causes the ring of  $c$  subunits to rotate (68,69). A “rotor stalk”, composed of  $\gamma\epsilon$ , connects the membrane intrinsic  $c$ -ring to the  $\alpha_3\beta_3$  subunits (61,70). The “stator stalk”, composed of  $b_2\delta$ , connects the  $a$  subunit to the  $\alpha$  subunit and remains stationary during catalysis (71,72). A number of “supernumerary” subunits are also present in more complex eukaryotic organisms and are thought to play regulatory roles (73-75).

The “binding change” mechanism of ATP synthesis was postulated by Paul Boyer (76,77) and remains true today. Essentially, the three  $\beta$  subunits can assume three different states: open, loose, or tight. In the open state, ADP and inorganic phosphate can freely enter or exit the substrate binding sites provided by the  $\beta$  subunit. A 120° rotation of the  $c$ -ring, effected by proton translocation down the electrochemical gradient, causes a conformational change and results in closure of the active site, achieving a loose state. Another 120° rotation of the  $c$ -ring causes the enzyme to adopt a tight state wherein ADP

and phosphate are covalently linked to produce ATP. A final 120° rotation of the *c*-ring causes the active site to open up and release the newly synthesized ATP molecule, and the  $\beta$  subunit cycles back to the open state once again. At any given time, each of the three different states is occupied by one of the three  $\beta$  subunits. Since there are 10-14 subunits in the *c*-ring, the cost to produce one molecule of ATP is anywhere between 3.3 to 4.6 H<sup>+</sup> translocated.

#### **1.4 Respiration in *Escherichia coli***

Aerobic respiration in prokaryotes such as *E. coli* is carried out by a simplified electron transfer chain wherein the canonical complex III and cytochrome *c* proteins are absent. Thus NADH dehydrogenases (either NuoA-N or Ndh), succinate dehydrogenase (SdhCDAB) and cytochrome oxidases (either CyoABCD or CydAB) are coupled via membrane soluble ubiquinone to carry out glycolytic aerobic respiration. In the absence of oxygen, non-fermentative energy conservation in *E. coli* may be carried out by alternative primary dehydrogenases and terminal reductases that utilize a diverse array of substrates as electron donor and acceptor (78). The constituent primary dehydrogenases and terminal reductases which make up the *E. coli* respiratory chain are depicted in Figure 1.2. Expression of each redox enzyme is governed by a complex regulatory hierarchy that ensures the largest available free energy is captured, thus resulting in the highest growth rate of the bacterium (78,79).

Oxygen availability is a major determinant of which terminal reductase is expressed. Global gene expression in aerobic and anaerobic environments is regulated by the ArcA/B (Anoxic Redox Control) two component system and the FNR (Fumarate and

Nitrate Reduction) protein. Under anaerobic conditions, ArcB acts as a sensor kinase that undergoes ATP-dependent autophosphorylation at a conserved His residue, followed by transphosphorylation of ArcA at an Asp residue (80,81). Phosphorylated ArcA activates operons involved in anaerobic metabolism and represses those involved in aerobic respiration (82-84). Under aerobic conditions, ArcB acts as a phosphatase that is specific to phosphorylated ArcA (85). The kinase activity of ArcB has been shown to depend on its dimerization via the formation of two cytoplasmic intermolecular disulfide bonds in response to the redox state of the quinone pool (86,87). Since different quinone species are expressed and utilized under reducing and oxidizing conditions, the Q-pool serves as an ideal control point to activate or repress the ArcA/B two component regulatory system.

The FNR protein of *E. coli* is a transcriptional regulator that also functions as an O<sub>2</sub> sensor *in vivo* (88-90). FNR polypeptide contains five Cys residues, four of which are essential in assembly of either a binuclear or tetranuclear [Fe-S] cluster, while the other Cys residue is non-essential and not involved in [Fe-S] ligation or protein function (91-93). In an oxygen rich environment, the FNR protein exists in the apo monomeric form where the [Fe-S] cluster is absent; upon an anoxic shift, a [4Fe-4S] cluster is assembled and FNR dimerization takes place (89,94,95). A somewhat labile [2Fe-2S] cluster has also been observed in FNR and it has been postulated that this is an intermediate form during degradation of [4Fe-4S]·FNR to apoFNR upon oxygen exposure (96,97). The active dimeric form of FNR interacts with a 22 base pair motif of inverted DNA sequence, located approximately 30-40 base pairs upstream of the transcriptional start site, to modulate gene expression (98,99). It is believed that binding of one FNR



homodimer at the promoter region upregulates gene expression while binding of tandem FNR dimers to the DNA represses transcription (100,101). In a genome-wide expression study for *E. coli* strain MG1655, Blattner *et al.* found that 184 operons encompassing 465 genes were either activated or repressed in a FNR-dependent manner when the bacterium was grown anaerobically (102). In particular, the *dmsABC* operon was positively regulated by FNR whereas repression of the *sdhCDAB* operon under anaerobic conditions was partially dependent on FNR (102-104).

An additional level of control imposed on the expression of oxidoreductases in *E. coli* is carried out by the NarX/L and NarQ/P two component regulatory systems. Similar to the ArcB/A system, NarX and NarQ are membrane bound protein kinases/phosphatases whereas NarL and NarP are cytoplasmic response regulators that can interact with DNA (105). NarX and NarQ are capable of activating a phosphorelay that includes autophosphorylation as well as transphosphorylation of NarL and NarP (106-108). The initial  $P_i$  substrate is donated directly by ATP. In a study carried out by Stewart and coworkers, it was found that the protein phosphatase activities of NarX and NarQ are 600 and 60-fold higher than their respective kinase activities, indicating a bias towards NarL and NarP inactivation. (109). The intricate interplay between the NarX/L and NarQ/P two component systems allows the bacterium to utilize the appropriate terminal electron acceptor that yields the highest free energy for pmf generation. In the presence of nitrate and nitrite, the response regulators NarL and NarP are phosphorylated and are able to activate genes involved in nitrate and nitrite metabolism as well as repress those involved in “secondary” anaerobic respiration and fermentation. Gene products such as NarGHI and NrfABCD are upregulated but operons such as *dmsABC* and

*frdABCD* are repressed (110-112). The expression of terminal reductases thus obeys a bioenergetic hierarchy since nitrate reductase is an electrogenic enzyme whereas dimethyl sulfoxide reductase and fumarate reductase are electroneutral (78).

### 1.5 Common Prosthetic Groups of Respiratory Enzymes

Substrate chemistry and electron transfer in respiratory chain enzymes are heavily reliant on cofactors assembled in these complexes, and removal of one or more of these redox centers in the protein often results in loss of function. Redox cofactors can undergo either a one or two electron oxidation/reduction reaction, and are present in many forms from a simple Cu atom or nickel-metal center to the more complex Mo-bisMGD or FAD molecules.

[Fe-S] clusters, consisting of iron and sulfur atoms at different stoichiometries, are commonly assembled as [2Fe-2S], [3Fe-4S], [4Fe-4S] or [8Fe-7S] clusters depending on the amino acid sequence of the protein scaffold. [Fe-S] clusters are generally coordinated by Cys residues in a non-covalent manner, although the side chains of Asp, His, or Ser, as well as backbone amides, can also serve as ligands (113). To date, three [Fe-S] cluster biosynthetic pathways have been identified: the *Isc* (iron sulfur cluster) system, the *Suf* (sulfur formation) system, and the *Nif* (nitrogen fixation) system. Generally, the *Isc* system is used for “housekeeping” cluster assembly, the *Suf* system is utilized under stress conditions (ie. oxidative stress) and the *Nif* system is used to assemble specialized clusters for specific enzymes (114). The first step in [Fe-S] cluster assembly is catalyzed by a cysteine desulfurase (*NifS*, *IscS* and *SufS*) and involves a reaction between L-cysteine and a pyridoxal phosphate cofactor in the enzyme that

results in a cysteinyl persulfide formation and alanine release (115). In addition to [Fe-S] cluster formation, cysteine desulfurases are also involved in the biosynthesis of other sulfur-containing compounds such as molybdopterin (116,117). The next step in [Fe-S] cluster biosynthesis involves scaffold proteins (IscU, IscA, NifU, SufU, SufA) which provide an intermediate assembly site for the [Fe-S] clusters or their precursors (118-122). The precise mechanism of how [2Fe-2S] and [4Fe-4S] clusters are built on these scaffold proteins remains unknown. Finally, the last step of [Fe-S] cluster biosynthesis involves a transfer of the assembled cluster from the scaffold protein to the target apoprotein. Other accessory proteins have also been identified to be crucial for [Fe-S] cluster assembly into respiratory chain enzymes. For instance, the Ssq1 and Jac1 proteins in *Saccharomyces cerevisiae* have been shown to interact with IscU and deletion of the *ssq1* or *jac1* gene results in decreased enzymatic activities of [Fe-S] proteins (123,124). In an independent study, the yeast Yah1 ferredoxin protein has also been shown to be involved in maturation of [Fe-S] proteins in the mitochondrion and in the cytosol (125). Frataxin, and the bacterial homologue CyaY, were found to be responsible for iron recruitment and delivery to IscU, leading to formation of a [2Fe-2S] cluster (126,127).

Aside from [Fe-S] clusters, iron can also be incorporated into respiratory chain enzymes as part of protoporphyrin rings to form heme molecules. The porphyrins, which include heme, chlorophyll and bacteriochlorophyll, belong to the class of cyclic tetrapyrrole macromolecules that are identified by a saturated ring system (128). In hemes, the nitrogen atoms of the four pyrrole rings provide four of six possible coordination points to the central iron atom. The common precursor to all tetrapyrroles is 5-aminolevulinic acid (ALA). Protoporphyrin synthesis from ALA involves a series of

enzymatic reactions catalyzed by porphobilinogen synthase, porphobilinogen deaminase, uroporphyrinogen III synthase, uroporphyrinogen decarboxylase, coproporphyrinogen III oxidase and protoporphyrinogen IV oxidase. The final step of heme biosynthesis is insertion of the Fe atom into the protoporphyrin ring by ferrochelatase. Modification of the porphyrin ring, as well as different attachments of the heme to the protein, gives different forms of heme (heme *a*, *b*, *c*, *d*, *l*, *m*, *o* or *s*). Proteins which contain at least one heme molecule are commonly known as cytochromes. The heme oxygenase enzyme is responsible for breaking down free heme, which releases carbon monoxide, biliverdin and iron (129). In respiratory enzymes such as the cytochrome oxidases and the *bc*<sub>1</sub> complex, assembly of the heme is absolutely essential for enzyme function. In the *E. coli* succinate dehydrogenase, the heme molecule is not required for electron transfer or quinone reduction (130), but has been proposed to act as an electron sink to minimize ROS generation (131). Aside from the respiratory chain, heme also plays a major role in other cellular processes including transcriptional regulation, transport of soluble gases (eg. hemoglobin and myoglobin) and catalysis of chemical reactions (catalases and peroxidases)(132-134).

Iron sulfur clusters and heme are transient one electron carriers that are common in respiratory enzymes. FAD and FMN are cofactors that can undergo two electron oxidation-reduction reactions. Covalent attachment of flavins to proteins was first noted in the Sdh enzyme by Singer and coworkers (135,136), but the FAD cofactor can also be housed non-covalently by the flavoprotein (137,138). However, the reduction potential of the covalent flavin is approximately 100-150mV higher than that of the non-covalent flavin (139). Flavin linkage can either occur at the 8 $\alpha$ -methyl group to a Tyr, His or Cys

residue, or via the C6 atom of the isoalloxazine ring to a Cys residue (140). Unlike the covalent attachment of hemes *c* to cytochromes by heme lyases, protein flavinylation appears to be an enzyme-free process. In the *S. cerevisiae* Sdh enzyme, formation of the  $8\alpha$ -*N*<sup>3</sup>-histidyl-FAD linkage requires correct targeting and folding of the Sdh subunit; covalent flavin attachment occurs after cleavage of the signal sequence and upon exposure to citric acid cycle intermediates (141-143). A common catalytic mechanism involving flavins is the reversible transfer of hydride with a nearby substrate (144-147).

## 1.6 Assembly and Targeting of Respiratory Enzymes

The biogenesis of respiratory enzymes is a complicated multi-step process that often involves synthesis of multiple polypeptides and their assembly, the incorporation of cofactors into the different subunits, as well as targeting and localization of the final product to either the bacterial cytoplasmic membrane or periplasm. All these conditions must be satisfied before the redox enzymes can carry out cellular respiration. As mentioned beforehand, specific proteins are required for heme and [Fe-S] cluster biosynthesis. In addition to these, protein-specific chaperones are often present to assist proper protein folding and insertion of the cofactors. For instance, the NarJ chaperone is specific for the NarGHI protein and the two are in fact co-expressed by induction of the *narGHJI* operon (148). The chaperone interacts with aponitrate reductase at two distinct sites (149). The first site coordinates the interaction between apoNarGH with the Mo-bisMGD biosynthetic machinery such that this enormous cofactor can be inserted into NarG (150). A second site of interaction between NarJ and apoNarGH takes place at the first 40 amino acids of NarG, and it is believed that this transient interaction prevents

membrane anchoring of the apoenzyme and maintains it in a soluble form that remains competent for cofactor insertion (149,151). Like NarJ, DmsD is a protein-specific chaperone that interacts with DmsABC (Chapter 2). In *E. coli*, assembly of succinate dehydrogenase does not appear to require a specific chaperone; in *S. cerevisiae* however, the mitochondrial protein Tcm62p is absolutely essential for Sdh assembly (152).

Membrane bound respiratory chain enzymes in *E. coli* are targeted to and inserted into the inner membrane by two major mechanisms. In the general secretory (Sec) pathway, nascent polypeptides are transported to the target destination before folding and assembly into the holoenzyme. The alternative twin arginine translocation (Tat or Mtt) pathway is used to transport folded proteins from the cytoplasm to the periplasm. Nascent peptides destined to be exported or inserted into the inner membrane typically contain a hydrophobic signal sequence that is recognized by either the signal recognition particle (SRP) or SecB. Binding of the SRP to the emerging peptide from the ribosome prevents further mRNA translation until the complex is targeted to the Sec translocon such that the peptide is inserted/translocated in a cotranslational manner. In contrast, the pathway involving the SecB chaperone is either late-cotranslational or posttranslational. The first high resolution structure of the conserved heterotrimeric translocon is that from *Methanococcus jannaschii* (153). Although crystallized as a monomer, the Sec translocon can come together to form higher oligomeric states (154,155). The structure of SecYEG is that of a closed channel wherein a short helix acts as a plug against a 20Å-wide cavity for peptide entry on the cytoplasmic side. The structure also has an overall 2-fold symmetry and the two halves are clamped together by the  $\gamma$ -subunit (SecE); separation of transmembrane helices 2/3 from 7/8 would then allow peptides to be laterally released

into the membrane bilayer (153). The core of the SecYEG complex also contains residues which are involved in recognition of the signal sequence, which is ultimately cleaved off by signal peptidase sometime during the translocation/insertion process. Energy needed to catalyze translocation of polypeptides is provided by the pmf as well as the ATPase activity of SecA, which has been shown to interact with the Sec translocon in the monomeric and dimeric states (156). In eukaryotes, a conserved system called the Sec61p complex plays a parallel role in the endoplasmic reticulum (157), while import of polypeptides into the mitochondrion is assisted by the TIM and TOM complexes. Other accessory or interacting proteins to the Sec translocon in *E. coli* include Ffh, FtsY, SecD, DecF, YajC and YidC; the role of the last protein is enigmatic in that it is essential for *E. coli* viability and is somehow involved in the biogenesis of inner membrane proteins in a Sec-dependent or Sec-independent manner (158).

The Tat machinery differs from the Sec pathway in that fully folded proteins are its substrates rather than nascent peptides. It is present in many bacteria, archaeobacteria and plants, but is absent in the vast majority of eukaryotic organisms including humans. In bacteria, the Tat pathway is required for numerous functions including biogenesis of respiratory chain enzymes, quorum sensing and motility, cell division, symbiosis and pathogenesis (159,160). Proteins that are to be secreted via the Tat pathway are labeled with a SRRXFLK “twin arginine” motif at the N-terminus (161) that is recognized by the TatBC complex (162). Interaction of TatBC with the signal sequence is dependent on the pmf (163), and it is thought that this event triggers a conformational change that exposes a TatA binding site on TatBC to complete the assembly of the TatABC translocase (164). It is unclear what the oligomeric state of TatA is (165), and it may be that TatA rings of

different sizes are formed to accommodate folded proteins of different dimensions. One enzyme of study in this thesis, DmsABC, uses the Tat transport machinery to reach the periplasm.



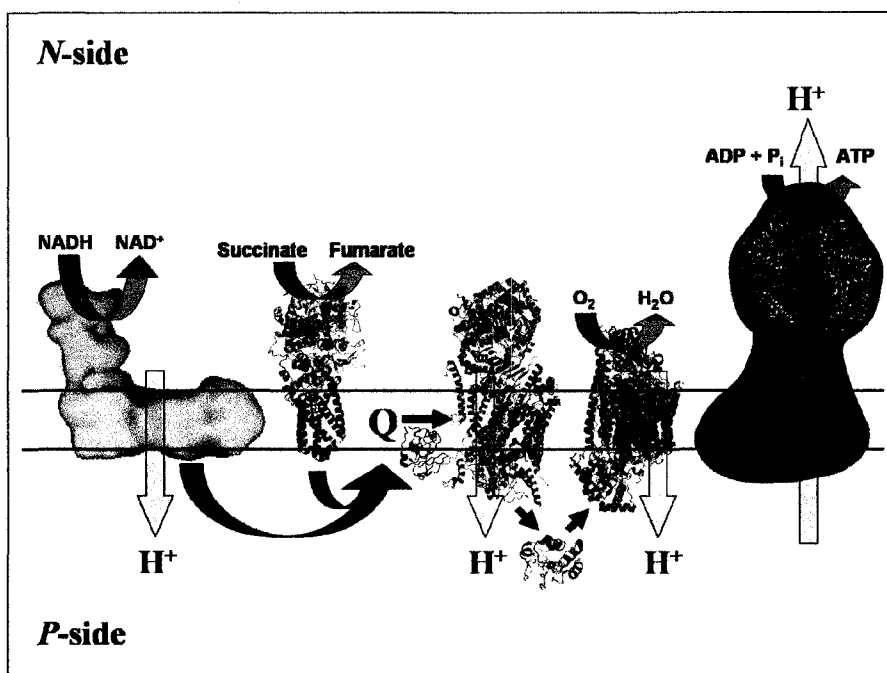


Figure 1.1. Overview of the canonical aerobic respiratory chain. Complexes I-V are membrane-bound and are sequentially arranged from left to right, while cytochrome *c* is shown as the lone soluble protein. The *P*-side is equivalent to the intermembrane space in mitochondria or the periplasmic space in bacteria such as *E. coli*. The *N*-side represents the mitochondrial matrix or bacterial cytoplasm. Electrons are donated into the electron transfer chain from NADH or succinate at complex I or II respectively, passed to complex III via the membrane soluble quinone pool, and passed to complex IV via cytochrome *c* where molecular oxygen is reduced to form water. In *E. coli*, complex III and cytochrome *c* are absent. Complexes I, III and IV are electrogenic and contribute to the proton motive force. Complex V, ATP synthase, can harness the transmembrane electrochemical potential to synthesize ATP. Pictures of complexes II (1NEK), III (1LON), IV (2EIJ) and cytochrome *c* (2B4Z) were prepared using PyMOL v.0.99. Electron microscopic structures of complex I and V were adapted from (11) and (66) respectively.

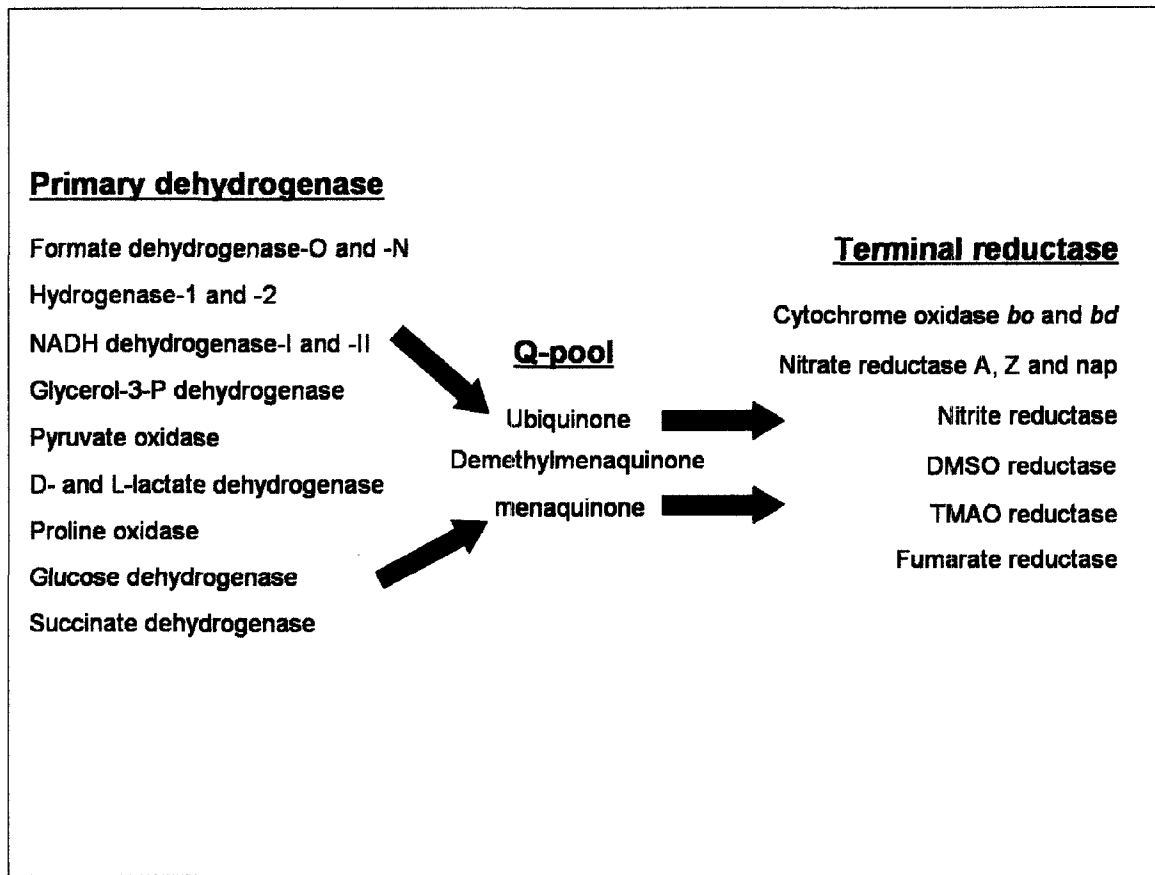


Figure 1.2. Variation in the *E. coli* Respiratory Chain. Depending on environmental conditions and substrate availability, the bacterium can express a range of primary dehydrogenases and terminal reductases to maximize proton motive force generation. The two enzymes in the respiratory chain are connected by the membrane soluble quinone pool.

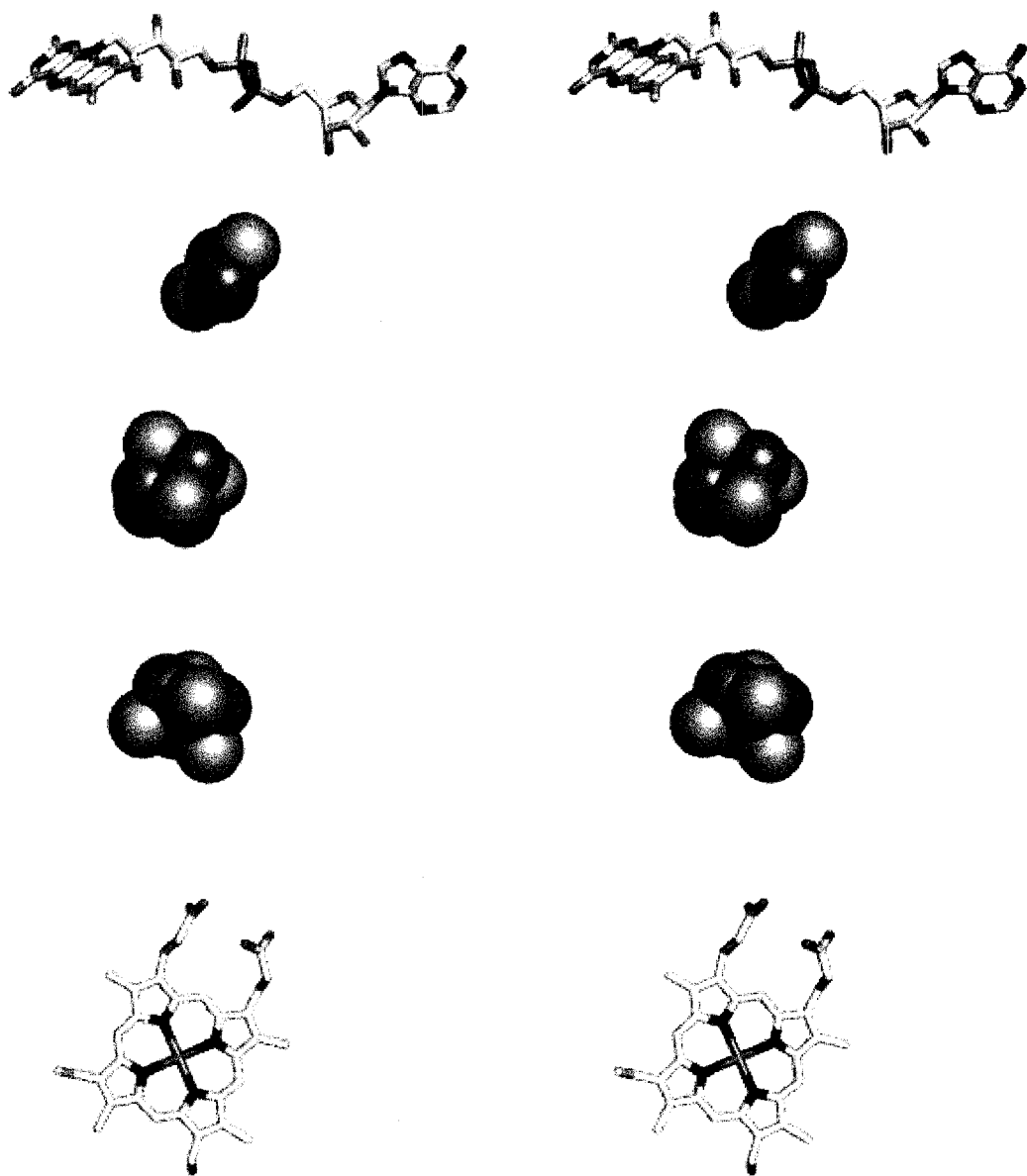


Figure 1.3. Stereo view of common prosthetic group in respiratory chain enzymes. Top to bottom: flavin adenine dinucleotide, [2Fe-2S] cluster, [4Fe-4S] cluster, [3Fe-4S] cluster, heme *b*. Atoms are colored as follows: C, white; O, red; N, blue; Fe, brown; S, yellow; P, orange. The iron-sulfur clusters are shown in a “sphere” representation whereas the flavin adenine dinucleotide and heme *b* are shown as “sticks”.

# Chapter 2

## *S*- and *N*-oxide Reductases

**A version of this chapter was published:**

**Cheng, VWT and Weiner JH. 31 August 2007, posting date. Chapter 3.2.8, *S*- and *N*-Oxide Reductases. In A. Böck, R. Curtiss III, J. B. Kaper, F. C. Neidhardt, T. Nyström, J. M. Slauch, and C. L. Squires (ed.), *EcoSal—Escherichia coli* and *Salmonella*: cellular and molecular biology. <http://www.ecosal.org>. ASM Press, Washington, D.C.**

## 2.1 Organization of the DMSO and TMAO Respiratory Chains

The dimethyl sulfoxide (DMSO) and trimethylamine *N*-oxide (TMAO) respiratory chains consist of a primary dehydrogenase and a terminal reductase which are functionally linked through menaquinone-8 (MQ) and demethylmenaquinone-8 (DMQ) (166). At least 15 primary dehydrogenases have been identified in *E. coli* (78) and while most of these enzymes will support anaerobic growth with DMSO or TMAO as the terminal oxidant, growth is normally observed with glycerol-3-phosphate or L-lactate as reductant. Formate and hydrogen can also be used if appropriate carbon sources (*i.e.* amino acids) are available (79). The respiratory chains terminating with either reductase, but not the terminal reductases themselves, generate the essential pmf across the cytoplasmic membrane (167). Terminal reductases which lack pmf capacity generally have their proton-consuming active site facing the periplasm and this is the case for TMAO reductase and possibly for DMSO reductase (Figure 2.1). Respiratory chain enzymes which do not generate a pmf directly are “electron sinks” whose sole function is to re-oxidize the Q-pool such that upstream dehydrogenases can continue to function and generate a transmembrane electrochemical gradient (167).

While the dehydrogenase and menaquinone are common to both electron transfer chains, the architectural organization of the terminal reductases differs (Figure 2.1). TMAO reductase is a soluble periplasmic molybdoprotein (TorA) which receives electrons via a transient interaction with a pentaheme *c*-type cytochrome (TorC) tethered to the membrane. TorC receives electrons directly from the MQ/DMQ pool (166). DMSO reductase is a trimeric, complex iron-sulfur molybdoenzyme in which a membrane anchor subunit (DmsC) communicates with the MQ/DMQ pool and funnels electrons

through a polyferredoxin electron transfer subunit (DmsB) to the catalytic site in DmsA. Both TMAO reductase and DMSO reductase have a molybdo-bis(molybdopterin guanine dinucleotide) (Mo-bisMGD) molecule at their active centers.

## **2.2 Dimethyl Sulfoxide Reductase**

### **2.2.1 Overview**

The ability to reduce DMSO to dimethyl sulfide (DMS) (Figure 2.2), a major intermediate in the global sulfur cycle, is widespread in both prokaryotes and eukaryotes (168,169). It is believed that DMS generated by degradation of dimethylsulfoniopropionate or by reduction of DMSO accounts for 50% of the biologically synthesized reduced sulfur in the environment and plays an important role in global climate control (170,171).

In the presence of hydrogen, formate or glycerol-3-phosphate as electron donor and DMSO as electron acceptor, and the absence of oxygen and nitrate, the enzyme DMSO reductase (DmsABC) is expressed to allow *E. coli* to respire anaerobically. The *E. coli* DMSO reductase is a heterotrimeric protein comprising a molybdopterin-containing catalytic subunit (DmsA), a ferredoxin-like electron transfer subunit (DmsB) and a membrane anchor subunit (DmsC) that interacts with the MQH<sub>2</sub>/MQ pool (Figure 2.1). Its enzymatic function involves the oxidation of MQH<sub>2</sub> to MQ, the transfer of two electrons from the membrane domain to the molybdenum active site, and the reduction of DMSO to DMS.

### **2.2.2 The *dms* Operon**

There are three open reading frames in the DMSO reductase operon located at 940 kbp (20 minutes) on the *E. coli* chromosome (Figure 2.3). They encode polypeptides with  $M_r$  values of 90.4/85.8 kDa, 23.1 kDa and 30.8 kDa, (DmsA preprotein/mature, B and C, respectively). Organization of the operon closely parallels that seen for fumarate reductase and formate dehydrogenase of *E. coli*. The 5' proximal gene encodes the molybdenum cofactor containing catalytic subunit followed by an electron transfer subunit which contains groups of cysteine residues for assembly of [4Fe-4S] clusters. The 3' distal gene encodes the membrane anchor and menaquinol binding subunit DmsC.

Transcription of the operon is dependent on the oxygenation state of the cell and the availability of nitrate and molybdenum but not *S*- or *N*-oxides. The transcriptional start site is under the control of two promoters, P1 and P2; both have A/T rich segments at the -35 and -10 positions (172) (Figure 2.4). Under anaerobic conditions, the global anaerobic transcription factor FNR binds to the sequence TTGATnnnnAACAA (FNR consensus is normally TTGATnnnnATCAA) located 48bp upstream of P1 to initiate transcription. (111,173) Transcription of the *dmsABC* operon is also under the regulation of the two component NarXL system. In the presence of nitrate, NarL is phosphorylated and binds to the P1 region such that FNR and RNA polymerase are unable to bind (111,112,173). The dominant repressive role of phosphorylated NarL over FNR ensures that nitrate is metabolized before DMSO to maximize pmf generation. A third level of control is provided by the ModE protein, which is required for both FNR activation and NarL repression of the *dmsABC* operon (111,172). The ModE protein also regulates the *modABCD* and *moaABCDE* operons in response to the presence of molybdate (174-176).

Interestingly, DmsABC expression is not dependent on substrate availability of DMSO or TMAO (111).

### 2.2.3 DmsA – The Catalytic Subunit

DmsA is the 85.8 kDa catalytic subunit that binds the Mo-bisMGD cofactor and is the site for DMSO reduction (177) (Figure 2.5). Exclusive supplementation with W (tungsten) in lieu of Mo during growth in minimal media renders the enzyme inactive and abolishes insertion of the metal-cofactor complex into DmsA despite proper targeting and assembly of DmsABC; however, overexpression of the enzyme or addition of both W and Mo to the minimal medium can rescue anaerobic growth on DMSO since small amounts of Mo can be salvaged and incorporated into approximately 10% of the DmsABC assembled (177). It is very likely that a high spin [4Fe-4S] cluster is coordinated by the conserved Cys residues at positions 18, 22, 26 and 59 of mature DmsA (see below) (*Note: residue numbers used herein often differ from the numbers in earlier publications as the existence of the tat leader was not known prior to 2000*). This cluster would communicate between the [4Fe-4S] clusters in DmsB and the Mo-bisMGD and would parallel the recent discoveries of a spectroscopically elusive [4Fe-4S] cluster in nitrate reductase and formate dehydrogenase (178-180).

The Mo-bisMGD cofactor in both TorA and DmsA (Figure 2.5) is a tricyclic ring system comprising a pterin group with a fused pyran ring that is attached via a phosphodiester linkage to a guanine nucleotide (181-184). The pyran ring of the pterin has two sulfur atoms attached in a dithiolene linkage. This cis-dithiolene provides bidentate coordination to the essential Mo atom at the active site of TMAO or DMSO



reduction. The dithiolene sulfurs of the two pterins provide a total of four sulfur ligands to the active site Mo. Further coordination of the Mo atom is provided by the hydroxyl sidechain of an amino acid and by an additional oxo group. Stable derivatives of the molybdopterin can be isolated, quantified and characterized by acid hydrolysis of the protein preparation followed by controlled oxidation of the cofactor (185). The transition metals Mo and W are found associated with molybdopterin. W catalyzes reactions of very low potential ( $<-420\text{mV}$ ) (186) whereas Mo catalyzes reactions of high redox potential (generally  $>0\text{mV}$ ). Molybdenum containing enzymes have been divided into three subfamilies based on the structure of the molybdenum center at the active site (187): the xanthine oxidase family, the sulfite oxidase family and the DMSO reductase family.

Although a three-dimensional structure of *E. coli* DmsA (EcDmsA) has not yet been determined, it has significant sequence similarity with the soluble, periplasmic DmsA of *Rhodobacter sphaeroides* and *Rh. capsulatus* (RhDmsA), both of which have been crystallized and their 3-dimensional structures elucidated (182,183,188,189). The RhDmsA protein possesses four distinct domains (Figure 2.6). Like EcDmsA, RhDmsA contains a Mo-bisMGD cofactor at the active site (see below). Domain IV forms a complex H-bonding network with the two pterin groups while domains II and III interact with the guanine nucleotides of the P-MGD (proximal to the active site) and Q-MGD (distal to the active site) molecules, respectively (182,183,188) (Figure 2.6). The substrate cavity/funnel leading to the active Mo atom is encircled by domains I, II and III to form a channel that is approximately  $10\text{\AA}$  wide and  $8\text{\AA}$  deep (Figure 2.7). Additionally, a conserved loop of polypeptide serves as a lid during the reaction cycle to

trap the substrate DMSO in the binding pocket. Domain IV sits at the “bottom” of the RhDmsA subunit and is where the [Fe-S] cluster in EcDmsA is predicted to be located and also the contact point with DmsB.

DmsA belongs in the DMSO reductase superfamily of molybdoenzymes which can be distinguished by the presence of two pyranopterin molecules per Mo atom and the covalent attachment of a GMP molecule to each pyranopterin via a phosphate bond (187,190,191). The coordination of the Mo atom in RhDmsA was somewhat controversial as the available crystal structures showed between 5 to 7 ligands interacting with the Mo (182,183,188,189). Early EXAFS (Extended X-Ray Absorption Fine Structure) studies on the *Rh. sphaeroides* (192,193) and the *Rh. capsulatus* (194) DMSO reductases also indicated differences between hexa- and heptacoordination, respectively. Currently, there is general consensus that the Mo is hexacoordinated with four ligands being provided by the dithiolenes of the bisMGD moieties, one provided by the hydroxymethyl sidechain of Ser147 and the last one provided by DMSO (195) (Figure 2.8). This organization is also observed in the TMAO reductase enzyme (184) and these enzymes have been classified as the Type III enzymes of the DMSO superfamily. This contrasts with other molybdoenzymes with Cys/SeCys or Asp sidechains as a Mo ligand in the Type I and Type II clades, respectively (187). In a recent EXAFS study by George *et al* (196) (Figure 2.8) of the active site of oxidized EcDmsA it was found that mono-oxo Mo<sup>VI</sup> species was coordinated by two molybdopterin dithiolenes and a serine with four Mo—S ligands at 2.43Å, one Mo=O at 1.71Å, and a longer Mo—O at 1.90Å. The coordination of Mo in EcDmsA is very similar to that in RhDmsA, suggesting similar active site structures for the two enzymes.

The apparent multiple coordination states of Mo coordination is believed to stem from movement of the Ser147 sidechain and the Mo atom as it cycles between the Mo(IV), Mo(V) and Mo(VI) states during catalysis (195). With reduction of DMSO and formation of the Mo-oxo intermediate, a Trp residue is responsible for H-bonding and stabilization of the oxo group (189). Residue Tyr114 has also been observed to interact with one of the oxo groups in the dioxo pentacoordinated structure in which the dithiolenes of the Q-pterin do not serve as ligands (183). It has been proposed that the heptacoordinated structure is the result of the superimposition of the penta and hexacoordinated states (188). The hexacoordinated mono-oxo form is believed to be correct as it is supported by EXAFS experiments (192,193) as well as Raman spectroscopy (197,198). The pentacoordinate state is thought to be a “damaged” state of the enzyme (199) whereby the dithiolene ligands of the Q-pyranopterin are lost.

From studies on the *Rh. capsulatus* and *Rh. sphaeroides* DMSO reductases it appears that the active site undergoes complex structural transformations. The molybdenum site exists in multiple structural states and rearrangement of atoms/groups at the active site is facilitated in the Mo(V) state. Johnson *et al* (200) have suggested a catalytic cycle for RhDmsA which likely is similar for the EcDmsABC (Figure 2.9).

Mutagenesis studies on Tyr114 and Trp116 have provided insights into the catalytic mechanism of DMSO reduction and oxo group transfer to the Mo atom. First, it is important to note that the equivalent residue to Tyr114 is missing in TMAO reductase (184). Second, a Tyr114→Phe mutation in the *Rh. capsulatus* enzyme causes the  $K_m$  to increase and the  $k_{cat}/K_m$  ratio to decrease for both DMSO and TMAO substrates (201). Third, insertion of an equivalent Tyr into the active site of TorA leads to an increased

preference for utilizing DMSO over TMAO (200). Together, these experiments indicate the crucial role of Tyr114 to be breakage of the S-O bond during catalysis. Residue Trp116 has also been shown to play a crucial role. Site directed mutagenesis of Trp116→Phe in the *Rh. capsulatus* enzyme results in alterations of its UV-Vis absorption spectrum that become reminiscent of the protein in the “damaged” pentacoordinated state (199,202). Furthermore,  $k_{\text{cat}}$  values were decreased with respect to both DMSO and TMAO whereas  $K_{\text{m}}$  values were only moderately affected, suggesting that Trp116 plays more of a role in the catalytic cycle rather than substrate binding (202). In addition, the Trp116→Phe mutant also renders the Mo<sup>V/IV</sup> transition pH dependent compared to a pH independent oxidation exhibited by the wild-type enzyme. The data presented by Ridge *et al.* suggest that Trp116 plays a stabilization role in which it H-bonds to the Mo-oxo group to maintain the active site in a hexacoordinate state and prevent conversion to the inactive pentacoordinate Mo form (202). Importantly, these residues are not conserved in EcDmsA suggesting that other nearby residues fulfill the roles. Further research will be needed to elucidate the mechanism of EcDmsA.

In addition to its ability to reduce DMSO to DMS, the *E. coli* DMSO reductase can also reduce a variety of other *S*- and *N*-oxides (203). The promiscuity of the oxidant is believed to stem from the wide active site funnel leading from the aqueous milieu into the active site (204). Although the structure of *E. coli* DmsA is unavailable, results from mutagenesis studies on conserved residues in DmsA inspired by the RhDmsA X-ray crystallographic structure agree with this hypothesis. An extensive study by Simala-Grant and Weiner (203) showed that the major determinant of substrate reducibility lies in its compatibility with the substrate pocket as  $K_{\text{m}}$  values showed 20-fold larger variance than

$k_{\text{cat}}$  values over a range of 22 substrates;  $K_m$  values for sulfoxides and pyridine *N*-oxide were lowest, followed by aliphatic *N*-oxides. Mutational analyses suggest Thr132, Gly151, Ala162, Gln163 and Arg201 to be part of the active site funnel and are required for substrate binding and/or enzyme catalysis. In particular, large changes in the  $K_m$  value were observed in the Thr132Ser, Ala162Gln and Arg201Gln mutants when DMSO was used as an electron acceptor; interestingly, the Thr132Ser mutant did not exhibit a similar change in  $K_m$  value when pyridine *N*-oxide was used as the substrate. Finally, it is interesting to note that the *Rhodobacter* DMSO reductases selectively reduce the S-enantiomer of the sulfoxides whereas the *E. coli* DMSO reductase is selective for the R-enantiomer (205,206).

The midpoint potentials for the  $\text{Mo}^{\text{VI/V}}$  and  $\text{Mo}^{\text{V/IV}}$  transitions have been determined by potentiometric titration and EPR spectroscopy to be -15mV and -175mV, respectively (207). Protein film voltammetry studies on DmsABC have shown that the enzyme activity is maximal within a narrow window of electrode potential that coincides with the appearance of the Mo(V) species (208). In fact, two switches at critical potentials were seen to control two one-electron processes separating three distinct states of the enzyme. Based on the elaborate series of protein film voltammetry studies, it was proposed that the most influential step during catalysis is the reduction of Mo(V) to  $\text{Mo(IV)-H}^+$  (208). This characteristic of DmsABC is called “tunnel diode” behavior.

Available X-ray crystal structures of *E. coli* anaerobic complex molybdoenzymes — namely formate dehydrogenase-H, formate dehydrogenase-N and nitrate reductase — show the assembly of a [4Fe-4S] cluster in the catalytic subunit (178,180,209). This cluster has not been observed by biophysical techniques such as electron paramagnetic

resonance spectroscopy, possibly due to peptide flexibility and heterogeneity-induced spectral broadening. Mutational studies have shown that the cysteine group in DmsA can act as ligand to a [3Fe-4S] cluster in a Cys22Ser mutant (207,210). This particular mutation may act in a similar manner to the DmsB-Cys102Ser mutant (see below), where the -50mV [4Fe-4S] cluster is converted into a [3Fe-4S] cluster and electron transfer through this cluster is compromised (211,212). In fact, mutation of Cys22 to Ser or Ala abolishes growth on DMSO and cuts the enzyme activity by 50% (207). EPR studies show alterations to the interaction between the reduced -120mV cluster of DmsB and the Mo(V) atom in the Cys22Ser mutant suggesting that the engineered [3Fe-4S] cluster is in the path for electron tunneling from DmsB to DmsA (210). It is also plausible that the -120mV signal corresponds to the FS0 species and is only observed through its interaction with the Mo. In a DmsA-Arg61Ser mutant, this interaction is abolished, suggesting this residue to be directly on the path of electron flow and its mutation prevents reduction of the Mo atom (210).

#### **2.2.4 DmsB – The Electron Transfer Subunit**

DmsB is an electron relay subunit bridging the Mo-bisMGD active site and the Q-site, and is highly homologous to FdnH and NarH, the respective electron transfer subunits of formate dehydrogenase-N and nitrate reductase. The electron transfer subunits of DMSO reductase and formate dehydrogenase each contain four [4Fe-4S] clusters (180,213), differing from the composition of NarH which contains three [4Fe-4S] clusters and one [3Fe-4S] cluster (214,215). The DmsB primary sequence contains sixteen cysteine residues that serve as ligands to the four [4Fe-4S] clusters. The

consensus sequences for assembly of [Fe-S] clusters in DmsB resemble those in typical bacterial ferredoxins and appear four times as a C-X<sub>2</sub>-C-X<sub>n</sub>-C-X<sub>n</sub>-C motif, where the first three cysteines serve as ligands to one [4Fe-4S] cluster and the terminal cysteine interacts with a different [4Fe-4S] cluster (Figure 2.10). The four [Fe-S] clusters of DmsB are arranged in an almost linear fashion that facilitates rapid electron transfer between the Mo active site and the Q-site, and are called FS1 (closest to catalytic subunit), FS2, FS3, and FS4 (closest to the Q-site).

The four [4Fe-4S] clusters in DmsB have midpoint potentials ( $E_m$  values) of -50mV (FS4), -120mV (FS3), -330mV (FS2), and -240mV (FS1) (212,213). The relatively negative potentials of FS1 and FS2 compared to the  $E_m$  for the MQH<sub>2</sub>/MQ and DMSO/DMS couples (-100mV and +160mV, respectively) led to a debate about whether these clusters participated in the electron transfer relay or served a structural role. Elucidation of the X-ray crystallographic structures of FrdB (216), NarH (178), SdhB (131) and most importantly FdnH (180), clearly shows that all [Fe-S] clusters are involved in the electron relay. The very negative clusters may provide a barrier for electron flow, slowing the rate of electron transfer and providing better coupling between MQH<sub>2</sub> oxidation and DMSO reduction.

Comparison of the cysteine motifs in DmsB and NarH shows that DmsB-Cys102 coordinating FS4 is a Trp residue in nitrate reductase, and the [Fe-S] cluster is assembled as a [3Fe-4S] cluster in NarH as opposed to the [4Fe-4S] cluster in DmsB. Replacement of Cys102 with Ser, Tyr, Trp or Phe by site-directed mutagenesis allows conversion of FS4 from a [4Fe-4S] cluster to a [3Fe-4S] cluster with a concomitant increase in its midpoint potential from -50mV to +275mV (211). EPR studies on FS4 of the Cys102

mutants show that this cluster is magnetically and conformationally-linked to the MQH<sub>2</sub> binding site (212). Traditional enzymatic assays and growth experiments demonstrate that the DmsB-Cys102Ser mutation renders the enzyme inactive as a DMSO reductase, but Q-pool coupling assays show the mutant enzyme to remain functional in the reverse direction to donate electrons to the MQ (212). How the protein modulates the biophysical properties of FS4 and how residues in the DmsB subunit affect MQH<sub>2</sub> binding and oxidation is one area of study in this thesis and is presented in Chapter 3.

### **2.2.5 DmsC – The Membrane Anchor Subunit**

DmsC is the 30.8 kDa membrane anchor subunit that tethers DmsAB to the cytoplasmic membrane. It is known that only the full-length DmsC can interact with DmsAB as truncated DmsC leads to accumulation of the soluble catalytic dimer in the cytoplasm (217). Hydropathy plots, such as those using the Kyte-Doolittle algorithm (218), of DmsC predict a subunit with eight distinct transmembrane  $\alpha$ -helices. Application of the “positive-inside” rule by von Heijne (219) suggests that both the N- and C-terminal ends of DmsC are located on the periplasmic side of the membrane with three Arg+Lys residues on the periplasmic side and eight on the cytoplasmic side. Fusion experiments using alkaline phosphatase and  $\beta$ -lactamase (217) have confirmed this proposed arrangement of DmsC and is shown in Figure 2.11. The subunit has three relatively large periplasmic loops, P1-P3, and four small cytoplasmic loops C1-C4. Comparative analyses and site-directed mutagenesis studies of conserved residues also reaffirms the proposed topological arrangement of DmsC (220).



The DmsC subunit plays an integral role in the binding of MQH<sub>2</sub> and its oxidation to MQ. Steady state and rapid reaction fluorescence quench titrations of DmsABC with the MQH<sub>2</sub> analogue 2-*n*-heptyl-4-hydroxyquinoline-*N*-oxide (HOQNO) indicate the presence of a single high affinity quinol binding site with a dissociation constant of 5nM (221). This differs from other anaerobic terminal oxidoreductases in *E. coli* such as fumarate reductase (222-225) and nitrate reductase (226) which have been proposed to contain more than one Q-site and can receive reducing power from both ubiquinol and menaquinol. Although structural information for fumarate reductase indicates the presence of both proximal and distal menaquinol binding sites, only the proximal menaquinol binding site is within electron transferring distance to the iron-sulfur clusters (227) and the role of the distal site remains to be determined. The crystal structure of nitrate reductase indicates that there are two clefts where quinol can bind. However, binding studies with the HOQNO and crystallographic studies with a benzoquinol analogue, pentachlorophenol, suggest there is only 1 quinol binding site (228). The lack of an X-ray crystallographic structure for DmsABC means that the presence of a non-dissociable Q-site that is undetectable by normal enzymology techniques cannot be discounted.

Other menaquinol-like molecules are oxidized by DmsABC. Two hydroxylated naphthoquinol analogues, reduced plumbagin (PBH<sub>2</sub>; 5-hydroxy-2-methyl-1,4-naphthoquinol) and reduced lapachol (LPCH<sub>2</sub>; 2-hydroxy-2-methyl-1,4-naphthoquinol), have been shown to be substrates. These compounds have optical, solubility and redox properties that make them suitable for use in studies of the enzymology of menaquinol oxidation (229).

The lack of cytochromes or any other redox active cofactor in the membrane anchor domain poses an interesting problem during MQH<sub>2</sub> oxidation: electrons from MQH<sub>2</sub> cannot dwell in the membrane anchor subunit as they do at the two *b*-hemes of NarI, but they must travel to the [4Fe-4S] clusters in the electron transfer subunit concomitant with MQH<sub>2</sub> oxidation. As such, the Q-site in DmsC has been demonstrated to be conformationally and functionally linked to the -50mV [4Fe-4S] cluster (FS4) in DmsB (212). In addition, a Tyr sidechain from the electron transfer subunit has also been suggested to point towards the Q-site and be involved in the binding and oxidation of MQH<sub>2</sub> (230). In comparison to nitrate reductase, the lack of hemes in DmsC might have consequences on its ability to carry out catalysis, and this is discussed in Chapter 3.

Two residues in DmsC – His65 and Glu87 – have been shown to exert negative effects on HOQNO binding and lapachol oxidation when mutated (212,220,221). Electron paramagnetic resonance studies on a DmsB-Cys102Ser/DmsC-His65Arg double mutant showed a clear functional link between the Q-site and the -50mV [Fe-S] cluster (FS4) (212). Incidentally, both residues are predicted to be in the first periplasmic loop of DmsC, between transmembrane  $\alpha$ -helices 2 and 3 (Figure 2.11), placing the Q-site on the periplasmic side of the membrane. Given that MQH<sub>2</sub> must donate electrons directly to DmsB, this implies a periplasmic location for DmsAB (see Section 2.2.7 for further discussion). Other residues—Leu66, Gly67, Arg71, Phe73, and Ser75—examined in DmsC are also located in this periplasmic loop, but they do not show enhanced or compromised activities associated with MQH<sub>2</sub> binding or oxidation when mutated (220).

## 2.2.6 MEMBRANE TARGETING AND TRANSLOCATION OF DMSO REDUCTASE

The DmsA subunit is synthesized as a pre-protein of 814 (90,400 Da) residues. A 45 amino acid *tat*-leader is removed to yield a mature protein of 769 (85,795 Da) amino acids. The DmsA polypeptide is translated and folded in the cytoplasm into a cofactor-containing protein together with DmsB before it is targeted to the cytoplasmic membrane as a catalytic dimer (231). The DmsA leader sequence contains two positively charged Lys near the N-terminus, two Arg residues at positions 16 and 17 consistent with typical twin arginine consensus sequences (S/T)-R-R-X-F-L-K, and an arginine near the cleavage site (161).

**<sup>1</sup>MKTKIPDAVLAAEVSRRLVKT AIGGLAMASSAL TLPFSRIAHA<sup>45</sup>**

The leader is presumably cleaved by leader peptidase but this has not been shown. Chromosomal deletion of the *tatABC* operon leads to accumulation of DmsAB in the cytoplasm and abolishment of growth on minimal media containing DMSO as terminal electron acceptor (232). Similarly, deletion of the leader sequence from DmsA does not allow full assembly and proper targeting of DmsABC, and in fact leads to degradation of DmsA *in vivo* (231). Thus the leader sequence also plays a protective role that prevents DmsA degradation in the cytoplasm. The DmsD protein encoded by the *ynfEFGHdmsD* operon is a specific chaperone which binds to the DmsA leader prior to targeting to the *tat* translocon (see Section 2.2.9) (233).

## 2.2.7 Topology of DmsABC

The membrane topology of the catalytic dimer, DmsAB, has been controversial for many years. The immature DmsA contains a leader sequence at its N-terminus that is recognized by the *tat* translocation machinery (231) and as such DmsA along with the leaderless DmsB appears to be a standard cofactor-containing substrate for *tat* translocation to the periplasm. Additionally, chromosomal deletion of the *tatABC* operon leads to accumulation of DmsAB in the cytoplasm and abolishes growth on minimal media containing DMSO (232). Unlike other *tat* substrates such as TorA (234), insertion of the MGD cofactor is not required for interaction with the *tat* translocase and a cofactor-less DmsABC is assembled on the membrane. Interestingly, the structure of the apo-form of NarGHI has been determined by X-ray crystallography and it appears as though the cofactor-less protein assembles with almost superimposable precision compared to the wild-type enzyme (179).

An earlier comprehensive study by Sambasivarao *et al* (235) used a number of biochemical and immunological approaches to examine the topology of DmsAB on the membrane. In these studies the conclusion reached was that DmsAB were located on the cytoplasmic side of the membrane. Traditional cold osmotic shock (236) and chloroform washing of whole cells (237), methods that normally release periplasmic proteins, did not release any DmsAB. While this might be expected if DmsAB are localized to the periplasm but are bound tightly to DmsC, no DmsAB are released in a DmsC deletion (238) where DmsAB should be free in the periplasm. The protease sensitivity of DmsAB was tested in cells with permeabilized outer membranes. No protease degradation was observed until the membranes were solubilized with Triton X-100 to destroy any topological constraints. Everted membrane vesicles prepared by French Pressure lysis

yielded protease sensitive DmsABC, but higher temperatures, higher pH and presence of solubilizing agents were required to achieve similar inactivation compared to the fumarate reductase control. Immunogold electron microscopy of thin sections using anti-DmsA and anti-DmsB antibody probes also indicated DmsAB to be oriented towards the cytoplasmic surface of the inner membrane. Attempts to construct fusions of alkaline phosphatase (PhoA) with either DmsA or DmsB did not yield any active PhoA in the periplasm (217). Many of the experiments of Sambasivarao *et al* (235) were carried out with both chromosomal and plasmid encoded DmsABC to eliminate artifacts due to overexpression. An independent experiment using the spin probe dysprosium(III)-EDTA also suggested a cytoplasmic location for the [Fe-S] clusters in DmsB (239).

In contrast to the Sambasivarao study, a later study by Stanley *et al.* (240) argued that the above experimental designs were flawed because: 1) overexpression of DmsABC from a multicopy plasmid might cause overloading of the *tat* translocase, leading to a cytoplasmic buildup of DmsAB and 2) the PhoA protein requires formation of two intramolecular disulfides (241) but the *tat* system transports proteins in their folded states (242-245). Thus an inability to select for DmsA-PhoA and DmsB-PhoA fusions does not conclusively indicate a cytoplasmic location for the dimer. In fact, it was shown that PhoA and LacZ fusions are not ideal candidates to use when studying periplasmic proteins that are exported via the *tat* system, but Bla and Cat fusions remain active when transported through the *tat* translocon (240). A periplasmic location of DmsAB was first observed in a  $\Delta dmsC$  strain by Weiner *et al.* (246) but this result could not be reproduced (232) although it was confirmed by Stanley *et al.* (240). Indeed, cellular subfractionation of a  $\Delta dmsC$  strain wherein a His<sub>6</sub>-tag was attached to the chromosomal *dmsB* allowed the

majority of DMSO reductase activity as well as DmsB polypeptides to be detected in the periplasm by enzyme assays and immunoblotting, respectively (240).

A bioinformatic analysis by Rothery *et al* (247) of the topology of membrane anchor subunits of multisubunit reductases and dehydrogenases suggested that DmsAB are bound to the periplasmic surface of DmsC. Additionally, the bioenergetic study by Bogachev *et al* (167) showed that DmsABC does not generate a pmf but serves as an electron sink, indicating that the quinol oxidase and DMSO reduction sites are on the same side of the membrane. Mutant studies of quinol binding in DmsC would place DmsAB on the periplasmic side. One additional result adds to the puzzle of DmsAB topology. A recent study by Lindenstrauss *et al* (248) showed that the *tat* proteins of *Rh. capsulatus* could correctly target the *E. coli* TorA, AmiA, and FdnGH subunits but could not target DmsAB, suggesting that there is something unique about the assembly of this latter complex.

Overall, the arguments for a periplasmic location of DmsAB are more convincing than the case presented for a cytoplasmic topology. An alternative model for the assembly of DmsABC is a “ball-in-glove” model where DmsAB sits deeply-embedded in the membrane but is surrounded by the eight helices of DmsC. This possibility could account for both cytoplasmic and periplasmic observations of DmsAB, and can reinforce the theory that DmsC prevents DmsAB from entering the periplasm (246). In this case, only an X-ray crystallographic structure would provide the answer to this lasting puzzle.

### **2.2.8 YnfEFGH/DmsD – A Dms Parologue**

The DMSO reductase enzyme has a paralogue in the *E. coli* genome: *ynfEFGHdmsD* (249). It is found at 1.65 kbp on the *E. coli* chromosome (Figure 2.3). This is not surprising as both the *torCAD* (250,251) and *narGHJI* operons (252,253) have paralogues. The role of the *ynf* operon remains an enigma. While there is some evidence from transcriptome studies that *ynfEFGH* are expressed, there is no evidence that this paralogue has any functional role. Strains carrying a  $\Delta dmsABC$  mutation are unable to grow using DMSO or other *S*-oxides as a terminal electron acceptor and immunoblot analysis using polyclonal anti-DmsA and anti-DmsB antibodies fail to reveal any cross-reacting polypeptides (238) in cells grown anaerobically on minimal medium with fumarate as terminal electron acceptor. However, it has been shown that YnfEFG produced by recombinant expression techniques do cross-react with anti-DmsA and anti-DmsB antibodies. The *dmsD* (*ynfI*) open reading frame in the operon encodes a specific chaperone that has an essential role in assembly of DmsABC (233) (see Section 2.2.9) and it is possible that the *ynf* operon has survived to provide a source of DmsD protein.

The DNA region upstream of *ynfE* has been examined for regulatory and promoter sequences and it appears that overlapping elements are used to control transcription of the *ynf* and *dms* operons. A putative FNR box upstream of the *ynfE* promoter has been identified (249), implying anaerobic expression of the paralogue. Two potential NarL binding sites have also been spotted (254) in the promoter region to allow nitrate repression of the *ynf* operon, preserving the substrate hierarchy of metabolizing nitrate before DMSO as a terminal electron acceptor. Response to molybdate availability is controlled by a potential ModE binding site (254) that was discovered by MatInspector (255). Two  $\sigma^{70}$  promoters have been identified by a computational approach (256); one

upstream of *ynfE* and one upstream of *ynfF* (249). The  $\sigma^{70}$  promoter for *ynfF* is located in the coding sequence of *ynfE* and presumably regulates transcription of *ynfFGHdmsD*. Upstream of *ynfE*, two binding sites for the general stress response regulator transcription factor RpoS (257) are present to initiate mRNA synthesis. Shine-Dalgarno sequences are located immediately upstream of *ynfE* and *ynfF* and are ideal for initiation of translation.

The gene products YnfE and YnfF are tandem duplications and are highly homologous to DmsA, showing 66% identity and an additional 15% similarity to the catalytic subunit. Both begin with typical *Tat* leader sequences responsible for membrane translocation and targeting. Both YnfE and YnfF also retain conserved amino acids which are thought to be critical in Mo-bisMGD binding and catalytic activity. The electron transferring subunit YnfG is the most conserved and is 94% identical plus 3% similar to DmsB. YnfH is the membrane anchor and quinol binding subunit. It is only 57% identical to DmsC and is predicted to be a transmembrane protein comprising 8 transmembranal  $\alpha$ -helices. DmsD is unique to the *ynf* operon.

Lubitz and Weiner (249) attempted to characterize the *ynf* open reading frames by constructing chimeric proteins between the Dms and Ynf polypeptides. The putative anchor subunit, YnfH, can interact with DmsAB to form a trimeric enzyme with MQH<sub>2</sub> oxidase and DMSO reductase activity. The YnfG paralogue can substitute for DmsB as an electron transfer subunit and can interact functionally with both DmsC/YnfH and DmsA/YnfF. The YnfF subunit is more restrictive as it preferentially interacts and accepts electrons from YnfGH but is unable to do so from DmsBC. Coexpression of YnfE and YnfF in conjunction with YnfG/DmsC could not complement growth on



DMSO in a  $\Delta dmsABC$  strain, whereas the YnfFG/DmsC chimera can do so effectively, indicating that YnfE interferes with assembly of the terminal reductase.

When YnfFGH is over-expressed using multicopy plasmids it can functionally replace DmsABC as a DMSO reductase, however growth on glycerol-DMSO minimal medium yielded approximately 50% cell mass when the former enzyme is utilized compared to the latter enzyme. Enzymological studies of YnfFGH and YnfFG/DmsC showed that they can also use a broad array of *S*- and *N*-oxides as is the case with DmsABC but the turnover numbers are relatively poor. (203,249) The best substrate for YnfFGH appears to be hydroxypyridine *N*-oxide, followed sequentially by isonicotinic acid *N*-oxide, pyridine *N*-oxide, 2-chloropyridine *N*-oxide, DMSO and finally TMAO (249). The possibility that *ynfEFGH* encodes a hydroxypyridine *N*-oxide reductase was refuted given that this substrate does not upregulate expression of the enzyme nor does the enzyme augment growth on minimal media containing hydroxypyridine *N*-oxide. The physiological substrate and function for the *ynfEFGH* gene products remain unknown.

### **2.2.9 DmsD – A DMSO Reductase Specific Chaperone**

The DmsD protein, initially named YnfI, has been shown to be a chaperone necessary for DmsABC maturation (233). Unexpectedly this gene is part of the *ynfEFGHdmsD* operon rather than the *dmsABC* operon. DmsD is a peripheral membrane protein localized to the *E. coli* inner membrane under anaerobic conditions in wild-type *E. coli* or a  $\Delta dmsABC$  strain, but DmsD is retained in the cytoplasm under aerobic conditions or in a  $\Delta tatABCDE$  strain (258). It was first purified as a protein which

interacts with the twin-arginine leader of DmsA and subsequently shown to interact with premature forms of DmsA and TorA (259). This finding is quite surprising given that the DmsA and TorA leader sequences are not functionally interchangeable (231). A three-dimensional structure of the DmsD homologue from *Salmonella typhimurium* LT2 has been deposited in the Protein Data Bank (Figure 2.12).

Binding of DmsD to pre-DmsA has been studied extensively by biophysical techniques. Fusion of the DmsA leader at the N-terminus of glutathione *S*-transferase allowed interaction with DmsD whereas a C-terminal fusion did not (260). Binding of DmsD to the DmsA leader occurs with 1:1 stoichiometry with relatively strong affinity; a  $K_d$  of 0.2 $\mu$ M was derived from isothermal titration calorimetry (260). DmsD has been purified and can be separated into three different states: monomer, dimer, and a heterogeneously-folded monomer containing multiple conformations (261). Interestingly, all three forms of DmsD can interact with the DmsA leader *in vitro* (260).

Although DmsD interacts with the leader sequence of DmsA, it does not appear that DmsD is necessary for proper translocation and targeting of periplasmic components since the DmsA leader can still target green fluorescent protein to the periplasm in a  $\Delta$ *dmsD* strain (233). It has therefore been proposed that DmsD acts as a chaperone for cofactor insertion into DmsA (233), much like the TorD chaperone for TorA maturation and Mo-bisMGD insertion. (262,263) As noted above, DmsD is not associated with the membrane in a  $\Delta$ *tatABCDE* strain suggesting that it binds to the *tat* complex and it has been shown that TatB and TatC are needed for the interactions (258). Thus, DmsD is seen as a DmsA chaperone necessary for cofactor insertion into DmsA and assists in its initial interaction with the *tat* machinery.

## 2.3 Trimethylamine *N*-oxide Reductase

### 2.3.1 TMAO in the Natural Environment

Trimethylamine *N*-oxide (TMAO) is found at low levels in seawater and phytoplankton. It is found in the tissues of salt water organisms including fish, cephalopods, mollusks, crustaceans and seaweed where it can be as much as 1% w/w (168). Salt water fish maintain a high intracellular osmolarity similar to the osmolarity of seawater by using TMAO in combination with urea as osmolytes (264). Interestingly, TMAO stabilizes proteins in solution by enhancing hydrogen bonding to water molecules and may play a role in the formation of disulfide bonds (265). This counteracts the denaturing effect of urea. TMAO is not found in fresh water fish which reside in an environment of low osmolarity. The product of TMAO reduction is trimethylamine (TMA) which is responsible for the pungent smell of rotting fish. Humans can detect TMA at concentrations of less than 1 ppb. Some species of bacteria grow anaerobically using TMAO as an alternate electron acceptor. TMAO reductase activity has been found in marine bacteria (*Shewanella*, *Vibrio* and *Photobacterium*), in photosynthetic bacteria (*Rhodobacter*) and in enterobacteria like *E. coli* and *S. typhimurium* (168,266). TMAO is reduced to TMA by bacteria associated with or contaminating the marine organisms. *E. coli* or *S. typhimurium* do not further metabolize TMA and thus it is not used as a carbon or nitrogen source. In methylotrophs the oxidation of TMA to TMAO is the initial step in the utilization of TMA as carbon, oxygen and energy source. In the early 70's Kim & Chang (267) observed that TMAO gave increased cell yield of cells grown anaerobically on glucose supplemented with TMAO and they proposed that reduction must be associated with anaerobic respiration that supported oxidative phosphorylation. The

TMAO/TMA half reaction is +0.130V which is less than the nitrate/nitrite couple (+0.42V), but higher than the fumarate/succinate couple (+0.031V) (254) and in line with the 3-4  $H^+/2e^-$  as measured by Takagi (268). Because TMAO reduction to TMA consumes protons, anaerobic growth on TMAO results in alkalization of the growth medium (Figure 2.13).

The early data on the number of distinct TMAO reductases (1 constitutive and 3-4 inducible) are confused (254). We now know that under most physiological anaerobic growth conditions there is one inducible, periplasmic TMAO reductase encoded by the *torCAD* operon which uses only TMAO as reductant and a membrane-bound enzyme complex encoded by *dmsABC* which reduces both DMSO and TMAO although it has been proposed that TMAO is the natural substrate for this enzyme (254).

### 2.3.2 The *tor* Locus

The *tor* (trimethylamine *N*-oxide reduction) locus of *E. coli* was originally identified by Ishimoto (268) in the early 1980's by mutagenesis and the TorA structural gene was mapped to a region that is homologous with the location of *tor* on the *Salmonella typhimurium* genome (269). The *tor* locus is located at approximately 1053 and 1061 mBP (22 min) on the *E. coli* MG1655 chromosome and consists of two parts: the *torCAD* structural operon and an adjoining region encoding the *torRTS* regulatory operon (269) (Figure 2.3). *torT* is encoded on the same strand as *torCAD* while *torR* and *torS* are divergently encoded.

### 2.3.3 Tor Regulation

The expression of the *torCAD* operon is controlled by anaerobiosis and TMAO (270). Surprisingly, although TorA will only reduce TMAO and methylmorpholine-*N*-oxide, the *torCAD* operon can be induced by a range of *S*- and *N*-oxide compounds including DMSO (271). Induction of the *torCAD* operon occurs in a somewhat unusual and complicated process (272). Anaerobiosis induces expression about 10-fold based on a *torA'-lacZ* reporter fusion but the *torCAD* operon is unusual in that the anaerobic induction is not under the control of the FNR (273) or ArcA (82) global regulatory proteins and no FNR or ArcA boxes can be found in the region upstream of the *torC* promoter (270,274). *torA* expression is not affected by ModE which mediates molybdenum regulation of *dmsABC* (172). Further *torA* expression is not subject to the hierarchical control whereby substrates with higher redox potentials are preferentially induced (270,275) and lacks the NarL consensus binding sequence (276). Regulation of *torCAD* is mediated by a group of three open reading frames located adjacent to the *torCAD* operon, *torS*, *torT* and *torR* which are divergently expressed (Figure 2.3).

The regulation by TorA expression is strictly dependent on TMAO and is mediated by a two-component histidine/aspartate kinase phosphotransfer relay (277). *torS* was originally identified by insertion mutagenesis (278) and encodes a membrane-bound sensor protein for TMAO. Although TorA only utilizes TMAO and 4-methylmorpholine-*N*-oxide as substrates, a wide variety of *S*- and *N*-oxide compounds including DMSO can induce *torCAD* expression via TorS binding (271). The TorS sensor histidine kinase contains an N-terminal periplasmic domain which senses the signal. Jourlin *et al* (278) have identified a three amino acid deletion mutation in this domain (presumably in the TMAO detector site) which results in full constitutive expression in the absence of

TMAO, confirming that the periplasmic domain senses TMAO. The kinase domain (transmitter domain) of 240 amino acids is located in the cytoplasm. This domain contains four motifs including the active site where a histidine is autophosphorylated when TMAO is detected (279). A linker region is located between the sensor and transmitter domain which includes a transmembrane  $\alpha$ -helix. It plays an essential role in propagating conformational changes from the periplasm to the histidine kinase transmitter domain and mutations have been isolated in this domain which gives some expression of *torCAD* in the absence of TMAO. This phosphoryl group is transferred to an aspartate on the response regulator, TorR (receiver domain), leading to transcription of *torCAD*.

Phosphotransfer by two-component regulatory systems occurs via one of two mechanisms (280). In the simple two-step mechanism the sensor kinase directly phosphorylates the response regulator. A more complex four-step mechanism utilizes a sensor kinase with two or three phosphorylation sites. TorS falls into the latter category as it involves three phosphorylation sites and is termed an “unorthodox kinase” (281). The additional phosphorylation sites are found in a histidine phosphotransferase domain which contains a receiver domain and an alternate transmitter domain at the C-terminus. A similar architecture is seen in ArcB (282). ArcB is part of the ArcA/ArcB two-component regulatory system for anaerobic repression of certain respiratory enzymes (82). All three phosphorylation sites on TorS (His443  $\rightarrow$  Asp723  $\rightarrow$  His850  $\rightarrow$  Asp(TorR)) are required for TMAO induction of *torCAD*. TorS can rapidly dephosphorylate phospho-TorR when TMAO is removed and this appears to work by a reverse phosphorelay as His850 and Asp723 are essential for dephosphorylation (283).

The unorthodox kinase proteins often have an additional phosphatase that regulates the signal transduction at intermediate checkpoints. In the case of the TorSR system, a novel protein, TorI, interacts with the effector domain of TorR to inhibit *torCAD* expression without affecting TorR binding to DNA (284). TorI is a very small protein of 66 amino acids. It appears that TorI prevents TorR from interacting with RNA polymerase thus limiting recruitment of the polymerase to the *torCAD* promoter. TorI has no effect on signal transduction or the phosphorelay mechanism. Homologues of TorI bearing 100% identity include *hkaC* of the coliphage HK620 and gene 18 of *Shigella* phage Sf6, suggesting that TorI is of phage origin and belongs to the defective prophage KplE1 which is present on the *E. coli* genome (285). Elantak *et al* have shown that TorI has excisionase activity and excises the cryptic prophage KplE1. The solution structure of TorI has been determined (285) and although it lacks sequence similarity, the three-dimensional structure is highly homologous to the  $\lambda$ Xis, Mu bacteriophage repressor and transposase.

An additional level of regulation of *torCAD* is mediated by apo-TorC (286). Immature TorC lacking the hemes cannot interact with TorA but can interact with the periplasmic domain of TorS inhibiting the TorS kinase and thus negatively regulating expression of *torCAD*. This regulation is highly specific to apo-TorC, and cannot be replaced by other immature *c*-type cytochromes. The regulation depends on the mono-heme carboxy terminal domain of TorC and not on the tetra-heme amino terminal domain.

TorR is the 25 kDa response regulator protein of the two-component regulatory system that controls expression of *torCAD* in response to TMAO (274). TorR is a

member of the OmpR family of response regulators (287-289). TorR binds to the short *torR-torC* intergenic regulatory region which contains four direct repeats of a decameric consensus sequence (*tor* box) (CTGTTTCATAT – box 1, 2 and 3) (CCGTTCATCC – box 4) (Figure 2.14) located in the untranslated nucleotide region between the divergently expressed *tor* operon and *torR* (Figure 2.3). TorR protein binds to the *torC* regulatory region based on DNA footprinting and gel retardation assays. Three regions are protected by TorR binding (274) (Figure 2.14): one of 24 nucleotides covers boxes 1 and 2, the second is upstream of the -35 region and covers box 3 and the third is downstream of the -35 sequence and covers the fourth *tor* box. Mutating any one box results in dramatic decrease of *tor* expression based on a *torA'-lacZ* reporter construct indicating that all four boxes are required. The upstream boxes, 1 and 2, display high affinity binding and form a nucleoprotein complex that covers the *torR* transcription start site. Simon *et al* (274) have proposed that unphosphorylated TorR dimer binds to boxes 1 and 2. In the presence of TMAO, TorR is transphosphorylated by TorS leading to the cooperative formation of a tetramer attached to boxes 1 and 2. One subunit then binds to box 4 and subsequently another subunit contacts the very low affinity box 3. This complex positions the promoter for RNA polymerase binding and transcription of *torCAD*. All 4 boxes must be close to each other and on the same side of the DNA helix for induction of *torCAD* (290). High-level expression of TorR mimics the presence of the inducer TMAO indicating that if there is enough protein available, it can bypass the need for histidine phosphorylation (272). The anaerobic regulator of *torCAD* is unknown and it does not appear that TorR plays a role in anaerobic regulation. The expression of *torR* itself is negatively autoregulated and is independent of TMAO and TorS (290) suggesting that both



unphosphorylated and phosphorylated TorR can bind. It only involves TorR binding to the high affinity sites boxes 1 and 2, thus preventing RNA polymerase from binding.

The *torT* gene encodes a periplasmic protein of 35.7 kDa. Transposon insertion within *torT* dramatically reduces expression of a *torA'-lacZ* fusion reporter (278). TorT bears some sequence similarity to the periplasmic ribose binding protein and it has been proposed that TorT serves as a ligand binding protein to deliver TMAO to the sensor kinase TorS in the cytoplasmic membrane. In support of this TorT has been found to be dispensable and excess TorR in a *torT* mutant results in partial constitutive expression of *torA'-lacZ*.

#### **2.3.4 TorA – The Catalytic Subunit**

TorA is the catalytic subunit responsible for converting TMAO to TMA. It is assembled with the Mo-bisMGD cofactor in the cytoplasm with the help of the TorD chaperone (Section 2.3.6) and translocated to the periplasm via the *tat* translocon (246,291). TorA is active only with TMAO and 4-methylmorpholine-*N*-oxide and does not have any *S*-oxide activity. This differs from DMSO reductase which is active with a wide range of *S*- and *N*-oxides (203).

TorA is a member of the DMSO reductase molybdenum cofactor family and several structures have been determined for members of this family including formate dehydrogenase-H (209), two DMSO reductases (182,183), formate dehydrogenase-N (180) and nitrate reductase (178). Although the structure of *E. coli* TorA has not been determined, the structure of the homologue from *Shewanella massilia* has been reported

at 2.5Å resolution (Figure 2.15) (184). Like RhDmsA discussed above, TorA is organized into four domains around the Mo-bisMGD cofactor.

In addition to the dithiolene sulfurs, further coordination of the Mo atom is provided by the hydroxyl sidechain of Ser149 and by an additional oxo group. Substrates reach the Mo via a funnel from the surface. Czjzek *et al* (184) tried to rationalize the substrate specificity of TorA compared to DMSO reductase as an active center issue, as TMAO reductase only reduces TMAO yet DMSO reductase has wide substrate specificity (203). One possibility focuses on Tyr114 of RhDmsA which is missing in TorA and this may be crucial for reduction of *S*-oxide compounds but not *N*-oxides. Another important difference is the number and arrangement of charged groups lining the inner surface of the funnel-like entrance. Finally a surface loop at the entrance to the funnel which is well defined in the TorA sequences is more flexible in the DmsA structure and may play a role in substrate accessibility.

Usually attempts to grow *E. coli* with tungsten result in the accumulation of molybdoenzyme lacking cofactor or enzyme with little or no activity. Interestingly, Buc and colleagues (292) were able to replace the transition metal Mo in *E. coli* TorA with W. The W-substituted TorA enzyme is active and now uses both TMAO and DMSO. This observation downplays the theory of a critical Tyr residue being responsible for the difference in the ability to reduce *S*- and *N*-oxides. The W-substituted enzyme is also more heat resistant.

### **2.3.5 TorC – The Porphyrin Cytochrome**

The TorC protein is a pentaheme *c*-type cytochrome that is essential for TMAO respiration (293). The protein is synthesized as a 390 amino acid precursor. TorC is translocated to the periplasm via the classical Sec system (294). A 28 amino acid N-terminal leader is cleaved from the mature enzyme yielding a 362 amino acid (40.47 kDa) mature protein that is bound to the cytoplasmic membrane by a membrane anchor at the amino end. The bulk of TorC faces the periplasm where it can interact with TorA. TorC must interact with the menaquinol pool in the membrane and must have a MQH<sub>2</sub> binding site; however, no information is available on the residues which make up this site.

The complexity of the TorA maturation and translocation machinery is matched by that needed to assemble TorC onto the outer surface of the cytoplasmic membrane. TorC is largely matured using the standard cytochrome *c* maturation machinery. After translocation via the *sec* system, the cysteines in the CXXCH are rapidly oxidized by DsbA/DsbB which converts TorC to a prefolded form that precedes maturation (294). Final maturation involves reduction of the cysteine disulfides and requires the gene products of *ccmABDEFGH* and *dsbD* (294).

TorC is composed of two domains. The N-terminal half is a member of the NapC/NirT family of *c*-type cytochromes and encodes four CXXCH motifs binding four *c*-type cytochromes (295). The C-terminal half has an additional CXXCH domain found only in TorC and DorC type proteins at residues 329-333 (296). Gon (293) cloned the amino (TorC<sub>N</sub>) and carboxy (TorC<sub>C</sub>) halves independently using the TorT leader to direct TorC<sub>C</sub> to the periplasm. Neither domain alone supported growth suggesting that the entire TorC protein was needed.

Attempts to over-express TorC have been hampered by the limited capacity of *E. coli* to make *c*-type cytochromes encoding the *c*-type cytochrome biosynthetic activity (294) even when the *ccm* genes are added on another plasmid. The *ccm* genes were under the arabinose promoter so that expression could be exquisitely controlled. Very low levels of arabinose were used (0.0005%) to avoid overloading the *c*-type cytochrome biosynthetic system. TorC maturation is prevented by TorC overproduction, DTT addition or disruption of the *ccm* genes involved in holoTorC production.

TorC has a typical *c*-type cytochrome spectrum. In the oxidized state the Soret band at 411 nm is observed. In the reduced state bands were seen at 417 nm (Soret), 523 nm and 552 nm. Redox potentiometry of TorC indicated  $E_m$  values of -177mV corresponding to two hemes, -98mV corresponding to two hemes and +114mV corresponding to one heme. The negative potential hemes were localized to the amino terminal half and the positive heme to the carboxy terminal half of the protein. This suggests that electrons flow from the amino terminal half to the carboxyl terminal domain and then to TorA.

Gon *et al* (293) examined the physical interaction of TorC with TorA. They found that TorC migration on native polyacrylamide gels was retarded by TorA, suggesting that the two proteins interact. These binding studies were extended using Histidine-tagged and purified TorC<sub>N</sub> and TorC<sub>C</sub> halves of TorC by surface plasmon resonance. Surprisingly they found that the TorC<sub>C</sub> half does not interact with TorA but the TorC<sub>N</sub> interacts with a  $K_d$  of  $4.5 \times 10^{-8}$  M. When intact TorC was used they noted that binding was in two steps with  $K_{d1}=1.7 \times 10^{-8}$  M and  $K_{d2}=3.0 \times 10^{-6}$  M. This suggests a model in which TorA folds around TorC such that TorC<sub>N</sub> can bind TorA and TorC<sub>C</sub> interacts with the molybdopterin

cofactor in TorA (293). Based on the ease with which TorC is released by osmotic shock this interaction must be relatively transient in the cell.

### 2.3.6 TorD – The Chaperone Protein

The third gene in the *tor* operon is not part of the functional complex. It is a 22 kDa cytoplasmic protein related to a large number of prokaryotic homologues with similarities ranging from 20-64%. The TorD family has been divided into four groups or clades using an unrooted phylogenetic tree (297) and several of these clades are also related by molybdoenzyme classification (298). The clade which includes the *E. coli* TorD also contains *S. massilia* TorD (266), *R. capsulatus* DorC (296) and *R. sphaeroides* DmsB (299). It is related to the Type III molybdoenzymes and is thus also defined as Type III. Although these proteins are clearly related, the TorD of *S. massilia* could not replace *E. coli* TorD for either *in vitro* binding studies or *in vivo* complementation (297). Proteins of Type II which includes the DmsD and YcdY proteins could not replace TorD for complementation although they did compete for TorD binding to TorA.

The TorD protein of *S. massilia* has been the subject of structural investigation. This protein is 33% identical in sequence to *E. coli* TorD and exists in multiple oligomeric states. Interconversion between the monomeric and dimeric states required destabilization of the native fold of the protein (300). The 2.4Å X-ray crystallographic structure of the dimeric form of *S. massilia* TorD has been solved (301) and it reveals a dumbbell-like structure with extreme domain swapping between the two subunits. TorD is an intertwined dimer with a globular domain of all  $\alpha$ -helical composition.

During the last few years considerable information has become available on the chaperone function of TorD with TorA. Pommier *et al* (262) originally showed that in *E. coli*, the absence of TorD led to a loss of TorA activity. However, a significant amount of TorA was still present in the periplasm. These studies suggest that TorD alters the conformation of apoTorA (lacking the Mo-bisMGD cofactor) to allow for better cofactor insertion. It was found that when the activation was carried out *in vitro* with purified components apoTorA was activated only in presence of TorD and MobA (MobA converts Mo-MPT to Mo-MGD). In a strain deficient in TorD and the MGD cofactor, TorA was proteolytically digested; however, an excess of TorD prevented the proteolytic degradation. The proteolytic degradation was particularly obvious at elevated temperatures (42°C) (302). Using surface plasmon resonance and native polyacrylamide gel electrophoresis it could be shown that TorD physically binds to apo-TorA (263).

More recent experiments by Sargent *et al* (303) and Iobbi-Nivol *et al* (263,297,301,302,304,305) indicate that TorD has a dual role: to act in the maturation of apo-TorA with MGD as noted above and to act as an escort for TorA to the *tat* translocation system (246,306). These two roles are independent. The latter role is to prevent the export of immature TorA. Using a mutant of TorA lacking the Tat signal sequence it could be shown that the truncated protein still binds Mo-bisMGD and the binding was stimulated by TorD, as normal. It was shown (307) that TorD bound to the TorA signal sequence. Using a synthetic TorA leader it could be shown that TorD bound to the TorA leader (303) and this binding involved portions of the leader independent of the SRRxFLK motif. Hatzixanthis *et al* further showed that TorD is a GTP binding protein. No GTPase activity could be measured and the role of GTP is unclear although it

may be regulatory. Interestingly addition of TorA to a GTP-TorC mixture results in increased GTP affinity.

### 2.3.7 The *torYZ* Operon

The *E. coli* chromosome contains a paralogue of the *torCAD* operon at 42.1 minutes (1952 - 1956 kbp on the MG1655 chromosome) (Figure 2.3) termed *torYZ*, originally termed *yecKtorZ*. Unlike the *torCAD* operon the paralogue lacks a gene related to the *torD* chaperone protein. The existence of a paralogue to the *tor* operon is similar to the *nar* and *dms* operons which also contain paralogues on the chromosome (249,253). In all cases the paralogue is expressed at relatively low levels.

*torZ* was originally characterized as BisZ, a second biotin sulfoxide (BSO) reductase in *E. coli* (250) and it is 63% identical to BisC while only 44% identical to TorA. TorZ accounted for only 4% of the BSO reductase activity in *E. coli*. However, Gon *et al* (251) have shown that unlike BSO reductase, TorZ has a typical *tat* leader similar to TorA and DmsA and the mature protein is located in the periplasm. Gon *et al* (251) have shown that translocation is dependent on a functional *tat* system. TorZ has wide catalytic activity to *S*- and *N*-oxide compounds and importantly it displays higher activity with TMAO than BSO. Upstream of *torZ* is the 1 kbp open reading frame *torY(yecK)* that is co-transcribed with *torZ*. This open reading frame encodes a membrane-bound pentaheme cytochrome, TorY, that is homologous to TorC and the corresponding subunit of the Dor system of *Rh. capsulatus*. *E. coli* contains only six pentaheme cytochromes, two involved in the periplasmic nitrate reductase (Nap) (308), two involved in nitrite reduction (Nrf) (308), TorC and TorY. TorY can support

anaerobic respiration with TorZ in a strain lacking *torCAD* and *dmsABC* when it is expressed from a *ptac* promoter in the presence of IPTG. Thus TorYZ can form a respiratory system capable of supporting anaerobic growth on TMAO, DMSO and BSO. Unlike TorCA, TorYZ is also able to support growth on BSO and DMSO in a strain lacking *torCAD* and *dmsABC* indicating that TorZ has a much broader substrate specificity than TorA.

Like the expression of the *ynfEFGHdmsD* operon (251), expression of *torYZ* remains an enigma. Expression is very low and the operon under control of the native promoter is not induced by TMAO, DMSO or BSO and it is unable to support growth on *S*- or *N*-oxides when the *torCAD* or *dmsABC* operons are mutated. As the activity profile of TorZ is not identical to TorA or DmsA perhaps it has a unique activity and the inducer has not yet been discovered.

A major difference between the *torCAD* operon and *torYZ* is the absence of a TorD like chaperone. As noted above TorD has multiple roles in the assembly of TorA. Gon *et al* (251) have shown that TorD is not required for TorZ maturation suggesting that TorZ maturation is chaperone independent or a chaperone is encoded elsewhere on the chromosome. A similar situation exists for DmsA where the DmsD chaperon is encoded in the *ynf* operon and not in the *dmsABC* operon. The lack of a chaperone may account for the very low level of TorZ expression.

## **2.4 Summary**

The major attributes amongst DmsABC, TorCA, and their respective homologues are listed in Table 2.1. All four proteins are synthesized with a *tat* leader in the premature



soluble domain and are thus targeted to the periplasm by the *Tat* translocon; however, the arguments for DmsABC remain debatable and the case for YnfFGH has yet to be fully explored although a periplasmic location could be conjectured based on its strong sequence and functional relation to DmsABC. Assembly of DmsABC and TorCA requires the chaperones DmsD and TorD respectively. YnfFGH assembly has not been tested in the absence of DmsD, but their genetic codes are located in one operon. The assembly of TorYZ has been shown to be chaperone-independent. The expression of DmsABC and its paralogue YnfFGH are positively regulated by the FNR protein under anaerobic conditions. TorCA is also expressed under anaerobic conditions, although via an unknown mechanism, and is additionally controlled by the presence of *S*- and *N*-oxides. In terms of substrate utilization, it is interesting to note that DmsABC, YnfFGH, and TorYZ can reduce a variety of *S*- and *N*-oxides; in contrast, the native TorCA can only reduce *N*-oxides but the W-substituted TorCA can reduce *S*- and *N*-oxides.

Although the two paralogues YnfFGH and TorYZ have enzyme activity towards *S*- and *N*-oxides, their physiological functions remain a mystery since their expressions are almost negligible and are negatively dominated by expressions of DmsABC and TorCA, respectively. It is possible that the *ynfEFGH* and *torYZ* operons are evolutionary remains of inefficient enzyme systems that have been functionally replaced by the *dmsABC* and *torCA* gene loci. Even the DmsABC and TorCA enzymes themselves have overlapping abilities to reduce certain *N*-oxides. Such duplicate systems might be a compensatory mechanism established by bacteria such as *E. coli* to survive in environments that limit energy conservation.

	DmsABC	YnfFGH	TorCA	TorYZ
Location of soluble domain	Periplasm	ND	Periplasm	Periplasm
Assembly chaperone	DmsD	ND	TorD	--
Induction of expression	Anaerobiosis (FNR)	Anaerobiosis (FNR)	Anaerobiosis, S- and N-oxides	ND
Reduction of S-oxides	YES	YES	NO	YES
Reduction of N-oxides	YES	YES	YES	YES

Table 2.1. Summary of attributes for the four enzymes discussed in this review. ND: not determined.

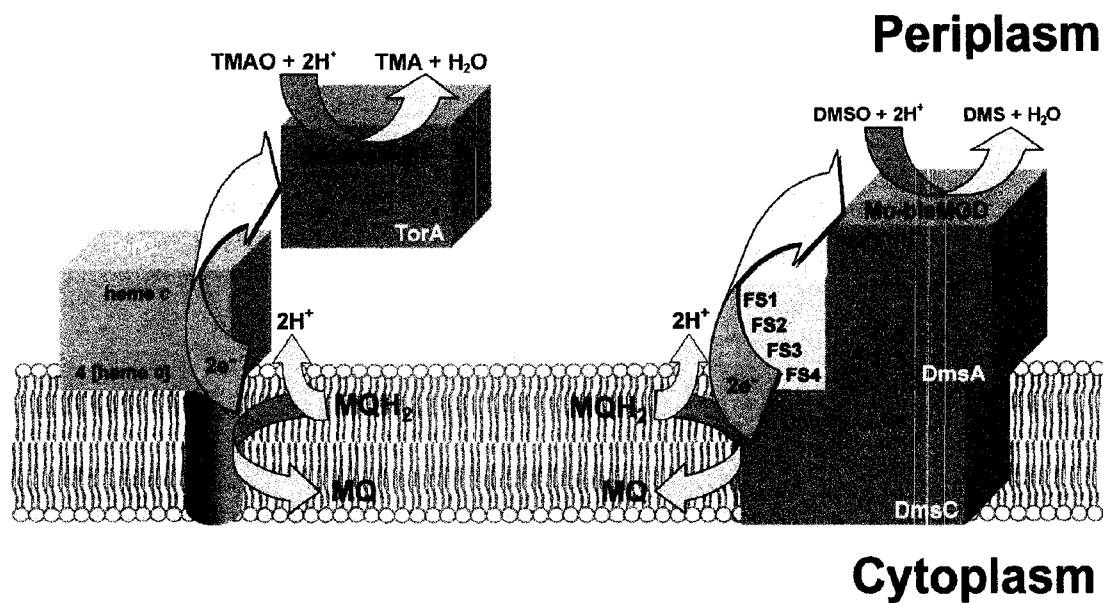


Figure 2.1. A schematic representation of the TMAO and DMSO reductases. MQ and MQH<sub>2</sub> are the oxidized and reduced forms of menaquinol-8. FS1-FS4 are the four [4Fe-4S] clusters in DmsB. The topology of DmsAB is shown oriented towards the periplasm but see text for further discussion.

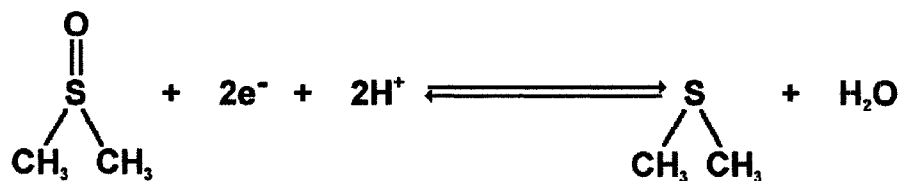


Figure 2.2. The reaction catalyzed by DMSO reductase.

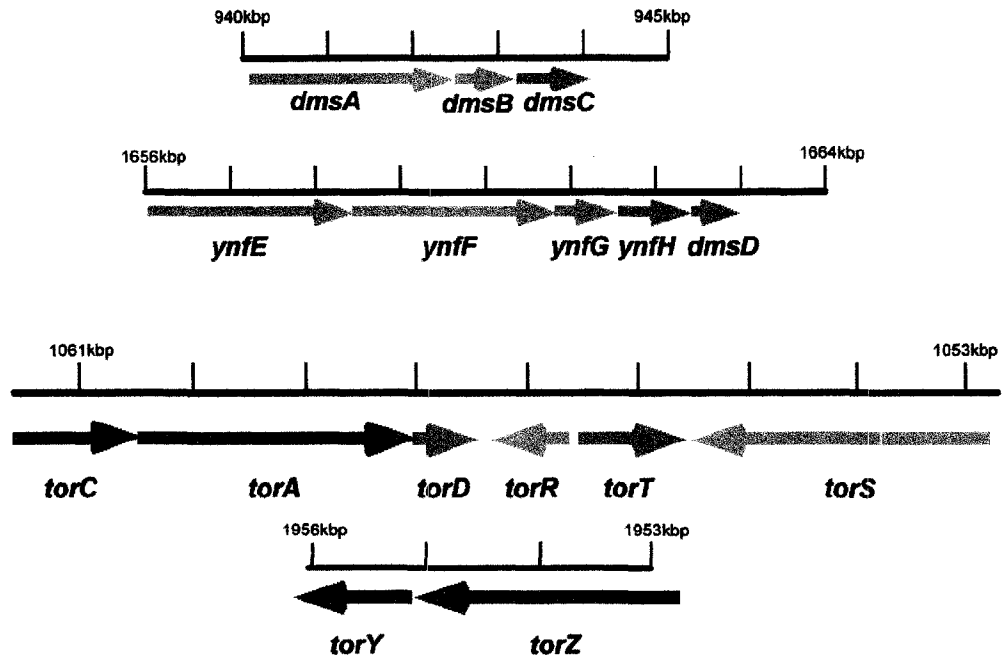


Figure 2.3. Organization of the chromosomal regions encoding *dmsABC*, *ynfEFGHdmsD*, *torCAD*, *torRTS* and *torYZ* operons.

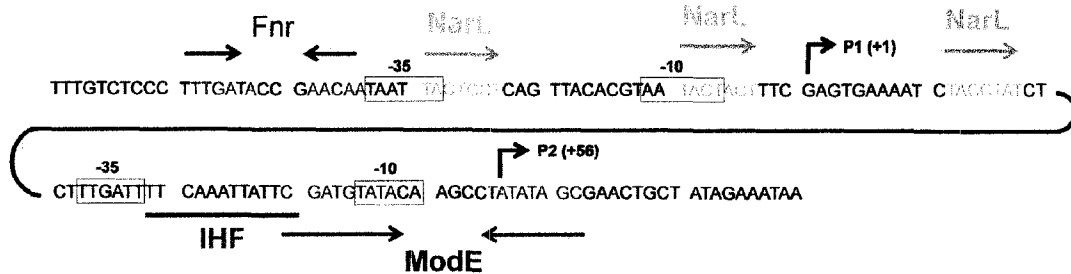


Figure 2.4. Organization of the upstream region preceding *dmsA*. The known promoter P1 is marked as is the putative promoter P2. The -10 and -35 promoter regions are shown in blue boxes. Three direct repeat NarL boxes are noted by the orange arrows. The Fnr box centered at -41.5 is shown in green. The integration host factor consensus sequence is underlined in blue and the ModE consensus is shown in red.

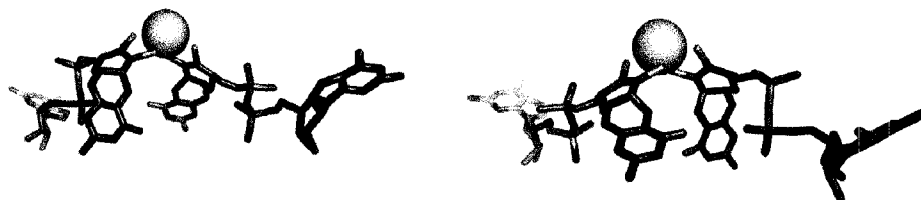


Figure 2.5. Opposite views of the Mo-bisMGD cofactor. The molybdenum is coordinated by two dithiolene sulfurs from each of the two molybdopterin guanine dinucleotides (MGD).

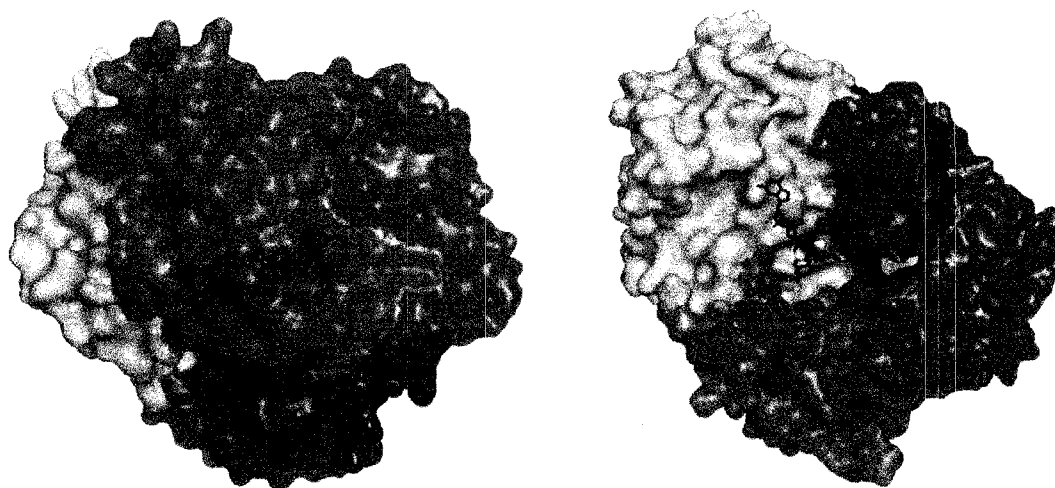


Figure 2.6. Space filling structures (PDB file 3DMR) of DMSO reductase from *Rhodobacter Capsulatus*. The left panel shows a “side” view while right panel shows a “top” view looking into the active site funnel. Domain I, green; Domain II, purple; Domain III, orange; Domain IV, black. The Mo atom is colored yellow while the MGD portions are shown as sticks. Images were generated using PyMol v.0.99 (DeLano Scientific LLC.).

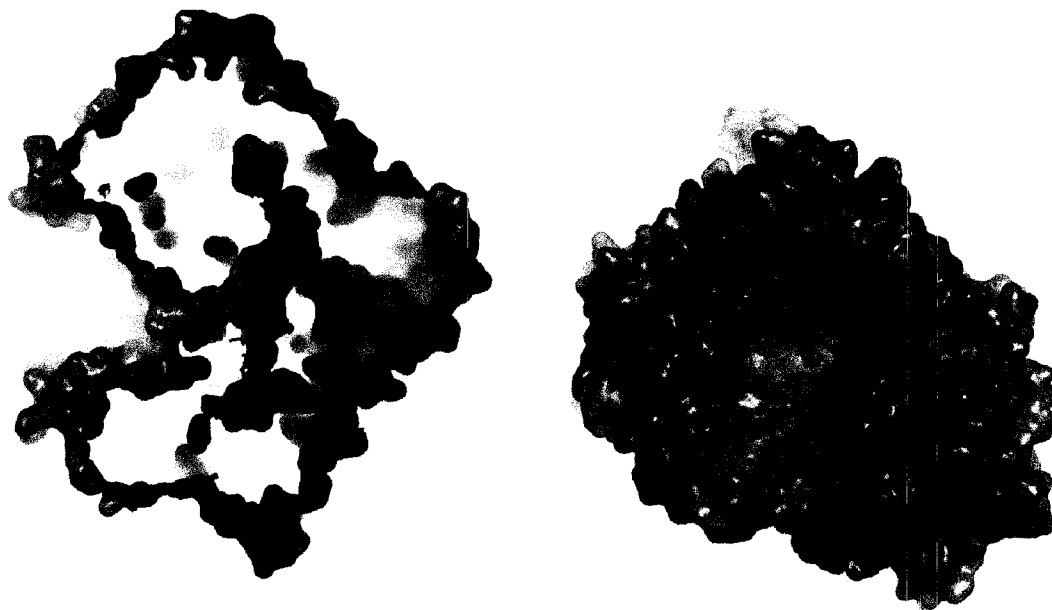


Figure 2.7. The active site funnel in *Rhodobacter capsulatus* DMSO reductase (PDB file 3DMR). Shown in purple are the oxo ligands to the Mo atom. The sliced view on the left shows the active site funnel leading to the Mo-bisMGD cofactor. The view on the right is directed straight into the active funnel to show the accessibility of the Mo-bisMGD. Images were generated using PyMol v.0.99 (DeLano Scientific LLC.).

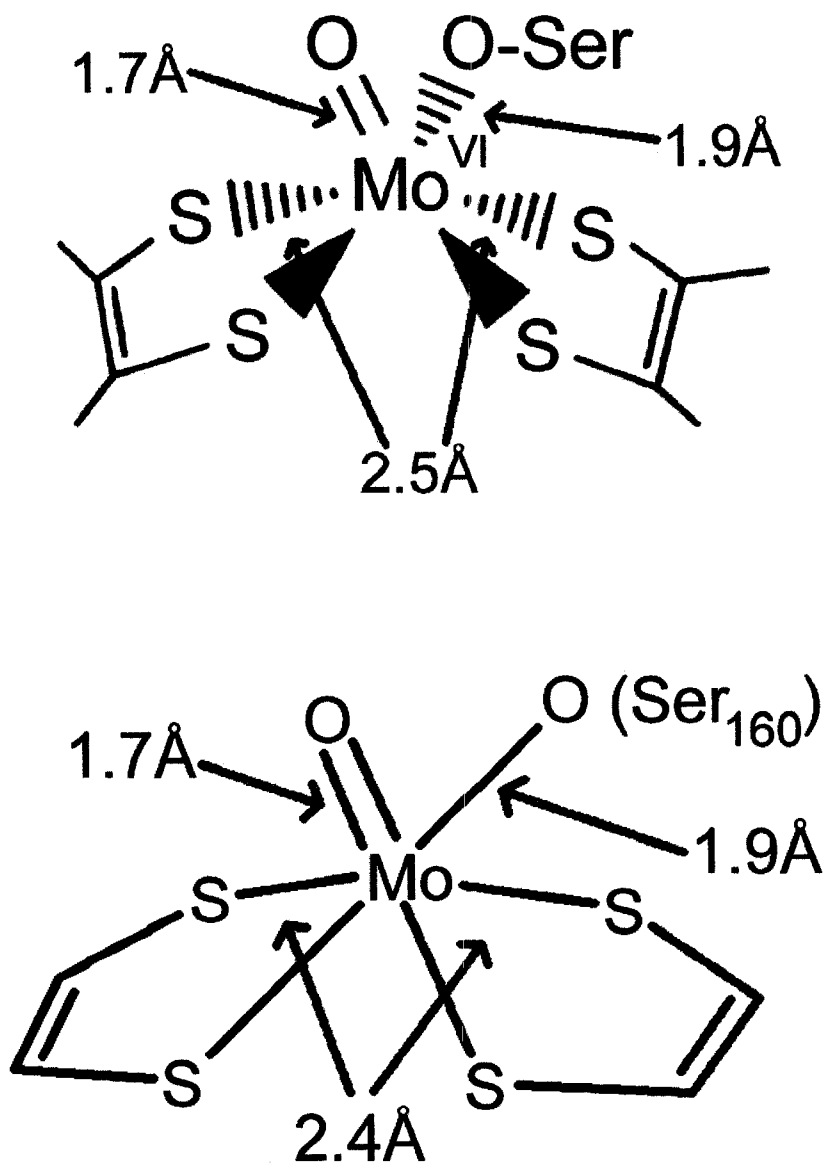


Figure 2.8. Coordination of the Molybdenum atom. Top, chemical structure of the Mo-bisMGD cofactor from *Rhodobacter capsulatus* DMSO reductase in the oxidized form. The Mo atom is coordinated by four dithiolene sulfurs from two molybdopterin molecules, one oxo ligand and the oxygen atom from the sidechain of Serine 147. The bond lengths are taken from (188). Bottom, EXAFS analysis of the active site Mo-bisMGD in *Escherichia coli* DmsA (196).

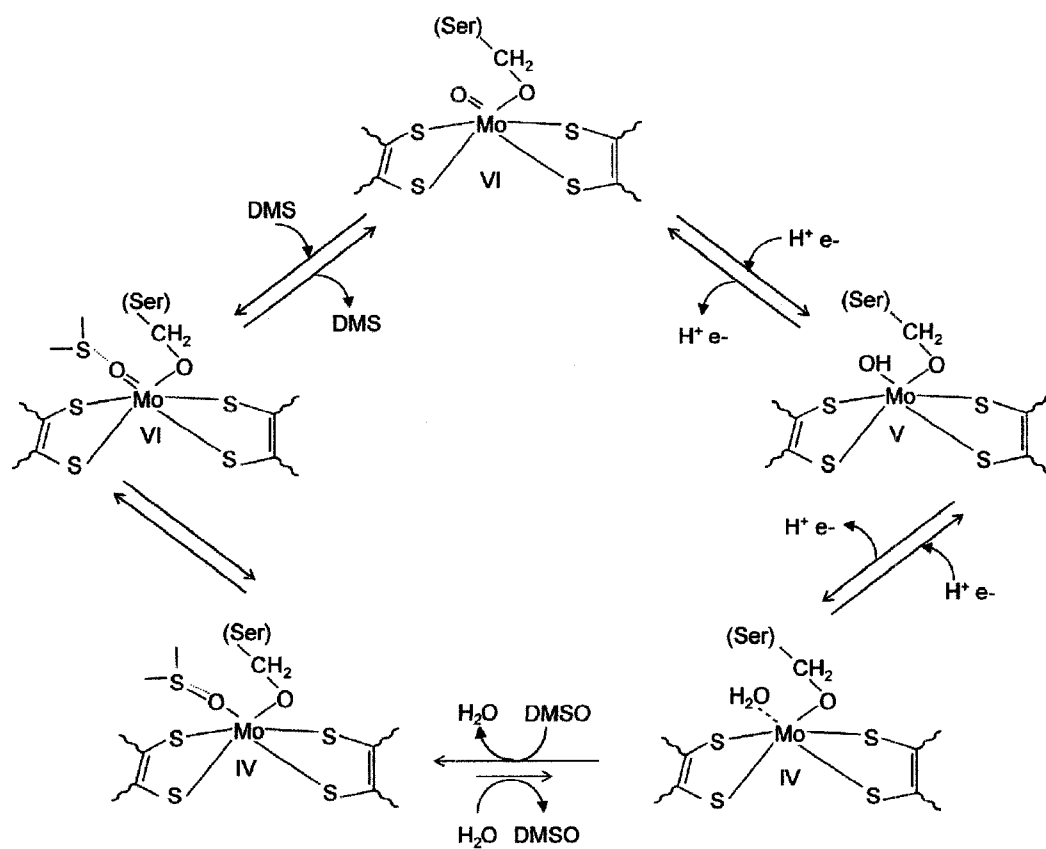


Figure 2.9. Suggested catalytic mechanism for the catalytic cycle of *Rhodobacter* DMSO reductase, as proposed by Johnson *et al* (200).







Figure 2.12. Ribbon model for the structure of *Salmonella typhimurium* DmsD (PDB file 1S9U). Two sulfate molecules (red/yellow) and five Di(hydroxyethyl)ether molecules were cocrystallized. The dotted yellow line shows residues 117 to 122 which are disordered in the crystals. Image was generated using PyMol v.0.99 (DeLano Scientific LLC.).

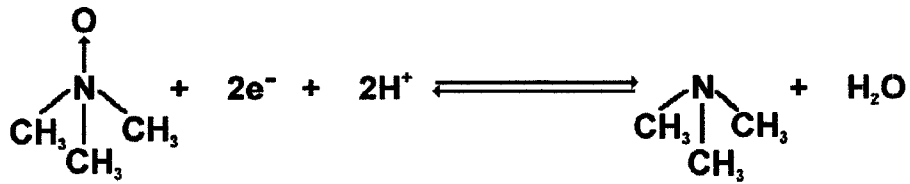


Figure 2.13. The reaction catalyzed by TMAO reductase.

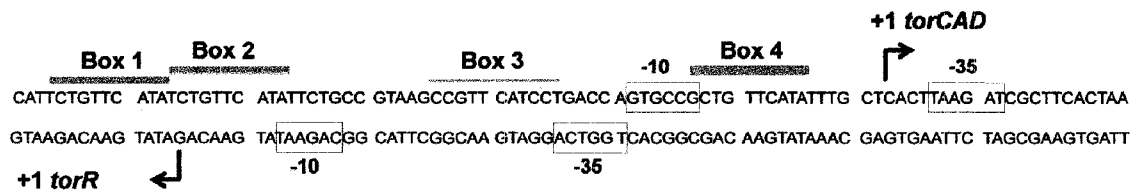


Figure 2.14. Organization of the divergently expressed intragenic region between *torC* and *torR*. The -10 and -35 promoter regions are shown in blue boxes. Four direct decameric *tor* boxes are noted by an orange bar. The thickness of the bar roughly approximates the affinity of TorR for the DNA.

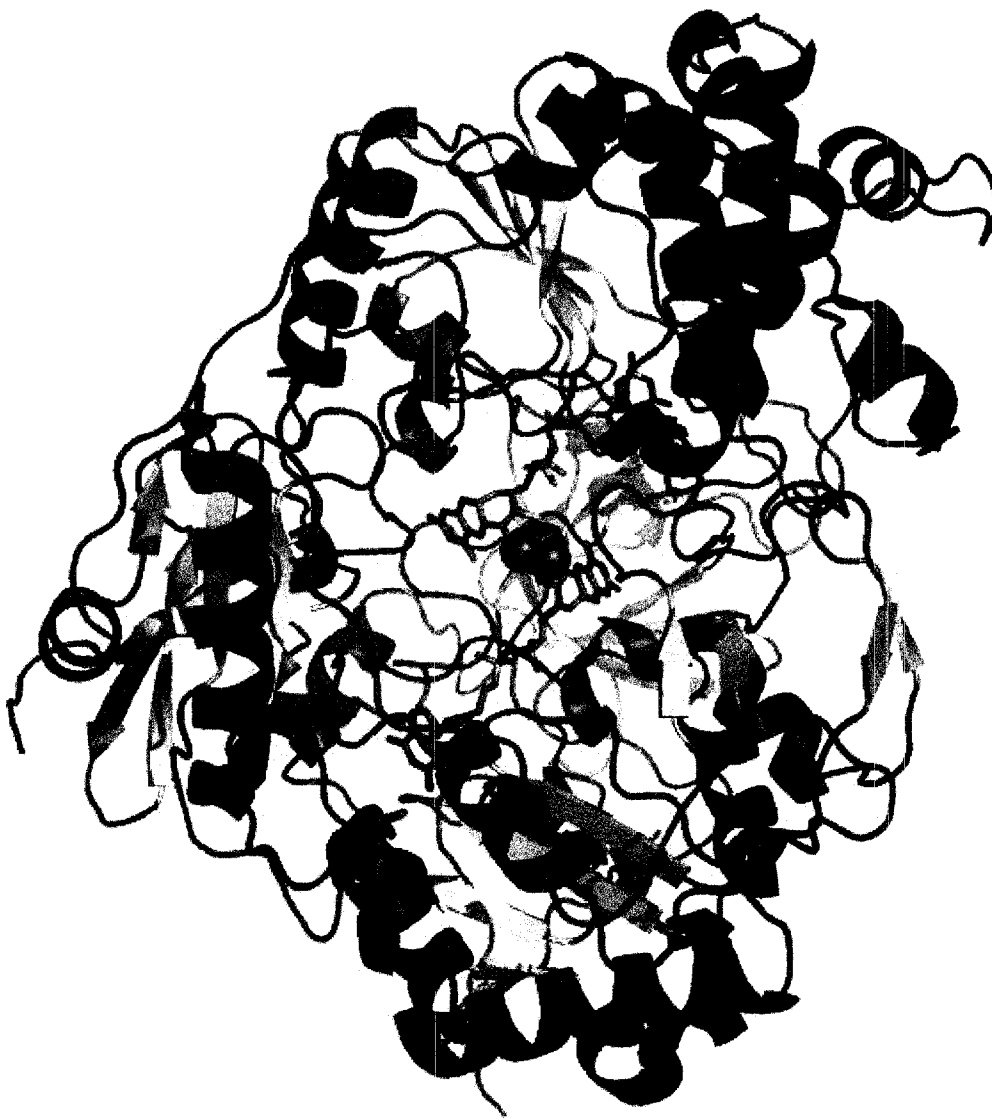


Figure 2.15. The structure of TorA from *Shewanella massilia* (PDB file 1TMO). Two oxo ligands (red), the Mo atom (blue) and the two MGD molecules can be seen when looking directly into the active site. Image was generated using PyMol v.0.99 (DeLano Scientific LLC.).

## **Chapter 3**

### **Investigation of the Environment Surrounding**

#### **Iron-Sulfur Cluster 4 of *Escherichia coli***

#### **Dimethylsulfoxide Reductase**

**A version of this chapter was published:**

**Cheng, V.W.T., Rothery, R.A., Bertero, M.G., Strynadka, N.C. and Weiner,**

**J.H. (2005) *Biochemistry* 44, 8068-77.**

### 3.1 Introduction

DmsABC is an archetype of an important family of bacterial [Fe-S]-molybdoenzymes that includes the *E. coli* formate dehydrogenases (FdnGHI and FdoGHI) (180,309,310), the *E. coli* membrane-bound nitrate reductases (NarGHI and NarZYV) (178,179,311), *Salmonella typhimurium* thiosulfate reductase (PhsABC) (312), and *Wolinella succinogenes* polysulfide reductase (PsrABC) (313,314). Each member of this family has a catalytic subunit containing a molybdenum cofactor in the form of Mo-bisMGD and a [4Fe-4S] cluster (FS0), an electron transfer subunit containing four [Fe-S] clusters (four cluster protein, FCP), and a hydrophobic membrane anchor subunit. The various prosthetic groups of these enzymes catalyze overall reactions that transfer two electrons through the FCP to or from a quinol-binding site (Q-site) that is associated with the membrane anchor domain.

DmsB shows a high degree of homology with FdnH and NarH, both of which are FCP subunits of membrane-bound heterotrimeric redox enzymes that recently have had their x-ray crystallographic structures elucidated to high resolution (178,180). The four [Fe-S] clusters of these subunits are arranged in an almost linear fashion that facilitates electron shuttling between the active site and the Q-site, and are called FS1 (closest to catalytic subunit), FS2, FS3, and FS4 (closest to the Q-site). The four [4Fe-4S] clusters in DmsB have midpoint potentials ( $E_m$  values) of -50mV (FS4), -120mV (FS3), -330mV (FS2), and -240mV (FS1) (212,213). NarH contains three [4Fe-4S] clusters and one [3Fe-4S] cluster, with  $E_m$  values of +180mV (FS4, [3Fe-4S] cluster), -50mV (FS3), -420mV (FS2), and +130mV (FS1) (179,315,316). Thus, the profiles of the  $E_m$  values are quite

similar for DmsB and NarH (Figure 3.1). The  $E_m$  values for the [4Fe-4S] clusters of FdnH have yet to be determined.

In addition to DmsABC and NarGHI, a number of *E. coli* respiratory chain enzymes containing [Fe-S] clusters have been examined in detail by redox potentiometry, including menaquinol:fumarate oxidoreductase (FrdABCD) (317,318) and succinate:ubiquinone oxidoreductase (SdhCDAB) (319). Two aspects of the redox potentiometry of [Fe-S] clusters are under intense study: (i) the role of the  $E_m$  value in defining the electron transfer rates through a string of clusters (19,320,321); and (ii) the role of the coordination environment in defining the  $E_m$  value (322,323). A number of factors have been proposed to control [Fe-S] cluster  $E_m$ , including: (i) the local hydrogen bonding network, (ii) the local electrostatic field, (iii) solvent accessibility, and (iv) backbone amides (322-328). DmsABC is a model enzyme in which we can evaluate factors that may modulate [Fe-S] cluster  $E_m$  values and inter-center electron transfer rates.

One fundamental difference between FdnGHI/NarGHI and DmsABC is the presence of *b*-type hemes in the transmembrane subunits of the former enzymes and the absence of heme in the latter enzyme. Thus in DmsABC, there is a direct transfer of electrons from MQH<sub>2</sub> to FS4 (211) in a manner similar to that observed for the transfer of electrons from the Q<sub>p</sub> site to the [3Fe-4S] cluster of FrdABCD (216,329,330). In the structure of FdnH, the sidechain of a conserved Tyr residue is pointing towards the FdnI subunit and interacts with the proximal heme. Since DmsABC does not contain heme, we hypothesize that the equivalent residue in DmsB (Tyr104) may play an important role in MQH<sub>2</sub> binding and oxidation, and may be critical in directing electrons from MQH<sub>2</sub> to

FS4. A related question arises regarding the role of heme(s) in the family of FrdABCD/SdhCDAB enzymes in different organisms, wherein zero, one, or two hemes may be present in the membrane anchor domain (330,331).

In this study, we have investigated the role of the protein environment in influencing the redox properties of the FS4 cluster of DmsB by using a combination of site-directed mutagenesis, redox potentiometry, and EPR spectroscopy. In order to eliminate spectral complications arising from spin-spin interactions between multiple reduced [4Fe-4S] clusters of DmsB, we have evaluated the effects of point mutations in a DmsB<sup>C102S</sup> mutant that contains a high potential [3Fe-4S] FS4 cluster (FS4<sup>[3Fe-4S]</sup>) that is magnetically isolated in its oxidized form. We have also evaluated the effects of the mutants on MQH<sub>2</sub> binding and on the kinetics of the enzyme containing the native [4Fe-4S] cluster form of FS4 (FS4<sup>[4Fe-4S]</sup>). These studies will aid in generating an understanding of the factors controlling the  $E_m$  of [Fe-S] clusters and their effects on the electron transfer rate.

### 3.2 Experimental Procedures

*Homology Modeling.* Sequence identity searches were conducted with the BLAST program (332). Threading calculations were performed with the program MODELLER 6.0a (333) using the *E. coli* FdnH structure as the template (PDB code 1KQF). The quality of the DmsB model was validated with the program PROCHECK (334). The model generated represents 84.6% of the residues in most favorable regions, 13.3% in additional allowed regions, and 2.1% in generously allowed regions.



*Bacterial Strains and Plasmids* - The *E. coli* strains used in this study include HB101 (*supE44 hsdS20 (r<sub>B</sub>-m<sub>B</sub>-) recA13 ara-14 proA2 lacY1 galK2 rpsL20 xyl-5 mtl-1*; lab collection), TG1 (*supE hsdΔ5 thi Δ(lac-proAB) F'*[*traD36 proAB<sup>+</sup> lacI<sup>q</sup> lacZΔM15*]; Amersham Biosciences), DSS301 (TG1,  $\Delta$ *dmsABC*; lab collection (238), and TOPP2 (*rif<sup>r</sup> [F', proAB, lacI<sup>q</sup>ZΔM15, Tn10,(tet<sup>r</sup>)]*; Stratagene). The plasmids used for cloning and expression include pBR322 (Tet<sup>R</sup>Amp<sup>R</sup>; Pharmacia), pTZ18R (Amp<sup>R</sup>*lacZ'*; Pharmacia), pDms160 (*dmsABC* cloned into EcoRI-Sall fragment of pBR322; lab collection (211)), pDms170 (pDms160 derivative; lab collection (210)), pBTZ (EcoRI-SacI fragment of pDms160 cloned into pTZ18R; this study), and pBTZ1021 (EcoRI-SacI fragment of pDms160 encoding the DmsB<sup>C102S</sup> mutation (211) cloned into pTZ18R; this study).

*Cloning* - Mutagenic oligonucleotides were designed with the addition/deletion of restriction sites in the DNA sequence to facilitate the screening process, and were purchased from Sigma Canada. Mutants were generated using the QuickChange Site-Directed Mutagenesis kit from Stratagene, with the pBTZ and pBTZ1021 plasmids as templates for the QuickChange reactions. DpnI was purchased from Invitrogen, and DNA purification kits were purchased from Qiagen. Mutants were verified by DNA sequencing (DNA core facility, Department of Biochemistry, University of Alberta), and cloned back into the pDms160 expression vector. The mutant plasmids were then transformed into both *E. coli* HB101 and DSS301 for biochemical studies. Preparation of competent cells and transformations of plasmids into competent cells were carried out as described in *Molecular Cloning: A Laboratory Manual* (335).

*Growth of Bacteria* - Variants of the expression plasmid pDms160 containing the desired DmsB mutations were transformed into DSS301 cells. The ability of the mutant

enzymes to support respiratory growth using DMSO was evaluated by growing the cells anaerobically at 37°C in glycerol-DMSO minimal medium and monitoring cell turbidity using a Klett-Summerson spectrophotometer equipped with a No. 66 filter as previously described (336). For preparation of membranes, HB101 cells were allowed to grow anaerobically for 48 hours in 19L glycerol-fumarate medium whereas DSS301 cells were grown for 24 hours in 1L glycerol-fumarate medium (211).

*Preparation of Membranes* - Membranes were prepared by French pressure cell lysis and differential centrifugation as previously described (213). Essentially, cells were pelleted and concentrated, washed and resuspended in 50mM MOPS / 5mM EDTA buffer (pH 7). Cells were French pressed after adding dithiothreitol and phenylmethanesulfonyl fluoride (PMSF) to final concentrations of 1mM and 0.2mM, respectively. Membranes were washed and pelleted by centrifugation in a Beckman 50.2Ti rotor at 150,000g for 90 minutes, then homogenized in 50mM MOPS / 5mM EDTA buffer (or 100mM MOPS / 5mM EDTA buffer for EPR samples) and flash frozen with liquid N<sub>2</sub>. Protein concentrations were determined by a modified Lowry assay containing 1% (w/v) SDS (337).

*Enzyme Assays* - The benzyl viologen (BV<sup>+</sup>)-dependent reduction of trimethylamine *N*-oxide (TMAO) has been previously described (213). The extinction coefficient of BV<sup>+</sup> is 7.4 mmol<sup>-1</sup> cm<sup>-1</sup>, measured at its absorbance maximum of 570nm. The lapachol (LPCH<sub>2</sub>)-dependent anaerobic reduction of TMAO has also been previously described (229). The extinction coefficient for LPCH<sub>2</sub> is 2.66 mmol<sup>-1</sup> cm<sup>-1</sup>, measured at a wavelength of 481nm.

*HOQNO Fluorescence Quench (FQ) Titrations* - 2-*n*-heptyl-4-hydroxyquinoline-*N*-oxide (HOQNO) binding was monitored by fluorescence according to van Ark and Berden (338). 2 $\mu$ L aliquots of 0.1mM HOQNO were added to the sample, and fluorescence was measured at an excitation wavelength of 341nm and an emission wavelength of 479nm. The experiment was carried out at protein concentrations of 0.25, 0.50, and 0.75 mg mL<sup>-1</sup>. The concentration of HOQNO binding sites and the dissociation constant of HOQNO were estimated by fitting the data according to Okun *et al.* (339) using the equation:

$$F_{\text{obs}} = (f_{\text{bound}} - f_{\text{free}}) \times \{ Q - (Q^2 - n_s[E_{\text{tot}}] \times [I_{\text{tot}}])^{1/2} \} + f_{\text{free}} \times [I_{\text{tot}}]$$

$$\text{with } Q = 0.5 \times ([I_{\text{tot}}] + K_d + n_s \times [E_{\text{tot}}]) \quad \text{and} \quad [I_{\text{tot}}] = [I_{\text{bound}}] + [I_{\text{free}}]$$

The terms  $f_{\text{bound}}$  and  $f_{\text{free}}$  refer to the fluorescence of bound and free HOQNO respectively ( $f_{\text{bound}}$  is zero for HOQNO).  $[I_{\text{tot}}]$ ,  $[I_{\text{bound}}]$ , and  $[I_{\text{free}}]$  are the concentrations of total, bound, and free HOQNO, respectively.  $[E_{\text{tot}}]$  is the total concentration of enzyme (given as nmol DmsABC / mg total protein in Table 2) and  $n_s$  is the number of inhibitor binding sites (For DmsABC,  $n_s = 1$ ) (221).

*EPR Spectroscopy* - Membrane vesicles were prepared in 100mM MOPS / 5mM EDTA (pH 7) buffer to a final protein concentration of approximately 30mg mL<sup>-1</sup>. Membranes were prepared in 100mM MES / 5mM EDTA (pH 6) and 100mM acetate / 5mM EDTA (pH 5) for pH studies. Redox titrations were carried out at 25°C under argon in an anaerobic chamber as previously described (212,316), and the following redox dyes were added to a final concentration of 50 $\mu$ M: quinhydrone ( $E_{m,7} = +286\text{mV}$ ), 2,6-dichloroindophenol ( $E_{m,7} = +217\text{mV}$ ), 1,2-naphthoquinone ( $E_{m,7} = +125\text{mV}$ ), toluylene blue ( $E_{m,7} = +115\text{mV}$ ), phenazine methosulfate ( $E_{m,7} = +80\text{mV}$ ), thionine ( $E_{m,7} =$

+60mV), duroquinone ( $E_{m,7} = +7\text{mV}$ ), methylene blue ( $E_{m,7} = -11\text{mV}$ ), resorufin ( $E_{m,7} = -50\text{mV}$ ), indigotrisulfonate ( $E_{m,7} = -80\text{mV}$ ), indigodisulfonate ( $E_{m,7} = -125\text{mV}$ ), anthraquinone-2-sulfonic acid ( $E_{m,7} = -225\text{mV}$ ), phenosafranine ( $E_{m,7} = -255\text{mV}$ ), benzyl viologen ( $E_{m,7} = -360\text{mV}$ ), and methyl viologen ( $E_{m,7} = -440\text{mV}$ ). All samples were prepared in 3mm internal diameter quartz EPR tubes and were rapidly frozen in liquid nitrogen-chilled ethanol before storing in liquid nitrogen. EPR spectra were recorded using a Bruker Elexsys E500 EPR spectrometer equipped with an Oxford Instruments ESR900 flowing helium cryostat. Instrument conditions and temperatures are described in the individual figure legends, and spectra were corrected for tube calibration. EPR studies were only carried out on enzymes which have both the desired mutation in DmsB and the DmsB<sup>C102S</sup> mutation so that a magnetically isolated oxidized [3Fe-4S] signal can be observed.

### 3.3 Results

*Selection of Residues for Mutagenesis.* Both *E. coli* FdnH and DmsB contain four [Fe-S] clusters which are coordinated by four ferredoxin-like Cys motifs (340). Alignment of DmsB with FdnH reveals 37% sequence identity between the two proteins. A significant difference between the two is that FdnH has a transmembrane C-terminal tail (180) whereas DmsB is predicted to be entirely membrane-extrinsic (238). A ClustalW alignment of the local amino acids from FdnH and DmsB immediately surrounding FS4 shows significant sequence similarity and inferred structural similarity (Fig. 3.2). To aid in the selection of targets for mutagenesis and subsequent analysis, a structural model of DmsB was generated with the program MODELLER 6.0 (333) using

the FdnH 1.6Å resolution X-ray crystal structure as the template. The amino acid residues in DmsB which were subjected to site-directed mutagenesis studies are indicated in Figures 3.2 and 3.3. These were chosen on the basis of their proximity (<10Å) to FS4 in the FdnH structure and in the DmsB model. A variety of charged, apolar, and aromatic residues were selected for site-directed mutagenesis studies. Figure 3.4 shows an overlay of the DmsB model with the FdnH structure. The DmsB model superimposes onto the FdnH structure with a root mean square deviation (rmsd) of 0.636Å for 151 common C-α atoms.

*Expression of DmsB Mutants.* Mutants of DmsABC were evaluated for their ability to support anaerobic growth in glycerol-DMSO minimal medium (Table 3.1). *E. coli* DSS301 cells ( $\Delta dmsABC$ ) transformed with plasmids encoding the DmsAB<sup>P80A</sup>C, DmsAB<sup>D95A</sup>C, DmsAB<sup>D97A</sup>C, and DmsAB<sup>Y104A</sup>C mutants exhibit shorter doubling times (3.0 to 4.2 hours) than the wild-type enzyme (6.3 hours), whereas cells transformed with plasmids encoding the DmsAB<sup>H85F</sup>C, DmsAB<sup>H85T</sup>C, DmsAB<sup>R103A</sup>C, DmsAB<sup>H106A</sup>C, and DmsAB<sup>H106E</sup>C mutants have longer doubling times (8.5 to 12.4 hours). The increased and decreased rates of growth of the aforementioned DmsB mutants can be correlated with the amount of DmsABC protein targeted to the membrane as determined by SDS-PAGE and immunoblotting (data not shown), as well as with the BV<sup>+</sup>:DMSO specific enzyme activities observed (Table 3.1). Enzyme expression levels also agree with the FQ data on membranes prepared from *E. coli* HB101 (see below, Table 3.2); FQ titrations were not carried out for mutants expressed in DSS301 due to the high level of expression of fumarate reductase in this strain. Cells transformed with plasmids encoding the DmsAB<sup>P80H</sup>C, DmsAB<sup>P80D</sup>C, DmsAB<sup>S81G</sup>C, DmsAB<sup>S81H</sup>C, and DmsAB<sup>Y104D</sup>C mutants

are unable to support anaerobic growth in glycerol-DMSO. DSS301 cells expressing the DmsAB<sup>Y104E</sup>C mutant show a much longer doubling time (~20 hours) compared to DSS301 expressing the wild-type enzyme. For mutants that do not support growth, mutant enzymes are still observed in membrane preparations as detected by immunoblotting (data not shown) and the presence of BV<sup>+</sup>:TMAO activities (Table 3.1).

*Enzyme Activities of wild-type and mutant DmsABC.* Membrane preparations from *E. coli* DSS301 harboring the mutant plasmids were tested for their ability to accept electrons from either BV<sup>+</sup> or LPCH<sub>2</sub>, and transfer them to TMAO (Table 3.1). The BV<sup>+</sup>:TMAO assay detects whether DmsAB is assembled and is independent of a functional Q-site within DmsC, whereas the LPCH<sub>2</sub>:TMAO assay requires a functional heterotrimer. A comparison of the BV<sup>+</sup>:TMAO activity to the LPCH<sub>2</sub>:TMAO activity can then be used to examine electron transfer from the Q-site to FS4 since such a ratio is independent of the amount of enzyme in the preparation and is therefore an intrinsic property of the DmsABC variant in question. In general, the levels of BV<sup>+</sup>:TMAO specific activities correlate closely to the amount of mutant enzyme expressed in the cytoplasmic membrane, as determined by SDS-PAGE and immunoblotting (data not shown), as well as FQ titrations with HOQNO (see below, Table 3.2). Comparison of the ratios of BV<sup>+</sup>:TMAO activity to LPCH<sub>2</sub>:TMAO activity indicates that the majority of DmsB mutants have ratios of approximately 35, which is equivalent to that of the wild-type enzyme. The DmsAB<sup>P80A</sup>C and DmsAB<sup>Y104A</sup>C mutants however, have ratios of 149 and 92 respectively, which are dramatically higher than that of the wild-type enzyme. These two mutants also exhibit an altered K<sub>m</sub> value for lapachol. The K<sub>m</sub> values for LPCH<sub>2</sub> of the wild-type, the DmsAB<sup>P80A</sup>C mutant and the DmsAB<sup>Y104A</sup>C mutant are

approximately 100 $\mu$ M, 47 $\mu$ M and 210 $\mu$ M, respectively. The corresponding  $k_{\text{cat}}$  values are approximately 64 s<sup>-1</sup>, 79 s<sup>-1</sup>, and 114 s<sup>-1</sup>, respectively.

*HOQNO FQ Titrations.* HOQNO is a MQH<sub>2</sub> analog inhibitor whose fluorescence in solution is quenched when bound to DmsABC (221). FQ titrations were carried out at three different enzyme concentrations to accurately estimate the affinity of the enzyme for HOQNO ( $K_d$  values) and the concentration of binding sites (Table 3.2). Mutations of K77, H85, D95, D97, R103, and H106 in DmsB do not affect the affinity of the enzyme for HOQNO; however, residues P80, S81 and Y104 appear to play an important role in defining the HOQNO binding site. The mutations DmsB<sup>P80A</sup>, DmsB<sup>P80D</sup> and DmsB<sup>P80H</sup> increase the  $K_d$  for HOQNO from 5nM to 10nM, 17nM, and 20nM respectively; mutations of DmsB<sup>S81G</sup> and DmsB<sup>S81H</sup> both increase the  $K_d$  to 20nM. Interestingly, the DmsB<sup>Y104A</sup> mutant has the same affinity for HOQNO as the wild-type enzyme, whereas the DmsB<sup>Y104D</sup> mutation increases the  $K_d$  to 10nM and the DmsB<sup>Y104E</sup> mutation increases the  $K_d$  to 18nM. The DmsB<sup>C102S</sup> mutant does not affect HOQNO binding, but the DmsB<sup>C102W</sup> mutant increases the  $K_d$  to 17nM. These results support the assertion that the function of FS4 is closely coupled to that of a dissociable Q-site within the DmsC subunit (see Discussion) (212).

*Modulation of the [3Fe-4S]  $E_m$  value.* FS4<sup>[4Fe-4S]</sup> of DmsB can be converted to a [3Fe-4S] form (FS4<sup>[3Fe-4S]</sup>) by mutagenesis of DmsB<sup>C102</sup> to a range of alternative residues (211). In a DmsB<sup>C102S</sup> mutant, FS4<sup>[3Fe-4S]</sup> has an  $E_m$  of +275mV compared to a value of -50mV for FS4<sup>[4Fe-4S]</sup> of the wild-type enzyme (212). The high potential of FS4<sup>[3Fe-4S]</sup> renders its EPR spectrum free from overlapping signals arising from the other three [4Fe-4S] clusters of DmsB (FS1-3), and also from complications arising from spin-spin

interactions with these centers. This greatly simplifies analyses of the effects that the DmsB mutants have on the EPR lineshape and the  $E_m$  value. Double mutants were therefore made which contained the mutation of interest and the DmsB<sup>C102S</sup> mutation. Potentiometric titrations of DmsB double mutants were performed and the intensities of the  $g=2.03$  peaks were plotted versus the ambient redox potential. The Nernst equation was used to fit the data points, and the resultant  $E_m$  values are shown in Table 3.3. FS4<sup>[3Fe-4S]</sup> of the DmsB<sup>C102S</sup> single mutant has an  $E_m$  of +275mV, which agrees with the previously reported value (211). In general, mutations of positively charged residues to apolar and non-charged residues cause a small  $\Delta E_m$  of approximately -15 to -25mV for FS4<sup>[3Fe-4S]</sup>. Mutations of acidic residues to alanine residues do not affect the  $E_{m,7}$  of the [3Fe-4S] cluster. The DmsB<sup>C102S/Y104E</sup> mutant causes a large  $\Delta E_m$  from +275mV to +145mV. A similar mutant, DmsB<sup>C102S/Y104D</sup>, also causes a large  $\Delta E_m$  from +275mV to +150mV. Another mutant, DmsB<sup>C102S/Y104E/H106F</sup>, exhibits an  $E_m$  of +130mV for FS4<sup>[3Fe-4S]</sup>.

*Effects of HOQNO and pH on FS4.* Expression of the mutants in *E. coli* TOPP2 reaches levels at which EPR spectra of oxidized inner membranes are dominated by the spectrum of FS4<sup>[3Fe-4S]</sup>. Incubation of oxidized DmsAB<sup>C102S</sup>C mutant enzyme with HOQNO (five times molar excess) elicits a lineshape change that is manifested by a shift in the position of the  $g_{xy}$  feature of the FS4<sup>[3Fe-4S]</sup> EPR spectrum (Figures 3.5C & D) (211). The DmsB<sup>C102S/Y104D</sup> and DmsB<sup>C102S/Y104E</sup> mutations have negligible effects on the EPR lineshape of FS4<sup>[3Fe-4S]</sup> (Figures 3.5E & G). Although HOQNO binding was observed for these two mutants in FQ titrations, it did not elicit the expected change in their oxidized FS4<sup>[3Fe-4S]</sup> spectra (Figures 3.5F & H). Preliminary studies with a



DmsB<sup>Y104W</sup> mutant show that its  $g_{xy}$  feature of the FS4<sup>[3Fe-4S]</sup> spectrum can be shifted upfield in the presence of HOQNO despite having a lower affinity for the inhibitor (unpublished data). This suggests that an aromatic residue is essential for the observation of an HOQNO-induced EPR lineshape change.

The potentiometric effect of acidic substitutions of DmsB<sup>Y104</sup> on the  $E_m$  of FS4<sup>[3Fe-4S]</sup> (a large  $-\Delta E_m$ ) and the retention of high-affinity HOQNO binding prompted us to evaluate the potentiometric effects of inhibitor binding on the DmsB<sup>C102S/Y104D</sup> mutant. In the presence of 50 $\mu$ M HOQNO, the  $E_m$  of the DmsB<sup>C102S</sup> single mutant remains unaltered ( $E_m = +275$ mV). However, when a potentiometric titration is performed on the DmsB<sup>C102S/Y104D</sup> mutant in the presence of HOQNO, the  $E_m$  of the FS4<sup>[3Fe-4S]</sup> cluster is increased from +150mV to +230mV (Figure 3.6). Given the inability of HOQNO to increase the  $E_m$  of FS4<sup>[3Fe-4S]</sup> in the DmsB<sup>C102S</sup> mutant, we determined if a decrease in pH can bring about a corresponding increase in  $E_m$  in this particular mutant. In pH studies, the  $E_{m,7}$ ,  $E_{m,6}$ , and  $E_{m,5}$  of the FS4<sup>[3Fe-4S]</sup> in the DmsB<sup>C102S</sup> mutant remain relatively unchanged at +275mV, +295mV, and +277mV, respectively. Interestingly, by lowering the  $E_{m,7}$  of FS4 to +150mV via the DmsB<sup>C102S/Y104D</sup> mutation, the  $E_m$  of the cluster becomes dependent on pH and the  $E_{m,6}$  and  $E_{m,5}$  are approximately +165mV and +200mV, respectively.

### 3.4 Discussion

By constructing and utilizing a model of DmsB based on the crystal structure of FdnH, we have identified the amino acids which are in close proximity to FS4, the [4Fe-4S] cluster closest to the membrane anchor subunit. This region of DmsABC is of interest

because, unlike NarGHI and FdnGHI, DmsABC lacks heme in its membrane anchor subunit and the Q-site must communicate directly with FS4. To investigate the role of these amino acids, we examined the enzymatic activity, HOQNO binding and the redox properties of FS4 using a site-directed mutagenesis approach. We found that electron transfer from the MQH<sub>2</sub> binding site to the [Fe-S] clusters of DmsB is affected in the DmsB<sup>P80</sup>, DmsB<sup>S81</sup> and DmsB<sup>Y104</sup> mutants. Q-site and FS4<sup>[3Fe-4S]</sup> mutants of DmsABC do not affect the ability of DmsABC to accept electrons from BV<sup>+</sup>, but hinder its ability to accept electrons from the MQH<sub>2</sub> analog LPCH<sub>2</sub> (211,212,220). The ratio of BV<sup>+</sup>:TMAO to LPCH<sub>2</sub>:TMAO activities were not altered significantly in the DmsB<sup>D95A</sup> and DmsB<sup>D97A</sup> mutants, indicating the lack of effect of these mutants on electron transfer from the Q-site to FS4. However, both BV<sup>+</sup>:TMAO and LPCH<sub>2</sub>:TMAO activities of these two mutants are higher than those of the wild-type enzyme by approximately five-fold; this is caused, in part, by the increased expression of the DmsB<sup>D95A</sup> and DmsB<sup>D97A</sup> mutants, as supported by the FQ data (Table 3.2) and immunoblotting (data not shown). Thus the removal of an acidic residue near the DmsB-DmsC interface seems to allow either increased assembly of DmsABC and/or decreased degradation of DmsABC, as well as increasing the rate of electron flux through DmsB. Because the ratio of BV<sup>+</sup>:TMAO to LPCH<sub>2</sub>:TMAO activities is an intrinsic property of the enzyme and is independent of the amount of enzyme in a given preparation, the increased ratios for the DmsAB<sup>P80A</sup>C and DmsAB<sup>Y104A</sup>C mutant enzymes strongly indicate an impediment of electron transfer from the Q-site to FS4. To examine the redox properties of these mutations, we utilized a DmsB<sup>C102S</sup> mutation that converts FS4 from a [4Fe-4S] cluster (FS4<sup>[4Fe-4S]</sup>) to a [3Fe-4S] cluster (FS4<sup>[3Fe-4S]</sup>) that is EPR-visible and magnetically

isolated in its oxidized form. In the corresponding double mutants (DmsB<sup>C102S/P80A</sup> and DmsB<sup>C102S/Y104A</sup>), the  $E_m$  of the FS4<sup>[3Fe-4S]</sup> cluster remains unchanged at approximately +275mV. Given that the  $E_m$  of FS4<sup>[4Fe-4S]</sup> remains unchanged in the single mutants, we surmise that the rate of electron transfer through the cofactors in DmsB is most likely unaffected in these mutants, but communication between the MQH<sub>2</sub> binding site and FS4 is disrupted.

The altered enzyme kinetics in the DmsAB<sup>P80A</sup>C and DmsAB<sup>Y104A</sup>C mutants suggest that these two residues play an important role in enzyme turnover. When the DmsB<sup>P80</sup> residue is changed to residues which have larger side chains, MQH<sub>2</sub> is either unable to bind or cannot be oxidized, and electrons are not transferred from the Q-site to FS4. This phenomenon also holds true for the DmsB<sup>S81G</sup>, DmsB<sup>S81H</sup>, DmsB<sup>C102W</sup>, and DmsB<sup>Y104D</sup> mutants. These mutations may distort the Q-site architecture by directly disrupting ligand interaction(s) or by indirectly altering the conformation of DmsC such that the Q-site is altered. Not only can distortions of the Q-site lead to lowered affinity of the enzyme for MQH<sub>2</sub>, but it can also affect MQH<sub>2</sub> oxidation by displacing key residues involved in the catalytic cycle. This is not surprising since the three residues in FdnH corresponding to DmsB<sup>P80</sup>, DmsB<sup>S81</sup>, and DmsB<sup>Y104</sup> are located at the interface between the soluble dimer and the membrane anchor subunit in the FdnGHI structure (Figure 3.3) (180). In fact, the equivalent Tyr residue in FdnH directly interacts with the proximal heme of FdnI. The absence of heme in DmsC suggests that MQH<sub>2</sub> donates electrons directly to FS4 in a manner essentially identical to that seen in *E. coli* fumarate reductase where electrons are donated directly from the Q<sub>p</sub>-site to the electron transfer subunit (216,227,329,330). The difference in HOQNO binding affinity between the DmsB<sup>C102S</sup>

( $K_d=5\text{nM}$ ) and DmsB<sup>C102W</sup> ( $K_d=17\text{nM}$ ) mutants implies that the Trp sidechain sterically hinders a Q-site located in the DmsB-DmsC interface region. Examination of the NarGHI structure lends support to this suggestion (178); the indole sidechain of NarH<sup>W220</sup> points towards the proximal heme ( $b_p$ ) of NarI within the NarH-NarI interface region. In the crystal structure of SdhCDAB, the equivalent proline residue (SdhB<sup>P160</sup>) at the SdhB-SdhCD interface is shown to be one of two residues that “sandwiches” the bound UQ molecule (131). Furthermore, mutation of this proline residue in human complex II results in an autosomal dominant disease called hereditary paraganglioma (341). Overall, given the FQ data presented herein and previously published data (212), we propose that the Q-site of DmsABC is in a location equivalent to those of FrdABCD and SdhCDAB.

Tyrosine residues have been implicated in the reaction scheme of many redox enzymes including *E. coli* cytochrome  $bo_3$  (342), yeast cytochrome  $bc_1$  complex (343), cytochrome  $c$  oxidases (37,38) and Photosystem II (344,345). The DmsB<sup>Y104</sup> mutations resulted in enzymes with quite different properties. The DmsAB<sup>Y104D</sup>C mutant enzyme does not support growth in DMSO whereas DmsAB<sup>Y104E</sup>C is able to support growth but at a much slower rate. There is also a correlation between side chain length and the observed  $K_d$  for HOQNO with the DmsB<sup>Y104D/E</sup> mutants. In contrast, the DmsAB<sup>Y104A</sup>C mutant enzyme is able to support growth in DMSO and binds HOQNO with high affinity. Thus, DmsB<sup>Y104</sup> plays an important, but non-essential, role in MQH<sub>2</sub> binding and oxidation. In the DmsB<sup>Y104A</sup> mutant, it is likely that another residue is shifted into the position of the Tyr side chain and can complement its role in quinol oxidation and/or electron transfer. In the DmsAB<sup>Y104D</sup>C mutant, the Asp residue is unable to perform the equivalent function. In the DmsAB<sup>Y104E</sup>C mutant however, the Glu carboxylate sidechain

is able to perform the equivalent function as a Tyr hydroxyl but at a much lower efficiency, as indicated by the slower growth in minimal media and the low LPCH<sub>2</sub>:TMAO activity. If DmsB<sup>Y104</sup> functions as a proton acceptor in the mechanism of MQH<sub>2</sub> oxidation, then its hydroxyl group must be H-bonded or be positioned near a positively charged sidechain such that its pK<sub>a</sub> is lowered to allow protonation/deprotonation to readily occur at near-neutral pH values. Examination of the DmsB model and the FdnH structure reveals that no residues from DmsB can provide such a side chain to interact with DmsB<sup>Y104</sup>, suggesting that this modulating residue is most likely provided by DmsC.

Table 3.3 lists the mutations made in DmsB and their effects on the  $E_m$  of FS4. The most significant  $\Delta E_m$  observed is from mutation of DmsB<sup>Y104</sup> to Asp and Glu, which lowers the  $E_m$  of the [3Fe-4S] cluster from +275mV to +150mV and +145mV, respectively. The DmsB<sup>C102S/Y104D</sup> and DmsB<sup>C102S/Y104E</sup> mutants both abolish the upfield shift of the peak-trough ( $g_{xy}$ ) observed in their oxidized spectra in the presence of HOQNO (Figure 3.5), despite the observation of HOQNO binding in FQ titrations for the corresponding single mutants. This would suggest that an aromatic residue is essential for communication between the Q-site and FS4 and the HOQNO-dependent lineshape change observed in the spectrum of FS4<sup>[3Fe-4S]</sup>. Bulky aromatic residues have been suggested to play a role in modulating the  $E_m$  of [Fe-S] clusters (323,346), and the mutagenesis of DmsB<sup>Y104</sup> in this study clearly supports this view. However, Agarwal and coworkers found that a conserved Tyr in ferredoxins near a [4Fe-4S] cluster did not play a role in modulating the  $E_m$  of that cluster, but rather prevented solvent accessibility and cluster degradation (347).

The DmsB<sup>C102S/P80A</sup> mutation does not alter the  $E_m$  of FS4<sup>[3Fe-4S]</sup>. This observation is quite surprising, since backbone amide hydrogens are postulated to play a dominant role in modulating the  $E_m$  of [Fe-S] clusters through H-bonding interactions (323-328), and the DmsB<sup>P80A</sup> mutation introduces an amide that points directly at FS4 based on the structures of FdnGHI and NarGHI (178,180). A plausible explanation for this is that the maximum allowable  $E_m$  for this particular [3Fe-4S] cluster may be approximately +275mV. This rationale is supported by results from pH titrations as well as the effect of HOQNO binding on FS4. At pH 7, 6, and 5, the  $E_m$  values of the DmsB<sup>C102S</sup> single mutant are independent of pH, whereas the DmsB<sup>C102S/Y104D</sup> mutation causes the  $E_m$  of FS4<sup>[3Fe-4S]</sup> to increase with decreasing pH. FS4<sup>[3Fe-4S]</sup> in the DmsB<sup>C102S</sup> mutant has an  $E_{m,7}$  of +275mV in the presence and absence of HOQNO, whilst in the DmsB<sup>C102S/Y104D</sup> mutant it has an  $E_{m,7}$  of +230mV in the presence of HOQNO and an  $E_{m,7}$  of +150mV in its absence. In addition, mutations of basic residues around FS4 cause the  $E_{m,7}$  to decrease, while no increase in the  $E_{m,7}$  is observed when acidic residues were mutated. The data strongly suggest that the maximum allowable  $E_m$  of DMSO reductase FS4<sup>[3Fe-4S]</sup> is approximately +275mV. This contrasts with other systems in which [Fe-S] cluster  $E_m$  values can clearly exceed this value (348,349). Experiments are in progress to determine the reason for the apparent upper limit for the  $E_m$  value of FS4<sup>[3Fe-4S]</sup>.

The DmsAB<sup>C102S</sup>C mutant enzyme is unable to support growth in glycerol-DMSO minimal medium, yet is clearly able to bind the MQH<sub>2</sub> analog HOQNO. The endergonic rate-limiting step in electron transfer through both DMSO reductase and nitrate reductase is for electrons to travel from FS4 to FS2 (Figure 3.1). The  $\Delta E_{m,7}$  for the FS4-FS2 pair is -600mV in NarH, -280mV in DmsB, -460mV in the DmsB<sup>C102S/Y104D/H106F</sup> mutant, and

-605mV in the DmsAB<sup>C102S</sup>C mutant. The DmsAB<sup>C102S</sup>C mutant enzyme is non-functional although the  $\Delta E_{m,7}$  for the FS4-FS2 pair is -605mV, which is comparable to the value of -600mV for NarH. One plausible explanation for this inconsistency lies in the  $E_m$  for nitrate reduction versus the reduction of DMSO. The  $E_m$  for nitrate reduction is much higher compared to  $E_m$  of NarGHI FS4, but the  $E_m$  for DMSO reduction becomes less than the  $E_m$  of FS4 in the DmsAB<sup>C102S</sup>C mutant enzyme, making it energetically unfavorable for the electron to travel from FS4 to the substrate. A second possibility lies in the fact that NarGHI possesses two heme moieties in the membrane intrinsic domain which are lacking in DmsABC. Recently, a model by which electrons travel through NarGHI was proposed by our laboratory (350), whereby multiple electrons enter into heme  $b_d$ , heme  $b_p$ , and FS4 sequentially before the first electron surmounts the thermodynamically unfavorable FS4-FS2 energy hill. In this model, electrons from heme  $b_d$  and heme  $b_p$  can “push” an electron from FS4 to FS2. In DmsABC however, this is impossible since it lacks heme in its membrane anchor subunit. Although the DmsB<sup>C102S/Y104D</sup> and DmsB<sup>C102S/Y104E</sup> mutations dramatically decrease the  $E_m$  of FS4, they are also unable to support growth on a glycerol-DMSO minimal medium. In light of our understanding that DmsB<sup>Y104</sup> plays a role in the catalytic cycle of the enzyme, it is not surprising that these mutants are unable to perform their physiological function despite a large drop in the  $E_m$  of FS4.

In this study, a Tyr residue was discovered to play a major role in controlling the redox properties of a [Fe-S] cluster and for communication between a [Fe-S] cluster and the Q-site. Data obtained from other mutants created around this [Fe-S] cluster also indicate that positively charged residues may be responsible for fine-tuning the  $E_m$  of the

[Fe-S] cluster by approximately 15-25mV per charge. The DmsB<sup>C102S/Y104D/H106F</sup> triple mutation shows that these two effects are additive in controlling the redox properties of the [Fe-S] cluster. By examining the structure of FdnGHI and the model of DmsABC, one can also surmise that certain charged residues may fine-tune the  $E_m$  of multiple redox centers during enzyme turnover. DmsB residues Pro80, Ser81, and Tyr104 are located at the interface between the soluble dimer and the membrane anchor domain, and were shown to be important residues for MQH<sub>2</sub> binding and oxidation. These observations support a model for MQH<sub>2</sub> oxidation by DmsABC in which the Q-site donates electrons directly to FS4 (212). Such a model is very similar to that observed for FrdABCD in which the Q-site donates electrons directly to the [3Fe-4S] cluster (216,330).

Overall, the data presented herein illustrate the crucial role of FS4 as the first electron acceptor in the electron relay system defined by the four [4Fe-4S] clusters of DmsB. We have demonstrated that the high  $E_m$  value of this cluster in its [3Fe-4S] form is a significant barrier to electron transfer through DmsB, and that alterations in its immediate environment can have a significant effect on the Q-site of DmsC. A comparison of the constituent cofactors in DmsABC to those in NarGHI suggests a possible role of the heme in the latter enzyme to allow physiological electron transfer despite a large (-600mV) endergonic step. These studies represent a significant step towards understanding the factors that regulate electron fluxes through [Fe-S] clusters in redox enzymes, and contribute to an emerging understanding of the thermodynamic barriers that govern electron transfer.



DmsB Mutant	Doubling Time (hrs)	BV <sup>+</sup> :TMAO Specific Activity	LPCH <sub>2</sub> :TMAO Specific Activity	BV <sup>+</sup> /LPCH <sub>2</sub> Activity Ratio
Wild-type				
DmsABC	6.3	35.4 ± 1.9	0.97 ± 0.01	36 ± 2
K77A	4.2	34.0 ± 0.0	1.10 ± 0.05	31 ± 1
P80A	3.0	115.9 ± 3.0	0.78 ± 0.03	149 ± 7
P80H	NG	9.2 ± 0.2	0	N/A
P80D	NG	18.5 ± 0.1	0	N/A
S81H	NG	8.6 ± 0.1	0	N/A
S81G	NG	12.7 ± 0.4	0	N/A
H85F	12.4	22.1 ± 0.5	0.69 ± 0.00	32 ± 1
H85T	11.7	24.1 ± 0.4	0.72 ± 0.02	34 ± 1
D95A	3.4	147.9 ± 5.3	5.56 ± 0.39	27 ± 2
D97A	3.6	166.6 ± 2.2	6.12 ± 0.25	27 ± 1
R103A	13.5	35.2 ± 1.9	0.81 ± 0.01	43 ± 2
Y104A	4.2	79.5 ± 4.6	0.86 ± 0.03	92 ± 6
Y104D	NG	12.0 ± 0.8	0	N/A
Y104E	~20	13.8 ± 0.8	0.32 ± 0.02	43 ± 4
H106A	11.4	14.4 ± 0.4	1.18 ± 0.02	12 ± 1
H106E	8.5	14.9 ± 0.2	0.43 ± 0.01	35 ± 1

Table 3.1. The growth rates of the DmsB mutants in glycerol-DMSO minimal media, and the BV<sup>+</sup>- and LPCH<sub>2</sub>-dependent reduction of TMAO. Mutant enzymes were expressed in *E. coli* DSS301 cells lacking a chromosomal copy of DMSO reductase. Enzyme specific activities are given in mmol (min x mg total protein)<sup>-1</sup> with one standard deviation of error. NG: No growth. N/A: Not applicable, the BV<sup>+</sup>/LPCH<sub>2</sub> activity ratio cannot be determined because the LPCH<sub>2</sub>:TMAO specific activity is zero.

DmsB Mutant	Estimated $K_d$ (nM)	[DmsABC] (nmol (mg membrane protein) <sup>-1</sup> )
Wild-type DmsABC	5	0.60
K77A	5	0.57
P80A	10	0.74
P80D	17	0.60
P80H	20	0.48
S81G	20	0.24
S81H	20	0.24
H85F	5	0.38
H85T	5	0.26
D95A	5	0.88
D97A	5	1.16
C102S ([3Fe-4S])	5	0.57
C102W ([3Fe-4S])	17	0.27
R103A	5	0.42
Y104A	5	0.80
Y104D	10	0.63
Y104E	18	0.34
H106A	5	0.47

Table 3.2. HOQNO FQ titrations of DmsB mutants expressed in HB101 cells. Titrations were carried out at three different protein concentrations and a best fit curve fitted to all three plots simultaneously to estimate the dissociation constants for HOQNO. Mutations of DmsB<sup>P80</sup>, DmsB<sup>S81</sup>, DmsB<sup>C102</sup> and DmsB<sup>Y104</sup> seem to have an effect on the affinity of the enzyme for HOQNO.

DmsB Mutant	FS4 $E_{m,7}$ (mV)	Significant $\Delta E_{m,7}$ (mV)
C102S	275	-
K77A/C102S	260	-15
P80A/C102S	270	-
H85F/C102S	255	-20
H85T/C102S	260	-15
D95A/C102S	283	-
D95K/C102S	277	-
D97A/C102S	273	-
R103A/C102S	250	-25
Y104A/C102S	280	-
Y104D/C102S	150	-125
Y104E/C102S	145	-130
Y104D/H106F/C102S	130	-145
H106A/C102S	260	-15
H106I/C102S	250	-25
H106E/C102S	271	-

Table 3.3. Mutations made in DmsB and the resultant  $E_m$  values of the [3Fe-4S] cluster. Mutant enzymes were expressed in HB101 cells. The signal of the engineered FS4 was detected at a temperature of 12K, a microwave power of 20mW at 9.38 GHz, and a modulation amplitude of 10  $G_{pp}$  at 100 KHz. The heights of the  $g = 2.03$  peak of the [3Fe-4S] cluster in the oxidized state were plotted against the redox potentials in which the membranes were poised, and the Nernst equation fitted to the data to determine  $E_{m,7}$  values.

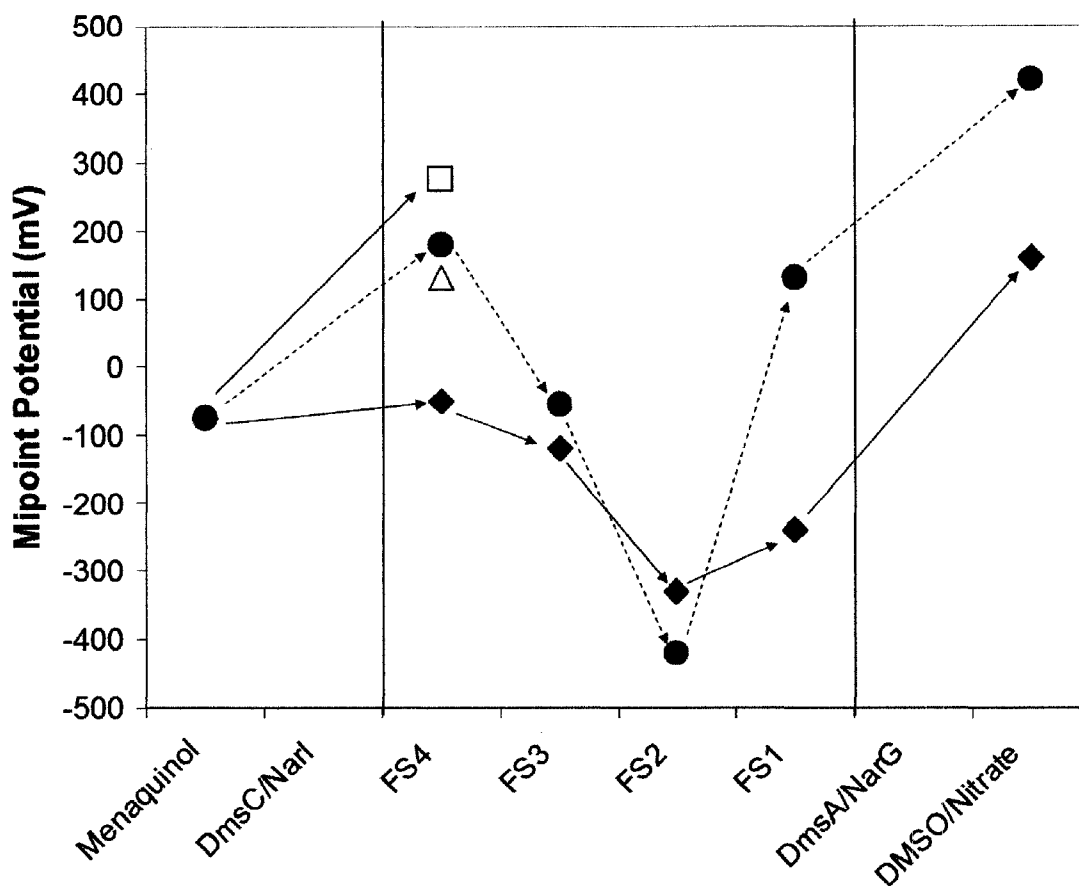


Figure 3.1. Electron transfer through DmsB (◆) and NarH (●). The  $E_m$  values of each [Fe-S] cluster in both electron transfer subunits are shown. The FS4 of the DmsAB<sup>C102S</sup>C (□) and the DmsAB<sup>C102S/Y104D/H106F</sup>C mutants (Δ) are also shown. Both the DmsAB<sup>C102S</sup>C and the DmsAB<sup>C102S/Y104D/H106F</sup>C mutant enzymes are non-functional. Note that the  $\Delta E_{m,7}$  for the FS4-FS2 pair is -600mV in NarH, -280mV in DmsB, -460mV in DmsB<sup>C102S/Y104D/H106F</sup>, and -605mV in DmsB<sup>C102S</sup>.

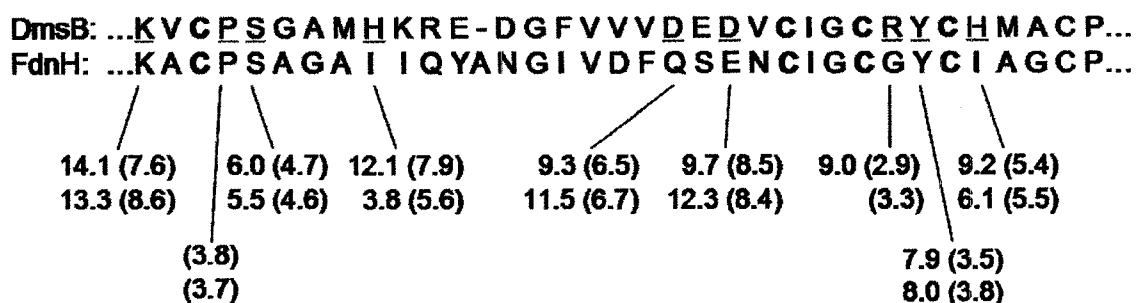


Figure 3.2. Local alignment of the amino acids around FS4 of DmsB with that of FdnH. The four cysteines in bold are ligands to FS4<sup>[4Fe-4S]</sup>. Underlined residues indicate the positions at which DmsB mutants were generated. Indicated are the distances of the DmsB (top) and FdnH (bottom) amino acid side chains (and backbone amides) to FS4 in Å.

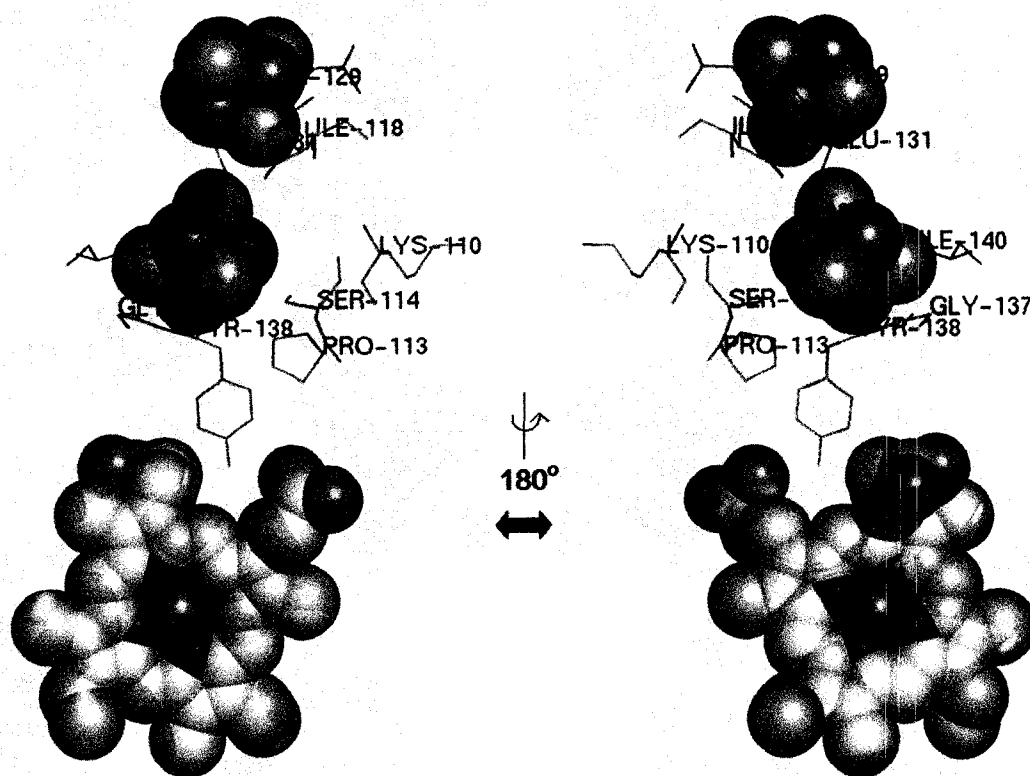


Figure 3.3. Crystal Structure of FdnGHI (PDB file 1KQF), magnified and centered on FS4. Highlighted are the equivalent residues in FdnH which were studied by site-directed mutagenesis in DmsB. The proximal heme of FdnI is also shown. Note that the proline, serine, and tyrosine residues are all located at the interface between the FdnH electron transfer subunit and the FdnI membrane anchor subunit, and that the latter residue plays a critical role by interacting with the proximal heme of FdnI. Pro113, Ser114, and Tyr138 of FdnH are equivalent to Pro80, Ser81, and Tyr104 of DmsB, respectively. Image was generated using PyMol v.0.96 (DeLano Scientific LLC.).



Figure 3.4. A three-dimensional alignment of the backbones of the DmsB model (yellow) and the structure of FdnH (blue). Using 151 common C- $\alpha$  atoms, a rmsd value of 0.636Å was calculated from the superimposition of the two structures. Note that the FdnH subunit contains a C-terminal transmembrane tail which is absent in DmsB. An important residue, DmsB<sup>Y104</sup>, has its side chain shown in the figure.

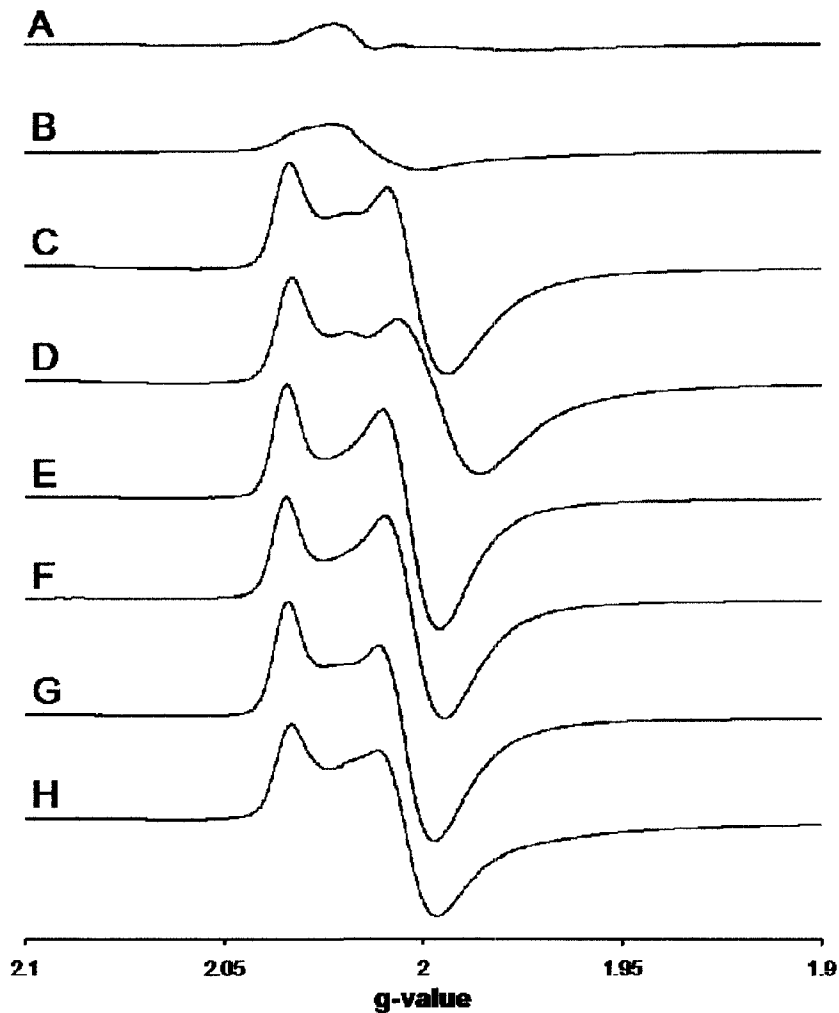


Figure 3.5. Oxidized EPR spectra of the engineered [3Fe-4S] cluster in DmsB in the absence and presence of HOQNO. When no DmsABC is expressed (A), or when only wild-type DmsABC is expressed (B), only the [3Fe-4S] cluster signal from fumarate reductase is observed. In the presence of 50 $\mu$ M HOQNO, the peak-trough centered at  $g=2.00$  corresponding to FS4<sup>[3Fe-4S]</sup> of the DmsAB<sup>C102S</sup>C mutant enzyme (C) is shifted upfield (D). In the DmsAB<sup>C102S/Y104D</sup>C and DmsAB<sup>C102S/Y104E</sup>C mutant enzymes, the EPR lineshape of the FS4<sup>[3Fe-4S]</sup> oxidized spectra are unchanged (E & G), and the upfield shift of the peak-trough is not observed in the presence of HOQNO (F & H).



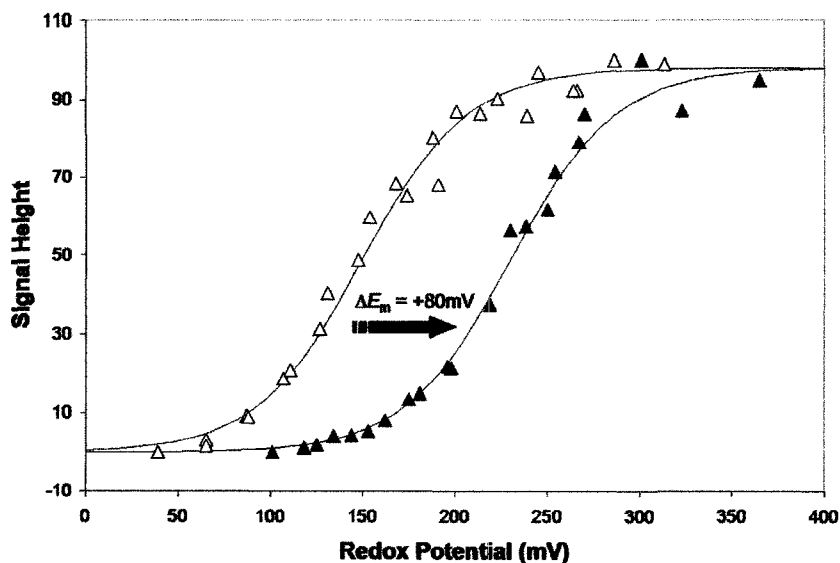
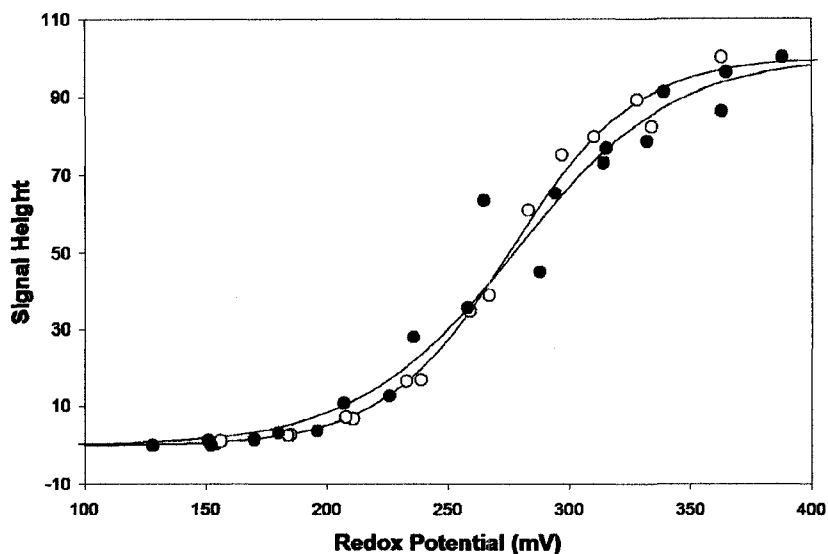


Figure 3.6. Redox titrations of FS4 from the DmsB<sup>C102S</sup> single mutant (top) and the DmsB<sup>C102S/Y104D</sup> double mutant (bottom). In both the absence (○) and presence (●) of HOQNO, the  $E_m$  of the [3Fe-4S] cluster in the DmsAB<sup>C102S</sup>C mutant enzyme is approximately +275mV. In the DmsAB<sup>C102S/Y104D</sup>C mutant enzyme however, the  $E_m$  of the [3Fe-4S] cluster shifts from +150mV in the absence (Δ) of HOQNO to +230mV in the presence (▲) of HOQNO.

## **Chapter 4**

# **Succinate:ubiquinone Oxidoreductase**

## 4.1 Overview

Sdh from *E. coli* and mitochondria is comprised of four subunits containing five unique redox cofactors. SdhAB is called the catalytic dimer and is oriented towards the cytoplasm in bacteria or the matrix in mitochondria; it is anchored to the bacterial/mitochondrial inner membrane via non-covalent interactions with the SdhCD subunits. The enzyme is obligatory for aerobic metabolism and functions as a link between the Krebs/tricarboxylic acid (TCA) cycle and the aerobic respiratory chain. The physiological role of Sdh is to couple succinate oxidation ( $E_m = +30\text{mV}$ ) to ubiquinone reduction ( $E_m = +100\text{mV}$ ) where reducing energy is transferred from the former substrate to the latter molecule. This is accomplished using an electron transfer relay comprised of a FAD molecule in SdhA, three [Fe-S] clusters in SdhB, and possibly the heme *b* that is sandwiched between SdhCD. The edge-to-edge distances between neighboring cofactors are all within the 14Å limit for rapid electron transfer (Figure 4.1).

Included in the large superfamily of complex II enzymes is fumarate reductase (Frd) which is also encoded in the *E. coli* genome but excluded in most eukaryotic organisms. The soluble FrdAB catalytic dimer is highly homologous to SdhAB, but a large disparity exists in regards to the sequences and 3-dimensional structures between SdhCD and FrdCD. Based on the variations of the membrane soluble domain, a classification system was used to categorize the different enzymes (331). The Type A enzymes have membrane anchors made from two peptide chains and house two heme molecules, while Type B enzymes also assemble two hemes to the membrane domain but it is made from a single polypeptide. *E. coli* Sdh is denoted Type C since its membrane

intrinsic domain is comprised of two polypeptide chains that assemble a single heme molecule, whereas *E. coli* Frd is denoted Type D because it lacks heme.

#### 4.2 The *sdh* operon

The genes encoding the tetrameric Sdh enzyme are grouped into the *sdhCDAB* operon that is located at 755.6 kbp (16.4') on the *E. coli* K-12 chromosome. The gene order is the same as that found in other gram-negative bacteria such as *Paracoccus denitrificans* and *Coxiella burnettii*. This contrasts to the *frdABCD* operon in which the flavoprotein and electron transfer subunits are encoded upstream of the membrane soluble subunits (351,352). In organisms that encode a Type B enzyme, such as *Bacillus subtilis* and *Wolinella succinogenes*, the single gene encoding the membrane anchor precedes those that encode the catalytic dimer (353-355). In most eukaryotes, the polypeptides of complex II are strictly nuclear encoded. This differs from respiratory chain complexes I, III, IV and V, which are encoded partly by nuclear DNA and partly by mitochondrial DNA. Exceptions to this rule include Sdh from *Porphyra purpurea* (a photosynthetic red alga) and *Reclinomonas americana* (a heterotrophic zooflagellate) wherein the *sdh2*, *sdh3* and *sdh4* genes are localized in the mitochondrion (356).

Transcription of the *sdh* and *frd* operons in *E. coli* is inversely dependent on oxygen availability and is effected through the ArcA/B and FNR response regulators.  $\beta$ -galactosidase activity, used commonly as a reporter enzyme for gene expression, was observed to be ~10 fold higher from an aerobic bacterial culture compared to an anaerobic culture when the reporter gene was positioned behind the *sdh* promoter (82); the reverse holds true for the *frd* promoter (357). Under anaerobic conditions, the amount

of Sdh expressed is negligible and is insufficient to completely rescue a  $\Delta frd$  strain to grow anaerobically on glycerol-fumarate minimal medium (358). However, if the *sdhCDAB* genes were cloned behind the *frd* promoter such that expression of Sdh is inducible under anoxic or microaerophilic conditions, the enzyme can work in reverse to carry out fumarate-dependent oxidation of menaquinol ( $E_m = -100\text{mV}$ ) and can complement a  $\Delta frd$  strain to grow anaerobically on glycerol-fumarate (359). Conversely, a  $\Delta sdh$  *E. coli* strain can be rescued to grow aerobically on succinate minimal medium when complemented with a plasmid encoding the Frd enzyme (225). Anaerobic overexpression of SdhCDAB from the  $P_{FRD}$ -*sdhCDAB* fusion construct, as well as overexpression of FrdABCD behind its native promoter on a plasmid, leads to formation of lipid-protein tubular structures that are composed of Sdh/Frd and enriched in cardiolipin (359-361).

One interesting organism that possesses both Sdh and Frd is the parasitic nematode *Ascaris suum*. During larval development from a fertilized egg to third stage larvae, the organism is a free living aerobe; after parasitization the organism becomes an adult and lives anaerobically in the host small intestine. Presently, aerobic Sdh and anaerobic Frd activities are believed to stem from two isoforms of an enzyme that differ in the flavoprotein subunit and the smaller cytochrome *b* subunit (362). Interestingly, the iron-sulfur protein and the larger cytochrome *b* subunit appear to be indifferent toward Sdh and Frd function as they are identical during the two distinct phases of the *A. suum* life cycle (363,364).

In addition to oxygen availability, expression of the two enzymes is also controlled by catabolite repression. Addition of glucose to aerobic medium decreased Sdh

expression by a factor of 3, but no changes were observed when succinate was added (82). Under anaerobic conditions, the presence of nitrate strongly represses transcription of the *frd* operon to prevent futile expenditure of ATP towards terminal reductases that do not contribute to the proton motive force (78,110) (see Section 1.4). The *frdABCD* genes, but not *sdhCDAB*, are also activated by the DcuS/DcuR two component system, which responds to the external presence of C<sub>4</sub>-dicarboxylates (365,366).

### 4.3 Sdh and Disease Phenotypes in Humans

Mutations mapped to different locations in Sdh have been associated with a number of diseases that have a wide spectrum of phenotypes. Missense mutations in SdhA have been identified in patients with Leigh syndrome (367,368). Mutations which lead to a decrease in succinate:cytochrome *c* activity can lead to abnormal muscular growth, optic atrophy, ataxia and development of Kearns-Sayre syndrome (369,370). Truncation, frame-shift and point mutations in either *sdhB*, *sdhC* or *sdhD* can lead to tumorigenesis in the form of familial pheochromocytoma and paraganglioma. An online database at [http://chromium.liacs.nl/lovd\\_sdh/home.php](http://chromium.liacs.nl/lovd_sdh/home.php) tracks the unique Sdh variants that have been sequenced, along with the possible associated disease phenotype.

The mechanism of tumorigenesis is under debate. One hypothesis suggests that mutations in the SdhB, SdhC or SdhD subunits cause an increase in superoxide production, which results in oxidative damage to DNA, lipids and proteins, leading to genomic instability. Another hypothesis also involves ROS production but involves stabilization of hypoxia-inducible factor (HIF)-1 $\alpha$  via inhibition of HIF prolyl hydroxylase, resulting in upregulation and expression of genes involved in cell

proliferation and tumorigenesis. Since succinate inhibits prolyl hydroxylase competitively, succinate build-up due to decreased Sdh activity can also directly lead to HIF-1 $\alpha$  stabilization without ROS production.

In fumarate reductase, reactive oxygen species have been shown to be produced at or near the FAD molecule (371). Using *sdh* sequence information from patients with hereditary paraganglioma, equivalent mutants were generated in the *E. coli* and *S. cerevisiae* proteins and studied. The majority of these point mutations is close to the heme *b* or the Q<sub>p</sub>-site and leads to increased production of superoxide and ROS during enzyme turnover (372-374), while other studies did not yield the same results (375). At present, it is impossible to decisively point out which combination of factors lead to cancer formation.

#### 4.4 X-ray Crystallographic Structures

The *E. coli* Sdh enzyme has been successfully overexpressed, purified, crystallized, and its 3-dimensional structure elucidated to a resolution of 2.6Å (131,376,377). Similarly, the porcine and avian mitochondrial complex II structures have also been determined to maximum resolutions of 2.4Å and 1.7Å respectively (378-380). Although the asymmetric unit in the different crystals range from a monomer to a trimer of Sdh and may represent the physiological form *in vivo*, the functional unit is clearly monomeric since distances between cofactors from neighbor Sdh subunits are longer than the proposed 14Å limit for electron tunneling (19). Some competitive inhibitors which have been co-crystallized with Sdh include Atpenin A5, 2-thenoyltrifluoroacetone (TTFA) and 3-nitropropionate (Figure 4.2).

The FrdABCD enzyme from *E. coli* has also been crystallized and its structure was in fact available before those of Sdh (216,227). The crystal structure of the *W. succinogenes* quinol:fumarate oxidoreductase has also been solved (381) and its overall structure is highly comparable to that of Sdh. Because of the ease of genetic manipulation, the majority of biochemical and biophysical data on mono-heme tetrameric Sdh were gathered from the *E. coli* (EcSdh) and *S. cerevisiae* (ScSdh) enzymes.

#### 4.5 SdhA – The Catalytic Subunit

SdhA (64.4 kD) is the catalytic subunit where interconversion between succinate and fumarate is catalyzed (Figure 4.3). Its primary sequence is highly homologous with that of FrdA wherein the amino acid residues are 64% similar and 44% identical (382). A more striking conservation amongst the complex II homologs is apparent via a 3-dimensional structural alignment of the catalytic subunits from available X-ray crystal structures (131,144,216,378,380,383), which shows a root mean square deviation of 1.5Å over 744 C<sub>α</sub> carbons (131). Despite the high degree of similarity between SdhA and FrdA, significant differences exist between the two in their abilities to carry out succinate oxidation and fumarate reduction.

At the active site, a FAD cofactor is present to carry out catalysis (384). Covalent attachment of the FAD to the Sdh protein appears to be an enzyme-free process, but substrate binding at the active site speeds up bond formation between the 8 $\alpha$ -methyl group and the imadazole side chain of the conserved SdhA<sup>H45</sup> residue (8 $\alpha$ -N<sup>3</sup>-histidyl-FAD) (Figure 4.4) (143). The two-electron reduction potentials of the covalent FAD molecules in Sdh and Frd, as determined by redox titration and EPR spectroscopy, range



from -80mV to -185mV at pH 8 (224,385-387). These values are 100-150mV higher than those of the non-covalent FAD as found in the soluble flavocytochrome  $c_3$  from *Shewanella frigidimarina* (139). pH studies on the reduction potential of the FAD cofactor in *E. coli* Frd reveal an  $E_m$  shift of approximately -30mV/pH, indicating the redox transition between FAD and FADH<sub>2</sub> involves 2 e<sup>-</sup> and 1 H<sup>+</sup> (386). This contrasts with studies done on the bovine Sdh which show a -30mV/pH dependence above pH 7.7 and a -60mV/pH variance below pH 7.7 (385), coinciding with the pK<sub>a</sub> value for the N-1 position of the flavin isoalloxazine ring (224,388). Replacement of the conserved His residue with Ser, Cys, Tyr or Arg in QFR did not impair proper assembly and localization of the enzyme, but resulted in non-covalent insertion of FAD that greatly compromised enzyme activity (389). Mutants lacking covalently bound flavin in *B. subtilis* Sdh are also able to assemble correctly to the membrane (390).

It is widely accepted that chemical reaction of the FAD with the dicarboxylate substrate occurs via hydride transfer as well as protonation/deprotonation by a nearby acidic/basic residue (144-147). In solution, unbound fumarate is a linear molecule constrained by its double bond; in crystal structures of fumarate reductase wherein fumarate was co-crystallized, the molecule is no longer linear (391,392). It is believed that the strain across the double bond may help stabilize the transition state element during hydride transfer between the flavin and the dicarboxylate substrate (144,391).

From protein film voltammetry studies as well as conventional spectrophotometric kinetic assays, it was observed that the ability of EcSdh to reduce fumarate decreases with increasing electrode potential above the -60mV threshold (393-395). This phenomenon where the rate of fumarate reduction actually decreases with an

increase in driving force has been described as the “tunnel diode” behavior of Sdh. In contrast, voltammetry techniques show that EcFrd exhibits normal kinetic behavior as its ability to reduce fumarate is proportional to electrochemical driving force (386).

Sidechains of several amino acids have been shown to play major roles in substrate binding, as well as succinate oxidation and fumarate reduction, in EcSdh and EcFrd (Figure 4.4). The structurally equivalent residues Gln-50/Glu-49 in SdhA/FrdA play opposing roles in their respective enzymes, whereby a Gln residue allows the enzymes to work better as a succinate oxidase and a Glu residue biases the enzymes toward fumarate reduction (396). Recently, two conserved Thr residues that were postulated to be important in Sdh and Frd enzyme function were studied by Cecchini and coworkers (147). The two Thr residues (SdhA-T244 and SdhA-T254) mark the beginning and end to an 11-amino acid loop that contains an absolutely conserved His-Pro-Thr motif as well as other residues important for enzyme catalysis. SdhA-T244 is a hinge between the FAD-binding and capping domains and interacts with SdhA-R248, which forms part of the proton shuttle with SdhA-E245 and SdhA-R287 (144,145,383,397); SdhA-T254 directly H-bonds to the substrate in the active site. Substitution of SdhA-T254 with an Ala residue resulted in significant loss of enzyme activity, most likely due to decreased abilities to bind substrate and to stabilize the transition state. The SdhA-T244A mutation resulted in lower expression level of Sdh, as well as increased rates of proteolysis during purification. Since SdhA-T244 H-bonds to SdhA-R248, it was suggested that loss of enzyme activity in the SdhA-T244A mutant enzyme stems from either an alteration of the  $pK_a$  of the proton shuttle or a shift in SdhA-R248 side chain conformation such that protons cannot be transferred to SdhA-E245 (147).

#### 4.6 SdhB – The Electron Transfer Subunit

The electron transfer subunit SdhB contains three iron-sulfur clusters that are spectrally distinct in electron paramagnetic resonance (EPR) studies. The [2Fe-2S] cluster (FS1) is coordinated by Cys55, Cys60, Asp63 and Cys75, and it is EPR visible in the reduced state at a temperature of 40K. Residues Cys149, Cys152, Cys155 and Cys 216 coordinate the [4Fe-4S] cluster (FS2) which is also EPR visible in the reduced state but at a temperature of 12K. Sidechains of Cys159, Cys206 and Cys 212 are ligands to the [3Fe-4S] cluster (FS3) which is EPR visible in the oxidized state at 12K. The three [Fe-S] clusters have  $E_m$  values of +10mV (FS1), -175mV (FS2) and +65mV (FS3) (319). Thus, relative to the rest of the electron transfer chain, the [4Fe-4S] cluster has an unusually low reduction potential and may serve as an energy barrier against physiological electron transfer. How the protein environment modulates the  $E_m$  value of [Fe-S] clusters, and how these changes affect electron transfer, is one aspect of redox chemistry that is examined in this thesis and is discussed in Chapters 6 and 7.

#### 4.7 SdhCD – The Membrane Anchor Domain

As opposed to the soluble catalytic SdhAB dimer, the membrane intrinsic SdhCD domain does not share sequence or structural homology with the Frd enzyme. One major difference between Frd and Sdh is the assembly of a low spin heme  $b_{556}$  molecule in the latter enzyme, which is bis-coordinated by residues SdhC-H84 and SdhD-H71. The edge-to-edge distances are 11.4Å between the [3Fe-4S] cluster and the heme, 7.6Å between the [3Fe-4S] cluster and UQ, and 6.5Å between UQ and the heme. Although the short

distances to/from heme *b* imply rapid electron transfer between the redox active species, the cofactor appears to lie outside the physiological electron transfer chain from succinate to ubiquinone and thus its role in enzyme catalysis was of great debate. Adding to the confusion were the different midpoint potentials of heme *b* in the *E. coli* and bovine enzymes, which were reported to be +35mV and -185mV, respectively (398,399). Since EcFrd has been demonstrated to produce a significantly higher amount of ROS than EcSdh (371), it was suggested that the heme cofactor acts as an electron sink to minimize ROS generation (131). Making this hypothesis more plausible was the fact that mutations around the quinone binding site resulted in increased ROS generation during enzyme turnover (372,373). Initial attempts to preclude heme assembly by substitution of the His ligands by either Leu or Gln managed to alter subtle properties of the heme but did not prevent its assembly into EcSdh (398). A recent attempt by Weiner and coworkers replaced the His ligands with Tyr residues and found that heme insertion was abolished, presumably because formation of a His-Tyr H-bond prevented its assembly into the enzyme (130). The heme-free Sdh variant retained significant physiological and reverse activities and did not show increased ROS production during catalysis. However, stability of the tetramer seemed to be perturbed since its enzyme activity decreased over time in the presence of detergent. Thus the heme in Sdh is not essential for enzyme function or the suppression of ROS generation, but appears to play more of a structural role in the stabilization of the holoenzyme (130). This was also confirmed by studies done on ScSdh (400).

Another major difference between EcSdh and other members of the complex II family of enzymes is the number of quinone binding sites in the membrane intrinsic

domain. In crystal structures of *E. coli* and avian Sdh wherein UQ or quinone analogues were co-crystallized, only a Q<sub>P</sub>-site (proximal to SdhAB) was observed to be occupied (131,377,380). In contrast, biochemical evidence suggests the presence of a Q<sub>P</sub>-site and a Q<sub>D</sub>-site (distal to SdhAB) in ScSdh (401,402), both of which were successfully inserted into a three-dimensional homology model (403). The X-ray crystal structures of porcine Sdh and *E. coli* Frd also show two distinct quinone binding sites on opposite sides of the membrane (216,378). In Frd, the Q<sub>P</sub>- and Q<sub>D</sub>-sites are approximately 25Å apart, too far for electron transfer to take place at a meaningful rate (404). If the Frd enzyme were crystallized in the presence of HOQNO or 2-[1-*p*-chlorophenyl]ethyl]4,6-dinitrophenol (quinone analogue inhibitors), electron density at the Q<sub>P</sub>-site remained but that at the Q<sub>D</sub>-site was lost (227). It was thus proposed that inhibitor binding at the Q<sub>P</sub>-site exerts anti-cooperative binding behavior on the Q<sub>D</sub>-site, similar to the situation with the two quinone binding sites in the *bc*<sub>1</sub> complex (405). If the controversial Q<sub>D</sub>-site was present in the *E. coli* Sdh enzyme, its equivalent spatial location is occupied by the acyl chains of the bound cardiolipin molecule (406). The presence of two distinct sites for quinone reduction/oxidation, located on opposite sides of the membrane, could have severe bioenergetic consequences. The proton gradient would drive quinone reduction at the Q<sub>D</sub>-site and quinol oxidation at the Q<sub>P</sub>-site, which would dissipate the electrochemical gradient.

Variation also exists in other members of the complex II superfamily of enzymes in regards to subunit composition, heme cofactor and the number of Q-sites. For instance, the *Bacillus subtilis* Sdh and *Wolinella succinogenes* Frd enzymes are heterotrimeric entities that have only one transmembrane subunit. Further, they assemble two *b* hemes

that facilitate electron transfer to the Q<sub>D</sub>-site. EcSdh and EcFrd, as well as eukaryotic complex II, are electroneutral enzymes that do not generate pmf during catalysis. However, the heterotrimeric Sdh enzymes from *B. subtilis* and *B. licheniformis* have been shown to be electrogenic when functioning as a quinol:fumarate oxidoreductase (407) and its succinate:quinone oxidoreductase activity is dependent on the transmembrane potential (408,409). The *W. succinogenes* fumarate reductase catalyzes an electroneutral reaction that involves a scalar movement of protons across the membrane that is cancelled by a stoichiometric vectorial movement of protons (the “E-pathway”) (392,410,411).

The Q<sub>P</sub>-site is built from residues of the SdhB, SdhC and SdhD subunits and its ability to accommodate and reduce UQ has been extensively studied (Figure 4.4). Stable semiquinone species have been observed in Sdh preparations from bovine heart (412), *P. denitrificans* (413), and *E. coli* (414). In contrast, a semiquinone radical is not observed in the wild-type EcFrd enzyme but is stabilized in a FrdC-E29L mutant (415).

Mutations of conserved residues in the vicinity of the Q<sub>P</sub>-site in human complex II have been linked to diseases such as hereditary paragangliomas and pheochromocytomas. The developmental mechanism of these two diseases is not well understood, but it was postulated that tumor formation was associated with superoxide overproduction by aberrant Sdh enzymes (416). Increased hypersensitivity to oxygen has been documented in *Caenorhabditis elegans* when mutations occur in this area of Sdh. Nematodes carrying the *mev-1* mutation (G71E) in SdhC show decreased life spans and increased levels of superoxide anion production under hyperoxia (417,418). The equivalent *mev-1* (S94E) and Sdh2p-P190Q mutations in ScSdh also conferred

hypersensitivities to oxygen and paraquat in *S. cerevisiae*. The EcSdh mutants SdhC-I28E (equivalent to *mev-1*), SdhD-H71L (heme ligand) and SdhC-H91L showed increased ROS production *in vitro* that is sensitive to the Q-site inhibitor HOQNO (373).

Biochemical studies pre-dating any structural data on ScSdh indicated the importance of Sdh3p-F103, Sdh3p-H113, Sdh3p-W116, Sdh4p-F69, Sdh4p-S71 and Sdh4p-H99 in a structurally independent fashion; that is, ScSdh enzymes harboring these individual mutants are assembled and localized correctly without large structural perturbations, but they show large decreases in enzyme activities (401,402). From the available crystal structures of Sdh, other residues which are directly involved in UQ binding, reduction and re-oxidation have been identified and examined in EcSdh. Amino acid side chains that interact with the UQ molecule through H-bonding include SdhC-S27, SdhC-R31, SdhD-D82 and SdhD-Y83, and substitution of these residues resulted in loss of UQ reductase activity as well as the ubisemiquinone EPR radical signal (414). It was suggested these residues play a large part by stabilizing the UQ molecule in the binding pocket. In the first EcSdh crystal structure, the O4 oxygen of UQ was not in close proximity to any part of the Sdh protein to form H-bonds, but the O1 oxygen of UQ was observed to be interacting with the hydroxyl side chain of SdhD-Y83, leading to the hypothesis that this absolutely conserved residue serves as a proton donor during UQ reduction; (131). However, removal of the OH group in a SdhD-Y83F mutant retained approximately 15% succinate:Q oxidoreductase activity, implying that this residue is not essential for enzyme catalysis but plays a large role in UQ binding (414). A subsequent study by Lemire *et al* on the ScSdh labeled the equivalent Tyr residue to be needed for UQ binding as well as proton transfer to the UQ during catalysis (375). Incidentally, the

same study also showcased a Tyr to Cys substitution that mimics a hereditary paraganglioma mutation (419) but the mutant enzyme did not show increased ROS generation during catalysis (375). Subsequent structural studies on EcSdh using competitive Q-site inhibitors revealed that a deeper quinone binding site allows the O4 carbonyl group to potentially H-bond to SdhC-S27 and SdhB-H207 (377). Two independent studies have confirmed the former residue to be critical for quinone binding and enzyme function (414,420). As for SdhB-H207, the importance of this residue is an ongoing study in our laboratory, but mutational studies of the equivalent residue in the *Ustilago maydis* (421) and *Paracoccus denitrificans* (422) Sdh enzymes render it resistant to carboxin, a Q-site inhibitor specific to complex II enzymes. From these studies, a reaction mechanism at the Q<sub>p</sub>-site was proposed (377): i) UQ binds loosely at the Q<sub>p</sub>-site and is stabilized by SdhD-Tyr83; ii) reduction of the [Fe-S] clusters in SdhB leads to conformational changes that cause UQ to bind deeper into the Q<sub>p</sub>-site and is further stabilized by SdhB-H207 and SdhC-S27; iii) two electrons are singly donated to UQ from either the [3Fe-4S] cluster or the heme *b* to form a phenolate dianion species, followed by donation of two protons via HOH39; iv) donation of protons disrupts the H-bonding network and the proton delivery pathway, leading to dissociation of the fully reduced UQH<sub>2</sub> molecule from the Q<sub>p</sub>-site.

In the EcSdh crystal structure, a series of ordered water molecules that span the width of the protein connect the cytoplasm to the Q<sub>p</sub>-site and has been proposed to be the source of protons for UQ reduction (377). In the porcine and avian Sdh enzymes, the entrance to the water channel, as well as the water molecules, are not conserved. In



Chapter 5, we examine the water channel in *E. coli* Sdh by mutating residues that line the entrance to this channel.

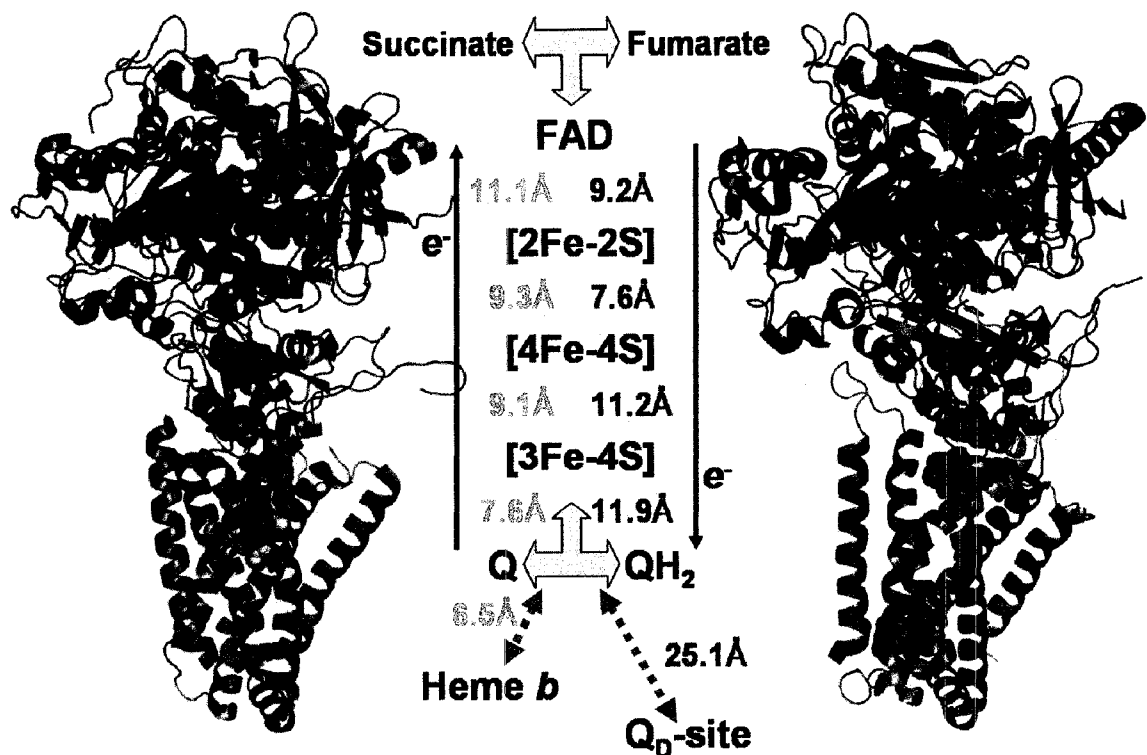


Figure 4.1. Overview of *Escherichia coli* succinate dehydrogenase (1NEK, left) and fumarate reductase (1LOV, right). The prosthetic groups, the direction of electron transfer, and the edge-to-edge distances between cofactors are indicated. Although the two enzymes are highly similar, major differences exist between the two homologues including the number of quinone binding sites, the location of the Q<sub>P</sub>-site, the presence of heme *b* in the membrane anchor domain, the midpoint potentials of the iron-sulfur clusters and the edge-to-edge distances between neighboring cofactors.

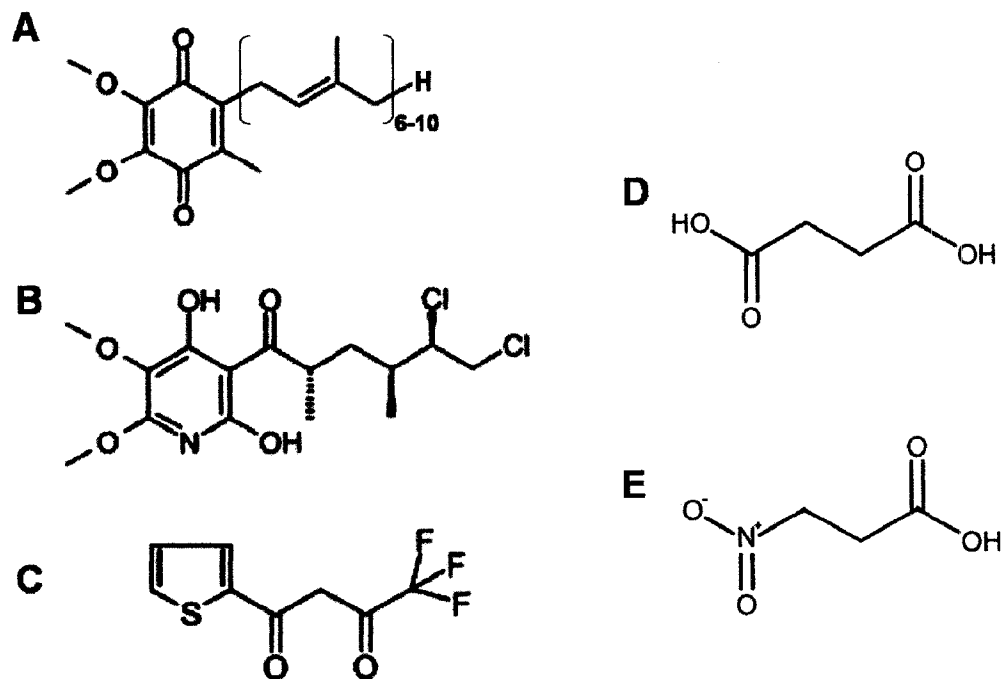


Figure 4.2. Competitive inhibitors which have been co-crystallized with Sdh. Atpenin 5 (B) and TTFA (C) are Q-site inhibitors that mimic ubiquinone (A). 3-nitropropionic acid (E) is a “suicide inhibitor” that irreversibly binds at the succinate (D) binding site.

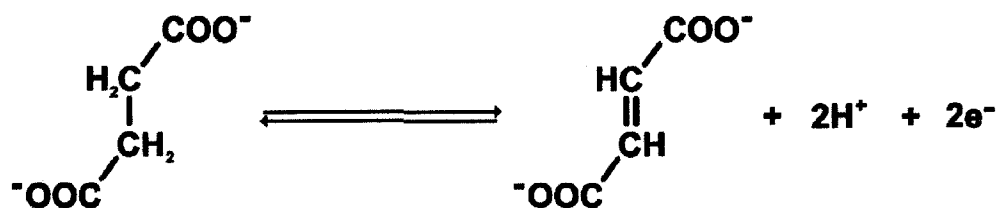


Figure 4.3. The reactions catalyzed by SdhA (forward) and FsdA (reverse).

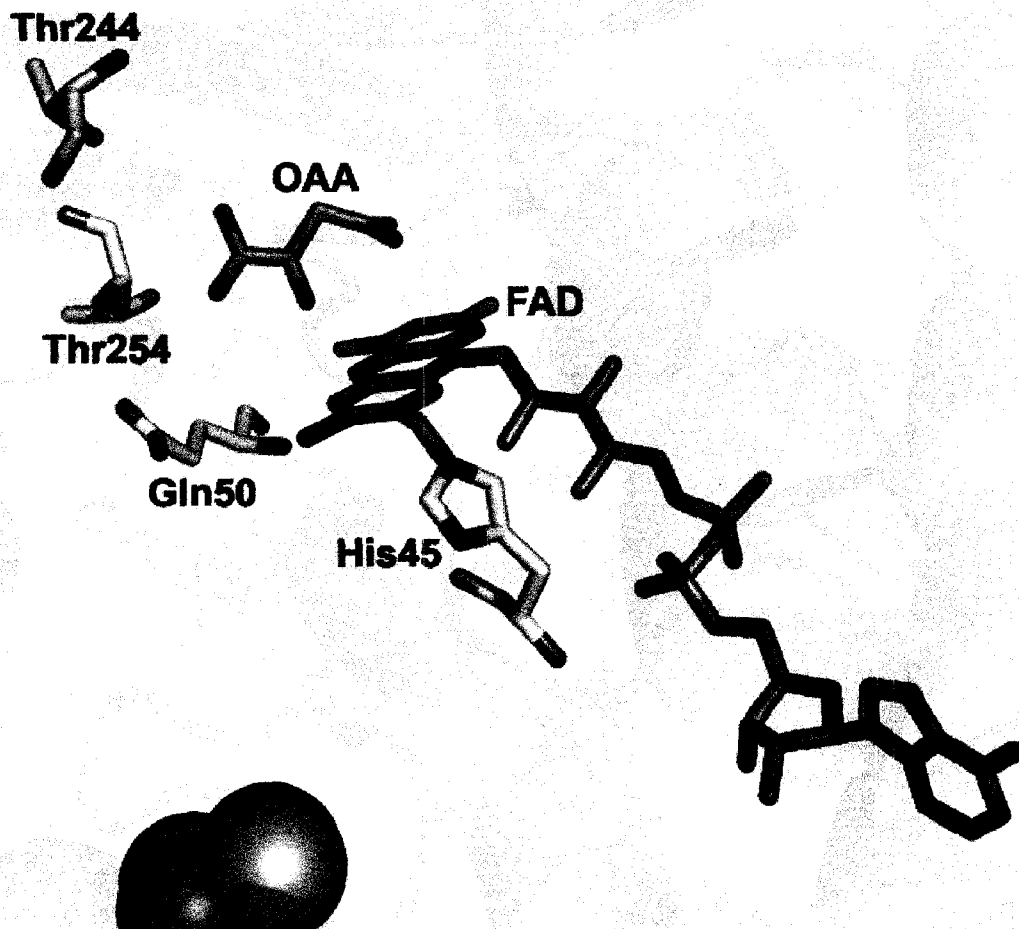


Figure 4.4. The succinate binding site in *Escherichia coli* succinate dehydrogenase. The flavin adenine dinucleotide (FAD) cofactor is covalently attached to SdhA via residue His45. The native enzyme was co-crystallized with the competitive inhibitor oxaloacetate (OAA). During catalysis, electrons are transferred from succinate to the FAD cofactor by a hydride transfer mechanism. Conserved residues Gln50, Thr244 and Thr254 have been shown to be important for substrate binding and succinate/fumarate interconversion.

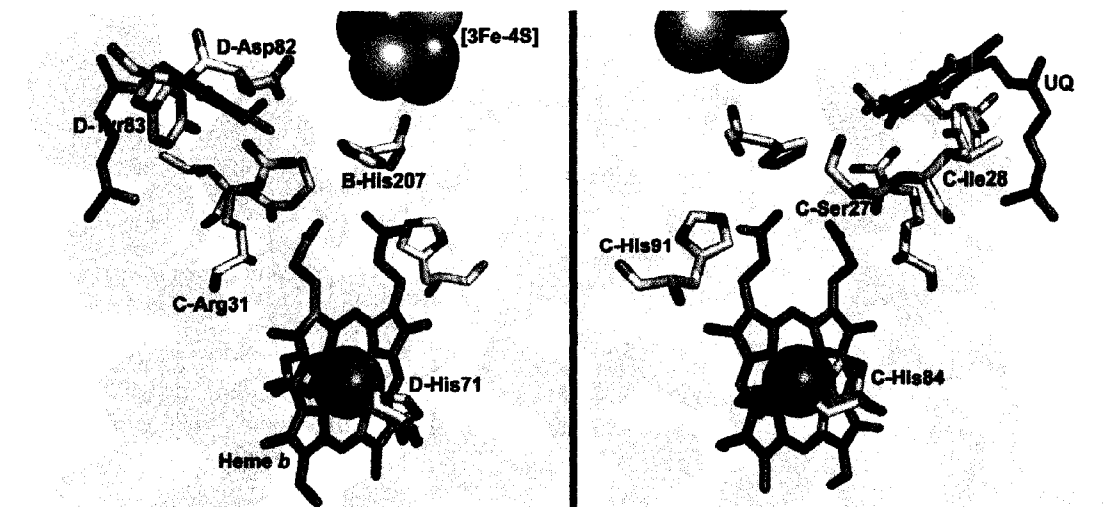


Figure 4.5. The ubiquinone binding pocket in *Escherichia coli* Sdh. The two images are 180° rotations of each other. The heme iron is bis-histidyl-coordinated and substitution of either His residue with Tyr leads to loss of the cofactor. Mutations of SdhC-His91 and SdhC-Ile28 leads to increased production of reactive oxygen species during enzyme turnover. Other residues labeled are important for ubiquinone binding and reduction.

## **Chapter 5**

# **Alternative Sites for Proton Entry from the Cytoplasm to the Quinone Binding Site in *Escherichia coli* Succinate Dehydrogenase**

**A version of this chapter was published:**

**Cheng, V.W.T., Johnson, A., Rothery, R.A. and Weiner, J.H. (2008) *Biochemistry*  
47, 9107-16.**

## 5.1 Introduction

The mitochondrial respiratory chain contains a complex electron relay system that converts chemical energy into a transmembrane electrochemical proton gradient. Complexes I, III and IV have been studied extensively and are known to translocate protons through either vectorial or scalar mechanisms. Complex II, commonly known as succinate:quinone oxidoreductase (SQR) or succinate dehydrogenase (Sdh), is the sole enzyme of the mitochondrial respiratory chain that is electroneutral. *Escherichia coli* possesses an Sdh that is essentially identical in structure and function to its mitochondrial counterpart (131,378,380) and represents an excellent model system for studying complex II enzymes.

Complex II enzymes have evolved with two basic overall architectures. The first is represented by the archetypical mitochondrial type enzyme that comprises a catalytic dimer (SdhAB) that is anchored to the matrix side of the membrane by two hydrophobic subunits (SdhCD). In *E. coli* and other bacteria such as *Paracoccus denitrificans*, the SdhCD subunits anchor SdhAB to the inner surface of the cytoplasmic membrane. An important subclass of complex II enzymes is represented by the heterotrimeric succinate dehydrogenase of *Bacillus subtilis* and the fumarate reductase of *Wolinella succinogenes*. These differ from the archetypical complex II in that they have only one membrane anchor subunit wherein two *b*-type hemes are integrated to provide an electron transfer relay to a periplasmically oriented quinone binding site (a Q<sub>D</sub>-site, distal to SdhB/FrdB). In the case of the true complex II archetypes, just a single heme *b* moiety is incorporated into the membrane anchor and only the Q<sub>P</sub>-site is functional. The presence of a Q<sub>D</sub>-site

has been observed in the homologous fumarate reductase enzyme from *E. coli* but its function remains controversial in mitochondrial and *E. coli* Sdh (216,227,378,402,423).

Because of the differences in subunit, heme, and Q-site compositions in the complex II superfamily, proton movement during quinone oxidation/reduction is extremely diverse. The *E. coli* and mitochondrial Sdh enzymes do not generate a proton motive force during catalysis as the two cytoplasmic protons consumed by quinone reduction are supplied by the succinate oxidation reaction. However, in Gram-positive bacteria such as *Bacillus sp.*, a heterotrimeric Sdh has been shown to be electrogenic when functioning as a quinol:fumarate oxidoreductase (407) and its succinate:quinone oxidoreductase activity is dependent on the transmembrane potential (408,409). The *W. succinogenes* fumarate reductase catalyzes an electroneutral reaction that involves a scalar movement of protons across the membrane that is cancelled by a stoichiometric vectorial movement of protons (392,410).

The reduction of ubiquinone to ubiquinol requires protons at the quinone binding site and few biochemical data are available on how protons are shuttled from the cytoplasm to this Q<sub>p</sub>-site. Crystallographic evidence supporting the existence of a conserved water-filled proton channel leading from the cytoplasm to the Q<sub>p</sub>-site is not obvious in the three available structures of tetrameric Sdh as there is a high degree of variation in the location of water molecules. A potential proton wire in the form of a water channel is observed in the *E. coli* structure (131,377) and we set out to determine whether the observed channel is crucial for enzyme function using a site-directed mutagenesis approach.



## 5.2 Experimental Procedures

*Bacterial Strains and Plasmids* – *E. coli* strain DW35 ( $\Delta frdABCD$ ,  $sdhC::kan$ ) (223) was used for all enzyme expression and growth studies. Expression of wild-type and mutant Sdh were anaerobically induced by using the plasmid pFAS, which encodes the *Sdh* operon under the control of the *frd* promoter (359). Laboratory strain TG1 (*supE hsd $\Delta$ 5 thi  $\Delta(lac-proAB)$  F[traD36 proAB<sup>+</sup> lacI<sup>q</sup> lacZ $\Delta$ M15]*; GE Healthcare) and plasmid pTZ18R (Amp<sup>R</sup>*lacZ'*; GE Healthcare) were used for molecular cloning and mutagenesis.

*Cloning* –The 3.7 kb KpnI-SphI fragment of pFAS was subcloned into pTZ18R and this recombinant plasmid was used as the template for site-directed mutagenesis (424). Sdh mutants were constructed using mutagenic oligonucleotides (Sigma), DpnI (Invitrogen) and Pfu DNA polymerase (Fermentas) in accordance to the QuikChange protocol (Stratagene). Mutants were verified by DNA sequencing (DNA Core Facility, Department of Biochemistry, University of Alberta) and cloned back into the pFAS expression vector. The mutant plasmids were then transformed into DW35 for biochemical studies. Preparation of competent cells and transformations of plasmids into competent cells were carried out as described in *Molecular Cloning: A Laboratory Manual* (335).

*Enzyme Expression and Preparation* – Wild-type and mutant enzymes were expressed in DW35 cells and isolated membranes enriched in Sdh were prepared by French pressure lysis followed by differential ultracentrifugation (424). All final membrane preparations containing activated enzymes were suspended in 100mM MOPS / 5mM EDTA / 1 mM malonate at pH 7.

*Growth Assays* – Aerobic growth on succinate and anaerobic growth on glycerol-fumarate were carried out as previously described (238,424). A Klett-Summerson colorimeter equipped with a no. 6 filter was used to monitor bacterial growth.

*SDS-PAGE* – Protein concentrations were estimated by the Lowry method (425) with the inclusion of 1% (w/v) sodium dodecyl sulfate in the mixture (337). 30 $\mu$ g of protein were resolved on a 12% SDS-PAGE gel (335) and visualized by Coomassie blue staining. Low molecular weight markers from Bio-Rad include phosphorylase b (97.4 kDa), bovine serum albumin (66.2 kDa), ovalbumin (45.0 kDa), carbonic anhydrase (31.0 kDa), soybean trypsin inhibitor (21.5 kDa) and lysozyme (14.4 kDa).

*Flavin Quantification* – Fluorometric quantification of the covalent flavin of Sdh was carried out in triplicate as described (426), using 5mg of protein as starting material.

*Enzyme Assays* – Succinate dependent reduction of 2-(4,5-dimethyl-2-thiazolyl)-3,5-diphenyl-2H-tetrazolium bromide (MTT,  $\epsilon = 17 \text{ mM}^{-1} \text{ cm}^{-1}$ ) was measured spectrophotometrically at 570nm in the presence of 750 $\mu$ M phenazine methosulfate (PMS) and 0.1% Triton X-100 (427). Succinate dependent reduction of Q<sub>0</sub> ( $\epsilon = 0.73 \text{ mM}^{-1} \text{ cm}^{-1}$ ) and fumarate dependent oxidation of plumbagin ( $\epsilon = 3.95 \text{ mM}^{-1} \text{ cm}^{-1}$ ) were monitored at 410nm and 419nm respectively. Turnover numbers were calculated based on covalent flavin (SdhA) concentrations. All assays were carried out using isolated membranes enriched in Sdh.

*Redox Titration and EPR Spectroscopy* – Redox titrations were carried out anaerobically under argon at 25°C on Sdh-enriched membranes at a total protein concentration of approximately 30mg mL<sup>-1</sup> in 100mM MOPS / 5mM EDTA (pH 7.0). The following redox mediators were used at a concentration of 25 $\mu$ M: 2,6-

dichloroindophenol, 1,2-naphthoquinone, toluylene blue, phenazine methosulfate, thionine, methylene blue, resorufin, indigotrisulfonate, indigocarmine, anthraquinone-2-sulfonic acid, and neutral red. EPR spectra were recorded using a Bruker Elexsys E500 EPR spectrometer equipped with an Oxford Instruments ESR900 flowing helium cryostat. Spectra of the [3Fe-4S] cluster were determined at 12K while that of heme *b* were determined at 9K, both at a microwave power of 20mW and a frequency of 9.38GHz. All spectra were corrected for internal EPR tube diameters. Presented data were gathered from two potentiometric titrations for each Sdh mutant, once via reduction by dithionite and once via oxidation by ferricyanide.

### 5.3 Results

Inspection of the *E. coli* Sdh crystal structure (PDB file 1NEK) (131) reveals a putative water channel leading from the cytoplasm to the Q<sub>P</sub>-site (377,423). Residues which line this water channel (<4Å away) are highlighted in Figure 5.1 wherein residues examined in this study are marked by asterisks. A list of mutants generated by site-directed mutagenesis is shown in Table 5.1, along with their predicted effects on the water channel as well as the conservation of the residue in the Sdh family.

A Coomassie blue-stained SDS-PAGE gel (Figure 5.2) shows that all Sdh mutant enzymes correctly assemble to the cytoplasmic membrane and Sdh expression levels, quantitated by covalent flavin content, correlate with the amount of protein detected.

The ability of the mutant Sdh enzymes to complement *E. coli* DW35 *in vivo* was examined using plasmid-mediated high level expression of the *sdh* operon. Figure 5.3a shows that all Sdh mutant enzymes were able to complement DW35 and support aerobic

growth on succinate minimal medium at essentially the same growth rate and growth density even though enzyme expression was induced by the anaerobic *frd* promoter. Since Sdh can readily function as a fumarate reductase under anaerobic conditions (359), we also tested the ability of the mutant enzymes to support anaerobic growth on glycerol-fumarate (G-F) medium. As expected, *E. coli* DW35 itself cannot grow on G-F minimal medium but can readily do so when transformed with the pFAS plasmid expressing wild-type (WT) Sdh (Figure 5.3b). Unlike the results seen for aerobic growth on succinate, the mutant enzymes displayed varying abilities to complement the deletion strain for growth on G-F. In particular the single mutants SdhC<sup>D95L</sup>DAB, SdhCDAB<sup>G227L</sup> and the double mutants containing the latter substitution (SdhC<sup>D95E</sup>DAB<sup>G227L</sup> and SdhC<sup>D95L</sup>DAB<sup>G227L</sup>) exhibited severely depressed growth.

The steady-state succinate:PMS/MTT assay is a non-physiological assay that measures succinate oxidase activity independent of Q<sub>P</sub>-site functionality. All membrane preparations containing the Sdh mutants, with the exception of SdhC<sup>D95E</sup>DAB, had comparable succinate:PMS/MTT activity relative to the WT enzyme at pH 7, pH 8 and in deuterium oxide (Table 5.2), indicating proper assembly and activation of the enzymes. Interestingly, the SdhC<sup>D95E</sup>DAB mutant had a succinate:PMS/MTT turnover rate that was approximately 50% higher than the WT enzyme at all three conditions. The succinate:Q<sub>0</sub> (succinate oxidation coupled to Q<sub>0</sub> reduction) and plumbagin:fumarate (plumbagin oxidation coupled to fumarate reduction) enzyme assays measure physiological and reverse activities of Sdh, respectively. At pH 7, WT Sdh catalyzed Q<sub>0</sub> reduction at a rate of 28 s<sup>-1</sup> and plumbagin oxidation at a rate of 31 s<sup>-1</sup>, whereas the mutant enzymes had slower rates of catalysis for both reactions (Tables 5.3 & 5.4). The double mutant

SdhC<sup>D95E</sup>DAB<sup>G227L</sup> also had slower rates of catalysis, but the SdhC<sup>D95L</sup>DAB<sup>G227L</sup> construct had wild-type kinetic parameters for succinate:Q<sub>0</sub> activity and remained impaired in the plumbagin:fumarate assay, resulting in a significantly higher Q<sub>0</sub>/plumbagin activity ratio at pH 7 (p-value < 0.001).

To further assess the functional efficiencies of the proton channel mutant enzymes, the assays were repeated at pH 8 where the H<sup>+</sup> concentration is decreased by 90%. At pH 8, the succinate:Q<sub>0</sub> and plumbagin:fumarate activities of the WT enzyme were determined to be 38 s<sup>-1</sup> and 16 s<sup>-1</sup> respectively, and are compromised in the proton channel mutants. The higher Q<sub>0</sub> reduction and lower plumbagin oxidation activities observed at pH 8 are consistent with previously published results (147,428). Worthy of note is the SdhCDAB<sup>G227L</sup> mutant which had similar turnover rates of Q<sub>0</sub> reduction and plumbagin oxidation. This contrasts to the other mutants, as well as the WT enzyme, which catalyze the forward reaction approximately twice as fast as the reverse reaction at pH 8 (Tables 5.3 & 5.4).

We also characterized the abilities of the mutant enzymes to function at pD 7.4 (measured as pH 7 using a pH electrode) in a deuterium oxide solvent. Using D<sub>2</sub>O to probe proton transfer reactions and rate-limiting steps in catalytic mechanisms is well established (429). The succinate:PMS/MTT, succinate:Q<sub>0</sub> and plumbagin:fumarate activities were determined to be 8 s<sup>-1</sup>, 10 s<sup>-1</sup> and 4 s<sup>-1</sup> respectively for the WT enzyme at pD 7.4. Figure 5.4 shows the physiological and reverse enzyme activities of the mutant enzymes relative to WT Sdh while Table 5.5 presents the results as ratios of comparative activities at pH 7 *versus* pD 7.4. Only a minor kinetic isotope effect (KIE) was observed in the succinate:PMS/MTT reaction. During Q<sub>0</sub> reduction the mutant enzymes show

similar KIE values compared to the WT enzyme (p-value > 0.1), but significant differences were observed in the plumbagin oxidation reaction (p-value < 0.001). We also observed a general increase in the KIE value for all mutant enzymes as well as the WT enzyme in the plumbagin:fumarate reaction compared to the succinate:Q<sub>0</sub> reaction.

We next determined the effects of the mutations on the EPR spectroscopic properties of the [3Fe-4S] cluster, which is in close proximity to the Q<sub>p</sub>-site; Figure 5.5 shows the effects of the mutations on its EPR lineshape. The SdhCDAB<sup>G227L</sup> mutant exhibits a minor broadening of the oxidized [3Fe-4S] peak-trough signal wherein the peak remains at g=2.02 and the trough shifts from g=1.99 to g=1.98. The SdhC<sup>D95E</sup>DAB<sup>G227L</sup> mutant, but not the SdhC<sup>D95L</sup>DAB<sup>G227L</sup> mutant, also experiences this broadening in the EPR lineshape of its [3Fe-4S] cluster. The SdhCD<sup>Q78L</sup>AB mutant shows an opposing effect where its trough is actually shifted from g=1.99 to g=2.00. Data from redox titrations suggest that only the SdhC<sup>D95L</sup>DAB mutant has an effect on the midpoint potential of the [3Fe-4S] cluster, which is shifted modestly from +52mV in the WT enzyme to +87mV (Table 5.6).

With respect to the EPR spectrum of the heme, the WT Sdh enzyme exhibits a broad signal that comprises two overlapping peaks located at g=3.66 and g=3.55. Some of the mutations presented herein appear to alter the relative intensities of these two peaks (Figure 5.6). SdhCDAB<sup>G227L</sup>, SdhC<sup>D95L</sup>DAB, SdhC<sup>E101L</sup>DAB and SdhCD<sup>Q78L</sup>AB, as well as the two double mutants, are able to elicit a downfield shift of the low-spin heme signal towards the g=3.66 species. Analyses of the heme *b* indicate that all mutations along the putative water channel cause a decrease in its *E<sub>m</sub>* value with the exception of the double mutant SdhAB<sup>G227L</sup>C<sup>D95L</sup>D (Table 5.6).

## 5.4 Discussion

In this study, we set out to determine if the water channel observed in the X-ray crystal structure of *E. coli* Sdh served as a H<sup>+</sup> delivery pathway from the cytoplasm to the Q<sub>P</sub>-site (131,377). Chains of electron densities interpreted to be water molecules are observed in the three known Sdh structures, but differences exist between the precise residues involved. In *E. coli* Sdh, the entrance to the proton pathway is surrounded by residues SdhB<sup>G227</sup> and SdhC<sup>E101</sup>, with SdhC<sup>D95</sup> nearby (131); in the two mammalian complex II structures (Figures 5.7 and 5.8), the water molecule at the hydrophobic/hydrophilic interface interacts with the sidechain of a glutamine residue that is equivalent to SdhD<sup>Q78</sup> in *E. coli* Sdh (378,380). Furthermore, the number and positions of water molecules along the proton pathway differ significantly amongst the three structures. Thus the role of these four residues in enzyme catalysis was examined.

Our data clearly indicate that mutations surrounding the putative water channel have little effect on the ability of the enzyme to support aerobic respiratory growth on succinate, but have a profound effect on anaerobic growth on glycerol-fumarate. At both pH 7 and pH 8, the Sdh mutant enzymes retained significant succinate:Q<sub>0</sub> oxidoreductase activity; thus their ability to sustain aerobic growth on succinate is not surprising. Given the high *in vitro* plumbagin:fumarate oxidoreductase activities observed in all the mutant enzymes, the variation of anaerobic growth rates on G-F minimal medium was unexpected. As the availability of ATP is limited during anaerobic growth on G-F, the poor growth rates of SdhCDAB<sup>G227L</sup>, SdhC<sup>D95L</sup>DAB, SdhC<sup>E101L</sup>DAB and the double mutants suggested that *in vivo* expression of the mutant enzymes was compromising the energy efficiency of the cells, possibly by making the membranes more permeable to H<sup>+</sup>

and thereby destroying the proton motive force. To rule out this possibility we monitored anaerobic growth on minimal media where dimethylsulfoxide was used as the terminal electron acceptor in place of fumarate (238). If the cells were leaky to  $H^+$  this should lead to compromised growth as was shown in Fig 3b, but this was not observed (data not shown). We also found that whole cells expressing the various mutant enzymes did not show a higher rate of  $H^+$  influx when exposed to an acid pulse (430). Thus the effects of the mutants examined herein appear to be specific to Sdh.

In  $D_2O$ , the mutant enzymes generally have similar rates of plumbagin oxidation but apparent decreased quinone reductase activities compared to the WT enzyme. This translates into a significantly larger KIE for the WT enzyme compared to the mutant enzymes in the plumbagin:fumarate assay, but not the succinate: $Q_0$  assay (Figure 5.4, Table 5.5). This implies that reversible proton transfer between the cytoplasm and the  $Q_P$ -site may be comprised of non-equivalent pathways using water molecules located at different locations. Specifically, there may be alternate water channels that are associated with different redox states of the heme (431). This latter explanation may account for the diversity and variation of the number and positions of the water molecules observed in the three crystal structures of Sdh.

In the kinetic data presented in Tables 5.3 and 5.4, two mutant enzymes stand out in particular: SdhCDAB<sup>G227L</sup>, which had a significant higher rate of  $Q_0$  reduction at pH 8 compared to pH 7, and SdhCD<sup>Q78L</sup>AB, which had higher  $k_{cat}/K_m$  values for the succinate: $Q_0$  reaction at pH 8 and the plumbagin:fumarate reaction at pH 7 relative to the WT enzyme. The altered kinetic properties of these two mutant enzymes is consistent with the fact that the two residues are located at the observed entrances to the membrane



intrinsic water channel in the *E. coli* and eukaryotic Sdh structures respectively. In an attempt to completely preclude solvent accessibility in the former enzyme, the double mutants SdhC<sup>D95E</sup>DAB<sup>G227L</sup> and SdhC<sup>D95L</sup>DAB<sup>G227L</sup> were created. Intriguingly, the SdhC<sup>D95L</sup>DAB<sup>G227L</sup> mutant enzyme had a comparable rate of succinate-dependent Q<sub>0</sub> reduction as the WT enzyme but remained compromised in its ability to carry out fumarate-dependent plumbagin oxidation. As discussed above, both double mutant enzymes were unable to rescue anaerobic growth of DW35 on G-F despite retaining significant plumbagin:fumarate activity. To explain this apparent paradox, we propose that the *E. coli* Sdh uses an alternative water channel to transport protons to/from the cytoplasm from/to the Q<sub>P</sub>-site when proton channel mutations close off the H<sup>+</sup> pathway. Examination of the *E. coli* Sdh structure revealed an alternative pathway for H<sup>+</sup> movement that involves residue SdhD<sup>D15</sup> and HOH45 (PDB file 1NEK). This pathway is not visible when the enzyme is viewed from the “side” (parallel to the membrane) but becomes apparent when viewed from the cytoplasm (Figure 5.9). Further, this pathway appears to be more efficient in that it involves only 5 ordered water molecules as opposed to a sequence of 13 water molecules which span the entire length of the protein as proposed by Horsefield *et al* (377). Most importantly, the location of HOH45 is also equivalent to the positions at which the water channel entrance is located in the pig and chicken Sdh enzymes, finally bringing a sense of coherency amongst the three Sdh structures.

The existence of multiple proton channels in redox enzymes is not newfound and has been extensively studied most notably in the cytochrome oxidase family of enzymes and the bacterial photosynthetic reaction center. In cytochrome *c* oxidase, up to three

possible proton pathways (D-, K- and H-pathways) may facilitate proton translocation across the energy conserving membrane. In a high resolution crystal structure of the *Rhodobacter sphaeroides* reaction center, multiple water channels were observed to connect the Q<sub>B</sub> molecule to the aqueous phase and converge at a key Asp residue near Q<sub>B</sub> (432,433). Single mutations of His-H126 and His-H128, residues located at the entrance to one of the water channels, did not affect proton uptake but double replacement of His with Ala impeded the rate of proton uptake by ~4-10 fold (434). The retention of proton uptake ability in the mutant reaction centers indicates other water channels are capable of proton conductance from the aqueous phase to the quinone molecule.

As our data suggest, the water channel entrance involving SdhD<sup>D15</sup> may only function *in vitro*, or is non-functional *in vivo* under anaerobic conditions. It is unclear why this may be the case, but one possible explanation involves the binding of menaquinol to the Q<sub>P</sub>-site *in vivo*. With regards to the porcine Sdh enzyme, it was proposed that the hydrophobic tail of the UQ molecule wraps around the SdhCD domain such that it induces closure to the Q<sub>D</sub>-site (378). In *E. coli* Sdh, it is conceivable by analogy that the isoprenoid tail of the quinone molecule can wrap around the membrane anchor domain such that the hydrophilic opening to the water channel via SdhD<sup>D15</sup> is blocked. Since plumbagin does not have any isoprenoid extensions, H<sup>+</sup> can enter/exit Sdh at SdhD<sup>D15</sup> even if the proton channel mutations studied herein close off the H<sup>+</sup> pathway further down the water chain. An alternate possibility to account for the discrepancy between the *in vivo* and *in vitro* activities is the presence of a weakly bound lipid that is washed off during enzyme preparation. Finally, the different oligomeric states of Sdh *in vivo* and *in vitro* could also account for the discrepancy since intersubunit contacts

between neighboring Sdh could deny accessibility at the SdhD<sup>D15</sup> entrance. However, this last scenario is unlikely since we did not employ any detergents during our enzyme preparations and used isolated membranes in all our assays.

Studies on the proton channel were recently carried out in the heme-free Sdh mutants from *E. coli* (130) and *Saccharomyces cerevisiae* (400). In the crystal structure, one of the propionate groups of the heme *b* interacts with the water channel (131); removal of the heme would most likely bring disorder to the existing water molecules and perhaps even allow additional water molecules into the void normally occupied by the heme. The *E. coli* and *S. cerevisiae* heme-free enzymes maintain approximately 50-70% of their catalytic activity at pH 7, similar to the results observed in this study. Thus the Q<sub>P</sub>-site appears to be relatively robust in that it can still carry out quinone reaction chemistry despite disruption of the water channel leading towards it, most likely because the final water molecule (HOH39) is still present and stabilized by residues SdhB<sup>H207</sup>, SdhC<sup>R31</sup> and SdhD<sup>D82</sup> (377). Given that the mutations studied herein affect the water channel it is conceivable that some long range effect might be propagated to the Q<sub>P</sub>-site. However, apparent K<sub>m</sub> values for Q<sub>0</sub> and plumbagin were only slightly affected in our enzyme assays. Furthermore, it is known that only an intact and functional Q<sub>P</sub>-site can bridge electron transfer from the [3Fe-4S] cluster to the heme *b* (414). Since the heme cofactor is reducible by succinate in all mutant enzymes (data not shown), it can be inferred that binding and release of endogenous quinone/quinol molecules are not significantly affected.

Oyedotun and Lemire had previously examined the strictly conserved Sdh3p-D117 residue in *S. cerevisiae* Sdh and discovered a long-range translational effect on the

flavin active site in the form of a *decreased* succinate:PMS turnover rate (401). In this study, a similar phenomenon was observed when the equivalent SdhC<sup>D95</sup> residue was substituted with a glutamate; however, the SdhC<sup>D95E</sup>DAB mutant, as well as the SdhC<sup>D95E</sup>DAB<sup>G227L</sup> mutant, showed an *increase* in succinate:PMS/MTT turnover. Thus it appears that SdhC<sup>D95</sup>, a residue that H-bonds to the water channel, has the ability to exert intersubunit control on the catalytic SdhAB dimer. Interestingly, the SdhC<sup>D95E</sup>DAB mutation also shifts the midpoint potential of the heme from +20mV to -40mV. To date, it remains uncertain what the exact function of the heme *b* is in Sdh. Clearly, it plays a role in enzyme stability, but it is not necessary for its assembly or for enzyme catalysis *in vitro* and *in vivo*, and it does not suppress generation of reactive oxygen species as some have suggested (130,131,400). Can it be that the heme acts as a redox sensor and communicates this information to the FAD site such that succinate oxidation and electron transfer are coupled to proton transfer and ubiquinone reduction?

Because the heme interacts with the water channel via H-bonds, spectroscopic data gathered on this cofactor would indicate whether its surroundings have been significantly altered. The reduced-*minus*-oxidized UV-visible spectra of the heme *b* in the mutant enzymes show no obvious deviation from that of the WT enzyme (data not shown). EPR analyses on the oxidized heme showed that the SdhCDAB<sup>G227L</sup>, SdhC<sup>D95L</sup>DAB, SdhC<sup>E101L</sup>DAB and SdhCD<sup>Q78L</sup>AB mutations cause a change in its EPR lineshape, indicating an alteration in the local environment or the conformation of this prosthetic group. Note that this change in EPR lineshape is not observed in the SdhC<sup>D95E</sup>DAB and SdhC<sup>E101D</sup>DAB mutant enzymes wherein the carboxylate sidechains are maintained. Rothery *et al.* have carried out redox titrations and *in silico* simulations

on the heme whereby a SdhC<sup>H91L</sup>DAB mutation shifts the EPR signal to the g=3.66 species and a SdhCD<sup>R20L</sup>AB mutation shifts the EPR signal to the g=3.55 species (unpublished data). It is believed that the two mutants alter the conformation of one of the propionate arms of the heme such that the H-bonding network involving the water channel is altered. All four leucine variants mentioned herein caused the equilibrium to shift towards the g=3.66 species, indicating that they all had the same disruptive effect on the water channel.

With this work on the H<sup>+</sup> pathway and water channel, an understanding of the complexity underlying the workings of the succinate dehydrogenase enzyme is beginning to emerge. Mutational analyses of SdhC<sup>D95</sup> provide a glimpse of how proton transfer may be coupled to succinate oxidation and possibly electron transfer in the catalytic dimer. We found that disruption of the water channel near its entrance into the hydrophobic SdhCD domain slows down, but does not completely inhibit, catalysis. *In vivo* activity, but not *in vitro* activity, was significantly altered when the mutants were forced to function as a fumarate reductase. Based on the structures of the pig and chicken Sdh, as well as our data, we present an alternative proton pathway that only appears to be functional *in vitro*. This pathway involves residue SdhD<sup>D15</sup>, which appears to be a worthy candidate for future experiments

Residue	Conservation	Mutation	Predicted effect on putative water channel
SdhB-G227	similar	G-->L	Adds hydrophobic bulk; blocks water channel entrance
SdhC-D95	yes	D-->E	Extends sidechain and alters H-bonding network
		D-->L	Eliminates potential H-bond to water channel
SdhC-E101	no	E-->D	Shortens sidechain and alters H-bonding network
		E-->L	Eliminates potential H-bond to water channel
SdhD-Q78	yes	Q-->L	Eliminates potential H-bond to water channel

Table 5.1. A list of residues studied by site-directed mutagenesis. ClustalW alignments with Sdh from human , pig, cow and chicken were performed and the conservation of the residue indicated. The mutation made at each position, as well as its rationale, are also listed.

	Turnover (s <sup>-1</sup> )					
	pH7		pH8		pD7.4	
WT Sdh	11.5	± 0.4	20.9	± 1.8	7.5	± 0.7
B-G227L	9.3	± 0.2	15.9	± 1.8	6.4	± 0.4
C-D95E	15.6	± 0.4	29.6	± 2.8	10.6	± 0.4
C-D95L	10.5	± 0.3	17.4	± 0.8	6.7	± 0.5
C-E101D	9.8	± 0.3	18.0	± 0.8	6.0	± 0.2
C-E101L	8.1	± 0.7	12.6	± 0.6	5.3	± 0.1
D-Q78L	9.9	± 0.6	20.8	± 0.3	6.0	± 0.2
B-G227L/C-D95E	19.9	± 1.6	N.D.		N.D.	
B-G227L/C-D95L	9.4	± 0.9	N.D.		N.D.	

Table 5.2. Succinate dependent reduction of PMS/MTT by mutant enzymes at pH 7, pH 8 and pD 7.4. Succinate was used as electron donor and reduction of MTT was measured in the presence of 750µM PMS. Turnover numbers were calculated based on the amount of covalent FAD determined. Triplicate readings were taken at each condition.

	Turnover ( $s^{-1}$ )		$K_m$ (mM)		$k_{cat}/K_m$ ( $s^{-1}mM^{-1}$ )	
	pH7	pH8	pH7	pH8	pH7	pH8
WT Sdh	27.5 ± 1.8	37.9 ± 3.4	0.18 ± 0.01	0.15 ± 0.01	157	248
B-G227L	14.5 ± 0.5	11.6 ± 1.3	0.16 ± 0.01	0.09 ± 0.01	90	127
C-D95E	16.1 ± 0.5	22.3 ± 1.8	0.18 ± 0.02	0.13 ± 0.01	91	173
C-D95L	16.8 ± 0.7	16.2 ± 2.3	0.13 ± 0.01	0.07 ± 0.01	125	246
C-E101D	14.7 ± 0.9	20.9 ± 1.5	0.13 ± 0.02	0.10 ± 0.01	111	207
C-E101L	12.6 ± 0.1	15.6 ± 1.8	0.10 ± 0.02	0.09 ± 0.01	124	168
D-Q78L	15.8 ± 0.1	17.4 ± 3.9	0.19 ± 0.03	0.06 ± 0.01	83	310
B-G227L/C-D95E	18.6 ± 0.6	N.D.	0.20 ± 0.01	N.D.	95	N.D.
B-G227L/C-D95L	24.8 ± 0.4	N.D.	0.16 ± 0.02	N.D.	151	N.D.

Table 5.3. Succinate-dependent reduction of  $Q_0$  by mutant enzymes. Rates of  $Q_0$  reduction were monitored spectrophotometrically at 410nm and were determined at varying concentrations of the quinone analogue.  $k_{cat}$  and  $K_m$  values were obtained by plotting  $1/v$  against  $1/[S]$  in a double-reciprocal plot using at least 8 activity measurements at different  $Q_0$  concentrations, and repeated at least once. N.D. = not determined.

	Turnover ( $s^{-1}$ )		$K_m$ (mM)		$k_{cat}/K_m$ ( $s^{-1}mM^{-1}$ )	
	pH7	pH8	pH7	pH8	pH7	pH8
WT Sdh	31.1 ± 1.7	15.9 ± 1.4	0.17 ± 0.02	0.17 ± 0.01	179	93
B-G227L	18.0 ± 0.8	9.1 ± 0.5	0.11 ± 0.01	0.13 ± 0.01	162	71
C-D95E	24.3 ± 3.5	12.7 ± 1.3	0.14 ± 0.03	0.19 ± 0.02	176	68
C-D95L	18.0 ± 3.7	8.6 ± 0.2	0.12 ± 0.01	0.16 ± 0.01	153	53
C-E101D	17.1 ± 1.4	10.4 ± 0.3	0.11 ± 0.01	0.14 ± 0.01	159	73
C-E101L	14.9 ± 1.7	7.7 ± 0.4	0.10 ± 0.01	0.11 ± 0.01	152	71
D-Q78L	16.7 ± 0.9	9.3 ± 0.4	0.08 ± 0.01	0.11 ± 0.01	210	85
B-G227L/C-D95E	23.0 ± 3.6	N.D.	0.128 ± 0.05	N.D.	179	N.D.
B-G227L/C-D95L	21.5 ± 0.4	N.D.	0.124 ± 0.03	N.D.	173	N.D.

Table 5.4. Fumarate dependent oxidation of reduced plumbagin by mutant enzymes. Rates of plumbagin oxidation were monitored spectrophotometrically at 419nm and were determined at varying concentrations of the quinone analogue.  $k_{cat}$  and  $K_m$  values were obtained by plotting  $1/v$  against  $1/[S]$  in a double-reciprocal plot using at least 8 activity measurements at different  $Q_0$  concentrations, and repeated at least once. N.D. = not determined.

	pH/pD Ratio		
	Succ:PMS/MTT	Succ:Q0	PBG:fumarate
WT Sdh	1.5	2.7	8.1
B-G227L	1.5	2.4	5.8
C-D95E	1.5	2.1	5.8
C-D95L	1.6	2.4	5.1
C-E101D	1.6	2.5	5.5
C-E101L	1.5	2.0	6.0
D-Q78L	1.7	2.6	5.5

Table 5.5. Kinetic isotope effect on enzyme activities. Enzymatic activities were measured by using concentrations of Q<sub>0</sub> and plumbagin that are at least 10x their K<sub>m</sub> values as determined at pH 7. The pH/pD ratios were determined by dividing the rate of substrate turnover at pH 7 by that obtained at pD 7.4.



Mutant	[3Fe-4S] $E_m$ (mV)	Heme <i>b</i> $E_m$ (mV)
WT	+ 52	+ 20
B-G227L	+ 60	- 5
C-D95E	+ 56	- 40
C-D95L	+ 87	+ 17
C-E101D	+ 51	+ 10
C-E101L	+ 55	+ 12
D-Q78L	+ 65	+ 8
B-G227L/C-D95E	+ 77	- 10
B-G227L/C-D95L	+ 86	+ 42

Table 5.6. Midpoint potentials of the [3Fe-4S] cluster and heme *b*. Two redox titrations on membrane preparations containing each Sdh construct were carried out at pH 7. Dithionite was used solely as a reductant in one titration (decreasing reduction potential) whereas ferricyanide was used solely as an oxidant in the other titration (increasing reduction potential). 200 $\mu$ L samples poised at varying reduction potentials were frozen with liquid nitrogen-chilled ethanol and analyzed by EPR. Data were obtained under the following instrument conditions: temperatures, 12 K ([3Fe-4S] cluster) and 9 K (heme *b*); microwave power, 20 mW at 9.38 GHz; modulation amplitude, 10 G<sub>pp</sub> at 100 KHz. The signal at  $g=2.02$  was used to determine the midpoint potential ( $E_{m,7}$ ) of the [3Fe-4S] cluster while the  $g=3.66$  signal was used for the heme *b*. Data from the two titrations were merged and the Nernst equation was fitted to obtain the  $E_{m,7}$  value of each cofactor. The error in  $E_{m,7}$  values is approximately  $\pm 10$  mV.

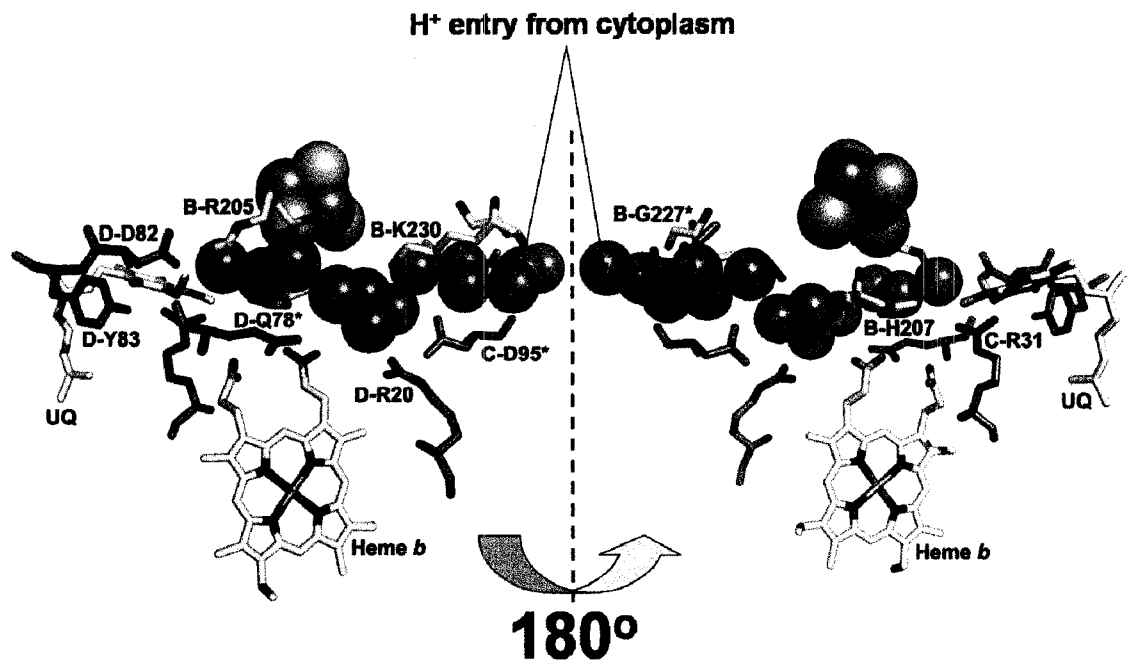


Figure 5.1. Two views of the putative water channel in *E. coli* Sdh leading from the cytoplasm to the Q-site. Protons required for ubiquinone reduction are acquired from the cytoplasm via this proposed water channel. Residues from SdhB, SdhC and SdhD interact with this channel, which passes near the [3Fe-4S] cluster and the heme *b*. Residues that are examined in this study are marked by an asterisk. Also shown are residues SdhC<sup>R31</sup>, SdhD<sup>D82</sup> and SdhD<sup>Y83</sup>, which have been implicated in the ubiquinone binding and reduction mechanism (377,414). The figure was generated from PDB file 1NEK using PyMOL v.0.99 (DeLano Scientific LLC.)

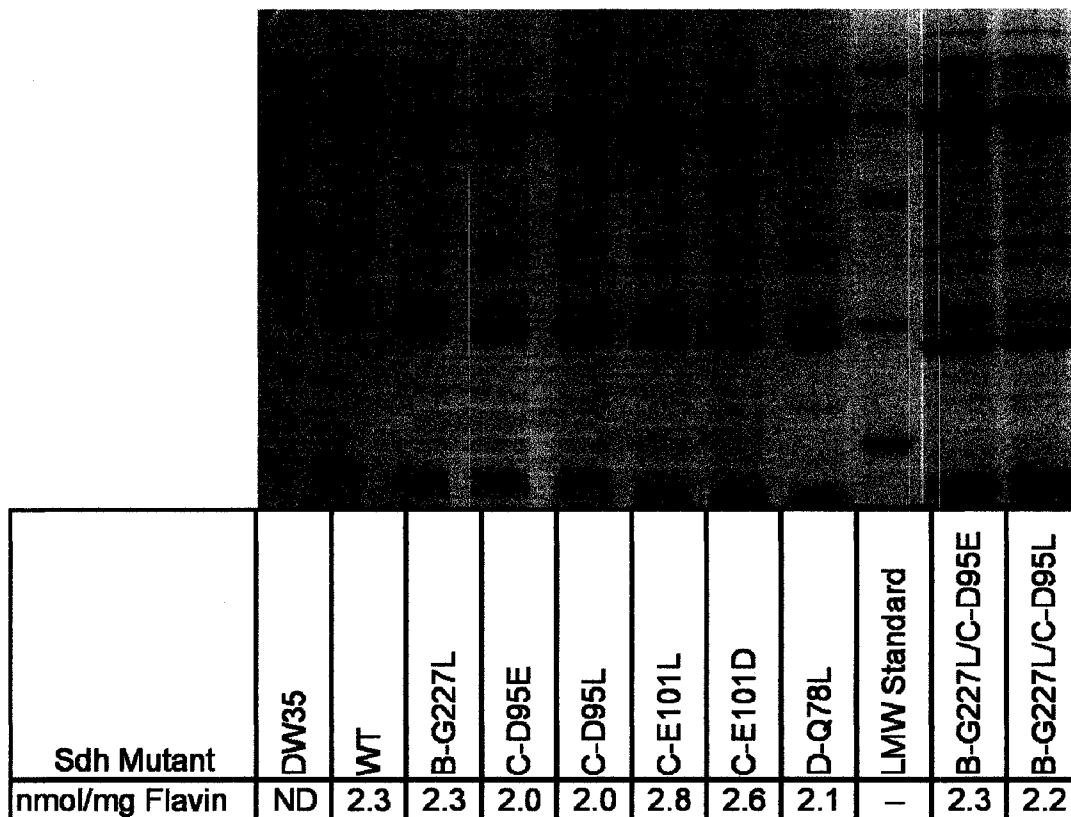


Figure 5.2. Assembly of mutant Sdh enzymes. 30  $\mu$ g of membrane proteins were separated on a 12% SDS polyacrylamide gel and stained by Coomassie blue. The concentrations of covalent flavin, determined as described in Experimental Procedures, in each enzyme preparation are also shown. ND: not determined.

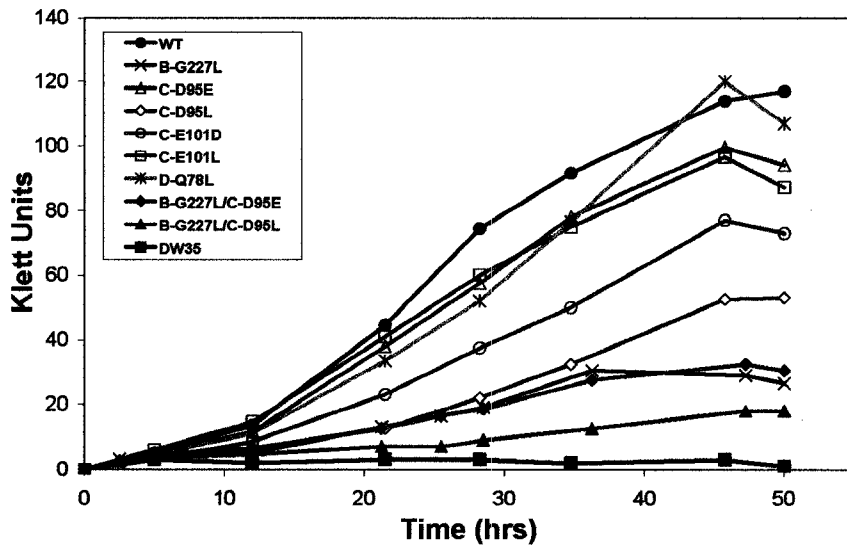
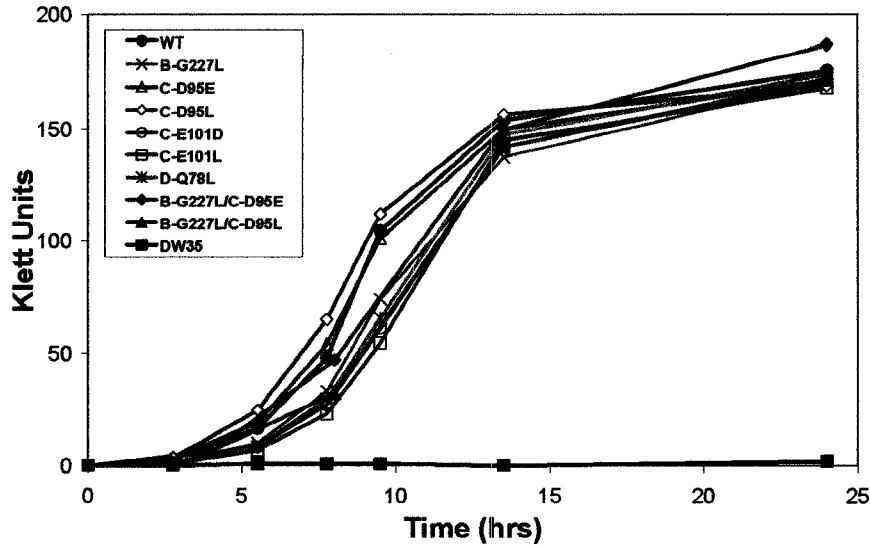


Figure 5.3. Growth of *E. coli* DW35 with and without expression of wild-type and mutant Sdh enzymes. Top, aerobic growth on succinate minimal medium. 25mL cultures in 125mL sidearm flasks were grown at 37°C with shaking. Bottom, anaerobic growth on glycerol-fumarate minimal medium. 125mL sidearm flasks filled with bacterial culture were grown at 37°C with magnetic stirring. Growth curves are representative of triplicate experiments wherein cell density measurements (Klett units) were collected from two separate and independent bacterial cultures at the times indicated.

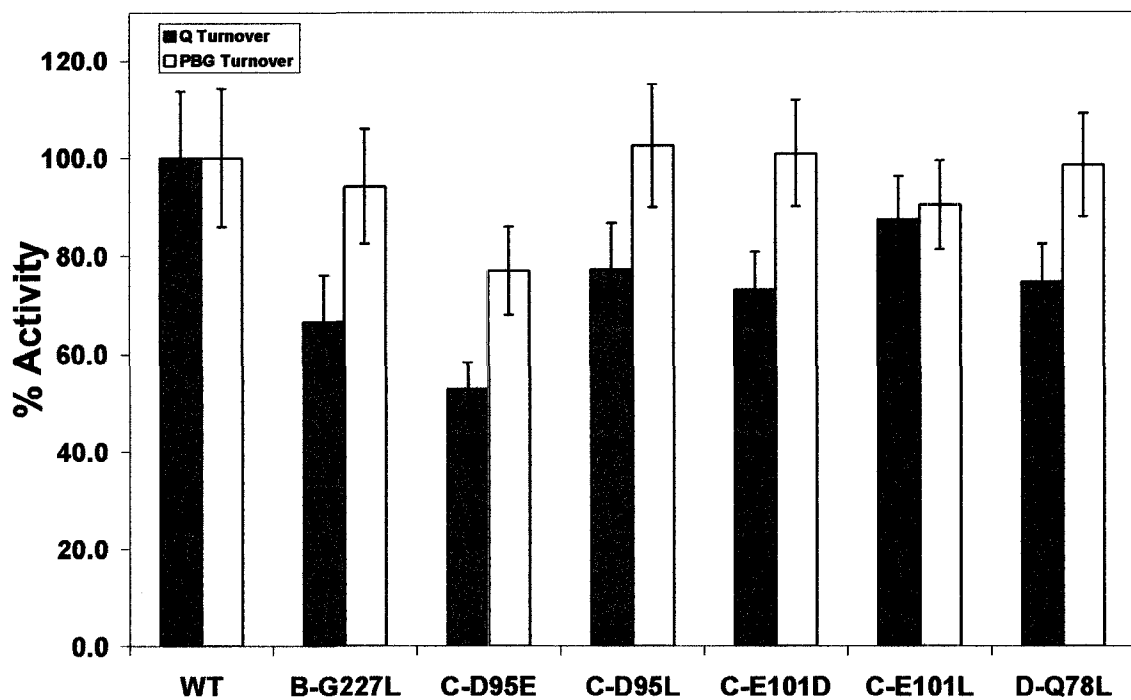


Figure 5.4. Relative enzyme activities in deuterium oxide. Succinate:Q<sub>0</sub> and plumbagin:fumarate oxidoreductase activities were determined at pD 7.4 (measured as pH 7.0 using a pH electrode). 100% activity, as measured from the wild-type Sdh enzyme, corresponds to turnover rates of 10 s<sup>-1</sup> and 4 s<sup>-1</sup> for the Succinate:Q<sub>0</sub> and plumbagin:fumarate assays, respectively. Q<sub>0</sub> reduction was monitored at a wavelength of 410nm while plumbagin oxidation was followed at 419nm. Enzyme activities of each Sdh preparation were gathered from three independent measurements and then normalized against their succinate:PMS/MTT activities.

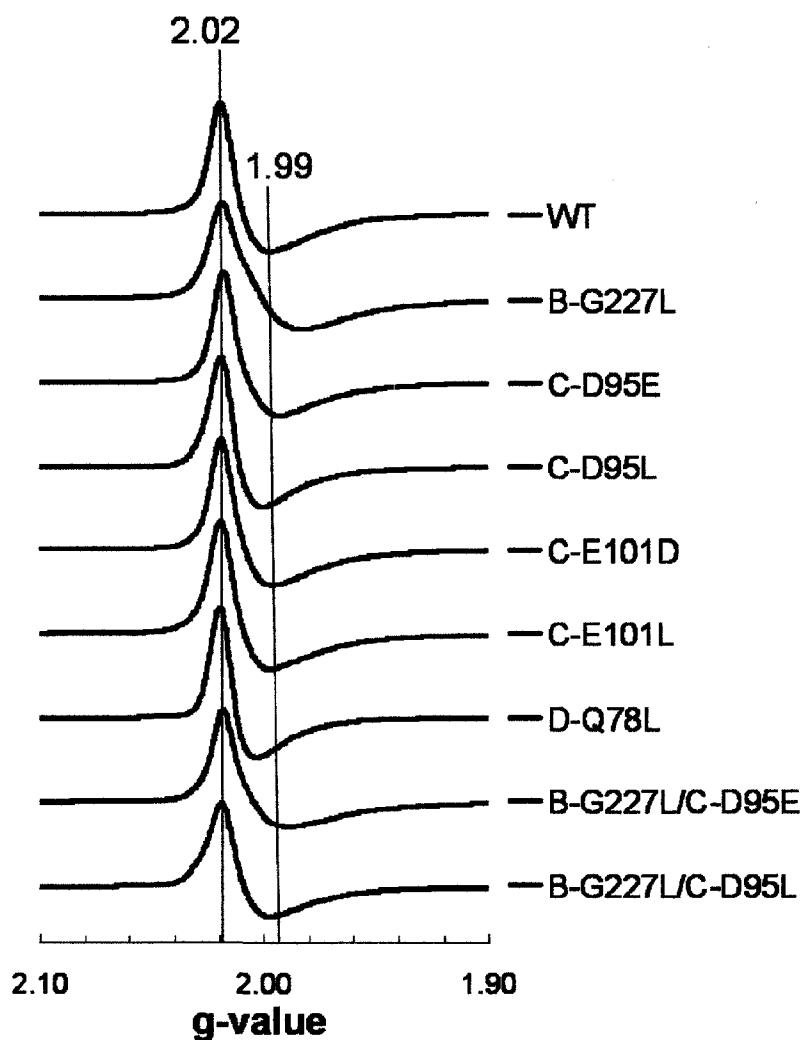


Figure 5.5. EPR spectra of the oxidized [3Fe-4S] cluster. Data were obtained under the following instrument conditions: temperature, 12 K; microwave power, 20 mW at 9.38 GHz; modulation amplitude, 10  $G_{pp}$  at 100 KHz. Spectra were taken during redox titrations wherein the [3Fe-4S] cluster is fully oxidized (poised at +118mV or higher). Each spectrum is collected from a 200 $\mu$ L sample at approximately 30 mg mL<sup>-1</sup> total protein concentration wherein the Sdh enzyme is present at approximately 2 nmol mg<sup>-1</sup>.

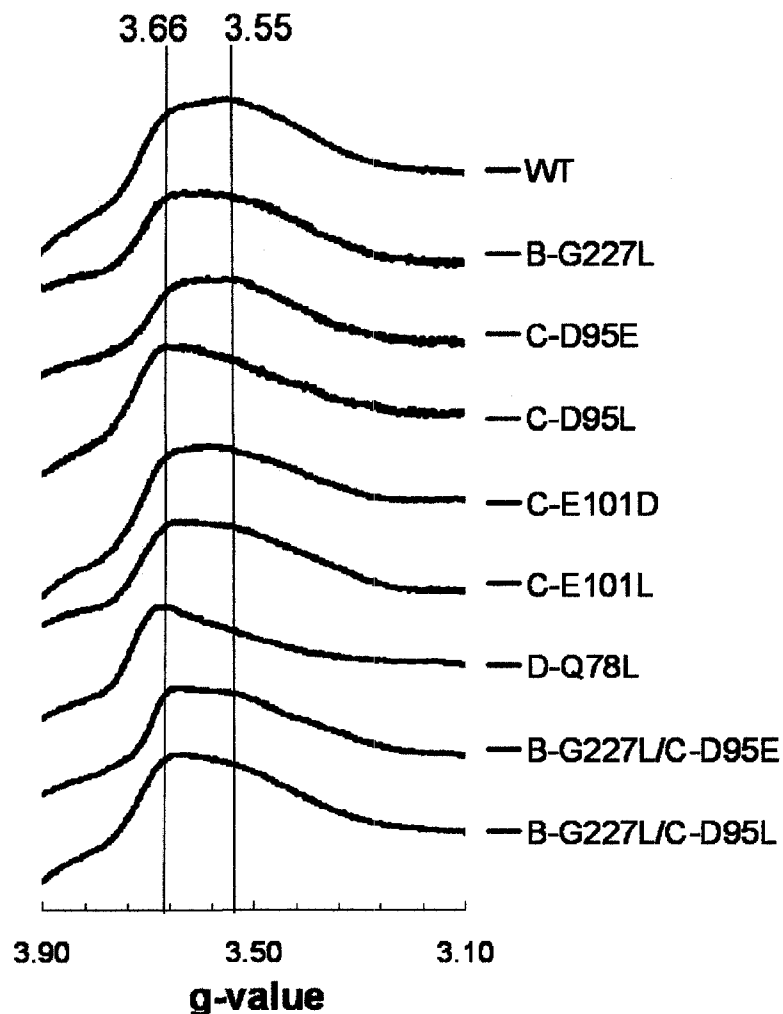


Figure 5.6. EPR spectra of the oxidized heme *b*. 3 scans of each sample were taken to form each individual spectrum. Data were obtained under the following instrument conditions: temperature, 9 K; microwave power, 20 mW at 9.38 GHz; modulation amplitude, 10 G<sub>pp</sub> at 100 KHz. Spectra were taken during redox titrations wherein the heme *b* is fully oxidized (poised at +117mV or higher). Each spectrum is collected from a 200 $\mu$ L sample at approximately 30 mg mL<sup>-1</sup> total protein concentration wherein the Sdh enzyme is present at approximately 2 nmol mg<sup>-1</sup>.

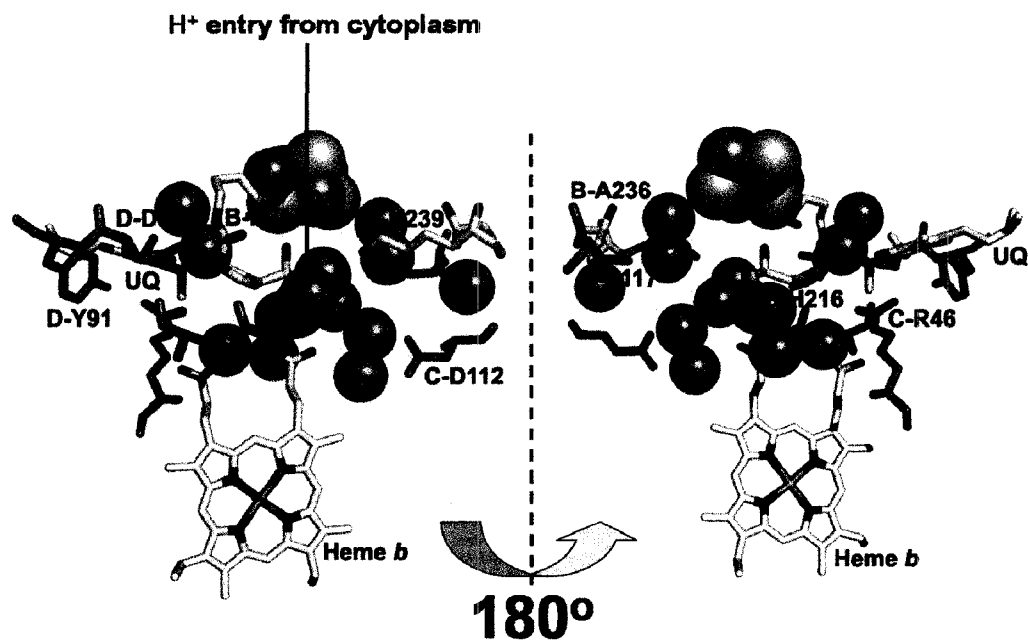


Figure 5.7. The observed water molecules in porcine Sdh. Identical views as those seen in Figure 5.1, with equivalent residues labeled. Surface rendering of the protein using PyMOL shows the entrance to the water channel lies at residue SdhD<sup>Q86</sup> in the pig Sdh. The figure was generated from PDB file 1ZOY using PyMOL v.0.99 (DeLano Scientific LLC.).



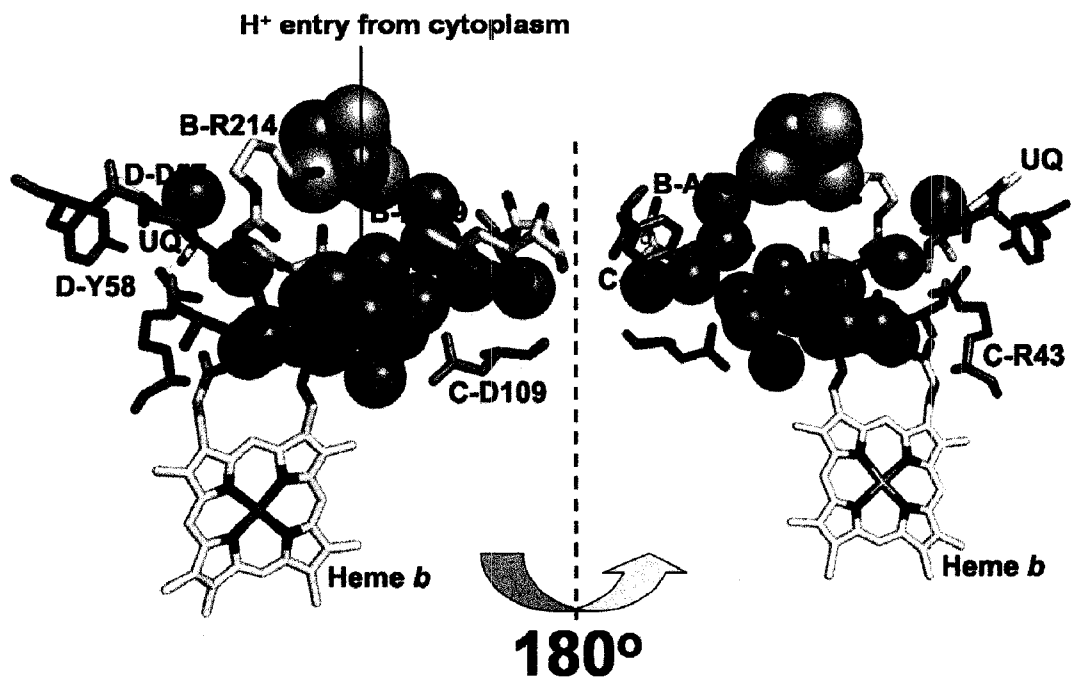


Figure 5.8. The observed water molecules in chicken Sdh. Identical views as those seen in Figure 5.1, with equivalent residues labeled. Surface rendering of the protein using PyMOL shows the entrance to the water channel lies at residue SdhD<sup>Q53</sup> in the chicken Sdh. The figure was generated from PDB file 1YQ3 using PyMOL v.0.99 (DeLano Scientific LLC.).

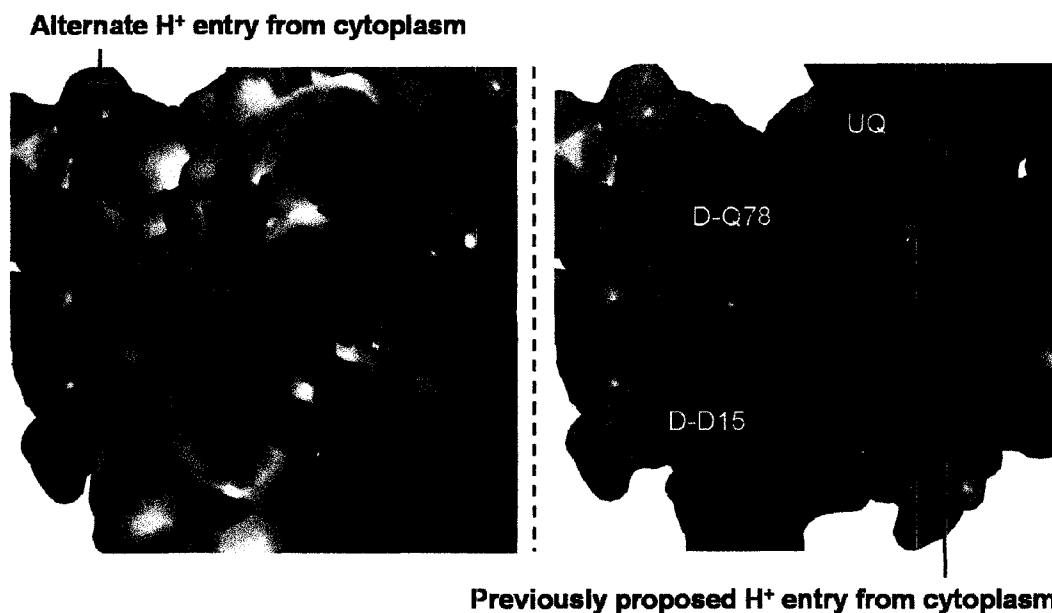


Figure 5.9. An alternative proton entry point in *E. coli* Sdh. Surface (left) and cut-away (right) perspectives of the observed water channel as viewed from SdhA towards the membrane. HOH45 in PDB file 1NEK can also serve as an entrance that brings protons from the cytoplasm to the Q<sub>P</sub>-site. This proton pathway also involves residue SdhD<sup>D15</sup> and only involves five ordered water molecules. HOH45 also corresponds to the observed proton entry point in the pig and chicken Sdh structures. The figure was generated from PDB file 1NEK using PyMOL v.0.99 (DeLano Scientific LLC.).

## **Chapter 6**

### **The Iron-Sulfur Clusters in *Escherichia coli***

### **Succinate Dehydrogenase Direct Electron Flow**

**A version of this chapter has been published:**

**Cheng, V.W.T., Ma, E., Zhao, Z., Rothery, R.A. and Weiner, J.H. (2006) *J Biol***

***Chem.* 281, 27662-27668.**

## 6.1 Introduction

Electron transport (ET) chains are ubiquitous and play a key role in energy conservation in both aerobic and anaerobic respiration. Cofactors such as iron-sulfur ([Fe-S]) clusters, hemes, and flavins comprise the ET relays of respiratory chain enzymes and mediate electron transfer from a powerful reductant with a relatively low midpoint potential ( $E_m$ ) to a final oxidant with a relatively high  $E_m$ . The ET chain usually involves cofactors from multiple enzymes and the membrane soluble ubiquinone or menaquinone pool, and the energetics of individual ET steps are not always downhill. In many redox enzymes, the exception often occurs in the form of an [Fe-S] cluster with an unusually low  $E_m$  located at an intermediate position in the ET relay (131,178,330,435). Thus during catalysis, electrons must surmount the energy barrier imposed by the low potential cluster despite the overall downhill reaction between the reductant and oxidant. Controversy continues to surround the issue as to whether  $E_m$  values of cofactors play a role in determining the rate of electron transfer through redox enzymes, especially that of the low potential cluster (19,139,230,387,436,437). It would thus be of great interest to use a genetically modifiable model system to study the effects of  $E_m$  modulation on observed catalytic rates of electron transfer.

Control of [Fe-S] cluster  $E_m$  values by the protein environment has been studied extensively in bacterial ferredoxins (322-328,347), but only a handful of studies have been done on [Fe-S] clusters in respiratory chain enzymes such as the  $bc_1$  complex (436,438) and yet even fewer studies on “simple” respiratory chain enzymes that utilize a single nonbifurcated electron pathway (230,387). Site-directed mutagenesis experiments which alter the cysteinyl ligands of [Fe-S] clusters have been performed on the *E. coli*

fumarate reductase (Frd) (317,318), nitrate reductase (315) and dimethylsulfoxide reductase (211). In most cases, alteration of the [Fe-S] cluster ligands resulted in enzymes which were not assembled or targeted correctly. These mutated enzymes often had undetectable enzyme activity; thus changes in midpoint potential could not be consistently correlated with changes in catalysis.

In this study, emphasis was placed on hydrophobic residues around the [4Fe-4S] cluster (FS2) of Sdh. Using the recently published high resolution x-ray crystallographic structure of Sdh (131), we generated site-directed mutants of SdhB<sup>I150</sup> and SdhB<sup>L220</sup> and determined their effects on  $E_m$  values of all three [Fe-S] clusters and the resultant changes in enzyme activity and rates of heme reduction. Since Sdh has been shown to produce reactive oxygen species (ROS) (371), we also addressed whether changes in enzyme turnover are consistent with changes in ROS production. Based on results obtained in this study, we propose a novel role for [Fe-S] clusters in ET relays whereby their midpoint potentials dictate the direction of electron transfer.

## 6.2 Experimental Procedures

*E. coli* strain DW35 ( $\Delta frdABCD$ ,  $sdhC::kan$ ) (223) was used for all enzyme expression and growth studies. Expression of wild-type and mutant Sdh was anaerobically induced by using the plasmid pFAS, which encodes the *sdh* operon under the control of the fumarate reductase promoter (359). Laboratory strain TG1 (*supE hsdΔ5 thi Δ(lac-proAB) F'[traD36 proAB<sup>+</sup> lacI<sup>q</sup> lacZΔM15]*; GE Healthcare) and plasmid pTZ18R (Amp<sup>R</sup>*lacZ'*; GE Healthcare) were used for molecular cloning and mutagenesis.

The 3.7kb KpnI-SphI fragment of pFAS was subcloned into pTZ18R and this recombinant plasmid was used for site-directed mutagenesis. Mutagenic oligonucleotides were designed with the addition/deletion of restriction sites in the DNA sequence to facilitate the screening process, and were purchased from Sigma Canada. Mutants were generated using the QuikChange Site-Directed Mutagenesis kit from Stratagene. DpnI was purchased from Invitrogen, and DNA purification kits were purchased from Qiagen. Mutants were verified by DNA sequencing (DNA core facility, Department of Biochemistry, University of Alberta), and the smaller 1.3 kb XhoI-SphI fragment cloned back into the pFAS expression vector. The mutant plasmids were then transformed into DW35 for biochemical studies. Preparation of competent cells and transformations of plasmids into competent cells were carried out as described in *Molecular Cloning: A Laboratory Manual* (335).

Wild-type and mutant SdhCDAB were expressed in DW35 cells. A 20mL starter culture of Terrific Broth grown at 37°C for 8 hours was used to inoculate 2L of Terrific Broth in a 4L flask. The culture was grown at 37°C for ~18 hours with shaking (160rpm). All media contained 100µg mL<sup>-1</sup> ampicillin, 100µg mL<sup>-1</sup> streptomycin and 40µg mL<sup>-1</sup> kanamycin. Cells were harvested by centrifugation followed by resuspension in 50mM MOPS / 5mM EDTA buffer (pH 7.0). Phenylmethanesulfonyl fluoride was added to a final concentration of 0.2mM and cells were lysed using a French press. Membranes were prepared by differential centrifugation as previously described (230). Enriched membranes were prepared by centrifugation on a 55% sucrose cushion at 150,000g for 90 minutes, and were diluted to 25mL. Malonate was added to a final concentration of 1mM and membranes were incubated at 30°C for 15 minutes to activate the Sdh enzyme. Two

subsequent spins at 150,000g for 90 minutes were carried out to wash the membranes using 50mM MOPS / 5mM EDTA / 1mM malonate buffer. The final membrane preparations were resuspended in 4mL of the above buffer and flash frozen with liquid N<sub>2</sub>. All steps were carried out at 4°C unless otherwise specified.

Anaerobic growth in minimal medium was carried out as described (238) using 50mM fumarate as the terminal electron acceptor and a Klett-Summerson colorimeter equipped with a no. 6 filter to monitor growth. Aerobic growth in succinate minimal media was carried out as the anaerobic growth experiment with the following exceptions: final volume decreased to 25mL, glycerol and fumarate were omitted, and succinate was added to a final concentration of 25mM.

Protein concentrations were estimated by the Lowry method (425) with the inclusion of 1% (w/v) sodium dodecyl sulfate in the mixture (337). 30µg of protein were incubated at 100°C for 5 minutes before separation by SDS-PAGE (335) and visualized by Coomassie blue staining. Low molecular weight markers from Bio-Rad include phosphorylase b (97.4 kDa), bovine serum albumin (66.2 kDa), ovalbumin (45.0 kDa), carbonic anhydrase (31.0 kDa), soybean trypsin inhibitor (21.5 kDa) and lysozyme (14.4 kDa). Fluorometric quantification of the covalent flavin of Sdh was carried out as described (426), using 5mg of protein as starting material.

Redox titrations were carried out anaerobically under argon at 25°C on Sdh-enriched membranes at a total protein concentration of approximately 30mg mL<sup>-1</sup> in 50mM MOPS / 5mM EDTA (pH 7.0). The following redox mediators were used at a concentration of 25µM: quinhydrone, 2,6-dichloroindophenol, 1,2-naphthoquinone, toluylene blue, phenazine methosulfate, thionine, duroquinone, methylene blue, resorufin,

indigotrisulfonate, indigodisulfonate, anthraquinone-2-sulfonic acid, phenosafranine, benzyl viologen, and methyl viologen. All samples were prepared in 3mm internal diameter quartz EPR tubes and were rapidly frozen in liquid nitrogen-chilled ethanol before storing in liquid nitrogen. EPR spectra were recorded using a Bruker Elexsys E500 EPR spectrometer equipped with an Oxford Instruments ESR900 flowing helium cryostat.  $E_m$  values for FS1 and FS3 were determined at 12K and 20mW while that of FS2 was determined at 40K and 2mW, all at a frequency of 9.38GHz. All spectra were corrected for internal EPR tube diameters. Presented data is representative of two independent potentiometric titrations for each Sdh mutant. Samples for spin quantitation measurements were prepared by oxidizing with 160 $\mu$ M potassium ferricyanide or reducing with 8mM sodium dithionite. Calculations were done using 1mM Copper-EDTA as standard.

Succinate dependent reduction of MTT ( $\epsilon = 17\text{mM}^{-1}\text{cm}^{-1}$ ) was measured spectrophotometrically at 570nm in the presence of 750 $\mu$ M phenazine methosulfate (PMS) and 0.1% Triton X-100 (427). Anaerobic succinate dependent reduction of  $Q_0$  ( $\epsilon = 0.73\text{mM}^{-1}\text{cm}^{-1}$ ) was monitored at 410nm; anaerobicity was achieved by saturating the assay buffer with  $N_2$  and the addition of glucose (20mM) and glucose oxidase (8.8 units  $\text{mL}^{-1}$ ) to the reaction cuvette. Anaerobic oxidation of plumbagin ( $\epsilon = 3.95\text{mM}^{-1}\text{cm}^{-1}$ ) in the presence of fumarate was measured at 419nm as described (229) in  $N_2$ -saturated buffer. Turnover numbers were calculated based on covalent flavin concentrations.

Stopped-flow experiments were carried out using a Sequential Bio SX-17MV stopped-flow spectrofluorimeter (Applied Photophysics Ltd., Leatherhead, U.K.) with a 1cm path length at 25 $^{\circ}$ C. Pre-steady state heme reduction was monitored by subtracting



$A_{575}$  from  $A_{560}$ . Sdh-enriched membranes at a total concentration of  $1\text{mg mL}^{-1}$  in  $\text{N}_2$ -saturated  $100\text{mM MOPS} / 5\text{mM EDTA}$  (pH 7.0) buffer were used. The assay was performed anaerobically in the presence of  $50\text{mM KCN}$  to eliminate overlapping heme absorbances from cytochromes *bd* and *bo*. Heme reduction was achieved by addition of  $10\text{mM succinate}$  and a time window of 10 seconds was monitored. Temporal changes in absorbance were averaged and fitted to the double exponential equation  $\Delta\text{Abs} = A_1e^{-k_1t} + A_2e^{-k_2t} + b$  where  $A_1$  and  $A_2$  are amplitudes,  $k_1$  and  $k_2$  are rate constants,  $t$  is time and  $b$  is the end point of the data trace.

Generation of ROS was monitored at  $A_{550}$  using the superoxide-dependent cytochrome *c* reduction assay ( $\epsilon^{(\text{Fe}^{2+} \text{ cytochrome } c)} - \epsilon^{(\text{Fe}^{3+} \text{ cytochrome } c)} = 21\text{mM}^{-1} \text{ cm}^{-1}$ ) as described (371,439). Essentially, Sdh enzyme, cytochrome *c*,  $\text{Q}_0$ , KCN, superoxide dismutase and succinate were added to final concentrations of  $1\mu\text{g mL}^{-1}$ ,  $10\mu\text{M}$ ,  $50\mu\text{M}$ ,  $10\text{mM}$ ,  $30\text{units mL}^{-1}$  and  $10\text{mM}$ , respectively.

### 6.3 Results

Using the published Sdh structure (PDB file 1NEN) (131), we elected to study two conserved hydrophobic residues located within  $4\text{\AA}$  of the  $[\text{4Fe-4S}]$  cluster, SdhB<sup>I150</sup> and SdhB<sup>L220</sup> (Figure 6.1). These two residues were chosen based on their proximity to FS2 with the objective of examining the role of the low potential  $[\text{4Fe-4S}]$  cluster in Sdh. Three mutants – I150E, I150H and L220S – were generated using site-directed mutagenesis and were analyzed by EPR spectroscopy and enzymatic assays.

We first examined whether mutation of a hydrophobic residue to a charged or polar residue in the middle of the electron transfer subunit had an impact on the proper

assembly and targeting of Sdh. Membrane preparations containing Sdh were analyzed by SDS-PAGE and the covalent flavin content was determined. The Coomassie blue-stained gel is depicted in Figure 6.2 and shows that although the SdhB subunits of mutant enzymes run anomalously compared to the wild-type (WT), mutant enzymes are assembled and correctly targeted to the cytoplasmic membrane. Table 6.1 shows the flavin content determined for each membrane preparation, indicating virtually no difference between the amount of mutant and WT Sdh enzymes targeted to the cytoplasmic membrane. DW35 membranes were not included in the flavin assay as no covalently-bound flavin was expected to be present. The concentrations of FS1 and FS3 as determined by spin quantitation are also shown in Table 6.1. The concentrations of FS2 are not shown due to the high intrinsic error in its determination (440).

Figure 6.3A shows the ability of the SdhB mutants to grow aerobically on succinate minimal media at 37°C. Clearly, the SdhB mutants were able to complement *E. coli* DW35 and support growth on succinate, with neither the growth rate nor the maximum growth density affected. It is well documented that Sdh can function as a fumarate reductase under anaerobic conditions (359) and we tested the ability of the mutants to support anaerobic growth on fumarate. *E. coli* DW35 did not grow on glycerol-fumarate (G-F) medium (Figure 6.3B) but grew well when complemented with the pFAS plasmid encoding the WT Sdh. Both SdhB<sup>I150</sup> mutants did not support growth on G-F minimal medium, whereas the SdhB<sup>L220S</sup> mutant showed growth similar to DW35/pFAS.

Potentiometric titrations and EPR spectroscopy were performed on the WT and mutant Sdh enzymes to determine the  $E_m$  values of the [Fe-S] clusters in SdhB.  $E_m$  values

of the FAD and heme were not determined as the mutations in SdhB were not expected to alter their redox behaviors. Table 6.1 lists the average  $E_m$  values determined for the WT and mutant enzymes in two independent experiments. Redox titration of the WT enzyme yielded  $E_m$  values of -15mV, -213mV and +55mV for FS1-FS3, respectively, which are in reasonable agreement with previously published values (319). In the SdhB<sup>I150E</sup> mutant, the  $E_m$  value of FS2 was decreased by approximately 70mV to -285mV with no major changes in the  $E_m$  values of FS1 and FS3. A similar case was observed with the SdhB<sup>I150H</sup> mutant, where  $E_m$  values of FS1 and FS3 were unchanged while an average  $E_m$  value of -338mV was recorded for FS2, a decrease of 125mV compared to the WT enzyme. The SdhB<sup>L220S</sup> mutant did not alter  $E_m$  values of FS1 or FS2, but surprisingly altered the  $E_m$  value of FS3 by lowering it to -20mV.

Steady state activity assays using the non-physiological acceptor PMS/MTT to measure the assembly and quantity of enzyme in the membrane showed that the I150 mutants and the WT had comparable succinate:PMS/MTT activity and so were assembled to similar levels (Figure 6.4). The L220S mutant showed a 50% decrease in PMS/MTT activity after taking into account the covalent flavin contents. Using the succinate:Q<sub>0</sub> assay as a measure of physiological Sdh activity, all three mutants showed a decrease in activity. The turnover rate decreased approximately 65% for the I150 mutants and almost 80% for the L220S mutant. When plumbagin was used to measure the fumarate reductase activity of the mutant enzymes, we found the I150E mutant to have the smallest effect and the L220S mutant the largest decrease in activity.

The ability of the heme *b* to be reduced by succinate was measured using the stopped-flow technique (Figure 6.5). Activated enzyme was reduced by addition of

succinate and the  $A_{560}$  was monitored on a 10-second time window. Triplicate traces were averaged and fitted to a double exponential equation from which we found  $k_1$  to be significantly decreased in the I150 mutants while  $k_1$  and  $k_2$  were  $\sim 0$  in the L220S mutant.  $k_1$  was decreased from  $6.44 \text{ s}^{-1}$  (WT enzyme) to  $1.05 \text{ s}^{-1}$  and  $1.35 \text{ s}^{-1}$  in the I150E and I150H mutants, respectively.  $A_1$  for the WT, I150E and I150H enzymes were  $-4.82 \times 10^{-3}$ ,  $-5.12 \times 10^{-3}$  and  $-3.09 \times 10^{-3}$ , respectively. No changes in  $k_2$  and  $A_2$  were observed in the I150 mutants.

Finally, we examined the ability of the SdhB mutants to produce ROS during enzyme turnover. Since it has been demonstrated that both Sdh and Frd can produce ROS, the former enzyme at the Q-site and the latter enzyme at the FAD site (371,372), we inquired whether a bottleneck in the electron transfer rate in Sdh affects ROS production. Also, we wanted to confirm whether the decrease in enzyme turnover in the SdhB mutants is indeed due to slower electron transfer rate, or whether it is a side effect of shortcircuiting the electron pathway by increased solvent exposure when the hydrophobic residues were replaced by hydrophilic amino acids. Figure 6.6 shows that in all the SdhB mutants, ROS generation during physiological turnover was decreased compared to the WT enzyme, which correlates with the decreased rates of succinate:Q<sub>0</sub> turnover.

## 6.4 Discussion

In this study, we examined the role of hydrophobic residues around the low potential [4Fe-4S] cluster of Sdh, as well as the intimate relationship between enzyme turnover, electron transfer rate and cofactor midpoint potential. Extensive studies on

bacterial ferredoxins have yielded insights into how the  $E_m$  of [Fe-S] clusters are generally controlled by the surrounding amino acids and degree of solvent exposure (322-328,347). Specifically, it was found that in the *Azotobacter vinelandii* ferredoxin I protein, mutation of Phe residues to His can increase  $E_m$  values of nearby [Fe-S] clusters by 100 to 200mV (323). We found that conversion of SdhB<sup>I150</sup> to Glu lowered the  $E_m$  value of FS2 from -213mV to -285mV; when the same residue was altered to His, the  $E_m$  value of FS2 surprisingly showed an additional decrease in  $E_m$  value to -338mV. This is the opposite effect to that observed in the ferredoxin I protein by Chen *et al.* We strongly believe that there is a functional relationship between Ile/Glu/His and a nearby [Fe-S] cluster as we have also observed similar decreases in  $E_m$  values of a [Fe-S] cluster in DMSO reductase when a nearby Ile residue is mutated to Glu and His (unpublished data). An alternative explanation may be offered by residue SdhB<sup>C154</sup>, which has been proposed to H-bond to FS2 such that it raises the apparent  $E_m$  value of the cluster in Sdh (387). In the x-ray crystallographic structure (131), C154 is a possible H-bond donor to one of the cysteine ligands of FS2, but is 7.5Å from I150. Glu and His mutants of I150 may cause local perturbations in the structure such that it H-bonds to C154, thus eliminating the C154-Sy H-bond to FS2 and thereby decreasing the  $E_m$  of the [4Fe-4S] cluster. H-bonds to [Fe-S] clusters have been shown to contribute between 50 and 200mV to the overall  $E_m$  of [Fe-S] clusters (323,436,441).

The observation that the L220S mutant has no significant effect on FS2 but instead decreased the  $E_m$  value of FS3 is much harder to rationalize. In the published Sdh structure, the L220 residue is close to FS3, but is also pointing away from FS3. It is possible that the L220S mutation induces some conformational change in the electron

transfer subunit that affects the redox behavior of FS3 but not that of FS1 or FS2. An X-ray crystallography structure of the L220S mutant would be needed to completely understand why FS3 was unexpectedly affected in this mutant.

When we examined the enzymatic activities of the SdhB<sup>I150</sup> mutants, it was found that both had decreased succinate:Q<sub>0</sub> and plumbagin:fumarate activities despite having similar succinate:PMS/MTT activities. In terms of FS2  $E_m$  values, the WT enzyme had the highest midpoint potential, followed by I150E and I150H. This trend can be correlated to succinate:Q<sub>0</sub> and plumbagin:fumarate activities, where the WT enzyme has the highest turnover, followed by the I150E and I150H mutants. Thus if we raise the energetic barrier against ET, we slow down the rate of electron flux or steady state turnover of the enzyme, in both the forward and reverse directions. Thus far, we have been unable to raise the  $E_m$  value of FS2 to verify whether the converse is true. Although we have observed a *direct* relationship between  $E_m$  values of FS2 and turnover rates in Sdh, it is interesting to point out that an *inverse* relationship was recently observed between  $E_m$  values of FS2 and turnover in Frd (387). Increases in cofactor  $E_m$  values which result in increases in enzymatic activity have also been observed in the Rieske protein (436) and recently in the *Blastochloris viridis* reaction center (437).

The turnover rates observed in the L220S mutant were also decreased compared to the wildtype enzyme. We believe that the decreased activities are the result of altering the  $E_m$  value of FS3, which is adjacent to and may exchange electrons directly with the Q-site. Experiments done on the *Saccharomyces cerevisiae* bc<sub>1</sub> complex, *E. coli* DMSO reductase, and *E. coli* fumarate reductase have shown that alteration of the  $E_m$  value of

the [Fe-S] cluster adjacent to the Q-site can cause major changes in enzyme activity (211,436,442).

The trend seen in the *in vitro* enzyme assays for the three SdhB mutants was not reflected in the aerobic or anaerobic growth in minimal medium. The mutant enzymes were able to complement *E. coli* DW35 for aerobic growth on succinate minimal media, presumably because the over-expressed level of Sdh overcomes their decreased succinate:Q<sub>0</sub> activities (359). It is intriguing to note that, despite having the lowest plumbagin:fumarate turnover, the L220S mutant was able to support growth on glycerol-fumarate minimal media whereas the I150 mutants could not. We propose that this phenomenon arises from the energetic restrictions in electron transfer. In the WT enzyme, the  $\Delta E_m$  for the FS3→FS2 transition is -268mV. In the I150E and I150H mutants, this  $\Delta E_m$  value increases to -340mV and -383mV, respectively. Thus the electrons have a higher energy barrier to surmount when the I150E and I150H mutants are functioning as a fumarate reductase, and are apparently unable to do so *in vivo*. In the L220S mutant however, the  $\Delta E_m$  for the FS3→FS2 transition is now only -203mV, less than the value calculated for the WT Sdh. We propose that the  $E_m$  values of the [Fe-S] clusters in Sdh are poised such that *in vivo*, the forward reaction of succinate oxidation is favored compared to that of fumarate reduction. Since the active sites of Sdh are already biased towards succinate oxidation and ubiquinone reduction (224,330,423), the [Fe-S] clusters exert an additional level of control over the directionality of electron transfer such that the succinate:UQ reaction is preferred in Sdh. This hypothesis can also be applied to the homologous *E. coli* Frd enzyme, wherein FS1-FS3 have  $E_m$  values of -35mV, -310mV, and -65mV, respectively (440). Thus the ET relay in Frd would favor electron transfer

from FS3 to FS1. The effects of  $E_m$  values in relation to electron transfer have also been previously examined in DMSO reductase (230).

In terms of ROS production, we did not see any significant change relative to the succinate:Q<sub>0</sub> activity in the SdhB mutants. The imposition of a higher energy barrier in the I150 mutants slows down electron transfer, meaning that cofactors upstream of FS2 such as the FAD are more likely to be reduced. Since Sdh produces ROS at the Q-site (371,372), we might expect less ROS to be produced from the I150E and I150H mutants. Indeed, we saw decreases in ROS production in all three mutants which correlate with the decreases in physiological turnover rates. This suggests that ROS production only occurs during the UQ→UQH<sub>2</sub> reduction step, rather than a simple leakage of electrons to molecular oxygen from the ET chain.

In this study, the midpoint potentials of the [4Fe-4S] and [3Fe-4S] clusters of Sdh were individually lowered by point mutations of hydrophobic residues to charged and polar residues. Lowering the  $E_m$  values of these [Fe-S] clusters led to decreases in *in vitro* enzyme turnover rates. Based on results obtained in this study, we propose that the  $E_m$  values of the [Fe-S] clusters in Sdh act as a checkpoint such that the forward reaction of succinate oxidation is the preferred reaction over the fumarate reduction reaction.



Membranes	Quantitation of Sdh (nmol/mg protein)			Midpoint Potentials (mV)		
	[Flavin]	[FS1]	[FS3]	FS1	FS2	FS3
WT	3.2	4.7	4.0	-15 ± 15	-213 ± 3	55 ± 15
I150E	3.2	4.2	4.2	-33 ± 13	-285 ± 10	55 ± 10
I150H	3.3	3.9	4.2	-30 ± 5	-338 ± 17	35 ± 0
L220S	2.6	5.3	3.6	-18 ± 8	-223 ± 3	-20 ± 10

Table 6.1. Quantitation of cofactors and midpoint potentials (mV) of [Fe-S] clusters in Sdh. Membrane fractions containing over-expressed wild-type or mutant SdhB were assayed for covalent flavin content as described in Materials and Methods. Concentrations of FS1 and FS3 were determined by spin quantitation.  $E_m$  values were determined by redox titration in combination with EPR spectroscopy. The FS1 and FS3 signals were monitored at 12K and 20mW, while the signal for FS2 was followed at 40K and 2mW. EPR spectra were all obtained at a frequency of 9.38GHz with a modulation amplitude of 10G<sub>pp</sub> at 100KHz. The average and range of  $E_m$  values from two independent redox titrations are shown.

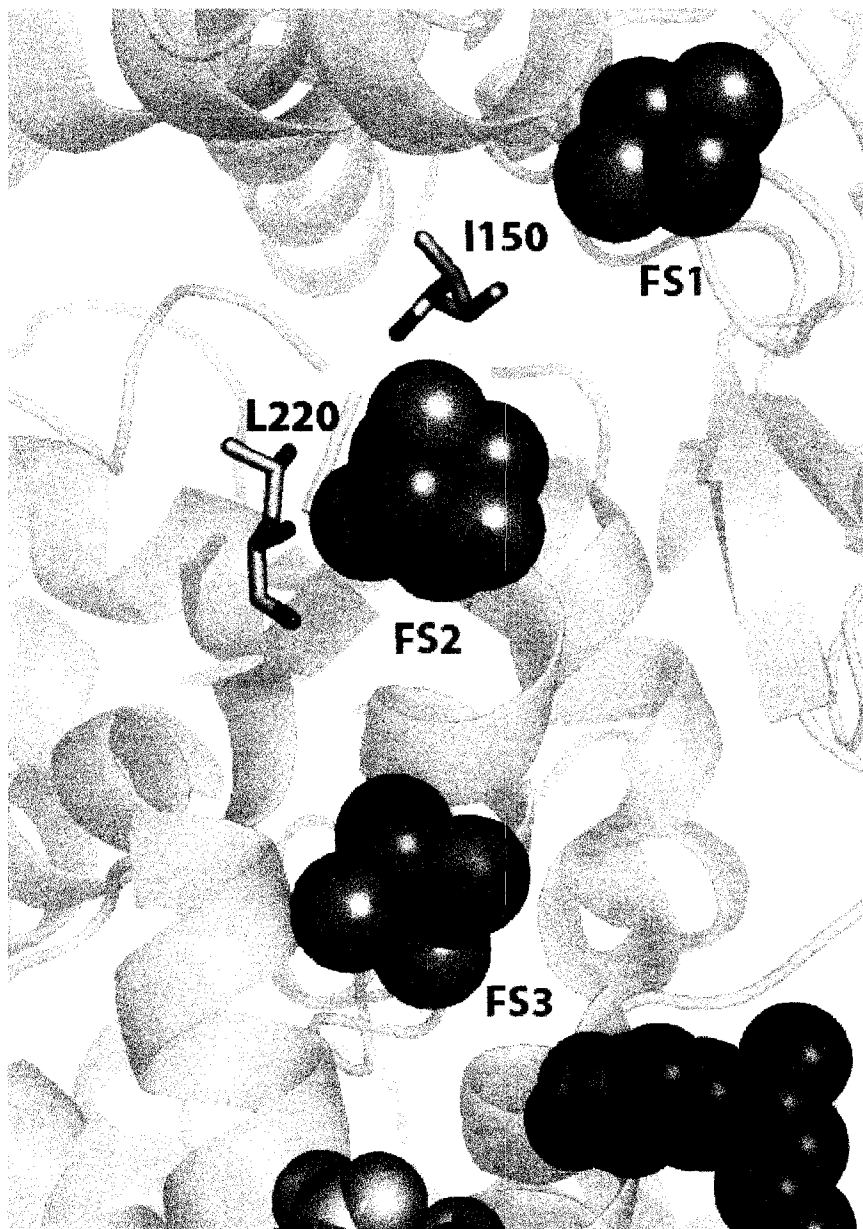


Figure 6.1. Iron-sulfur clusters in SdhB. Physiological electron transfer within SdhB is FS1→FS2→FS3. Shown are the two hydrophobic residues which were studied by site-directed mutagenesis. The figure was generated from PDB file 1NEN using PyMOL visualization software (DeLano Scientific LLC).

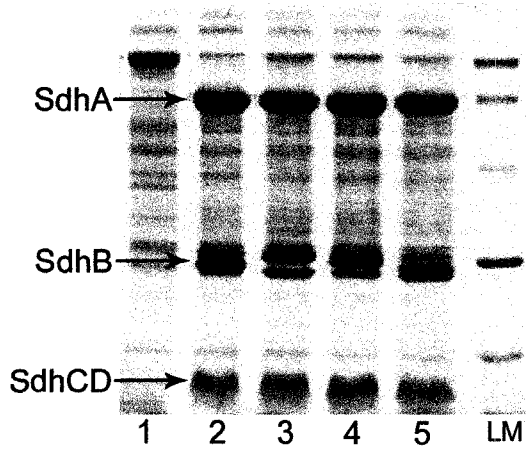


Figure 6.2. SDS-PAGE gel stained by Coomassie blue. Lanes 1-5 contains 30 $\mu$ g of membrane preparations from *E. coli* cells DW35, DW35/pFAS, DW35/pFAS-SdhB<sup>I150E</sup>, DW35/pFAS-SdhB<sup>I150H</sup> and DW35/pFAS-SdhB<sup>L220S</sup>, respectively. LM, low molecular mass standards from Bio-Rad. The individual Sdh subunits are marked.

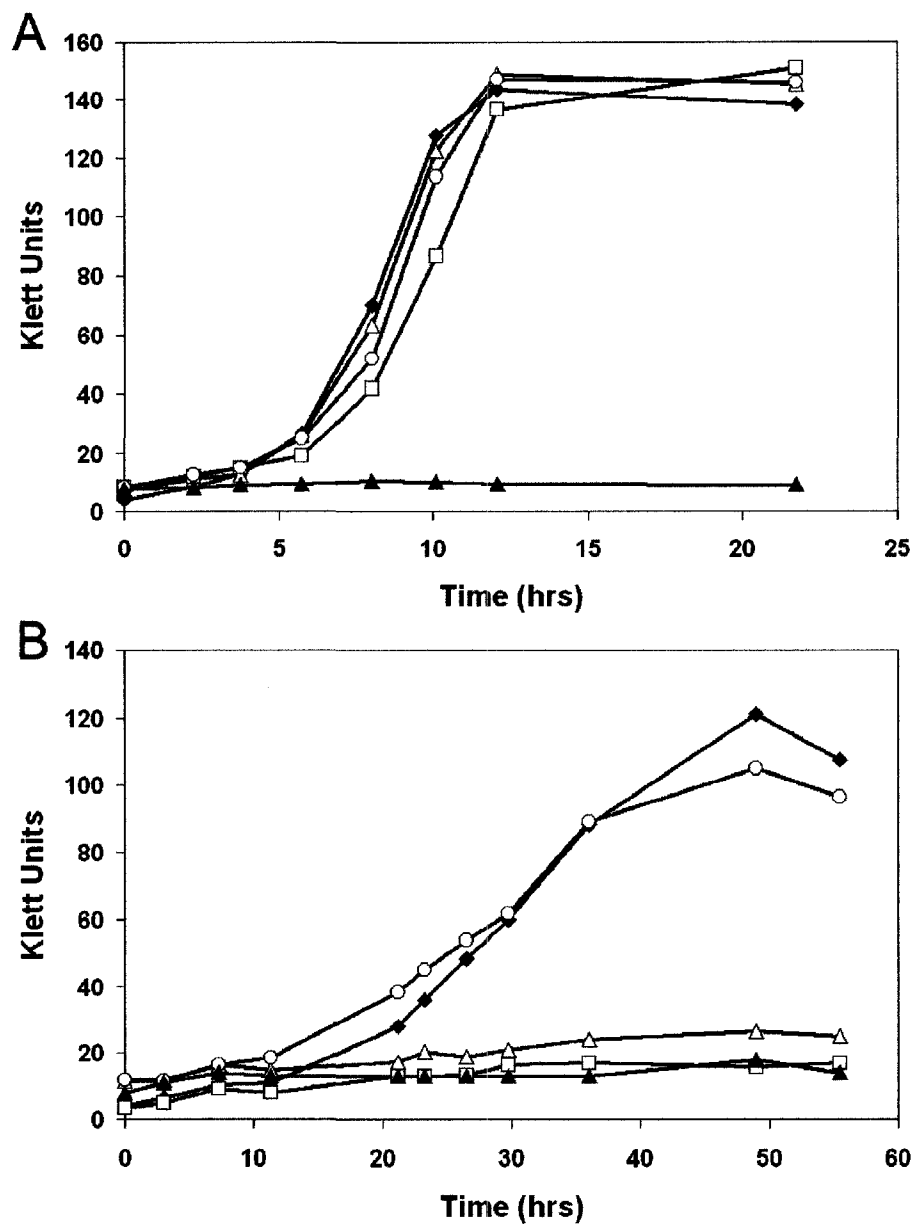


Figure 6.3. Aerobic growth with succinate as electron donor (top) and anaerobic growth with fumarate as electron acceptor (bottom). Cells were grown as described in Section 6.2. Klett readings are plotted as a function of time for the DW35 strain (▲), and the DW35 strain harboring the wildtype Sdh (◆), SdhCDAB<sup>I150E</sup> (△), SdhCDAB<sup>I150H</sup> (□) and SdhCDAB<sup>L220S</sup> enzymes (○).

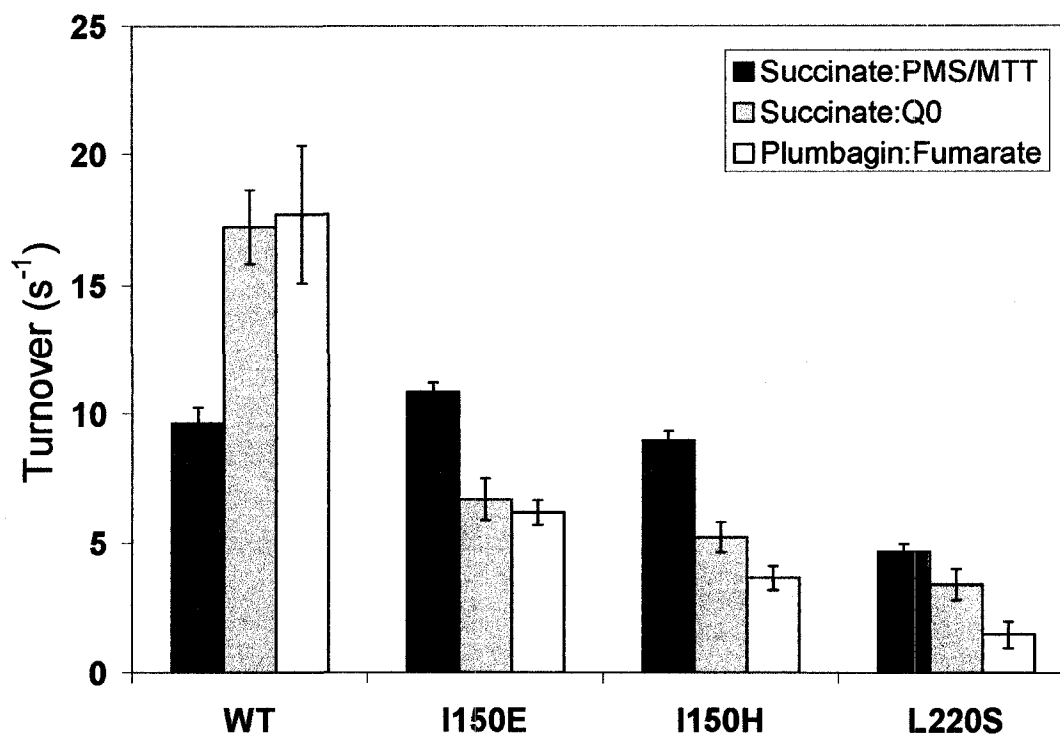


Figure 6.4. Physiological and non-physiological enzyme activities of SdhB mutants. Succinate:PMS/MTT activity assays for proper assembly and targeting of the enzyme to the cytoplasmic membrane. Succinate:Q<sub>0</sub> is the physiological assay that requires a functional holoenzyme. The plumbagin:fumarate assay tests the ability of the enzyme to function in reverse as a fumarate reductase. Turnover is given as mol substrate per mol enzyme per second; error bars indicate 1 standard deviation of error from at least 4 measurements.

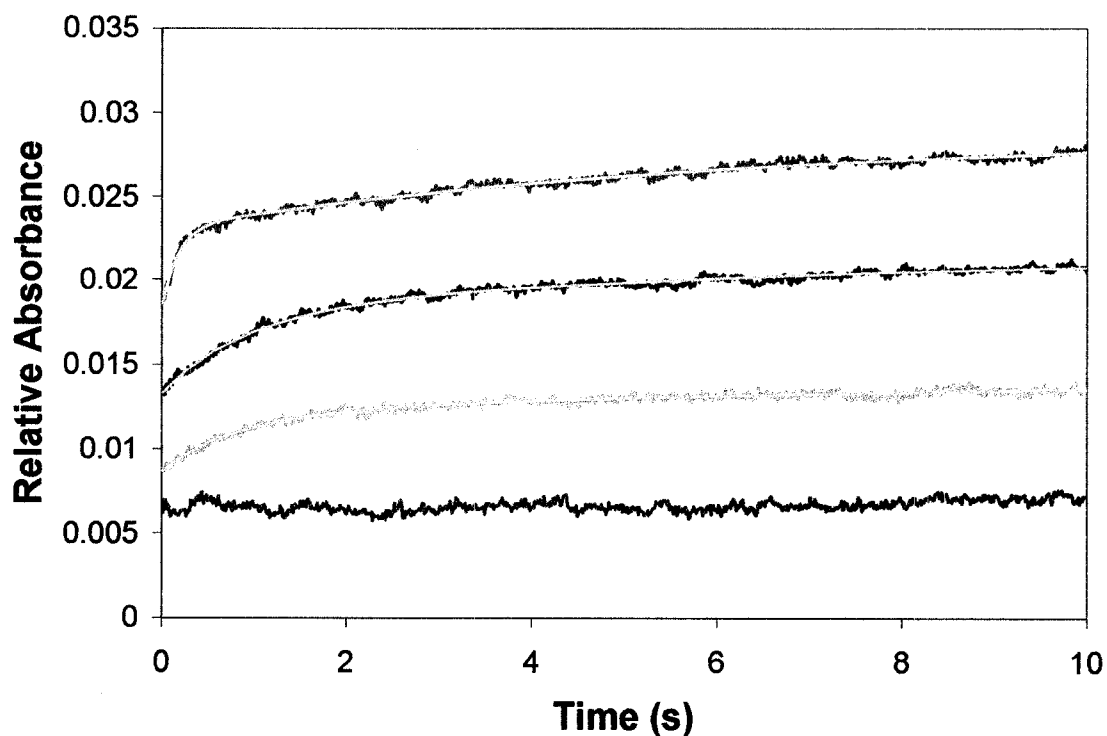


Figure 6.5. Stopped-flow traces of heme reduction by succinate in SdhB mutants. Blue, wild-type enzyme; red, SdhB<sup>I150E</sup>, orange, SdhB<sup>I150H</sup>, green, SdhB<sup>L220S</sup>. The traces were obtained by subtracting  $A_{575}$  from  $A_{560}$  and were fitted (grey) to a double exponential equation.  $k_1$  values for traces A-D were  $6.44 \text{ s}^{-1}$ ,  $1.05 \text{ s}^{-1}$ ,  $1.35 \text{ s}^{-1}$ , and  $\sim 0 \text{ s}^{-1}$ , respectively.  $k_2$  values were not altered significantly between wildtype and mutant enzymes.

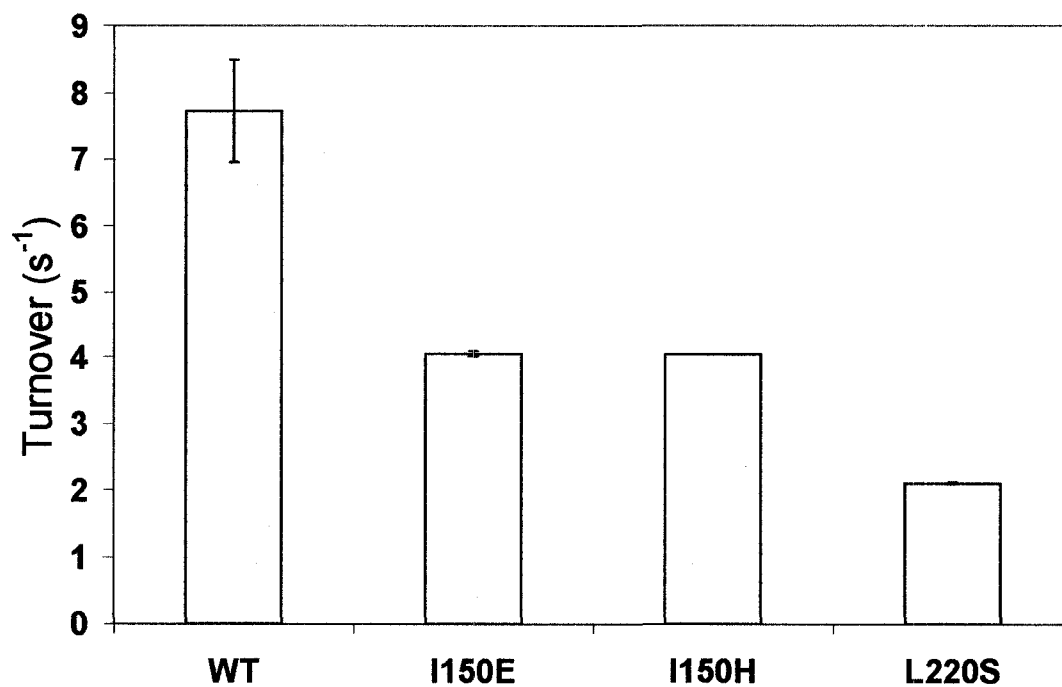


Figure 6.6. Production of reactive oxygen species by SdhB mutants during enzyme turnover. ROS production was determined by subtracting values obtained in the presence of superoxide dismutase from those observed in the absence of superoxide dismutase. All SdhB mutants showed a decrease in ROS production compared to the wildtype Sdh. Turnover is given as mol ROS produced per mol enzyme per second, and is an average value from 2 independent measurements.

## **Chapter 7**

### **Calculation and Observation of Electron Transfer in *Escherichia coli* Succinate Dehydrogenase**



## 7.1 Introduction

Succinate dehydrogenase (Sdh, or complex II in eukaryotes) contains a small portion of the entire electron transfer (ET) chain involved in aerobic metabolism and oxidative phosphorylation, particularly in the mitochondrion. The relay of electrons from either complex I (NADH,  $E^{\circ} = -315\text{mV}$ ) or complex II (succinate,  $E^{\circ} = +30\text{mV}$ ) to cytochrome oxidase ( $\text{O}_2$ ,  $E^{\circ} = +815\text{mV}$ ) involves over 20 cofactors that include iron-sulfur clusters, hemes, copper atoms, and dissociable ubiquinone/ubiquinol molecules. These cofactors are responsible for harnessing the reducing energy by scalar and vectorial generation of proton motive force; the exception lies with complex II which is non-electrogenic. Examination of the midpoint potentials ( $E_m$ ) of all the cofactors indicate ET energetics are not exclusively exergonic (443) and that endergonic ET to a prosthetic group with an unusually low  $E_m$  value may serve as a rate-limiting step. For instance, the [4Fe-4S] cluster in Sdh has an  $E_m$  value that is 230mV lower than neighboring [Fe-S] clusters and a further decrease in its  $E_m$  value by site-directed mutagenesis limits the rate of enzyme turnover in both the forward and reverse directions (424).

Theoretical treatments of ET rates involve four elements which are thought to govern ET between neighboring redox cofactors: packing density, edge-to-edge distance, difference in free energies, and changes in reorganization energy associated with the ET step (19). Because ET rates are predicted to be on the microsecond timescale while turnover of redox enzymes generally occur on the millisecond timescale, ET through redox enzymes is generally not considered to be the rate-limiting step in oxidoreductases. However, numerous case studies have demonstrated that alteration of the midpoint potentials of redox cofactors can predictably influence the rate of enzyme turnover

(211,424,436,437). Although natural designs of redox enzymes afford a wide range of parameters to allow competent ET, it should nonetheless be coordinated with reactions at the active sites which are coupled to proton chemistry such that straying electrons are minimized to avoid short circuit and reactive oxygen species generation (371,443,444).

The X-ray crystallographic structure of the *E. coli* Sdh is available (131) and provides important spatial and geometric details needed to carry out a detailed study of ET rates in this particular enzyme. In addition, the unique composition of the [Fe-S] clusters in SdhB (FS1, [2Fe-2S] cluster with  $E_{m,7} = +15\text{mV}$ ; FS2, [4Fe-4S] cluster with  $E_{m,7} = -213\text{mV}$ ; FS3, [3Fe-4S] cluster with  $E_{m,7} = +55\text{mV}$ ) allows unambiguous identification of their individual redox states using electron paramagnetic resonance (EPR) spectroscopy (319,424). Furthermore, a novel freeze-hyperquench (FHQ) technique was recently developed to study enzyme catalysis on the microsecond timescale (445). The combination of the above advantages presents a unique opportunity to study experimental ET mechanisms and compare their kinetics to theoretical models of ET.

Using the *E. coli* Sdh as a model system, we were able to identify specific aspects of ET and enzyme turnover that were not predicted from conventional wisdom. This includes the rates of sequential ET through Sdh after succinate oxidation as well as the mechanisms of physiological ET. Based on the experimental observations of ET through Sdh, we propose a new model for ET in the Sdh enzyme that involves multiple turnovers of succinate until steady state is achieved.

## 7.2 Experimental Procedures

*Bacterial Strains and Plasmids* – *E. coli* strain DW35 ( $\Delta frdABCD$ ,  $sdhC::kan$ ) (223) was grown anaerobically to induce expression of wild-type and mutant Sdh from the pFAS plasmid, which encodes the *sdh* operon under the control of the fumarate reductase promoter (359). The SdhB<sup>I150H</sup> mutant examined herein was constructed in a previous study (424).

*Enzyme Expression and Preparation* – A 20mL starter culture of Terrific Broth grown at 37°C for 8 hours was used to inoculate 2L of Terrific Broth in a 4L flask. The culture was grown at 37°C for ~18 hours with shaking (160rpm). All media contained 100µg mL<sup>-1</sup> ampicillin, 100µg mL<sup>-1</sup> streptomycin and 40µg mL<sup>-1</sup> kanamycin. Cells were harvested by centrifugation followed by resuspension in 50mM MOPS / 5mM EDTA buffer (pH 7). Phenylmethanesulfonyl fluoride was added to a final concentration of 0.2mM and cells were lysed using a French press. Membranes enriched in Sdh were prepared by differential centrifugation as previously described (424) and resuspended in 20mM sodium phosphate / 5mM EDTA / 1mM malonate buffer (pH 8). Two additional ultracentrifugation steps were carried out wherein the membrane preparations were washed and resuspended in 100mM HEPES / 5mM EDTA without malonate.

*Protein Quantifications* – Protein concentrations were estimated by the Lowry method (425) with the inclusion of 1% (w/v) sodium dodecyl sulfate in the mixture (337).

*Heme Reduction* – Stopped-flow experiments were carried out using a Sequential Bio SX-17MV stopped-flow spectrofluorimeter (Applied Photophysics Ltd., Leatherhead, U.K.) with a 1cm path length at 22°C. Pre-steady state heme reduction was monitored by subtracting A<sub>410</sub> from A<sub>425</sub>. Sdh-enriched membranes at a total protein concentration of approximately 1mg mL<sup>-1</sup> in 100mM HEPES / 5mM EDTA (pH 8) buffer

were used. Heme reduction was achieved by addition of 200mM succinate and time windows of 10, 50, 100, and 1000 ms were monitored.

*Freeze-hyperquench Preparations of Sdh* – To study physiological electron flow through Sdh, 300 $\mu$ L of air-oxidized membranes resuspended in 100mM HEPES / 5 mM EDTA were mixed with an equal volume of 200mM succinate dissolved in 100mM HEPES / 5mM EDTA. The system flow rates and the distance from the mixer to the cold plate were varied to attain progressive time points from  $t = 0$  when mixing between enzyme and substrate is initiated (445). The dead time of the instrument setup is estimated to be  $75 \pm 15 \mu\text{s}$  and has been accounted for in our data and simulations. To achieve appropriate mixing on the  $\mu\text{s}$  and ms timescales, flow rates between 1.4 to 3.0 mL/min were used while the distance from the mixer to the cold plate was varied from 10mm to 61mm. The duration of the spray was varied according to the system flow rate such that approximately 500 $\mu$ L of frozen samples are collected in each experiment. The temperature of the reaction was approximately 10°C.

*Electron Paramagnetic Resonance Spectroscopy* – Redox titrations were carried out anaerobically under argon at 25°C on Sdh-enriched membranes at a total protein concentration of approximately 30mg mL<sup>-1</sup> in 100mM HEPES / 5mM EDTA (pH 8). The following redox mediators were used at a concentration of 25 $\mu$ M: quinhydrone, 2,6-dichloroindophenol, 1,2-naphthoquinone, toluylene blue, phenazine methosulfate, thionine, duroquinone, methylene blue, resorufin, indigotrisulfonate, indigodisulfonate, anthraquinone-2-sulfonic acid, phenosafranine, benzyl viologen, and methyl viologen. All samples were prepared in 3mm internal diameter quartz EPR tubes and were rapidly frozen in liquid nitrogen-chilled ethanol before storing in liquid nitrogen. EPR spectra

were recorded using a Bruker Elexsys E500 EPR spectrometer equipped with an Oxford Instruments ESR900 flowing helium cryostat.  $E_m$  values for FS1 and FS3 were determined at 12K and 20mW while that of FS2 was determined at 40K and 2mW, all at a frequency of 9.38GHz. All spectra were corrected for internal EPR tube diameters. In the FHQ studies, sample “flakes” were directly packed into EPR tubes for analyses. FS1 and FS3 were monitored at a non-saturating power of 20mW at a temperature of 12 K and frequency of 9.4GHz.

*Calculation and Simulation of Electron Transfer* – The following equations were used for theoretical treatments of electron transfer through Sdh:

$$\log_{10} k_{\text{exergonic}} = 13.0 - (1.2 - 0.8\rho)(R - 3.6) - 3.1(\Delta G + \lambda)^2/\lambda$$

$$\log_{10} k_{\text{endogonic}} = 13.0 - (1.2 - 0.8\rho)(R - 3.6) - 3.1(-\Delta G + \lambda)^2/\lambda - \Delta G/0.06$$

where  $k$  is the rate of ET in  $\text{s}^{-1}$ ,  $\rho$  is packing density and is estimated to be 0.76,  $R$  is the edge-to-edge distance in angstroms,  $\Delta G$  is the change in free energy based on the  $E_m$  values of the cofactors involved, and  $\lambda$  is the reorganization energy associated with the ET step (19).

### 7.3 Results

To study pre-steady state electron transfer through Sdh, we made membrane preparations enriched in Sdh that had been activated by the traditional protocol of incubation at 30°C for 15 minutes followed by resuspension in buffer that included 1mM malonate. This process eliminates the competitive inhibitor oxaloacetate that binds strongly to and co-purifies with Sdh. Using membrane preparations containing activated wild-type (WT) Sdh enzyme, we added succinate to initiate ET to the heme  $b$  and

monitored its reduction on the ms timescale using the stopped-flow technique. Addition of succinate resulted in heme reduction approximately 40ms after mixing (data not shown). We proceeded to re-wash and resuspend the membranes in different buffers at different pH to determine whether heme reduction can be initiated at a faster rate. Of the conditions tested — 100mM MOPS, pH 7; 20 mM P<sub>i</sub>, pH 8; 200mM P<sub>i</sub>, pH 8; 100mM HEPES, pH 8 — it was the latter that resulted in the shortest lag time for heme reduction, and subsequent washes of the membrane preparations in the different buffers did not alter the dead time any further.

For the WT Sdh enzyme, heme reduction was seen as early as the dead time of the instrument (~4 ms) and was completed after approximately 50 ms (Figure 7.1A). Observation of heme reduction on the 100 and 1000 ms timescales also confirmed that heme reduction reached a steady state after approximately 50 ms. The mutant enzyme of choice in this study, SdhCDAB<sup>I150H</sup>, has a lowered  $E_m$  value for FS2 and slower rates of enzyme turnover and heme reduction (424). After activation of SdhCDAB<sup>I150H</sup> and resuspension in HEPES buffer, heme reduction was observed after a lag time of 15 ms and attained steady state at 200 ms (Figure 7.1B). Reduction of heme *b* in both WT and mutant enzymes appears to be biphasic. For the WT enzyme, the first phase of heme reduction ( $t < 14\text{ms}$ ) could be fitted to either a first-order equation with  $A = -0.28$  and  $k = 400\text{s}^{-1}$  or a zero-order equation with  $k = 80\text{s}^{-1}$ ; the slow second phase ( $14\text{ms} < t < 50\text{ms}$ ) could only be fitted to a linear equation with  $k = 22\text{s}^{-1}$ . For the SdhCDAB<sup>I150H</sup> mutant, the first phase ( $t < 75\text{ms}$ ) of heme reduction appears linear with  $k = 8\text{s}^{-1}$ , whereas the second phase ( $75\text{ms} < t < 200\text{ms}$ ) had a rate of  $k = 2.4\text{s}^{-1}$ .

In the FHQ experiments, succinate was used as the reductant to donate electrons into Sdh and the reaction mixture was quenched anywhere between 130 $\mu$ s to 138ms. The air-oxidized membrane preparations were used as the  $t = 0$  data point while succinate-reduced samples were at the steady-state  $t = \infty$ . Reduction of FAD and the three [Fe-S] clusters were then analyzed by EPR spectroscopy, but only reduction of FS1 and FS3 were observed. Figure 7.2 and Figure 7.3 show the reduction of these two [Fe-S] clusters in WT Sdh and the SdhCDAB<sup>I150H</sup> mutant enzyme, respectively. Table 7.1 shows the attempts to fit the reduction profiles to either a single or double exponential first-order rate equation. In both the WT Sdh and SdhCDAB<sup>I150H</sup>, reduction of the [2Fe-2S] cluster reached approximately 40% whereas reduction of the [3Fe-4S] cluster reached 100%. In the WT enzyme reduction of FS1 and FS3 proceeded at approximately the same rate, where  $k_{\text{FS1}} = 65 \pm 16 \text{ s}^{-1}$  and  $k_{\text{FS3}} = 57 \pm 13 \text{ s}^{-1}$  (single exponential fits). In the SdhCDAB<sup>I150H</sup> mutant, electron buildup at FS1 occurred more rapidly and FS3 reduction occurred much more slowly, with  $k_{\text{FS1}} = 135 \pm 57 \text{ s}^{-1}$  and  $k_{\text{FS3}} = 7 \pm 9 \text{ s}^{-1}$ . We also attempted to fit the FS1 and FS3 reduction profiles to double exponential equations, and the results are shown in Figure 7.2, Figure 7.3 and Table 7.1. In the case of the SdhCDAB<sup>I150H</sup> mutant enzyme wherein ET rate is slowed, reduction of FS1 appears to be biphasic; this is much harder to envision in the WT enzyme from Figure 7.2.

In order to predict ET rates, we used PDB file 1NEK (131) to determine edge-to-edge distances between cofactors. The packing density,  $\rho$ , and the reorganization energy,  $\lambda$ , were estimated to be 0.76 and 0.70 respectively. We also performed redox titrations on the WT and mutant Sdh enzymes to determine the midpoint potentials of the [Fe-S] clusters at pH 8 (Table 7.2) such that  $\Delta G$  can be calculated. The  $E_{\text{m},8}$  values were similar

between the WT and SdhB<sup>I150H</sup> mutant for FS1 and FS3, but the  $E_{m,8}$  value of FS2 remained depressed by ~107mV in the mutant enzyme (Table 7.2). This is in agreement with previously published data at pH 7 (424). Simulation of ET using the equations described in Experimental Procedures (Section 7.3) yielded rates of  $14.1 \times 10^3 \text{ s}^{-1}$  for the FS1→FS2 transition and  $1.0 \times 10^9 \text{ s}^{-1}$  for the FS2→FS3 transition for the WT enzyme, and  $3.8 \times 10^3 \text{ s}^{-1}$  and  $1.5 \times 10^9 \text{ s}^{-1}$  for the same transitions in the SdhCDAB<sup>I150H</sup> mutant enzyme. This is much higher than the reduction rates of FS1 and FS3 observed in the FHQ experiments.

#### 7.4 Discussion

In this study, we employed the *E. coli* Sdh enzyme as a model system to compare experimental ET rates to those obtained from theoretical calculations. By observing reduction rates of the [2Fe-2S] and [3Fe-4S] clusters in WT Sdh and the SdhCDAB<sup>I150H</sup> mutant enzyme, we were able to discern information regarding ET rates and mechanisms.

In both the WT and SdhCDAB<sup>I150H</sup> mutant enzymes, FS1 was only ~40-50% reducible by succinate. This was true for FHQ samples as well as for membrane preparations that were mixed directly with succinate in an EPR tube and allowed to reach steady state (ie.  $t = \infty$ ); only when dithionite was used as a reductant did we see 100% reduction of FS1. This was somewhat expected since at pH 8, the midpoint potential of FS1 is -40mV in both mutant and WT enzymes, which is below the reduction potential of succinate (+30mV at pH 7). In terms of FS3, its  $E_{m,8}$  value was +44mV and +54mV in the WT and SdhCDAB<sup>I150H</sup> enzymes respectively, and thus it was completely reducible by both succinate and dithionite. The very low  $E_m$  values of the flavin and the [4Fe-4S]



cluster also prevented observation of the flavosemiquinone radical and the reduced FS2 signal in our FHQ studies.

The most significant observation from this study is the depressed rate of FS3 reduction in the SdhCDAB<sup>I150H</sup> mutant enzyme. In a previous study (424), the SdhB<sup>I150H</sup> mutation was shown to elicit a 125mV decrease in the  $E_{m,7}$  value of FS2, resulting in a ~65% loss in its ability to carry out succinate-dependent reduction of Q<sub>0</sub> and fumarate-dependent oxidation of plumbagin under steady-state conditions. In the freeze-hyperquench studies presented herein, pre-steady state reduction of FS3 in the SdhB<sup>I150H</sup> mutant proceeds at a rate that is ~20% of that observed for the WT enzyme (Table 7.1, single exponential fit). A slower rate of ET from succinate to FS3 implies that electrons might remain longer at FS1, and this appeared as an apparent higher rate of FS1 reduction in the SdhB<sup>I150H</sup> mutant compared to the WT enzyme in our observations.

The decreased ET rate through SdhB also translated to a slower rate of heme *b* reduction in the membrane anchor domain. The lag time before the initiation of heme reduction, the rates of heme reduction during both the first and second phases, as well as their durations, are all extended in the SdhCDAB<sup>I150H</sup> mutant enzyme. Pre-steady state kinetics on the *E. coli* Sdh heme *b* has not been previously studied, therefore we were somewhat surprised to see a biphasic heme reduction mechanism by the physiological substrate succinate. We surmise that these two distinct phases are the result of rapid electron transfer between the heme and the UQ species at the Q<sub>p</sub>-site. During the initial phase, electrons are passed from the FS3 to UQ to form ubisemiquinone, which in turn donates electrons to the heme *b*. During the second, slower phase of heme reduction, a second electron is transferred from FS3 to UQ to once again form ubisemiquinone, and

the heme can donate its electron to the Q<sub>P</sub>-site to form UQH<sub>2</sub>. Thus the second phase is slower than the first phase because, in addition to electrons reducing the heme, electrons are also leaving the heme to complete the UQ reduction mechanism in a subpopulation of enzyme. In Q<sub>P</sub>-site mutants wherein quinone binding is hindered, electron transfer to the heme *b* progresses at a much slower rate (414). Thus an alternate explanation that accounts for the two phases of heme reduction is that in the first phase, electrons can converge to the heme directly from FS3 or via the Q<sub>P</sub>-site, but upon quinone reduction and dissociation, the only source of electrons for heme *b* reduction is FS3.

Electron transfer through the porcine complex II enzyme had been previously modeled (443). The theoretical calculations revealed that a flavosemiquinone radical and the reduced [2Fe-2S] cluster form would build up on the microsecond timescale. However, we did not observe any [Fe-S] cluster reduction in the FHQ samples that were quenched at  $t < 0.7$ ms. We also did not observe any flavosemiquinone radical and FS2 reduction in all the FHQ samples prepared. The lack of cofactor reduction in the microsecond timescale might be the result of trace amounts of oxaloacetate and/or malonate in the membrane preparations, which compete with succinate for binding at the dicarboxylate binding site. The lag time for reduction may also be indicative of the time needed for succinate binding and hydride transfer to the FAD.

In the simulations of electron transfer, the ET reaction is typically “idealized” so that only 1 molecule of substrate would be consumed. For Sdh, this type of treatment would mean a single turnover of succinate that would donate 2 electrons into the enzyme. *In vivo*, such a scenario would hardly be realistic. Thus we carried out novel ET simulations *in silico* which models the main observations from our ET experiments and

these are shown in Figures 7.2 and 7.3. The most noticeable features of this simulation which parallels the FHQ data are: i) no FS2 reduction during the course of the reaction and ii) electron transfer steps in the SdhCDAB<sup>I150H</sup> mutant enzyme proceeds much slower than those of the WT Sdh. However, notable differences between the observed and theoretical ET in Sdh include the appearance of a flavosemiquinone and the extent to which FS1 gets reduced. This difference can be accounted for if we assume that UQ reduction and dissociation occurs faster than succinate binding and oxidation such that electrons do not build up in the early portion of the ET chain.

The studies presented herein detailed the experimental observations of electron transfer through the Sdh enzyme on the  $\mu$ s and ms timescales. We did not observe any cofactors to be reduced in the microsecond timeframe, presumably because succinate oxidation and hydride transfer to the FAD proceeds during this time window. Reduction of the [2Fe-2S] and [3Fe-4S] clusters, as well as heme *b* reduction, were all observed on the millisecond timescale. Analyses by stopped-flow indicated that heme *b* reduction proceeds via a biphasic mechanism wherein the second, slower step is associated with ubiquinone reduction. Finally, we presented a novel simulated model of electron transfer through a redox enzyme that involves multiple turnovers of substrate based on our freeze-hyperquench studies.

		Single Exponential			Double Exponential					
		A	k	t <sub>1/2</sub>	A <sub>1</sub>	k <sub>1</sub>	t <sub>1/2,1</sub>	A <sub>2</sub>	k <sub>2</sub>	t <sub>1/2,2</sub>
WT Sdh	FS1	-0.4257	0.065	10.707	-0.2424	0.014	50.7	-0.2235	0.207	3.3
	FS3	-0.9186	0.057	12.147	-0.627	0.016	44.5	-0.3687	0.361	1.9
SdhB-I150H	FS1	-0.3591	0.135	5.145	-0.2543	0.282	2.5	-0.2785	0.003	276.2
	FS3	-1.0033	0.007	98.667	-0.5017	0.007	98.7	-0.5017	0.007	98.7

Table 7.1. Parameters to fit first-order rate equations to observed FS1 and FS3 reduction. The single exponential equation is  $y = Ae^{(-kt)} + b$  where  $y$  is reduction of the cluster ( $0 < y < 1$ ),  $A$  is the steady state reduction level,  $k$  is the rate with units of  $\text{ms}^{-1}$ ,  $t$  is time in ms, and  $b$  is set to  $-A$  to allow the curve to start at  $(0,0)$ . The variables in the double exponential equation  $y = A_1e^{(-k_1t)} + A_2e^{(-k_2t)} + b$  have the same meaning as those in the single exponential equation but describe a biphasic kinetic behavior.

Membranes	Midpoint Potentials (mV)		
	FS1	FS2	FS3
WT Sdh	$-40 \pm 20$	$-235 \pm 10$	$44 \pm 1$
SdhCDAB <sup>I150H</sup>	$-40 \pm 3$	$-342 \pm 0$	$54 \pm 2$

Table 7.2. Midpoint potentials of the [Fe-S] clusters in WT and mutant Sdh. Redox titrations were performed at 25°C under wet argon at pH 8. The FS1 and FS3 signals were monitored at 12K and 20mW, while the signal for FS2 was followed at 40K and 2mW. EPR spectra were all obtained at a frequency of 9.38GHz with a modulation amplitude of 10G<sub>pp</sub> at 100KHz. The average and range of  $E_m$  values from two independent redox titrations are shown.

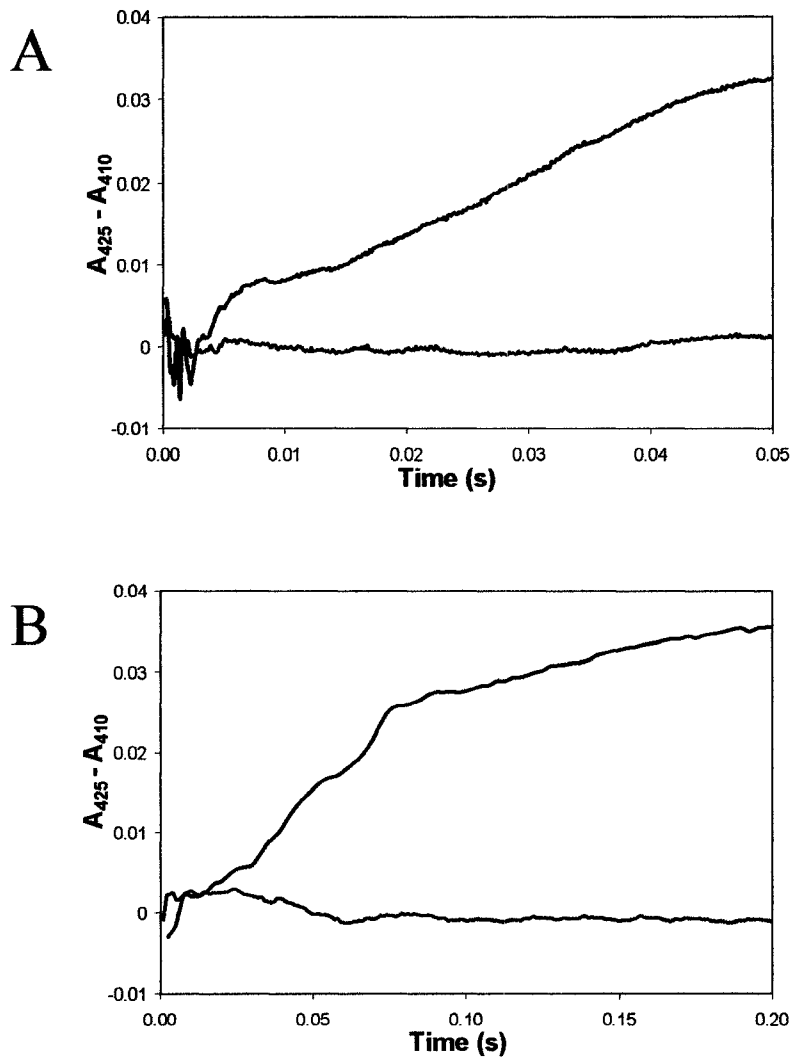


Figure 7.1. Pre-steady state heme reduction. Absorbance was monitored at 425 nm (Soret band) and 410 nm (baseline) on the 50 ms timescale using the stopped-flow technique. 200 mM succinate (black traces) was mixed with membranes enriched in either wild-type Sdh (A) or SdhCDAB<sup>I150H</sup> (B). Heme reduction was observed after 4 ms and was completed in approximately 50 ms for the wild-type enzyme. For the SdhCDAB<sup>I150H</sup> mutant enzyme, heme reduction was observed after 15ms and was completed in 200ms. When the same membrane preparations were mixed with HEPES/EDTA buffer (blue traces), no reduction was observed.

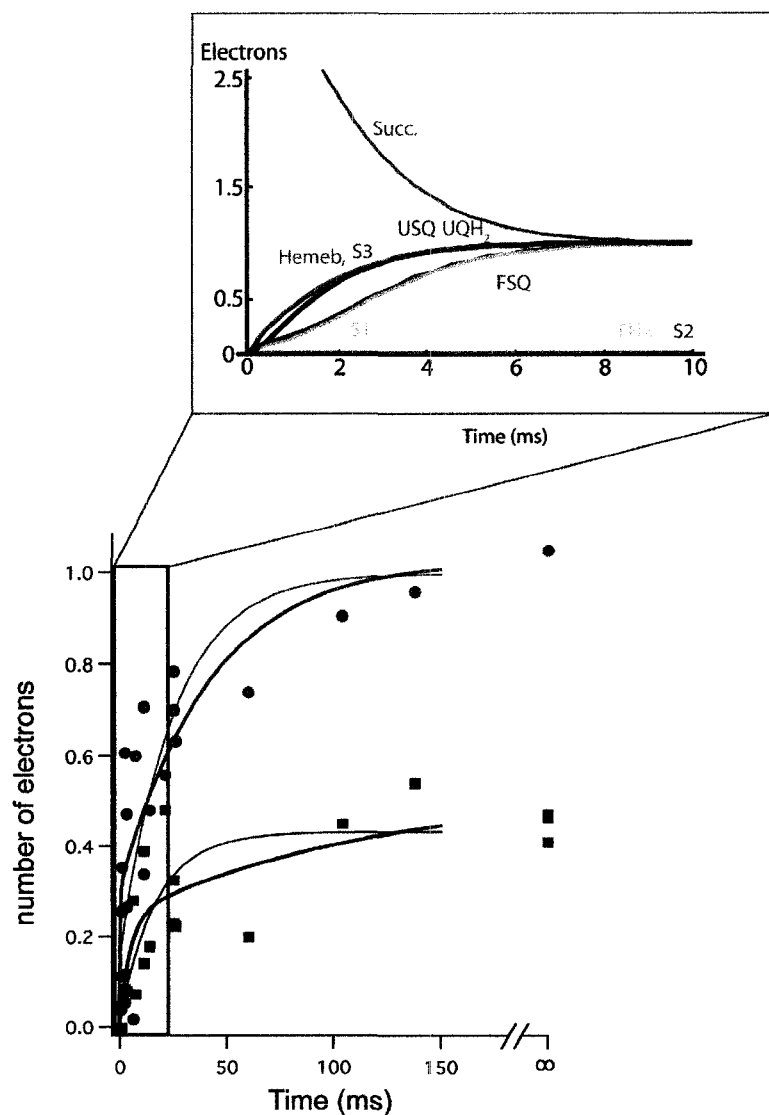


Figure 7.2. Electron transfer in SdhCDAB. Reduction of the [2Fe-2S] cluster (blue) and the [3Fe-4S] cluster (green) as determined by freeze-hyperquench and EPR spectroscopy are shown in the bottom panel and fitted to either a single exponential (thin line) or double exponential (thick line) first-order equation. Time point  $t = 0$  ms corresponds to Sdh in the air-oxidized state whereas  $t = \infty$  corresponds to Sdh enzymes which have been reduced by succinate. The top panel, created by Dr. Chris Moser and Elizabeth Chobot from the laboratory of Dr. Les Dutton, illustrates a 10 millisecond simulation of electron transfer in Sdh using theoretical equations.

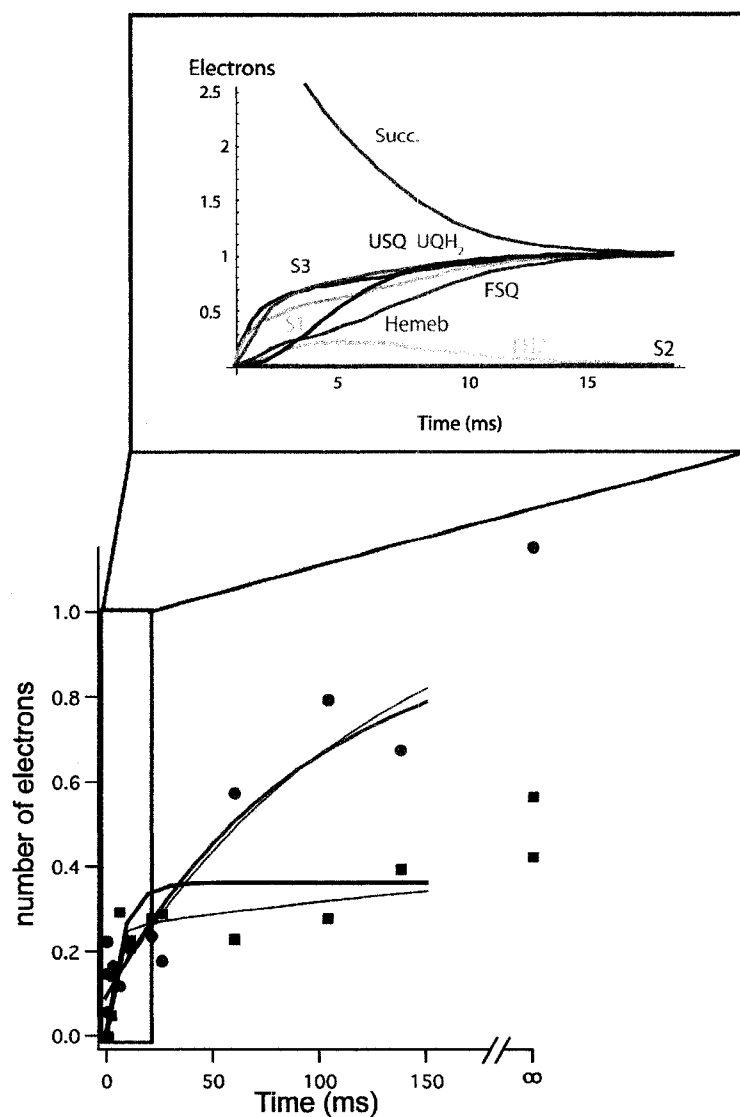


Figure 7.3. Electron transfer in SdhCDAB<sup>1150H</sup>. Reduction of the [2Fe-2S] cluster (blue) and the [3Fe-4S] cluster (green) as determined by freeze-hyperquench and EPR spectroscopy are shown in the bottom panel and fitted to either a single exponential (thin line) or double exponential (thick line) first-order equation. Time point  $t = 0$  ms corresponds to Sdh in the air-oxidized state whereas  $t = \infty$  corresponds to Sdh enzymes which have been reduced by succinate. The top panel, created by Dr. Chris Moser and Elizabeth Chobot from the laboratory of Dr. Les Dutton, illustrates a 20 millisecond simulation of electron transfer in Sdh using theoretical equations.

## **Chapter 8**

### **Conclusions, Summary, and Future Direction**



## 8.1 DMSO Reductase

In chapter 3 of this thesis, mutagenesis studies on the DmsB subunit were presented and the results indicate that not only is this subunit required for electron transfer, but residues of this subunit are also important for quinol binding and oxidation. Using the X-ray crystal structure of formate dehydrogenase-N as a 3-dimensional template, we began by building a structural model of DmsB. Based on this *in silico* model, residues Pro80, Ser81, Cys102 and Tyr104 of DmsB were predicted to be located at the DmsB-DmsC interface and our experiments indicated that they were critical for the binding of the MQH<sub>2</sub> inhibitor analog HOQNO and the transfer of electrons from MQH<sub>2</sub> to FS4. We evaluated mutant effects on the redox chemistry of FS4 by constructing double mutants (with a DmsB<sup>C102S</sup> mutation) in which FS4 is assembled as a [3Fe-4S] cluster. Mutations of positively charged residues around FS4 lowered its midpoint potential, but mutations of negatively charged residues had negligible effects. Substitution of DmsB<sup>Y104</sup> with either Asp or Glu elicited a much larger effect on the  $E_m$  of FS4, causing it to decrease by ~130mV. We found the  $E_m$  of FS4 in the DmsB<sup>C102S</sup> mutant to be insensitive to HOQNO as well as to changes in pH from 5 to 7, whereas the  $E_m$  of FS4 in the the DmsB<sup>C102S/Y104D</sup> double mutant increased in the presence of HOQNO and decreasing pH. Analyses of the mutants suggested that the maximum achievable  $E_m$  for FS4 in the [3Fe-4S] cluster form is approximately +275mV.

## 8.2 Succinate Dehydrogenase

When the *E. coli* Sdh crystal structure was published, it became the clear choice over DmsABC as the superior model to study structure-function relationships in redox

enzyme catalysis. Not only was a 3-dimensional map of the holoenzyme available, the distinct spectroscopic properties of the enzyme made results much simpler for interpretation. Furthermore, SdhCDAB could be over-expressed to higher levels than DmsABC and identical membrane preparation protocols yielded much higher enzyme concentrations.

One very interesting fact about the EcSdh structure was that there was high variation in the membrane anchor domain compared to other members belonging in the complex II superfamily, including the porcine (378) and avian (380) mitochondrial Sdh enzymes. A major difference amongst the three structures is the water channel leading from the cytoplasm to the Q<sub>P</sub>-site. In EcSdh, residues SdhB<sup>G227</sup>, SdhC<sup>D95</sup> and SdhC<sup>E101</sup> are located at or near the entrance of a water channel that has been proposed to function as a proton wire connecting the cytoplasm to the quinone binding site (377). However, the pig and chicken Sdh enzymes show an alternative entrance to the water channel via the conserved SdhD<sup>Q78</sup> residue. In the study presented in Chapter 5, site-directed mutants of these four residues were created and characterized. We showed that the observed water channel in the *E. coli* Sdh structure is the functional proton wire *in vivo*, while *in vitro* results indicate an alternative entrance for protons. *In silico* examination of the *E. coli* Sdh revealed a possible H-bonding network leading from the cytoplasm to the quinone binding site that involves SdhD<sup>D15</sup>, which is located at the equivalent spatial location as the entrance for the proton channel of porcine and avian Sdh. Based on our results we proposed an alternative proton pathway in EcSdh that might be functional only *in vitro*.

As mentioned, the electron transfer relay of respiratory chains often contains a [4Fe-4S] cluster with a relatively low midpoint potential that may serve as a rate-limiting

step in the ET process. We first began by studying the conserved hydrophobic residues around FS2 of Sdh (Chapter 6). Mutation of SdhB<sup>I150</sup> to either Glu or His brought about decreases in the  $E_m$  value of FS2, whereas mutation of SdhB<sup>L220</sup> to Ser surprisingly lowered the  $E_m$  value of FS3. It was discovered that a decrease in midpoint potential of either the [4Fe-4S] cluster or the [3Fe-4S] cluster was accompanied by decreased rates of Q<sub>0</sub> reduction and plumbagin oxidation. We also observed differential effects of these mutants to rescue growth on succinate and glycerol-fumarate minimal media. Based on our observations, we hypothesized that the midpoint potentials of the [Fe-S] clusters in the native Sdh enzyme are poised such that direction of ET from succinate to ubiquinone is favored.

However, with the magnitude of decrease observed in the  $E_m$  value of FS2 in the SdhCDAB<sup>I150H</sup> mutant, we did not see the expected decrease in enzyme activity that was predicted from theoretical calculations if we believe ET is rate-limiting. To further study the kinetics and mechanism of ET through Sdh, we performed freeze-hyperquench experiments on the  $\mu$ s and ms timescales (Chapter 7). In FHQ studies, no reduction of any cofactor was observed on the  $\mu$ s time window, indicating that succinate oxidation and hydride transfer to the FAD might occur during this period. Relative to the WT enzyme, the apparent rate of FS3 reduction in the SdhCDAB<sup>I150H</sup> mutant is much slower, but reduction of FS1 occurs at a faster rate, which is expected if the decreased  $E_m$  value of FS2 slows down ET through SdhB. Using the FHQ data, we were able to do *in silico* simulations of ET, wherein multiple molecules of succinate are oxidized, to account for our observed data.

### 8.3 Future Studies

With respect to DmsABC, one major hurdle towards unraveling the mechanism of DmsABC function is the lack of structural data. Purification and crystallization of EcDmsABC have been attempted on numerous occasions in our laboratory for over 15 years but we have had little success. Crystal structures of nitrate reductase (178) and formate dehydrogenase-N (180) are available, but these merely give a holistic view of how DmsABC and its cofactors are assembled. Crystal structures of the soluble DMSO reductase from *Rhodobacter* species have also been obtained (182,183), and the wealth of biochemical data that complements this have allowed us to obtain a good understanding of how DMSO reduction occurs (Chapter 2). However, some intriguing questions regarding the nature of the Mo-bisMGD cofactor remain. For instance, one of the pterin groups appears as a bicyclic dihydropterin species in the NarGHI structure, but appears as a tricyclic pyranopter in all other crystal structures of Mo-bisMGD enzymes. The bicyclic form has been proposed to be an intermediate during enzyme catalysis, and its role is being investigated in our laboratory using NarGHI as a model. Another question relating to the Mo-bisMGD cofactor is whether it donates electrons directly to DmsB, or do electrons transit through a [4Fe-4S] cluster in DmsA that has not been directly observed by EPR spectroscopy? This interesting question is also currently being addressed in our laboratory, but the structural information from NarGHI and FdnGHI, as well as the structure of polysulfide reductase (PsrABC) from *Thermus thermophilus* (446), give a strong argument for its presence in DmsA.

There is certainly a strong overlap between DmsABC and PsrABC in terms of the number and types of cofactors that are assembled, the number of transmembrane helices

and their orientations in the membrane anchor subunit, and their involvements in sulfur metabolism. In fact, residues equivalent to DmsB<sup>P80</sup>, DmsB<sup>S81</sup> and DmsB<sup>Y104</sup> in PsrABC are located at the PsrB-PsrC interface, validating the DmsB model that was generated *in silico* in Chapter 3. However, a closer look at the molybdenum and MQH<sub>2</sub> active sites hints at how these two enzymes may have divergently evolved. In DmsABC, a wide active site funnel is present to allow larger *S*- and *N*-oxide molecules to enter the active site; in PsrABC, this funnel is narrow, perhaps only to accommodate polysulfide. The coordination of the Mo atom is also different between the two enzymes; DmsA provides a Ser hydroxyl sidechain as one of the Mo ligands whereas PsrA provides a Cys sulfhydryl sidechain. This could partially account for the differences in reduction potentials of the reactions catalyzed by DmsABC (DMSO/DMS, +130mV) and PsrABC (S<sup>2-</sup><sub>4</sub>/HS<sup>-</sup>, -260mV), and it may play a key role in catalyzing sulfur reduction at the elevated temperatures of the *T. thermophilus* habitats.

The mechanism of MQH<sub>2</sub> oxidation is also poorly understood in DmsABC and PsrABC. Since there is no quinone binding motif, residues of DmsC which are involved in MQH<sub>2</sub> binding and oxidation cannot be easily identified. Controversy surrounding the cytoplasmic/periplasmic location of DmsABC also adds mystery to the location of the Q-site and how electrons are donated to DmsB. In the structure of PsrABC, the quinone binding site is situated on the proximal side of the membrane relative to the electron transfer subunit, and can in fact donate electrons directly to FS4 which is 7Å away (446). Although we might expect the Q-site in DmsABC to be similarly positioned compared to that in PsrABC, residues which were found to be involved in Q-site function in the former enzyme, namely DmsC<sup>H65</sup> and DmsC<sup>E87</sup>, are not conserved in the latter enzyme.

However, Psrc<sup>E67</sup> and Psrc<sup>H75</sup> are proposed to play a role in MQH<sub>2</sub> binding (446). It is possible that the His and Glu residues are conserved in the quaternary structure despite differing in positions in the primary sequence. Another major difference lies in the fact that DmsABC is an electroneutral enzyme (167) whereas PsrcABC is thought to generate a pmf (447). Using the structure of PsrcABC, Jormakka and coworkers proposed a transmembrane H<sup>+</sup> pathway that functions as a conformational H<sup>+</sup> pump (446), much like those in cytochrome oxidase or NADH dehydrogenase.

Just as it was the case with formate dehydrogenase-N, it is the ET subunit of PsrcABC that shows the highest sequence homology out of the three subunits when compared to DmsABC. Unfortunately, biophysical data describing the iron-sulfur clusters of PsrcB does not exist, so very little structure-function relationships can be extracted from the PsrcABC crystal structure.

Much information has been gathered from the Sdh crystal structures and the biochemical and biophysical data that accompany them, but many topics of interest remain to be studied. For instance, how many Q-sites are present in EcSdh and mitochondrial complex II, and does the presence of a Q<sub>D</sub>-site really dissipate the pmf? This last point has actually been proven in the *Bacillus* Sdh enzyme, which contains both a Q<sub>P</sub>- and a Q<sub>D</sub>-site. Uden and coworkers (407,409) hypothesize that because the succinate/MQ couple is endergonic in *Bacillus*, MQ reduction at the Q<sub>D</sub>-site must be driven by the pmf (*i.e.* H<sup>+</sup> from the periplasm). Thus by the same token, if a Q<sub>D</sub>-site is indeed present in EcSdh, one might test its functionality by observing growth of a *ubi*<sup>-</sup> strain on succinate minimal media. In the absence of the more electropositive UQ molecule, the bacterium will be forced to utilize MQ, which has a lower reduction

potential than the succinate/fumarate couple. This would mimic the scenario observed in *Bacillus*, and might force the Q<sub>D</sub>-site to become operative in EcSdh as it is oriented towards the periplasm and can therefore apply the pmf towards MQ reduction. One must be careful here in that a negative result does not absolutely mean the Q<sub>D</sub>-site is non-existent. First, the *Bacillus* Sdh has 2 hemes whereas EcSdh only has 1 heme; therefore the mechanism of ET might be different. Second, the EcSdh Q<sub>D</sub>-site is extremely hydrophobic and may only be involved in quinone binding but not reduction. In the *Bacillus* enzyme, the Q<sub>P</sub>-site has the ability to exert conformational changes to the holoenzyme that somehow affects electron transfer, but only in a specific direction (448). Finally, the terminal oxidase must be able to utilize MQH<sub>2</sub> as a substrate.

Another mystery pertaining to Sdh is the role of the heme. Why are one, two, or no hemes assembled in different members of the complex II family of enzymes? One “simple” explanation is that they are required for ET to the Q<sub>D</sub>-site. The *Bacillus subtilis* Sdh and *Wolinella succinogenes* Frd enzymes both have two hemes and both carry out quinone oxidation-reduction chemistry at the Q<sub>D</sub>-site. In contrast, Sdh and Frd enzymes which have one or no heme in the membrane domain exclusively use the Q<sub>P</sub>-site to reduce or oxidize the Q-pool. However, if this is true, then this begs the question of why EcSdh assembles a heme at all if ET to the Q<sub>D</sub>-site is unnecessary. Recently, postulates of its function have been downplayed since heme-free EcSdh and ScSdh can be assembled correctly and retain significant catalytic activity without increasing ROS production (130,400). To examine other possible roles that the heme *b* might play in EcSdh, our laboratory is currently attempting to change its midpoint potential by site-directed mutagenesis and by substituting the heme with synthetic protoporphyrin rings and non-

ferric metal centers. If the  $Q_D$ -site does exist in EcSdh, then the heme might act as a communication medium between it and the  $Q_P$ -site even if ET does not occur between the two Q-sites. One might also speculate that the heme might serve as a probe of the Q-pool and translate its redox state to the catalytic domain such that substrate binding and oxidation/reduction is controlled.

What is the role of the low potential iron-sulfur cluster in redox enzymes? In the field of bioenergetics, this was a dividing question before any crystal structures of linear ET chains were available. Some argued that its low potential excluded its role as an ET intermediate while others stood on the other side of the fence. With the surge of structural data that is becoming available, it is now clear that the low potential iron-sulfur cluster plays a critical role in electron transfer, more than the mere structural role as some have argued. So why is its midpoint potential so much lower than the reduction couples of the reactions catalyzed by the specific enzyme? In fact, why do the midpoint potentials of cofactors in an ET chain resemble an energetic rollercoaster instead of a simple energy slide? A thorough search of the literature would show that in the vast majority of case studies, the larger the  $E_m$  values deviate from those in the native enzyme, the larger the decrease in catalytic activity. This not only applies to the low potential iron-sulfur cluster, but to any cofactor in the ET chain. Thus it appears nature has engineered redox enzymes to be as efficient as possible, and there is an additional role the  $E_m$  values of cofactors play that we are unaware of. If this is true, additional variables might need to be introduced into the equation by Dutton *et al.* (19) to account for this unknown phenomenon such that a more accurate model of ET can be generated. It is possible that ET from one end of the redox enzyme to the other is accompanied by propagating



conformational changes that help substrate binding/release and lower transition state energies. For instance, the free energy from succinate oxidation can be coupled, via the electron transfer chain, to drive quinone reduction. It is well known that Sdh exhibits tunnel diode behavior such that its catalytic activity actually decreases with increasing driving force. The electrode potential at which Sdh begins to lose enzyme activity is close to the  $E_m$  value of the low potential [4Fe-4S] cluster. We know from Chapter 7 that FS2 remains oxidized after succinate oxidation, even when FS1 and FS3 are reduced. If FS2 is permanently reduced at very high driving forces, Sdh might be locked into a conformation that is unfavorable for catalysis.

In EcSdh, it was observed that electrons from FS3 preferentially tunnel to the Q<sub>P</sub>-site instead of the heme *b* (414). This phenomenon might be partly explained by the tandem Trp residues in SdhB (Trp163 and Trp164), which stack on top of the UQ molecule in the crystal structure (131). Some recent experiments have identified Tyr and Trp residues to be involved in catalysis by accelerating intraprotein electron transfer (449). Thus it would be of interest to create single and combined substitutions of SdhBW163 and SdhBW164 with Tyr, His or Ala.

In the complex II superfamily of enzymes, ScSdh is the only protein that requires an assembly chaperone. It is unclear when Tcm62p interacts with ScSdh during the assembly process and why this particular Sdh requires such an assembly factor whereas Sdh from more complicated organisms do not require a chaperone for proper folding and assembly (at least, no such chaperones have been identified). One significant difference between ScSdh and Sdh enzymes in general is that the latter enzymes use a *bis*-histidyl coordination scheme to interact with the heme *b* whereas ScSdh has an unusual His/Cys

*bis*-coordination scheme for heme stabilization. The role of Tcm62p in *S. cerevisiae* might be to help heme insertion into ScSdh, potentially by interacting with Sdh4p-Cys78. This hypothesis can be tested by observing whether a strain lacking the Tcm62p chaperone can sustain growth on succinate minimal medium by expressing the heme-free mutant enzyme.

Another interesting topic is how missense mutations at different locations in Sdh lead to varying disease phenotypes in humans, and what are the underlying mechanisms of disease manifestation that stem from Sdh? As discussed briefly in Chapter 4, this is thought to occur through either overproduction of ROS or cellular accumulation of succinate. The  $E_m$  value of FS2 in bovine complex II is -260mV, which is lower than that of EcSdh. In Chapter 6, we saw that decreasing the  $E_m$  value of FS2 allowed growth on succinate but not on glycerol-fumrate. In Chapter 5, we proposed an alternative  $H^+$  pathway via SdhD<sup>D15</sup> that is spatially conserved with the entrances of the  $H^+$  channels in the porcine and avian Sdh enzymes. This secondary  $H^+$  route allowed growth on succinate but not on glycerol-fumarate. Thus, it appears the mitochondrial Sdh have evolved at least two mechanisms to avoid fumarate reduction such that succinate oxidation is preferred and its accumulation can be prevented *in vivo*. As for the ability of Sdh to generate ROS, the precise location of where this occurs has yet to be pinpointed, but evidence strongly suggests the Q<sub>P</sub>-site to be the origin of ROS. Another possible location for ROS generation is the heme molecule itself. In hemoglobin, myoglobin, and cytochrome oxidases, hemes can stably interact with oxygen. Although the heme *b* in Sdh is hexacoordinated in a low spin state, it can actually be converted to the pentacoordination state in certain Sdh mutants; further, the membrane domain shows a

certain degree of flexibility in that different His residues can act as ligand to the heme (398). This degree of freedom around the heme may allow molecular oxygen to bind transiently and take up a lone electron from the heme, thereby generating superoxide. Such a scenario would partially explain why superoxide generation was decreased in a heme-free Sdh (130).

The work presented within this thesis has generated many answers, but more importantly, it has generated more intriguing and fundamental questions about bioenergetics and energy conservation which we did not even dream about. However, these are not questions for me to tackle, but perhaps for another PhD graduate student...

## References

1. Mitchell, P. (1967) *Fed Proc* **26**(5), 1370-1379
2. Gabel, C. V., and Berg, H. C. (2003) *Proc Natl Acad Sci U S A* **100**(15), 8748-8751
3. Oster, G., and Wang, H. (2003) *Trends Cell Biol* **13**(3), 114-121
4. Kotyk, A. (1983) *J Bioenerg Biomembr* **15**(6), 307-319
5. Marques, J. P., Schattat, M. H., Hause, G., Dudeck, I., and Klosgen, R. B. (2004) *J Exp Bot* **55**(403), 1697-1706
6. Bageshwar, U. K., and Musser, S. M. (2007) *J Cell Biol* **179**(1), 87-99
7. Brown, G. C., and Brand, M. D. (1988) *Biochem J* **252**(2), 473-479
8. Wikstrom, M. (1984) *FEBS Lett* **169**(2), 300-304
9. Hirst, J. (2003) *Proc Natl Acad Sci U S A* **100**(3), 773-775
10. Hofhaus, G., Weiss, H., and Leonard, K. (1991) *J Mol Biol* **221**(3), 1027-1043
11. Guenebaut, V., Vincentelli, R., Mills, D., Weiss, H., and Leonard, K. R. (1997) *J Mol Biol* **265**(4), 409-418
12. Grigorieff, N. (1998) *J Mol Biol* **277**(5), 1033-1046
13. Peng, G., Fritsch, G., Zickermann, V., Schagger, H., Mentele, R., Lottspeich, F., Bostina, M., Radermacher, M., Huber, R., Stetter, K. O., and Michel, H. (2003) *Biochemistry* **42**(10), 3032-3039
14. Guenebaut, V., Schlitt, A., Weiss, H., Leonard, K., and Friedrich, T. (1998) *J Mol Biol* **276**(1), 105-112
15. Walker, J. E. (1992) *Q Rev Biophys* **25**(3), 253-324

16. Hirst, J., Carroll, J., Fearnley, I. M., Shannon, R. J., and Walker, J. E. (2003) *Biochim Biophys Acta* **1604**(3), 135-150
17. Sazanov, L. A., and Hinchliffe, P. (2006) *Science* **311**(5766), 1430-1436
18. Hinchliffe, P., and Sazanov, L. A. (2005) *Science* **309**(5735), 771-774
19. Page, C. C., Moser, C. C., Chen, X., and Dutton, P. L. (1999) *Nature* **402**(6757), 47-52
20. Dutton, P. L., Moser, C. C., Sled, V. D., Daldal, F., and Ohnishi, T. (1998) *Biochim Biophys Acta* **1364**(2), 245-257
21. Xia, D., Yu, C. A., Kim, H., Xia, J. Z., Kachurin, A. M., Zhang, L., Yu, L., and Deisenhofer, J. (1997) *Science* **277**(5322), 60-66
22. Iwata, S., Lee, J. W., Okada, K., Lee, J. K., Iwata, M., Rasmussen, B., Link, T. A., Ramaswamy, S., and Jap, B. K. (1998) *Science* **281**(5373), 64-71
23. Hunte, C., Koepke, J., Lange, C., Rossmannith, T., and Michel, H. (2000) *Structure* **8**(6), 669-684
24. Zhang, H., Kurisu, G., Smith, J. L., and Cramer, W. A. (2003) *Proc Natl Acad Sci USA* **100**(9), 5160-5163
25. Esser, L., Elberry, M., Zhou, F., Yu, C. A., Yu, L., and Xia, D. (2008) *J Biol Chem* **283**(5), 2846-2857
26. Mitchell, P. (1975) *FEBS Lett* **56**(1), 1-6
27. Mitchell, P. (1975) *FEBS Lett* **59**(2), 137-139
28. Crofts, A. R. (2004) *Annu Rev Physiol* **66**, 689-733
29. Osyczka, A., Moser, C. C., and Dutton, P. L. (2005) *Trends Biochem Sci* **30**(4), 176-182

30. Tian, H., Yu, L., Mather, M. W., and Yu, C. A. (1998) *J Biol Chem* **273**(43), 27953-27959
31. Tian, H., White, S., Yu, L., and Yu, C. A. (1999) *J Biol Chem* **274**(11), 7146-7152
32. Wikstrom, M. K. (1977) *Nature* **266**(5599), 271-273
33. Oliveberg, M., Hallen, S., and Nilsson, T. (1991) *Biochemistry* **30**(2), 436-440
34. Branden, G., Gennis, R. B., and Brzezinski, P. (2006) *Biochim Biophys Acta* **1757**(8), 1052-1063
35. Yoshikawa, S., Muramoto, K., Shinzawa-Itoh, K., Aoyama, H., Tsukihara, T., Shimokata, K., Katayama, Y., and Shimada, H. (2006) *Biochim Biophys Acta* **1757**(9-10), 1110-1116
36. Tsukihara, T., Aoyama, H., Yamashita, E., Tomizaki, T., Yamaguchi, H., Shinzawa-Itoh, K., Nakashima, R., Yaono, R., and Yoshikawa, S. (1996) *Science* **272**(5265), 1136-1144
37. Ostermeier, C., Harrenga, A., Ermler, U., and Michel, H. (1997) *Proc Natl Acad Sci USA* **94**(20), 10547-10553
38. Yoshikawa, S., Shinzawa-Itoh, K., Nakashima, R., Yaono, R., Yamashita, E., Inoue, N., Yao, M., Fei, M. J., Libeu, C. P., Mizushima, T., Yamaguchi, H., Tomizaki, T., and Tsukihara, T. (1998) *Science* **280**(5370), 1723-1729
39. Abramson, J., Riistama, S., Larsson, G., Jasaitis, A., Svensson-Ek, M., Laakkonen, L., Puustinen, A., Iwata, S., and Wikstrom, M. (2000) *Nat Struct Biol* **7**(10), 910-917

40. Wikstrom, M., and Verkhovsky, M. I. (2006) *Biochim Biophys Acta* **1757**(8), 1047-1051
41. Fetter, J. R., Qian, J., Shapleigh, J., Thomas, J. W., Garcia-Horsman, A., Schmidt, E., Hosler, J., Babcock, G. T., Gennis, R. B., and Ferguson-Miller, S. (1995) *Proc Natl Acad Sci U S A* **92**(5), 1604-1608
42. Puustinen, A., and Wikstrom, M. (1999) *Proc Natl Acad Sci U S A* **96**(1), 35-37
43. Svensson-Ek, M., Abramson, J., Larsson, G., Tornroth, S., Brzezinski, P., and Iwata, S. (2002) *J Mol Biol* **321**(2), 329-339
44. Hosler, J. P., Ferguson-Miller, S., Calhoun, M. W., Thomas, J. W., Hill, J., Lemieux, L., Ma, J., Georgiou, C., Fetter, J., Shapleigh, J., and et al. (1993) *J Bioenerg Biomembr* **25**(2), 121-136
45. Hosler, J. P., Shapleigh, J. P., Mitchell, D. M., Kim, Y., Pressler, M. A., Georgiou, C., Babcock, G. T., Alben, J. O., Ferguson-Miller, S., and Gennis, R. B. (1996) *Biochemistry* **35**(33), 10776-10783
46. Branden, M., Sigurdson, H., Namslauer, A., Gennis, R. B., Adelloth, P., and Brzezinski, P. (2001) *Proc Natl Acad Sci U S A* **98**(9), 5013-5018
47. Cukier, R. I. (2005) *Biochim Biophys Acta* **1706**(1-2), 134-146
48. Lee, H. M., Das, T. K., Rousseau, D. L., Mills, D., Ferguson-Miller, S., and Gennis, R. B. (2000) *Biochemistry* **39**(11), 2989-2996
49. Salje, J., Ludwig, B., and Richter, O. M. (2005) *Biochem Soc Trans* **33**(Pt 4), 829-831
50. Senior, A. E. (1988) *Physiol Rev* **68**(1), 177-231

51. Senior, A. E., Nadanaciva, S., and Weber, J. (2002) *Biochim Biophys Acta* **1553**(3), 188-211
52. Zhou, Y., Duncan, T. M., and Cross, R. L. (1997) *Proc Natl Acad Sci U S A* **94**(20), 10583-10587
53. Yasuda, R., Noji, H., Yoshida, M., Kinosita, K., Jr., and Itoh, H. (2001) *Nature* **410**(6831), 898-904
54. Itoh, H., Takahashi, A., Adachi, K., Noji, H., Yasuda, R., Yoshida, M., and Kinosita, K. (2004) *Nature* **427**(6973), 465-468
55. Berry, R. M. (2005) *Curr Biol* **15**(10), R385-387
56. Abrahams, J. P., Leslie, A. G., Lutter, R., and Walker, J. E. (1994) *Nature* **370**(6491), 621-628
57. Abrahams, J. P., Buchanan, S. K., Van Raaij, M. J., Fearnley, I. M., Leslie, A. G., and Walker, J. E. (1996) *Proc Natl Acad Sci U S A* **93**(18), 9420-9424
58. Shirakihara, Y., Leslie, A. G., Abrahams, J. P., Walker, J. E., Ueda, T., Sekimoto, Y., Kambara, M., Saika, K., Kagawa, Y., and Yoshida, M. (1997) *Structure* **5**(6), 825-836
59. Wilkens, S., Dunn, S. D., Chandler, J., Dahlquist, F. W., and Capaldi, R. A. (1997) *Nat Struct Biol* **4**(3), 198-201
60. Bianchet, M. A., Hüllihen, J., Pedersen, P. L., and Amzel, L. M. (1998) *Proc Natl Acad Sci U S A* **95**(19), 11065-11070
61. Stock, D., Leslie, A. G., and Walker, J. E. (1999) *Science* **286**(5445), 1700-1705
62. Hausrath, A. C., Gruber, G., Matthews, B. W., and Capaldi, R. A. (1999) *Proc Natl Acad Sci U S A* **96**(24), 13697-13702



63. Matthey, U., Kaim, G., Braun, D., Wuthrich, K., and Dimroth, P. (1999) *Eur J Biochem* **261**(2), 459-467
64. Gibbons, C., Montgomery, M. G., Leslie, A. G., and Walker, J. E. (2000) *Nat Struct Biol* **7**(11), 1055-1061
65. Capaldi, R. A., and Schulenberg, B. (2000) *Biochim Biophys Acta* **1458**(2-3), 263-269
66. Rubinstein, J. L., Walker, J. E., and Henderson, R. (2003) *Embo J* **22**(23), 6182-6192
67. Leslie, A. G., and Walker, J. E. (2000) *Philos Trans R Soc Lond B Biol Sci* **355**(1396), 465-471
68. Fillingame, R. H., Jiang, W., and Dmitriev, O. Y. (2000) *J Exp Biol* **203**(Pt 1), 9-17
69. Kaim, G., Matthey, U., and Dimroth, P. (1998) *Embo J* **17**(3), 688-695
70. Capaldi, R. A., Schulenberg, B., Murray, J., and Aggeler, R. (2000) *J Exp Biol* **203**(Pt 1), 29-33
71. Jiang, W., and Fillingame, R. H. (1998) *Proc Natl Acad Sci U S A* **95**(12), 6607-6612
72. McLachlin, D. T., Coveny, A. M., Clark, S. M., and Dunn, S. D. (2000) *J Biol Chem* **275**(23), 17571-17577
73. Belogrudov, G. I., Tomich, J. M., and Hatefi, Y. (1996) *J Biol Chem* **271**(34), 20340-20345
74. Devenish, R. J., Prescott, M., Roucou, X., and Nagley, P. (2000) *Biochim Biophys Acta* **1458**(2-3), 428-442

75. Velours, J., and Arselin, G. (2000) *J Bioenerg Biomembr* **32**(4), 383-390
76. Boyer, P. D. (1989) *Faseb J* **3**(10), 2164-2178
77. Boyer, P. D. (1993) *Biochim Biophys Acta* **1140**(3), 215-250
78. Uden, G., and Bongaerts, J. (1997) *Biochim Biophys Acta* **1320**(3), 217-234
79. Gennis, R. B., and Stewart, V. (1996) Respiration. In: Neidhardt, F. C. (ed). *Escherichia coli and Salmonella*, 2 Ed., ASM Press, Washington, D.C.
80. Georgellis, D., Lynch, A. S., and Lin, E. C. (1997) *J Bacteriol* **179**(17), 5429-5435
81. Kwon, O., Georgellis, D., and Lin, E. C. (2000) *J Bacteriol* **182**(13), 3858-3862
82. Iuchi, S., and Lin, E. C. (1988) *Proc Natl Acad Sci U S A* **85**(6), 1888-1892
83. Brondsted, L., and Atlung, T. (1994) *J Bacteriol* **176**(17), 5423-5428
84. Lynch, A. S., and Lin, E. C. (1996) *J Bacteriol* **178**(21), 6238-6249
85. Georgellis, D., Kwon, O., De Wulf, P., and Lin, E. C. (1998) *J Biol Chem* **273**(49), 32864-32869
86. Georgellis, D., Kwon, O., and Lin, E. C. (2001) *Science* **292**(5525), 2314-2316
87. Malpica, R., Franco, B., Rodriguez, C., Kwon, O., and Georgellis, D. (2004) *Proc Natl Acad Sci U S A* **101**(36), 13318-13323
88. Kiley, P. J., and Beinert, H. (1998) *FEMS Microbiol Rev* **22**(5), 341-352
89. Crack, J., Green, J., and Thomson, A. J. (2004) *J Biol Chem* **279**(10), 9278-9286
90. Reinhart, F., Achebach, S., Koch, T., and Uden, G. (2008) *J Bacteriol* **190**(3), 879-886
91. Melville, S. B., and Gunsalus, R. P. (1990) *J Biol Chem* **265**(31), 18733-18736
92. Sharrocks, A. D., Green, J., and Guest, J. R. (1990) *FEBS Lett* **270**(1-2), 119-122

93. Green, J., Sharrocks, A. D., Green, B., Geisow, M., and Guest, J. R. (1993) *Mol Microbiol* **8**(1), 61-68
94. Green, J., Bennett, B., Jordan, P., Ralph, E. T., Thomson, A. J., and Guest, J. R. (1996) *Biochem J* **316** ( Pt 3), 887-892
95. Khoroshilova, N., Popescu, C., Munck, E., Beinert, H., and Kiley, P. J. (1997) *Proc Natl Acad Sci U S A* **94**(12), 6087-6092
96. Sutton, V. R., Mettert, E. L., Beinert, H., and Kiley, P. J. (2004) *J Bacteriol* **186**(23), 8018-8025
97. Achebach, S., Selmer, T., and Unden, G. (2005) *Febs J* **272**(16), 4260-4269
98. Guest, J. R., Green, J., Irvine, A. S., and Spiro, S. (1996) The FNR modulon and FNR-regulated gene expression. In: Lin, E. C., and Lynch, A. S. (eds). *Regulation of gene expression in Escherichia coli*, R. G. Landes & Co., Austin, Tex.
99. Lazazzera, B. A., Beinert, H., Khoroshilova, N., Kennedy, M. C., and Kiley, P. J. (1996) *J Biol Chem* **271**(5), 2762-2768
100. Marshall, F. A., Messenger, S. L., Wyborn, N. R., Guest, J. R., Wing, H., Busby, S. J., and Green, J. (2001) *Mol Microbiol* **39**(3), 747-753
101. Barnard, A. M., Green, J., and Busby, S. J. (2003) *J Bacteriol* **185**(20), 5993-6004
102. Kang, Y., Weber, K. D., Qiu, Y., Kiley, P. J., and Blattner, F. R. (2005) *J. Bacteriol.* **187**(3), 1135-1160
103. Bilous, P. T., Cole, S. T., Anderson, W. F., and Weiner, J. H. (1988) *Mol Microbiol* **2**(6), 785-795
104. Park, S. J., Chao, G., and Gunsalus, R. P. (1997) *J Bacteriol* **179**(13), 4138-4142

105. Darwin, A. J., Tyson, K. L., Busby, S. J., and Stewart, V. (1997) *Mol Microbiol* **25**(3), 583-595
106. Rabin, R. S., and Stewart, V. (1993) *J Bacteriol* **175**(11), 3259-3268
107. Cavicchioli, R., Chiang, R. C., Kalman, L. V., and Gunsalus, R. P. (1996) *Mol Microbiol* **21**(5), 901-911
108. Lee, A. I., Delgado, A., and Gunsalus, R. P. (1999) *J Bacteriol* **181**(17), 5309-5316
109. Noriega, C. E., Schmidt, R., Gray, M. J., Chen, L. L., and Stewart, V. (2008) *J Bacteriol* **190**(11), 3869-3876
110. Iuchi, S., and Lin, E. C. (1987) *Proc Natl Acad Sci U S A* **84**(11), 3901-3905
111. Cotter, P. A., and Gunsalus, R. P. (1989) *J Bacteriol* **171**(7), 3817-3823
112. Stewart, V. (1994) *Res Microbiol* **145**(5-6), 450-454
113. Johnson, D. C., Dean, D. R., Smith, A. D., and Johnson, M. K. (2005) *Annu Rev Biochem* **74**, 247-281
114. Ayala-Castro, C., Saini, A., and Outten, F. W. (2008) *Microbiol Mol Biol Rev* **72**(1), 110-125, table of contents
115. Zheng, L., White, R. H., Cash, V. L., Jack, R. F., and Dean, D. R. (1993) *Proc Natl Acad Sci U S A* **90**(7), 2754-2758
116. Kambampati, R., and Lauhon, C. T. (2000) *J Biol Chem* **275**(15), 10727-10730
117. Leimkuhler, S., and Rajagopalan, K. V. (2001) *J Biol Chem* **276**(25), 22024-22031
118. Agar, J. N., Krebs, C., Frazzon, J., Huynh, B. H., Dean, D. R., and Johnson, M. K. (2000) *Biochemistry* **39**(27), 7856-7862

119. Ollagnier-de-Choudens, S., Mattioli, T., Takahashi, Y., and Fontecave, M. (2001) *J Biol Chem* **276**(25), 22604-22607
120. Krebs, C., Agar, J. N., Smith, A. D., Frazzon, J., Dean, D. R., Huynh, B. H., and Johnson, M. K. (2001) *Biochemistry* **40**(46), 14069-14080
121. Ollagnier-de Choudens, S., Nachin, L., Sanakis, Y., Loiseau, L., Barras, F., and Fontecave, M. (2003) *J Biol Chem* **278**(20), 17993-18001
122. Smith, A. D., Jameson, G. N., Dos Santos, P. C., Agar, J. N., Naik, S., Krebs, C., Frazzon, J., Dean, D. R., Huynh, B. H., and Johnson, M. K. (2005) *Biochemistry* **44**(39), 12955-12969
123. Schilke, B., Voisine, C., Beinert, H., and Craig, E. (1999) *Proc Natl Acad Sci U S A* **96**(18), 10206-10211
124. Voisine, C., Cheng, Y. C., Ohlson, M., Schilke, B., Hoff, K., Beinert, H., Marszalek, J., and Craig, E. A. (2001) *Proc Natl Acad Sci U S A* **98**(4), 1483-1488
125. Lange, H., Kaut, A., Kispal, G., and Lill, R. (2000) *Proc Natl Acad Sci U S A* **97**(3), 1050-1055
126. Yoon, T., and Cowan, J. A. (2003) *J Am Chem Soc* **125**(20), 6078-6084
127. Layer, G., Ollagnier-de Choudens, S., Sanakis, Y., and Fontecave, M. (2006) *J Biol Chem* **281**(24), 16256-16263
128. Frankenberg, N., Moser, J., and Jahn, D. (2003) *Appl Microbiol Biotechnol* **63**(2), 115-127
129. Shibahara, S. (2003) *Tohoku J Exp Med* **200**(4), 167-186
130. Tran, Q. M., Rothery, R. A., Maklashina, E., Cecchini, G., and Weiner, J. H. (2007) *Proc Natl Acad Sci U S A* **104**(46), 18007-18012

131. Yankovskaya, V., Horsefield, R., Tornroth, S., Luna-Chavez, C., Miyoshi, H., Leger, C., Byrne, B., Cecchini, G., and Iwata, S. (2003) *Science* **299**(5607), 700-704
132. Furuyama, K., Kaneko, K., and Vargas, P. D. t. (2007) *Tohoku J Exp Med* **213**(1), 1-16
133. Wilson, M. T., and Reeder, B. J. (2008) *Exp Physiol* **93**(1), 128-132
134. Smulevich, G., Jakopitsch, C., Droghetti, E., and Obinger, C. (2006) *J Inorg Biochem* **100**(4), 568-585
135. Kearney, E. B., and Singer, T. P. (1955) *Biochim Biophys Acta* **17**(4), 596-597
136. Singer, T. P., Kearney, E. B., and Zastrow, N. (1955) *Biochim Biophys Acta* **17**(1), 154-155
137. Pealing, S. L., Black, A. C., Manson, F. D., Ward, F. B., Chapman, S. K., and Reid, G. A. (1992) *Biochemistry* **31**(48), 12132-12140
138. Schilling, B., and Lerch, K. (1995) *Mol Gen Genet* **247**(4), 430-438
139. Jeuken, L. J., Jones, A. K., Chapman, S. K., Cecchini, G., and Armstrong, F. A. (2002) *J Am Chem Soc* **124**(20), 5702-5713
140. Mewies, M., McIntire, W. S., and Scrutton, N. S. (1998) *Protein Sci* **7**(1), 7-20
141. Robinson, K. M., and Lemire, B. D. (1995) *Methods Enzymol* **260**, 34-51
142. Robinson, K. M., and Lemire, B. D. (1996) *J Biol Chem* **271**(8), 4061-4067
143. Robinson, K. M., and Lemire, B. D. (1996) *J Biol Chem* **271**(8), 4055-4060
144. Reid, G. A., Miles, C. S., Moysey, R. K., Pankhurst, K. L., and Chapman, S. K. (2000) *Biochim Biophys Acta* **1459**(2-3), 310-315

145. Pankhurst, K. L., Mowat, C. G., Rothery, E. L., Hudson, J. M., Jones, A. K., Miles, C. S., Walkinshaw, M. D., Armstrong, F. A., Reid, G. A., and Chapman, S. K. (2006) *J Biol Chem* **281**(29), 20589-20597
146. Lucas, M. F., and Ramos, M. J. (2006) *J Phys Chem B* **110**(21), 10550-10556
147. Tomasiak, T. M., Maklashina, E., Cecchini, G., and Iverson, T. M. (2008) *J Biol Chem* **283**(22), 15460-15468
148. Blasco, F., Dos Santos, J. P., Magalon, A., Frixon, C., Guigliarelli, B., Santini, C. L., and Giordano, G. (1998) *Mol Microbiol* **28**(3), 435-447
149. Vergnes, A., Pommier, J., Toci, R., Blasco, F., Giordano, G., and Magalon, A. (2006) *J Biol Chem* **281**(4), 2170-2176
150. Vergnes, A., Gouffi-Belhabich, K., Blasco, F., Giordano, G., and Magalon, A. (2004) *J Biol Chem* **279**(40), 41398-41403
151. Lanciano, P., Vergnes, A., Grimaldi, S., Guigliarelli, B., and Magalon, A. (2007) *J Biol Chem* **282**(24), 17468-17474
152. Dibrov, E., Fu, S., and Lemire, B. D. (1998) *J Biol Chem* **273**(48), 32042-32048
153. Van den Berg, B., Clemons, W. M., Jr., Collinson, I., Modis, Y., Hartmann, E., Harrison, S. C., and Rapoport, T. A. (2004) *Nature* **427**(6969), 36-44
154. Breyton, C., Haase, W., Rapoport, T. A., Kuhlbrandt, W., and Collinson, I. (2002) *Nature* **418**(6898), 662-665
155. Mori, H., Tsukazaki, T., Masui, R., Kuramitsu, S., Yokoyama, S., Johnson, A. E., Kimura, Y., Akiyama, Y., and Ito, K. (2003) *J Biol Chem* **278**(16), 14257-14264
156. Tziatzios, C., Schubert, D., Lotz, M., Gundogan, D., Betz, H., Schagger, H., Haase, W., Duong, F., and Collinson, I. (2004) *J Mol Biol* **340**(3), 513-524

157. Rapoport, T. A., Jungnickel, B., and Kutay, U. (1996) *Annu Rev Biochem* **65**, 271-303
158. Luirink, J., von Heijne, G., Houben, E., and de Gier, J. W. (2005) *Annu Rev Microbiol* **59**, 329-355
159. Berks, B. C., Palmer, T., and Sargent, F. (2005) *Curr Opin Microbiol* **8**(2), 174-181
160. Stevenson, L. G., Strisovsky, K., Clemmer, K. M., Bhatt, S., Freeman, M., and Rather, P. N. (2007) *Proc Natl Acad Sci U S A* **104**(3), 1003-1008
161. Berks, B. C. (1996) *Mol Microbiol* **22**(3), 393-404
162. Alami, M., Luke, I., Deitermann, S., Eisner, G., Koch, H. G., Brunner, J., and Muller, M. (2003) *Mol Cell* **12**(4), 937-946
163. Gerard, F., and Cline, K. (2007) *J Biol Chem* **282**(8), 5263-5272
164. Sargent, F. (2007) *Biochem Soc Trans* **35**(Pt 5), 835-847
165. Gohlke, U., Pullan, L., McDevitt, C. A., Porcelli, I., de Leeuw, E., Palmer, T., Saibil, H. R., and Berks, B. C. (2005) *Proc Natl Acad Sci U S A* **102**(30), 10482-10486
166. Uden, G. (1988) *Arch Microbiol* **150**(5), 499-503
167. Bogachev, A. V., Murtazina, R. A., and Skulachev, V. P. (1996) *J Bacteriol* **178**(21), 6233-6237
168. Barrett, E. L., and Kwan, H. S. (1985) *Annu Rev Microbiol* **39**, 131-149
169. Zinder, S. H., and Brock, T. D. (1978) *Arch Microbiol* **116**(1), 35-40
170. Kiene, R. P., and Bates, T. S. (1990) *Nature* **345**(6277), 702



171. Lovelock, J. E., Maggs, R. J., and Rasmussen, R. A. (1972) *Nature* **237**(5356), 452
172. McNicholas, P. M., Chiang, R. C., and Gunsalus, R. P. (1998) *Mol Microbiol* **27**(1), 197-208
173. Bearson, S. M., Albrecht, J. A., and Gunsalus, R. P. (2002) *BMC Microbiol* **2**, 13
174. Walkenhorst, H. M., Hemschemeier, S. K., and Eichenlaub, R. (1995) *Microbiol Res* **150**(4), 347-361
175. Grunden, A. M., Ray, R. M., Rosentel, J. K., Healy, F. G., and Shanmugam, K. T. (1996) *J Bacteriol* **178**(3), 735-744
176. McNicholas, P. M., Rech, S. A., and Gunsalus, R. P. (1997) *Mol Microbiol* **23**(3), 515-524
177. Rothery, R. A., Grant, J. L., Johnson, J. L., Rajagopalan, K. V., and Weiner, J. H. (1995) *J Bacteriol* **177**(8), 2057-2063
178. Bertero, M. G., Rothery, R. A., Palak, M., Hou, C., Lim, D., Blasco, F., Weiner, J. H., and Strynadka, N. C. (2003) *Nat Struct Biol* **10**(9), 681-687
179. Rothery, R. A., Bertero, M. G., Cammack, R., Palak, M., Blasco, F., Strynadka, N. C., and Weiner, J. H. (2004) *Biochemistry* **43**(18), 5324-5333
180. Jormakka, M., Tornroth, S., Byrne, B., and Iwata, S. (2002) *Science* **295**(5561), 1863-1868
181. Rajagopalan, K. V. (1991) *Adv Enzymol Relat Areas Mol Biol* **64**, 215-290
182. Schindelin, H., Kisker, C., Hilton, J., Rajagopalan, K. V., and Rees, D. C. (1996) *Science* **272**(5268), 1615-1621

183. Schneider, F., Lowe, J., Huber, R. S., 1996 #24}, Schindelin, H., Kisker, C., and Knablein, J. (1996) *J Mol Biol* **263**(1), 53-69
184. Czjzek, M., Dos Santos, J. P., Pommier, J., Giordano, G., Mejean, V., and Haser, R. (1998) *J Mol Biol* **284**(2), 435-447
185. Johnson, J. L., Hainline, B. E., Rajagopalan, K. V., and Arison, B. H. (1984) *J Biol Chem* **259**(9), 5414-5422
186. Kletzin, A., and Adams, M. W. (1996) *FEMS Microbiol Rev* **18**(1), 5-63
187. Hille, R. (1996) *Chem Rev* **96**(7), 2757-2816
188. McAlpine, A. S., McEwan, A. G., Shaw, A. L., and Bailey, S. (1997) *Journal of Biological Inorganic Chemistry* **2**(6), 690-701
189. McAlpine, A. S., McEwan, A. G., and Bailey, S. (1998) *J Mol Biol* **275**(4), 613-623
190. Johnson, J. L., Bastian, N. R., and Rajagopalan, K. V. (1990) *Proc Natl Acad Sci USA* **87**(8), 3190-3194
191. Hille, R. (1999) *Essays Biochem* **34**, 125-137
192. George, G. N., Hilton, J., and Rajagopalan, K. V. (1996) *J. Am. Chem. Soc.* **118**(5), 1113-1117
193. George, G. N., Hilton, J., Temple, C., Prince, R. C., and Rajagopalan, K. V. (1999) *J. Am. Chem. Soc.* **121**(6), 1256-1266
194. Baugh, P. E., Garner, C. D., Charnock, J. M., Collison, D., Davies, E. S., McAlpine, A. S., Bailey, S., Lane, I., Hanson, G. R., and McEwan, A. G. (1997) *Journal of Biological Inorganic Chemistry* **2**(5), 634-643

195. Li, H. K., Temple, C., Rajagopalan, K. V., and Schindelin, H. (2000) *J. Am. Chem. Soc.* **122**(32), 7673-7680
196. George, G. N., Doonan, C. J., Rothery, R. A., Boroumand, N., and Weiner, J. H. (2007) *Inorg Chem* **46**(1), 2-4
197. Garton, S. D., Hilton, J., Oku, H., Crouse, B. R., Rajagopalan, K. V., and Johnson, M. K. (1997) *J. Am. Chem. Soc.* **119**(52), 12906-12916
198. Bell, A. F., He, X., Ridge, J. P., Hanson, G. R., McEwan, A. G., and Tonge, P. J. (2001) *Biochemistry* **40**(2), 440-448
199. Bray, R. C., Adams, B., Smith, A. T., Bennett, B., and Bailey, S. (2000) *Biochemistry* **39**(37), 11258-11269
200. Johnson, K. E., and Rajagopalan, K. V. (2001) *J Biol Chem* **276**(16), 13178-13185
201. Ridge, J. P., Aguey-Zinsou, K. F., Bernhardt, P. V., Brereton, I. M., Hanson, G. R., and McEwan, A. G. (2002) *Biochemistry* **41**(52), 15762-15769
202. Ridge, J. P., Aguey-Zinsou, K. F., Bernhardt, P. V., Hanson, G. R., and McEwan, A. G. (2004) *FEBS Lett* **563**(1-3), 197-202
203. Simala-Grant, J. L., and Weiner, J. H. (1996) *Microbiology* **142** ( Pt 11), 3231-3239
204. Simala-Grant, J. L., and Weiner, J. H. (1998) *Eur J Biochem* **251**(1-2), 510-515
205. Abo, M., Tachibana, M., Okubo, A., and Yamazaki, S. (1995) *Bioorg Med Chem* **3**(2), 109-112
206. Hanlon, S. P., Graham, D. L., Hogan, P. J., Holt, R. A., Reeve, C. D., Shaw, A. L., and McEwan, A. G. (1998) *Microbiology* **144** ( Pt 8), 2247-2253

207. Trieber, C. A., Rothery, R. A., and Weiner, J. H. (1996) *J Biol Chem* **271**(44), 27339-27345
208. Heffron, K., Leger, C., Rothery, R. A., Weiner, J. H., and Armstrong, F. A. (2001) *Biochemistry* **40**(10), 3117-3126
209. Boyington, J. C., Gladyshev, V. N., Khangulov, S. V., Stadtman, T. C., and Sun, P. D. (1997) *Science* **275**(5304), 1305-1308
210. Rothery, R. A., Trieber, C. A., and Weiner, J. H. (1999) *J Biol Chem* **274**(19), 13002-13009
211. Rothery, R. A., and Weiner, J. H. (1991) *Biochemistry* **30**(34), 8296-8305
212. Rothery, R. A., and Weiner, J. H. (1996) *Biochemistry* **35**(10), 3247-3257
213. Cammack, R., and Weiner, J. H. (1990) *Biochemistry* **29**(36), 8410-8416
214. Blasco, F., Iobbi, C., Giordano, G., Chippaux, M., and Bonnefoy, V. (1989) *Mol Gen Genet* **218**(2), 249-256
215. Guigliarelli, B., Asso, M., More, C., Augier, V., Blasco, F., Pommier, J., Giordano, G., and Bertrand, P. (1992) *Eur J Biochem* **207**(1), 61-68
216. Iverson, T. M., Luna-Chavez, C., Cecchini, G., and Rees, D. C. (1999) *Science* **284**(5422), 1961-1966
217. Weiner, J. H., Shaw, G., Turner, R. J., and Trieber, C. A. (1993) *J Biol Chem* **268**(5), 3238-3244
218. Kyte, J., and Doolittle, R. F. (1982) *J Mol Biol* **157**(1), 105-132
219. von Heijne, G. (1992) *J Mol Biol* **225**(2), 487-494
220. Geijer, P., and Weiner, J. H. (2004) *Biochim Biophys Acta* **1660**(1-2), 66-74
221. Zhao, Z., and Weiner, J. H. (1998) *J Biol Chem* **273**(33), 20758-20763

222. Westenberg, D. J., Gunsalus, R. P., Ackrell, B. A., and Cecchini, G. (1990) *J Biol Chem* **265**(32), 19560-19567
223. Westenberg, D. J., Gunsalus, R. P., Ackrell, B. A., Sices, H., and Cecchini, G. (1993) *J Biol Chem* **268**(2), 815-822
224. Maklashina, E., Hellwig, P., Rothery, R. A., Kotlyar, V., Sher, Y., Weiner, J. H., and Cecchini, G. (2006) *J Biol Chem* **281**(36), 26655-26664
225. Guest, J. R. (1981) *J Gen Microbiol* **122**(2), 171-179
226. Wallace, B. J., and Young, I. G. (1977) *Biochim Biophys Acta* **461**(1), 84-100
227. Iverson, T. M., Luna-Chavez, C., Croal, L. R., Cecchini, G., and Rees, D. C. (2002) *J Biol Chem* **277**(18), 16124-16130
228. Bertero, M. G., Rothery, R. A., Boroumand, N., Palak, M., Blasco, F., Ginet, N., Weiner, J. H., and Strynadka, N. C. (2005) *J Biol Chem* **280**(15), 14836-14843
229. Rothery, R. A., Chatterjee, I., Kiema, G., McDermott, M. T., and Weiner, J. H. (1998) *Biochem J* **332** ( Pt 1), 35-41
230. Cheng, V. W., Rothery, R. A., Bertero, M. G., Strynadka, N. C., and Weiner, J. H. (2005) *Biochemistry* **44**(22), 8068-8077
231. Sambasivarao, D., Turner, R. J., Simala-Grant, J. L., Shaw, G., Hu, J., and Weiner, J. H. (2000) *J Biol Chem* **275**(29), 22526-22531
232. Sambasivarao, D., Dawson, H. A., Zhang, G., Shaw, G., Hu, J., and Weiner, J. H. (2001) *J Biol Chem* **276**(23), 20167-20174
233. Ray, N., Oates, J., Turner, R. J., and Robinson, C. (2003) *FEBS Lett* **534**(1-3), 156-160
234. Ize, B., Gerard, F., and Wu, L. F. (2002) *Arch Microbiol* **178**(6), 548-553

235. Sambasivarao, D., Scraba, D. G., Trieber, C., and Weiner, J. H. (1990) *J Bacteriol* **172**(10), 5938-5948
236. Neu, H. C., and Heppel, L. A. (1965) *J Biol Chem* **240**(9), 3685-3692
237. Ames, G. F., Prody, C., and Kustu, S. (1984) *J Bacteriol* **160**(3), 1181-1183
238. Sambasivarao, D., and Weiner, J. H. (1991) *J Bacteriol* **173**(19), 5935-5943
239. Rothery, R. A., and Weiner, J. H. (1993) *Biochemistry* **32**(22), 5855-5861
240. Stanley, N. R., Sargent, F., Buchanan, G., Shi, J., Stewart, V., Palmer, T., and Berks, B. C. (2002) *Mol Microbiol* **43**(4), 1005-1021
241. Sone, M., Kishigami, S., Yoshihisa, T., and Ito, K. (1997) *J Biol Chem* **272**(10), 6174-6178
242. Roffey, R. A., and Theg, S. M. (1996) *Plant Physiol* **111**(4), 1329-1338
243. Santini, C. L., Ize, B., Chanal, A., Muller, M., Giordano, G., and Wu, L. F. (1998) *Embo J* **17**(1), 101-112
244. Halbig, D., Wiegert, T., Blaudeck, N., Freudl, R., and Sprenger, G. A. (1999) *Eur J Biochem* **263**(2), 543-551
245. Sanders, C., Wethkamp, N., and Lill, H. (2001) *Mol Microbiol* **41**(1), 241-246
246. Weiner, J. H., Bilous, P. T., Shaw, G. M., Lubitz, S. P., Frost, L., Thomas, G. H., Cole, J. A., and Turner, R. J. (1998) *Cell* **93**(1), 93-101
247. Rothery, R. A., Kalra, N., Turner, R. J., and Weiner, J. H. (2002) *J Mol Microbiol Biotechnol* **4**(2), 133-150
248. Lindenstrauss, U., and Bruser, T. (2006) *J Bacteriol* **188**(22), 7807-7814
249. Lubitz, S. P., and Weiner, J. H. (2003) *Arch Biochem Biophys* **418**(2), 205-216
250. del Campillo Campbell, A., and Campbell, A. (1996) *J Mol Evol* **42**(2), 85-90

251. Gon, S., Patte, J. C., Mejean, V., and Iobbi-Nivol, C. (2000) *J Bacteriol* **182**(20), 5779-5786
252. Iobbi, C., Santini, C. L., Bonnefoy, V., and Giordano, G. (1987) *Eur J Biochem* **168**(2), 451-459
253. Blasco, F., Iobbi, C., Ratouchniak, J., Bonnefoy, V., and Chippaux, M. (1990) *Mol Gen Genet* **222**(1), 104-111
254. McCrindle, S. L., Kappler, U., and McEwan, A. G. (2005) *Adv Microb Physiol* **50**, 147-198
255. Quandt, K., Frech, K., Karas, H., Wingender, E., and Werner, T. (1995) *Nucleic Acids Res* **23**(23), 4878-4884
256. Salgado, H., Santos-Zavaleta, A., Gama-Castro, S., Millan-Zarate, D., Diaz-Peredo, E., Sanchez-Solano, F., Perez-Rueda, E., Bonavides-Martinez, C., and Collado-Vides, J. (2001) *Nucleic Acids Res* **29**(1), 72-74
257. Robison, K., McGuire, A. M., and Church, G. M. (1998) *J Mol Biol* **284**(2), 241-254
258. Papish, A. L., Ladner, C. L., and Turner, R. J. (2003) *J Biol Chem* **278**(35), 32501-32506
259. Oresnik, I. J., Ladner, C. L., and Turner, R. J. (2001) *Mol Microbiol* **40**(2), 323-331
260. Winstone, T. L., Workentine, M. L., Sarfo, K. J., Binding, A. J., Haslam, B. D., and Turner, R. J. (2006) *Arch Biochem Biophys* **455**(1), 89-97
261. Sarfo, K. J., Winstone, T. L., Papish, A. L., Howell, J. M., Kadir, H., Vogel, H. J., and Turner, R. J. (2004) *Biochem Biophys Res Commun* **315**(2), 397-403

262. Pommier, J., Mejean, V., Giordano, G., and Iobbi-Nivol, C. (1998) *J Biol Chem* **273**(26), 16615-16620
263. Ilbert, M., Mejean, V., Giudici-Orticoni, M. T., Samama, J. P., and Iobbi-Nivol, C. (2003) *J Biol Chem* **278**(31), 28787-28792
264. Wang, A., and Bolen, D. W. (1997) *Biochemistry* **36**(30), 9101-9108
265. Tulla-Puche, J., Getun, I. V., Woodward, C., and Barany, G. (2004) *Biochemistry* **43**(6), 1591-1598
266. Dos Santos, J. P., Iobbi-Nivol, C., Couillault, C., Giordano, G., and Mejean, V. (1998) *J Mol Biol* **284**(2), 421-433
267. Kim, K. E., and Chang, G. W. (1974) *Can J Microbiol* **20**(12), 1745-1748
268. Takagi, M., Tsuchiya, t., Ishimoto, M. (1981) *Journal of Bacteriology* **148**, 762-768
269. Mejean, V., Iobbi-Nivol, C., Lepelletier, M., Giordano, G., Chippaux, M., and Pascal, M. C. (1994) *Mol Microbiol* **11**(6), 1169-1179
270. Pascal, M. C., Burini, J. F., and Chippaux, M. (1984) *Mol Gen Genet* **195**(1-2), 351-355
271. Iobbi-Nivol, C., Pommier, J., Simala-Grant, J., Mejean, V., and Giordano, G. (1996) *Biochim Biophys Acta* **1294**(1), 77-82
272. Simon, G., Mejean, V., Jourlin, C., Chippaux, M., and Pascal, M. C. (1994) *J Bacteriol* **176**(18), 5601-5606
273. Spiro, S., and Guest, J. R. (1990) *FEMS Microbiol Rev* **6**(4), 399-428
274. Simon, G., Mejean, V., Jourlin, C., Chippaux, M., and Pascal, M. C. (1995) *J Bacteriol* **177**(1), 275



275. Stewart, V., and Parales, J., Jr. (1988) *J Bacteriol* **170**(4), 1589-1597
276. Goh, E. B., Bledsoe, P. J., Chen, L. L., Gyaneshwar, P., Stewart, V., and Igo, M. M. (2005) *J Bacteriol* **187**(14), 4890-4899
277. Stock, J. B., Ninfa, A. J., and Stock, A. M. (1989) *Microbiol Rev* **53**(4), 450-490
278. Jourlin, C., Bengrine, A., Chippaux, M., and Mejean, V. (1996) *Mol Microbiol* **20**(6), 1297-1306
279. Stock, A. M., and Mowbray, S. L. (1995) *Curr Opin Struct Biol* **5**(6), 744-751
280. Dutta, R., Qin, L., and Inouye, M. (1999) *Mol Microbiol* **34**(4), 633-640
281. Jourlin, C., Ansaldi, M., and Mejean, V. (1997) *J Mol Biol* **267**(4), 770-777
282. Ishige, K., Nagasawa, S., Tokishita, S., and Mizuno, T. (1994) *Embo J* **13**(21), 5195-5202
283. Ansaldi, M., Jourlin-Castelli, C., Lepelletier, M., Theraulaz, L., and Mejean, V. (2001) *J Bacteriol* **183**(8), 2691-2695
284. Ansaldi, M., Theraulaz, L., and Mejean, V. (2004) *Proc Natl Acad Sci U S A* **101**(25), 9423-9428
285. Elantak, L., Ansaldi, M., Guerlesquin, F., Mejean, V., and Morelli, X. (2005) *J Biol Chem* **280**(44), 36802-36808
286. Gon, S., Jourlin-Castelli, C., Theraulaz, L., and Mejean, V. (2001) *Proc Natl Acad Sci U S A* **98**(20), 11615-11620
287. Kondo, H., Nakagawa, A., Nishihira, J., Nishimura, Y., Mizuno, T., and Tanaka, I. (1997) *Nat Struct Biol* **4**(1), 28-31
288. Martinez-Hackert, E., and Stock, A. M. (1997) *J Mol Biol* **269**(3), 301-312
289. Itou, H., and Tanaka, I. (2001) *J Biochem (Tokyo)* **129**(3), 343-350

290. Ansaldi, M., Simon, G., Lepelletier, M., and Mejean, V. (2000) *J Bacteriol* **182**(4), 961-966
291. Palmer, T., Sargent, F., and Berks, B. C. (2005) *Trends Microbiol* **13**(4), 175-180
292. Buc, J., Santini, C. L., Giordani, R., Czjzek, M., Wu, L. F., and Giordano, G. (1999) *Mol Microbiol* **32**(1), 159-168
293. Gon, S., Giudici-Orticoni, M. T., Mejean, V., and Iobbi-Nivol, C. (2001) *J Biol Chem* **276**(15), 11545-11551
294. Thony-Meyer, L., and Kunzler, P. (1997) *Eur J Biochem* **246**(3), 794-799
295. Allen, J. W., Barker, P. D., and Ferguson, S. J. (2003) *J Biol Chem* **278**(52), 52075-52083
296. Shaw, A. L., Hochkoepler, A., Bonora, P., Zannoni, D., Hanson, G. R., and McEwan, A. G. (1999) *J Biol Chem* **274**(15), 9911-9914
297. Ilbert, M., Mejean, V., and Iobbi-Nivol, C. (2004) *Microbiology* **150**(Pt 4), 935-943
298. McDevitt, C. A., Hugenholtz, P., Hanson, G. R., and McEwan, A. G. (2002) *Mol Microbiol* **44**(6), 1575-1587
299. Mouncey, N. J., Choudhary, M., and Kaplan, S. (1997) *J Bacteriol* **179**(24), 7617-7624
300. Tranier, S., Mortier-Barriere, I., Ilbert, M., Birck, C., Iobbi-Nivol, C., Mejean, V., and Samama, J. P. (2002) *Protein Sci* **11**(9), 2148-2157
301. Tranier, S., Iobbi-Nivol, C., Birck, C., Ilbert, M., Mortier-Barriere, I., Mejean, V., and Samama, J. P. (2003) *Structure* **11**(2), 165-174

302. Genest, O., Ilbert, M., Mejean, V., and Iobbi-Nivol, C. (2005) *J Biol Chem* **280**(16), 15644-15648
303. Hatzixanthis, K., Clarke, T. A., Oubrie, A., Richardson, D. J., Turner, R. J., and Sargent, F. (2005) *Proc Natl Acad Sci U S A* **102**(24), 8460-8465
304. Genest, O., Seduk, F., Ilbert, M., Mejean, V., and Iobbi-Nivol, C. (2006) *Biochem Biophys Res Commun* **339**(3), 991-995
305. Genest, O., Seduk, F., Theraulaz, L., Mejean, V., and Iobbi-Nivol, C. (2006) *FEMS Microbiol Lett* **265**(1), 51-55
306. Berks, B. C., Sargent, F., and Palmer, T. (2000) *Mol Microbiol* **35**(2), 260-274
307. Jack, R. L., Buchanan, G., Dubini, A., Hatzixanthis, K., Palmer, T., and Sargent, F. (2004) *Embo J* **23**(20), 3962-3972
308. Grovc, J., Busby, S., and Cole, J. (1996) *Mol Gen Genet* **252**(3), 332-341
309. Berg, B. L., Li, J., Heider, J., and Stewart, V. (1991) *J Biol Chem* **266**(33), 22380-22385
310. Abaibou, H., Pommier, J., Benoit, S., Giordano, G., and Mandrand-Berthelot, M. A. (1995) *J Bacteriol* **177**(24), 7141-7149
311. Blasco, F., Guigliarelli, B., Magalon, A., Asso, M., Giordano, G., and Rothery, R. A. (2001) *Cell Mol Life Sci* **58**(2), 179-193
312. Heinzinger, N. K., Fujimoto, S. Y., Clark, M. A., Moreno, M. S., and Barrett, E. L. (1995) *J Bacteriol* **177**(10), 2813-2820
313. Krafft, T., Bokranz, M., Klimmek, O., Schroder, I., Fahrenholz, F., Kojro, E., and Kroger, A. (1992) *Eur J Biochem* **206**(2), 503-510
314. Dietrich, W., and Klimmek, O. (2002) *Eur J Biochem* **269**(4), 1086-1095

315. Guigliarelli, B., Magalon, A., Asso, M., Bertrand, P., Frixon, C., Giordano, G., and Blasco, F. (1996) *Biochemistry* **35**(15), 4828-4836
316. Rothery, R. A., Magalon, A., Giordano, G., Guigliarelli, B., Blasco, F., and Weiner, J. H. (1998) *J Biol Chem* **273**(13), 7462-7469
317. Manodori, A., Cecchini, G., Schroder, I., Gunsalus, R. P., Werth, M. T., and Johnson, M. K. (1992) *Biochemistry* **31**(10), 2703-2712
318. Kowal, A. T., Werth, M. T., Manodori, A., Cecchini, G., Schroder, I., Gunsalus, R. P., and Johnson, M. K. (1995) *Biochemistry* **34**(38), 12284-12293
319. Condon, C., Cammack, R., Patil, D. S., and Owen, P. (1985) *J Biol Chem* **260**(16), 9427-9434
320. Unciuleac, M., Warkentin, E., Page, C. C., Boll, M., and Ermler, U. (2004) *Structure (Camb)* **12**(12), 2249-2256
321. Page, C. C., Moser, C. C., and Dutton, P. L. (2003) *Curr Opin Chem Biol* **7**(5), 551-556
322. Stephens, P. J., Jollie, D. R., and Warshel, A. (1996) *Chem Rev* **96**(7), 2491-2514
323. Chen, K., Bonagura, C. A., Tilley, G. J., McEvoy, J. P., Jung, Y. S., Armstrong, F. A., Stout, C. D., and Burgess, B. K. (2002) *Nat Struct Biol* **9**(3), 188-192
324. Langen, R., Jensen, G. M., Jacob, U., Stephens, P. J., and Warshel, A. (1992) *J Biol Chem* **267**(36), 25625-25627
325. Jensen, G. M., Warshel, A., and Stephens, P. J. (1994) *Biochemistry* **33**(36), 10911-10924
326. Adman, E., Watenpaugh, K. D., and Jensen, L. H. (1975) *Proc Natl Acad Sci U S A* **72**(12), 4854-4858

327. Rayment, I., Wesenberg, G., Meyer, T. E., Cusanovich, M. A., and Holden, H. M. (1992) *J Mol Biol* **228**(2), 672-686
328. Jang, S. B., Seefeldt, L. C., and Peters, J. W. (2000) *Biochemistry* **39**(4), 641-648
329. Rothery, R. A., and Weiner, J. H. (1998) *Eur J Biochem* **254**(3), 588-595
330. Cecchini, G., Schroder, I., Gunsalus, R. P., and Maklashina, E. (2002) *Biochim Biophys Acta* **1553**(1-2), 140-157
331. Hagerhall, C. (1997) *Biochim Biophys Acta* **1320**(2), 107-141
332. Altschul, S. F., Madden, T. L., Schaffer, A. A., Zhang, J., Zhang, Z., Miller, W., and Lipman, D. J. (1997) *Nucleic Acids Res* **25**(17), 3389-3402
333. Fiser, A., and Sali, A. (2003) *Methods Enzymol* **374**, 461-491
334. Laskowski, R. A., MacArthur, M. W., Moss, D. S., and Thornton, J. M. (1993) *J Appl Cryst* **26**, 283-291
335. Sambrook, J., and Russell, D. W. (2001) *Molecular cloning : a laboratory manual*, 3rd Ed., Cold Spring Harbor Laboratory Press, Cold Spring Harbor, N.Y.
336. Bilous, P. T., and Weiner, J. H. (1985) *J Bacteriol* **162**(3), 1151-1155
337. Markwell, M. A., Haas, S. M., Bieber, L. L., and Tolbert, N. E. (1978) *Anal Biochem* **87**(1), 206-210
338. Van Ark, G., and Berden, J. A. (1977) *Biochim Biophys Acta* **459**(1), 119-127
339. Okun, J. G., Lummen, P., and Brandt, U. (1999) *J Biol Chem* **274**(5), 2625-2630
340. Berks, B. C., Page, M. D., Richardson, D. J., Reilly, A., Cavill, A., Outen, F., and Ferguson, S. J. (1995) *Mol Microbiol* **15**(2), 319-331

341. Astuti, D., Latif, F., Dallol, A., Dahia, P. L., Douglas, F., George, E., Skoldberg, F., Husebye, E. S., Eng, C., and Maher, E. R. (2001) *Am J Hum Genet* **69**(1), 49-54
342. Wang, J., Rumbley, J., Ching, Y. C., Takahashi, S., Gennis, R. B., and Rousseau, D. L. (1995) *Biochemistry* **34**(47), 15504-15511
343. Wang, Y., and Beattie, D. S. (2002) *J Bioenerg Biomembr* **34**(2), 81-88
344. Barry, B. A., and Babcock, G. T. (1987) *Proc Natl Acad Sci U S A* **84**(20), 7099-7103
345. Babcock, G. T., Barry, B. A., Debus, R. J., Hoganson, C. W., Atamian, M., McIntosh, L., Sithole, I., and Yocum, C. F. (1989) *Biochemistry* **28**(25), 9557-9565
346. Ryle, M. J., Lanzilotta, W. N., and Seefeldt, L. C. (1996) *Biochemistry* **35**(29), 9424-9434
347. Agarwal, A., Li, D., and Cowan, J. A. (1995) *Proc Natl Acad Sci U S A* **92**(21), 9440-9444
348. Heering, H. A., Bultink, B. M., Hagen, W. R., and Meyer, T. E. (1995) *Biochemistry* **34**(45), 14675-14686
349. Ambler, R. P., Daniel, M., Meyer, T. E., and Cusanovich, M. A. (1999) *Arch Biochem Biophys* **369**(1), 143-148
350. Zhao, Z., Rothery, R. A., and Weiner, J. H. (2003) *Biochemistry* **42**(18), 5403-5413
351. Cole, S. T., Grundstrom, T., Jaurin, B., Robinson, J. J., and Weiner, J. H. (1982) *Eur J Biochem* **126**(1), 211-216

352. Cole, S. T. (1982) *Eur J Biochem* **122**(3), 479-484
353. Magnusson, K., Philips, M. K., Guest, J. R., and Rutberg, L. (1986) *J Bacteriol* **166**(3), 1067-1071
354. Phillips, M. K., Hederstedt, L., Hasnain, S., Rutberg, L., and Guest, J. R. (1987) *J Bacteriol* **169**(2), 864-873
355. Lauterbach, F., Kortner, C., Albracht, S. P., Uden, G., and Kroger, A. (1990) *Arch Microbiol* **154**(4), 386-393
356. Burger, G., Lang, B. F., Reith, M., and Gray, M. W. (1996) *Proc Natl Acad Sci U S A* **93**(6), 2328-2332
357. Jones, H. M., and Gunsalus, R. P. (1987) *J Bacteriol* **169**(7), 3340-3349
358. Spencer, M. E., and Guest, J. R. (1973) *J Bacteriol* **114**(2), 563-570
359. Maklashina, E., Berthold, D. A., and Cecchini, G. (1998) *J Bacteriol* **180**(22), 5989-5996
360. Weiner, J. H., Lemire, B. D., Elmes, M. L., Bradley, R. D., and Scraba, D. G. (1984) *J Bacteriol* **158**(2), 590-596
361. Elmes, M. L., Scraba, D. G., and Weiner, J. H. (1986) *J Gen Microbiol* **132**(6), 1429-1439
362. Amino, H., Osanai, A., Miyadera, H., Shinjyo, N., Tomitsuka, E., Taka, H., Mineki, R., Murayama, K., Takamiya, S., Aoki, T., Miyoshi, H., Sakamoto, K., Kojima, S., and Kita, K. (2003) *Mol Biochem Parasitol* **128**(2), 175-186
363. Amino, H., Wang, H., Hirawake, H., Saruta, F., Mizuchi, D., Mineki, R., Shindo, N., Murayama, K., Takamiya, S., Aoki, T., Kojima, S., and Kita, K. (2000) *Mol Biochem Parasitol* **106**(1), 63-76

364. Iwata, F., Shinjyo, N., Amino, H., Sakamoto, K., Islam, M. K., Tsuji, N., and Kita, K. (2008) *Parasitol Int* **57**(1), 54-61
365. Zientz, E., Bongaerts, J., and Uden, G. (1998) *J Bacteriol* **180**(20), 5421-5425
366. Golby, P., Davies, S., Kelly, D. J., Guest, J. R., and Andrews, S. C. (1999) *J Bacteriol* **181**(4), 1238-1248
367. Bourgeron, T., Rustin, P., Chretien, D., Birch-Machin, M., Bourgeois, M., Viegas-Pequignot, E., Munnich, A., and Rotig, A. (1995) *Nat Genet* **11**(2), 144-149
368. Horvath, R., Abicht, A., Holinski-Feder, E., Laner, A., Gempel, K., Prokisch, H., Lochmuller, H., Klopstock, T., and Jaksch, M. (2006) *J Neurol Neurosurg Psychiatry* **77**(1), 74-76
369. Rivner, M. H., Shamsnia, M., Swift, T. R., Trefz, J., Roesel, R. A., Carter, A. L., Yanamura, W., and Hommes, F. A. (1989) *Neurology* **39**(5), 693-696
370. Arpa, J., Campos, Y., Gutierrez-Molina, M., Cruz-Martinez, A., Arenas, J., Caminero, A. B., Palomo, F., Morales, C., and Barreiro, P. (1994) *Acta Neurol Scand* **90**(4), 281-284
371. Messner, K. R., and Imlay, J. A. (2002) *J Biol Chem* **277**(45), 42563-42571
372. Guo, J., and Lemire, B. D. (2003) *J Biol Chem* **278**(48), 47629-47635
373. Zhao, Z., Rothery, R. A., and Weiner, J. H. (2006) *Biochem Cell Biol* **84**(6), 1013-1021
374. Szeto, S. S., Reinke, S. N., Sykes, B. D., and Lemire, B. D. (2007) *J Biol Chem* **282**(37), 27518-27526



375. Silkin, Y., Oyedotun, K. S., and Lemire, B. D. (2007) *Biochim Biophys Acta* **1767**(2), 143-150
376. Tornroth, S., Yankovskaya, V., Cecchini, G., and Iwata, S. (2002) *Biochim Biophys Acta* **1553**(1-2), 171-176
377. Horsefield, R., Yankovskaya, V., Sexton, G., Whittingham, W., Shiomi, K., Omura, S., Byrne, B., Cecchini, G., and Iwata, S. (2006) *J Biol Chem* **281**(11), 7309-7316
378. Sun, F., Huo, X., Zhai, Y., Wang, A., Xu, J., Su, D., Bartlam, M., and Rao, Z. (2005) *Cell* **121**(7), 1043-1057
379. Huang, L. S., Shen, J. T., Wang, A. C., and Berry, E. A. (2006) *Biochim Biophys Acta* **1757**(9-10), 1073-1083
380. Huang, L. S., Sun, G., Cobessi, D., Wang, A. C., Shen, J. T., Tung, E. Y., Anderson, V. E., and Berry, E. A. (2006) *J Biol Chem* **281**(9), 5965-5972
381. Lancaster, C. R. (2002) *Biochim Biophys Acta* **1565**(2), 215-231
382. Wood, D., Darlison, M. G., Wilde, R. J., and Guest, J. R. (1984) *Biochem J* **222**(2), 519-534
383. Mowat, C. G., Moysey, R., Miles, C. S., Leys, D., Doherty, M. K., Taylor, P., Walkinshaw, M. D., Reid, G. A., and Chapman, S. K. (2001) *Biochemistry* **40**(41), 12292-12298
384. Walker, W. H., and Singer, T. P. (1970) *J Biol Chem* **245**(16), 4224-4225
385. Ohnishi, T., King, T. E., Salerno, J. C., Blum, H., Bowyer, J. R., and Maida, T. (1981) *J Biol Chem* **256**(11), 5577-5582

386. Leger, C., Heffron, K., Pershad, H. R., Maklashina, E., Luna-Chavez, C., Cecchini, G., Ackrell, B. A., and Armstrong, F. A. (2001) *Biochemistry* **40**(37), 11234-11245
387. Hudson, J. M., Heffron, K., Kotlyar, V., Sher, Y., Maklashina, E., Cecchini, G., and Armstrong, F. A. (2005) *J Am Chem Soc* **127**(19), 6977-6989
388. Williamson, G., and Edmondson, D. E. (1985) *Biochemistry* **24**(26), 7790-7797
389. Blaut, M., Whittaker, K., Valdovinos, A., Ackrell, B. A., Gunsalus, R. P., and Cecchini, G. (1989) *J Biol Chem* **264**(23), 13599-13604
390. Hederstedt, L. (1983) *Eur J Biochem* **132**(3), 589-593
391. Leys, D., Tsapin, A. S., Nealsen, K. H., Meyer, T. E., Cusanovich, M. A., and Van Beeumen, J. J. (1999) *Nat Struct Biol* **6**(12), 1113-1117
392. Madej, M. G., Nasiri, H. R., Hilgendorff, N. S., Schwalbe, H., and Lancaster, C. R. (2006) *Embo J* **25**(20), 4963-4970
393. Sucheta, A., Ackrell, B. A., Cochran, B., and Armstrong, F. A. (1992) *Nature* **356**(6367), 361-362
394. Ackrell, B. A., Armstrong, F. A., Cochran, B., Sucheta, A., and Yu, T. (1993) *FEBS Lett* **326**(1-3), 92-94
395. Pershad, H. R., Hirst, J., Cochran, B., Ackrell, B. A., and Armstrong, F. A. (1999) *Biochim Biophys Acta* **1412**(3), 262-272
396. Maklashina, E., Iverson, T. M., Sher, Y., Kotlyar, V., Andrell, J., Mirza, O., Hudson, J. M., Armstrong, F. A., Rothery, R. A., Weiner, J. H., and Cecchini, G. (2006) *J Biol Chem* **281**(16), 11357-11365

397. Doherty, M. K., Pealing, S. L., Miles, C. S., Moysey, R., Taylor, P., Walkinshaw, M. D., Reid, G. A., and Chapman, S. K. (2000) *Biochemistry* **39**(35), 10695-10701
398. Maklashina, E., Rothery, R. A., Weiner, J. H., and Cecchini, G. (2001) *J Biol Chem* **276**(22), 18968-18976
399. Yu, L., Xu, J. X., Haley, P. E., and Yu, C. A. (1987) *J Biol Chem* **262**(3), 1137-1143
400. Oyedotun, K. S., Sit, C. S., and Lemire, B. D. (2007) *Biochim Biophys Acta* **1767**(12), 1436-1445
401. Oyedotun, K. S., and Lemire, B. D. (1999) *J Biol Chem* **274**(34), 23956-23962
402. Oyedotun, K. S., and Lemire, B. D. (2001) *J Biol Chem* **276**(20), 16936-16943
403. Oyedotun, K. S., and Lemire, B. D. (2004) *J Biol Chem* **279**(10), 9424-9431
404. Ohnishi, T., Moser, C. C., Page, C. C., Dutton, P. L., and Yano, T. (2000) *Structure* **8**(2), R23-32
405. Gutierrez-Cirlos, E. B., and Trumpower, B. L. (2002) *J Biol Chem* **277**(2), 1195-1202
406. Hederstedt, L. (2003) *Science* **299**(5607), 671-672
407. Schnorpfel, M., Janasch, I. G., Biel, S., Kroger, A., and Unden, G. (2001) *Eur J Biochem* **268**(10), 3069-3074
408. Schirawski, J., and Unden, G. (1998) *Eur J Biochem* **257**(1), 210-215
409. Madej, M. G., Nasiri, H. R., Hilgendorff, N. S., Schwalbe, H., Unden, G., and Lancaster, C. R. (2006) *Biochemistry* **45**(50), 15049-15055

410. Lancaster, C. R., Sauer, U. S., Gross, R., Haas, A. H., Graf, J., Schwalbe, H., Mantele, W., Simon, J., and Madej, M. G. (2005) *Proc Natl Acad Sci U S A* **102**(52), 18860-18865
411. Lancaster, C. R., Haas, A. H., Madej, M. G., and Mileni, M. (2006) *Biochim Biophys Acta* **1757**(8), 988-995
412. Ruzicka, F. J., Beinert, H., Schepler, K. L., Dunham, W. R., and Sands, R. H. (1975) *Proc Natl Acad Sci U S A* **72**(8), 2886-2890
413. Hung, S. C., Grant, C. V., Peloquin, J. M., Waldeck, A. R., Brit, R. D., and Chan, S. I. (2000) *J Biol Inorg Chem* **5**(5), 593-602
414. Tran, Q. M., Rothery, R. A., Maklashina, E., Cecchini, G., and Weiner, J. H. (2006) *J Biol Chem* **281**(43), 32310-32317
415. Hagerhall, C., Magnitsky, S., Sled, V. D., Schroder, I., Gunsalus, R. P., Cecchini, G., and Ohnishi, T. (1999) *J Biol Chem* **274**(37), 26157-26164
416. Rustin, P., Munnich, A., and Rotig, A. (2002) *Eur J Hum Genet* **10**(5), 289-291
417. Ishii, N., Fujii, M., Hartman, P. S., Tsuda, M., Yasuda, K., Senoo-Matsuda, N., Yanase, S., Ayusawa, D., and Suzuki, K. (1998) *Nature* **394**(6694), 694-697
418. Senoo-Matsuda, N., Yasuda, K., Tsuda, M., Ohkubo, T., Yoshimura, S., Nakazawa, H., Hartman, P. S., and Ishii, N. (2001) *J Biol Chem* **276**(45), 41553-41558
419. Milunsky, J. M., Maher, T. A., Michels, V. V., and Milunsky, A. (2001) *Am J Med Genet* **100**(4), 311-314
420. Yang, X., Yu, L., He, D., and Yu, C. A. (1998) *J Biol Chem* **273**(48), 31916-31923

421. Broomfield, P. L., and Hargreaves, J. A. (1992) *Curr Genet* **22**(2), 117-121
422. Matsson, M., and Hederstedt, L. (2001) *J Bioenerg Biomembr* **33**(2), 99-105
423. Cecchini, G., Maklashina, E., Yankovskaya, V., Iverson, T. M., and Iwata, S. (2003) *FEBS Lett* **545**(1), 31-38
424. Cheng, V. W., Ma, E., Zhao, Z., Rothery, R. A., and Weiner, J. H. (2006) *J Biol Chem* **281**(37), 27662-27668
425. Lowry, O. H., Rosebrough, N. J., Farr, A. L., and Randall, R. J. (1951) *J Biol Chem* **193**(1), 265-275
426. Singer, T. P., and Edmondson, D. E. (1980) *Methods Enzymol* **66**, 253-264
427. Kita, K., Vibat, C. R., Meinhardt, S., Guest, J. R., and Gennis, R. B. (1989) *J Biol Chem* **264**(5), 2672-2677
428. Maklashina, E., and Cecchini, G. (1999) *Arch Biochem Biophys* **369**(2), 223-232
429. Cleland, W. W. (2005) *Arch Biochem Biophys* **433**(1), 2-12
430. King, S. C., and Wilson, T. H. (1990) *J Biol Chem* **265**(17), 9645-9651
431. Berghuis, A. M., and Brayer, G. D. (1992) *J Mol Biol* **223**(4), 959-976
432. Stowell, M. H., McPhillips, T. M., Rees, D. C., Soltis, S. M., Abresch, E., and Feher, G. (1997) *Science* **276**(5313), 812-816
433. Abresch, E., Paddock, M. L., Stowell, M. H., McPhillips, T. M., Axelrod, H. L., Soltis, S. M., Rees, D. C., Okamura, M. Y., and Feher, G. (1998) *Photosynthesis Research* **55**, 119-125
434. Adelroth, P., Paddock, M. L., Tehrani, A., Beatty, J. T., Feher, G., and Okamura, M. Y. (2001) *Biochemistry* **40**(48), 14538-14546

435. Nicholls, D. G., and Ferguson, S. J. (2002) *Bioenergetics 3*, Academic Press, Boston
436. Denke, E., Merbitz-Zahradnik, T., Hatzfeld, O. M., Snyder, C. H., Link, T. A., and Trumpower, B. L. (1998) *J Biol Chem* **273**(15), 9085-9093
437. Alric, J., Lavergne, J., Rappaport, F., Vermeglio, A., Matsuura, K., Shimada, K., and Nagashima, K. V. (2006) *J Am Chem Soc* **128**(12), 4136-4145
438. Gray, K. A., Davidson, E., and Daldal, F. (1992) *Biochemistry* **31**(47), 11864-11873
439. Messner, K. R., and Imlay, J. A. (2002) *Methods Enzymol* **349**, 354-361
440. Cammack, R., Patil, D. S., and Weiner, J. H. (1986) *Biochim Biophys Acta* **870**(3), 545-551
441. Leggate, E. J., and Hirst, J. (2005) *Biochemistry* **44**(18), 7048-7058
442. Rothery, R. A., Seime, A. M., Spiers, A. M., Maklashina, E., Schroder, I., Gunsalus, R. P., Cecchini, G., and Weiner, J. H. (2005) *Febs J* **272**(2), 313-326
443. Moser, C. C., Farid, T. A., Chobot, S. E., and Dutton, P. L. (2006) *Biochim Biophys Acta* **1757**(9-10), 1096-1109
444. Osyczka, A., Moser, C. C., Daldal, F., and Dutton, P. L. (2004) *Nature* **427**(6975), 607-612
445. Cherepanov, A. V., and De Vries, S. (2004) *Biochim Biophys Acta* **1656**(1), 1-31
446. Jormakka, M., Yokoyama, K., Yano, T., Tamakoshi, M., Akimoto, S., Shimamura, T., Curmi, P., and Iwata, S. (2008) *Nat Struct Mol Biol* **15**(7), 730-737

447. Hedderich, R., Klimmek, O., Kroger, A., Dirmeier, R., Keller, M., and Stetter, K. O. (1998) *FEMS Microbiol Rev* **22**(5), 353-381
448. Christenson, A., Gustavsson, T., Gorton, L., and Hagerhall, C. (2008) *Biochim Biophys Acta* **1777**(9), 1203-1210
449. Shih, C., Museth, A. K., Abrahamsson, M., Blanco-Rodriguez, A. M., Di Bilio, A. J., Sudhamsu, J., Crane, B. R., Ronayne, K. L., Towrie, M., Vlcek, A., Jr., Richards, J. H., Winkler, J. R., and Gray, H. B. (2008) *Science* **320**(5884), 1760-1762